Sensitivity Studies of the Neutronic Design of a Fission Converter-Based Epithermal Beam for Boron Neutron Capture Therapy

by

Shuichi Sakamoto

B. E., Nuclear Engineering (1990)
M. E., Nuclear Engineering (1992)
Kyoto University

Submitted to the Department of Nuclear Engineering
in Partial Fulfillment of the Requirements for the Degrees of

Master of Science in Nuclear Engineering
and
Nuclear Engineer

at the

Massachusetts Institute of Technology

June 1997

Copyright © 1997 Massachusetts Institute of Technology
All rights reserved.

Signature of Author: _____
Department of Nuclear Engineering
May 9, 1997

Certified by: _____
Prof. Otto K. Harling
Thesis Supervisor

_____
Prof. Jacquelyn C. Yanch
Thesis Reader

Accepted by: _____
Prof. Jeffrey P. Freidberg
Chairman, Department Committee on Graduate Students

MASSACHUSETTS INSTITUTE
OF TECHNOLOGY

JUL 10 1997

Sensitivity Studies of the Neutronic Design of a Fission Converter-Based Epithermal Beam for Boron Neutron Capture Therapy

by

Shuichi Sakamoto

Submitted to the Department of Nuclear Engineering
on May 9, 1997 in Partial Fulfillment of the Requirements for the Degrees of
Master of Science in Nuclear Engineering and Nuclear Engineer

ABSTRACT

This thesis presents sensitivity analyses of the neutronic designs of the main components of a fission converter-based epithermal neutron beam for neutron capture therapy. Results for the fission converter, the neutron filters and the collimator are presented. In the analyses of the fast neutron filter/moderator and collimator designs, great emphasis was laid on in-phantom figures of merit using a water-filled ellipsoidal head phantom to evaluate beam performance. In addition, various neutronic calculations required for the engineering design (e.g., reactivity insertion due to the fission converter) were performed. This study intensively employed the general purpose Monte Carlo radiation transport code MCNP (Monte Carlo N-Particle) for the analyses.

In the sensitivity analysis of the fission converter design, the effect of using different fuel configurations (multi-plate reactor type MITR-II fuel vs. single plate type fuel) was examined with the expectation that the reduced volume fraction of coolant in the single plate fuel fission converter might offset the disadvantage of the H_2O coolant which overmoderates a useful portion of the neutron spectrum without commensurate reduction of fast contamination. However, this analysis indicated that the fresh MITR-II fuel provides comparable beam performance to that of the single plate fuel and that an H_2O-cooled single plate fuel fission converter with the minimum coolant thickness (0.16 cm) does not improve beam performance significantly relative to a D_2O-cooled burned MITR-II fuel fission converter. Therefore, it is concluded that both burned and fresh MITR-II fuels are as efficient generators of epithermal neutron beams, especially with D_2O coolant, as is the single plate fuel. The effect of varying fuel spacing between the MITR-II fuel elements was also studied. This study showed that increasing spacing causes power to increase without affecting the epithermal neutron flux and the specific fast neutron dose. It was concluded that increases in the thickness of the coolant layers surrounding the fuel elements do not reduce fast neutron contamination enough to offset concomitant loss of beam intensity because the MITR-II fuel elements already have a large coolant volume fraction.

The sensitivity analysis of the filter/moderator design revealed that various combinations of the filter/moderator materials, i.e., Al-Al_2O_3, Al-AlF_3, Al-$(CF_2)_n$ and Al-C, will provide epithermal neutron beams with high intensity and high quality (epithermal neutron flux $\geq 10^{10}$n/cm^{2}s, specific fast neutron and photon doses $\leq 2*10^{-11}$cGycm^2/n). The filter/moderator designs with the optimized dimensions of these materials provide deep penetration of the beam (the AD's of

9.3-9.8 cm extend into the region beyond the centerline of the head phantom) and large therapeutic gain (the AR is around 5) for a boron-delivery compound such as BPA-fructose. Moreover, they produce advantage depth dose rates of 400-600 RBE cGy/min, which would enable a complete irradiation in a few minutes. This analysis also indicated that the variation of the neutron spectrum caused by the use of different filter/moderator configurations does not affect beam quality as long as the design goals on beam quality are met because fast neutron and photon contamination is maintained at a very low level compared to the irreducible background due to nitrogen and hydrogen capture. As for the use of the materials which would be accompanied with concern of decomposition and release of chemically active species (e.g., fluorine from aluminum fluoride or Teflon), this analysis suggested that one can take advantage of the shielding effect of a thick aluminum block by locating such materials behind it, where the radiation level and temperature would be reduced relative to a location near the fission converter.

The collimator analysis included the effect of using a beam delimiter made of a neutron absorber (i.e., lithiated polyethylene) and varying the size of the beam aperture on in-phantom beam performance. It showed that, although the use of a Li-poly delimiter increases the current-to-flux ratio (J/Φ) because of removal of neutrons impinging on the target with large angles, it does not improve beam penetration; on the contrary, the advantage depth is somewhat decreased with concomitant great reduction of the advantage depth dose rate. Therefore, in designing the collimator, one has to optimize the trade-off between the advantage of reduction of the neutron dose outside the beam aperture and the disadvantage of significant reduction of beam intensity and slight degradation of beam penetration when using a beam delimiter.

Thesis Supervisor: Otto K. Harling
Title: Professor of Nuclear Engineering

Dedication

To my wife, Yoko, who has helped me tremendously to accomplish my research, always saying "You should keep in mind that you have the most dedicated, patient wife in the world"

To my son, Kensuke, who likes to play around me very much when I am studying

and

To my parents, who are always supporting us

Acknowledgment

First of all, I would like to acknowledge Professor Otto K. Harling, my thesis supervisor, for his excellent guidance. His very kind, thoughtful advice encouraged me very much. I would also like to acknowledge Professor Jacquelyn C. Yanch, who read my thesis carefully and gave me thoughtful comments.

I would like to express my thanks to W. S. Kiger, whose various supports were essential to the accomplishment of this research. I would also like to thank wonderful people of the BNCT group, K. Riley, B. Sutharshan, J. Goorley, C. Chuang, Dr. R. Zamenhof and Dr. G. Solares for their various kinds of help. I am also grateful to Dr. J. Bernard, E. Lau and T. Newton, Dr. G. Kohse, E. Redmond, T. Lee, K. O'Connell, C. Medeiros and H. Bonder.

I gratefully acknowledge the Science and Technology Agency, which provided me an opportunity to work with such wonderful people.

This research was supported by the US Department of Energy under Contract DE-FG02-87ER 60600.

Table of Contents

Abstract.....3
Dedication.....5
Acknowledgment.....6
Table of Contents.....7
List of Figures.....10
List of Tables.....18

CHAPTER ONE 27

Introduction

1.1 Background 27
1.2 Previous Work on the Fission Converter 30
1.3 Objective.....41
1.4 Methodology of the Analysis 43
1.4.1 Criticality Calculation to Create the Thermal Column Surface Source 47
1.4.2 Fixed-Source Calculation to Generate a Surface Source at the Patient Position 48
1.4.3 Dose-Depth Profile Calculation in a Head Phantom 49
1.5 References.....52

CHAPTER TWO 55

Sensitivity Study Of The Fission Converter Design: Fuel Configuration And Fuel Spacing

2.1 Introduction.....55
2.2 Fuel Configuration - Multi-Plate Reactor Type Fuel vs. Single Flat Plate Type Fuel.....59
2.2.1 Performance of Single Plate Fuel Fission Converters.....67
2.2.2 Comparison of MITR-II Fuel and Single Plate Fuel Fission Converters..70
2.3 Fuel Spacing in the MITR-II Fuel Fission Converter.....75
2.4 Comparison of In-Phantom Beam Performance for H_2O and D_2O Cooling.....82
2.5 Conclusion.....86
2.6 References.....88

CHAPTER THREE 89

Sensitivity Study Of The Neutron Filter Design-Effect Of Variation Of The Neutron Spectrum

3.1 Introduction....89
3.2 Analysis of the Fast Neutron Filter/Moderator....94
3.2.1 Effect of the Arrangement or Ordering of Filter/Moderator Materials....94
3.2.2 Sensitivity Analysis of the Fast Neutron Filter/Moderator Using Combinations of Aluminum and Fluorine, Oxygen Containing Materials or Carbon....102
3.3 In-Phantom Beam Performance....130
3.4 Analysis of the Thermal Neutron Filter....149
3.5 Conclusion....152
3.6 References....154

CHAPTER FOUR 157

Sensitivity Study Of The Collimator Design-Effect Of Beam Directionality And Beam Size

4.1 Introduction....157
4.2 Definition of the Current-to-Flux Ratio (J/Φ) in MCNP....160
4.3 In-Air Analysis of the Collimator Design....165
4.4 In-Phantom Analysis....175
4.5 Conclusion....192
4.6 References....194

CHAPTER FIVE 196

Neutronic Calculations Related To The Engineering Considerations On The Fission Converter Beam

5.1 Introduction....196
5.2 Results of the Analysis....196
5.2.1 Effect of Change of the Cross-Sectional Area of the Fast Neutron Filter/Moderator....197
5.2.2 Effect of the Core Gamma Ray....198
5.2.3 Reactivity Insertion Due to the Fission Converter....202
5.2.4 Tritium Production Rate in the D_2O-Cooled Fission Converter....205
5.2.5 Heat Deposition in the Fission Converter....207
5.2.6 Transverse and Vertical Power Profiles in Individual Fuel Plates....210
5.2.7 Effect of Impurities in the Fast Neutron Filter/Moderator and Collimator Materials....214
5.2.8 Shielding of Photons Outside the Beam Aperture....220
5.3 Conclusion....228
5.4 References....229

CHAPTER SIX 231

Summary And Recommendations For Future Analysis

6.1 Summary....231

6.2 Recommendations for Future Analysis 236

6.3 References....238

APPENDIX 239

Numerical Results Of The MCNP Calculations For Transverse And Vertical Power Profiles

List of Figures

CHAPTER ONE

Introduction

Figure 1.1 34
Isometric view of MITR-II showing major components and experimental facilities
Figure 1.2 35
The thermal column duct with the aluminum gas box during reactor renovation in 1974-75. The main coolant pipes curve over the top of the duct where they connect to the core tank. The duct is the future location of the fission converter (Courtesy of W. S. Kiger).
Figure 1.3 37
Isometric view of MIT fission converter beam and medical irradiation facility. Drawing is roughly to scale (Courtesy of W. S. Kiger).
Figure 1.4 39
Plan view of the fission converter beam design proposed by Reference 12 (Courtesy of W. S. Kiger).
Figure 1.5 45
Previous methodology for MCNP calculations (Courtesy of W.S. Kiger)
Figure 1.6 46
Modified methodology of MCNP calculations for the fission converter beam design.

CHAPTER TWO

Sensitivity Study Of The Fission Converter Design: Fuel Configuration And Fuel Spacing

Figure 2.1 57
Plan view of the fission converter design proposed as the 'final design' in Reference 1. The area enclosed by the dashed rectangle is enlarged in Figure 2.2. All dimensions in cm (courtesy of W. S. Kiger).
Figure 2.2 58
Close-up view of the fission converter design proposed as the 'final design' in Reference 1. All dimensions in cm (Courtesy of W. S. Kiger).
Figure 2.3 62
Cross-sectional view of a fission converter design using a single flat plate fuel. The fuel meat of the single plate fuel has a thickness 5.3 cm for 20% EU and 1.1 cm for 93% EU. The coolant thickness on both sides of the fuel is varied from 0.16 cm to 1.0 cm.
Figure 2.4 65
Epithermal neutron flux as a function of coolant thickness, coolant type and fuel enrichment for single plate fission converters. These calculations used a neutron filter/moderator composed of 68 cm 70% AlF_3/30% Al + 2 cm Ti followed by a 0.04 cm Cd thermal neutron filter, an 8 cm thick Bi photon shield and a pyramidal collimator with a 15 cm thick lead lining. The filter/moderator is surrounded by a 10 cm thick lead reflector.

Figure 2.5 66
Specific fast neutron dose as a function of coolant thickness, coolant type and fuel enrichment for single plate fission converters. These calculations used a neutron filter/moderator composed of 68 cm 70% AlF_3/30% Al + 2 cm Ti followed by a 0.04 cm Cd thermal neutron filter, an 8 cm thick Bi photon shield and a pyramidal collimator with a 15 cm thick lead lining. The filter/moderator is surrounded by a 10 cm thick lead reflector.
Figure 2.6 73
Epithermal neutron flux vs. specific fast neutron dose at the patient position for different fuel configurations and coolants. Data labels denote coolant types and, for single plate fuel, coolant thicknesses on both sides of the plate are in parentheses. Statistical uncertainties are less than the size of the data points.
Figure 2.7 74
Partial neutron current spectra in the direction of the patient position at the interface between the coolant and the inner tank for fission converters using H_2O-cooled 20% enriched single plate fuel with 0.16 cm thick coolant layers, or eleven H_2O- or D_2O-cooled burned MITR-II fuel elements.
Figure 2.8 80
Power generation in the D_2O-cooled fission converters composed of eleven burned MITR-II fuel elements with varying fuel spacing. These calculations used a neutron filter/moderator composed of 68 cm 70% AlF_3/30% Al + 2 cm Ti followed by a 0.04 cm Cd thermal neutron filter, an 8 cm thick Bi photon shield and a pyramidal collimator with a 15 cm thick lead lining. The filter/moderator is surrounded by a 10 cm thick lead reflector.
Figure 2.9 81
Partial neutron current spectra in the direction of the patient position at the interface between the coolant and the rear inner tank wall for fission converters using eleven D_2O-cooled burned MITR-II fuel elements with varying fuel spacing.
Figure 2.10 84
Normalized neutron flux spectra at the patient position for H_2O and D_2O cooling in linear scale. These calculations used a fission converter composed of eleven burned MITR-II fuel elements (312 g ^{235}U per element) followed by a fast neutron filter/moderator of 68 cm 70% AlF_3/30% Al - 2 cm Ti, a 0.04 cm Cd thermal neutron filter, an 8 cm Bi photon shield and a pyramidal collimator with a 15 cm thick lead lining. The filter/moderator is surrounded by a 10 cm thick lead reflector. The reactor power was set at 5 MW.
Figure 2.11 85
Normalized neutron flux spectra at the patient position for H_2O and D_2O cooling in log scale. These calculations used a fission converter composed of eleven burned MITR-II fuel elements (312 g ^{235}U per element) followed by a fast neutron filter/moderator of 68 cm 70% AlF_3/30% Al - 2 cm Ti, a 0.04 cm Cd thermal neutron filter, an 8 cm Bi photon shield and a pyramidal collimator with a 15 cm thick lead lining. The filter/moderator is surrounded by a 10 cm thick lead reflector. The reactor power was set at 5 MW.

CHAPTER THREE

Sensitivity Study Of The Neutron Filter Design- Effect Of Variation Of The Neutron Spectrum

Figure 3.1 93
Schematic view of the fission converter beam design used in the sensitivity analysis of the neutron filter design, where the components to be varied are shown.

Figure 3.2 98
Partial neutron current spectra in the direction of the patient position at the interface between the fast neutron filter/moderator and the Cd thermal neutron filter. The fast neutron filter/moderator is composed of 71 cm thick Al and 27 cm thick AlF_3 (2115 kg Al and 858 kg AlF_3) with varying arrangements or ordering .
Figure 3.3 99
Partial neutron current spectra in the direction of the patient position at the interface between the fast neutron filter/moderator and the Cd thermal neutron filter. The fast neutron filter/moderator is composed of 83 cm thick Al and 19 cm thick AlF_3 (2473 kg Al and 831 kg AlF_3) with varying arrangements or ordering.
Figure 3.4 101
Partial neutron current spectra at the interface between the converter coolant (D_2O) and the rear inner tank wall in the upstream (i.e., backward) direction for the fast neutron filter/moderators composed of 83 cm Al + 19 cm Al_2O_3 with varying arrangements.
Figure 3.5 113
Epithermal neutron flux vs. specific fast neutron dose for various fast neutron filter/moderator designs composed of an Al block followed by an Al_2O_3 block. The label of each data point denotes the configuration of the filter/moderator design.
Figure 3.6 114
Epithermal neutron flux vs. specific fast neutron dose for various fast neutron filter/moderator designs composed of an Al block followed by an AlF_3 block. The label of each data point denotes the configuration of the filter/moderator.
Figure 3.7 115
Epithermal neutron flux vs. specific fast neutron dose for various fast neutron filter/moderator designs composed of an Al block followed by a Teflon $[(CF_2)_n]$ block. The label of each data point denotes the configuration of the filter/moderator
Figure 3.8 116
Comparison of the neutron flux spectra at the patient position generated by the fission converter beams with D_2O-cooled burned MITR-II fuel and the fast neutron filter/moderator designs using 71 cm Al - 22 cm AlF_3 (skm454) and 41 cm Al - 32 cm AlF_3 (skm457) shown in a linear scale. The reactor power was set at 5 MW.
Figure 3.9 117
Comparison of the neutron flux spectra at the patient position generated by the fission converter beams with D_2O-cooled burned MITR-II fuel and the fast neutron filter/moderator designs using 71 cm Al - 22 cm AlF_3 (skm454) and 41 cm Al - 32 cm AlF_3 (skm457) shown in a log scale. The reactor power was set at 5 MW.
Figure 3.10 118
Comparison of the neutron flux spectra at the patient position generated by the fission converter beams with D_2O-cooled burned MITR-II fuel and the fast neutron filter/moderator designs using 83 cm Al - 17 cm Al_2O_3 (skm451) and 58 cm Al - 24 cm Al_2O_3 (skm463) shown in a linear scale. The reactor power was set at 5 MW.
Figure 3.11 119
Comparison of the neutron flux spectra at the patient position generated by the fission converter beams with D_2O-cooled burned MITR-II fuel and the fast neutron filter/moderator designs using 83 cm Al - 17 cm Al_2O_3 (skm451) and 58 cm Al - 24 cm Al_2O_3 (skm463) shown in a log scale. The reactor power was set at 5 MW.

Figure 3.12 127
Epithermal neutron flux vs. specific fast neutron dose for various fast neutron filter/moderator designs using the combination of Al-Al_2O_3, Al-AlF_3, Al-$(CF_2)_n$ and Al-C. The label of each data point denotes the configuration of the filter/moderator design.
Figure 3.13 138
Dose-depth profile for unilateral irradiation produced by the fission converter beam with D_2O-cooled burned MITR-II fuel and the fast neutron filter/moderator design composed of 71 cm Al - 27 cm AlF_3 (skm308). The filter/moderator is followed by a 0.04 cm Cd thermal neutron filter, an 8 cm Bi photon shield and a pyramidal collimator with a 15 cm thick lead lining, and is surrounded by a 10 cm thick lead reflector. The beam aperture size is 20 cm*20 cm. The MITR reactor power was set at 5 MW. Boron uptake was assumed at 40 ppm ^{10}B in tumor with a tumor-to-normal uptake ratio of 3.5:1.
Figure 3.14 139
Comparison of dose-depth profiles for bilateral irradiations calculated for the fission converter beam with D_2O-cooled burned MITR-II fuel and measured for the MIT M67 beam at the reactor power of 5 MW. The doses are normalized so that the maximum normal tissue dose is equal to 1000 cGy. The fast neutron filter/moderator of the fission converter beam is composed of 71cm Al - 27cm AlF_3 (skm308). The filter/moderator is followed by a 0.04 cm Cd thermal neutron filter, an 8 cm Bi photon shield and a pyramidal collimator with a 15 cm thick lead lining, and is surrounded by a 10 cm thick lead reflector. The beam aperture size is 20 cm*20 cm. Boron uptake was assumed at 40 ppm ^{10}B in tumor with a tumor-to-normal uptake ratio of 3.5:1. The RBE's are 3.2 for neutrons, 1.0 for photons, 3.8 for boron in tumor, 1.35 for boron in normal tissue.
Figure 3.15 140
Profiles of epithermal and thermal neutron fluxes as a function of depth in the head phantom produced by the fission converter beam with D_2O-cooled burned MITR-II fuel and the fast neutron filter/moderator composed of 71 cm Al - 27 cm ALF_3 (skm308). The filter/moderator is followed by a 0.04 cm Cd thermal neutron filter, an 8 cm Bi photon shield and a pyramidal collimator with 15 cm thick lead lining, and is surrounded by a 10 cm thick lead reflector. The beam aperture size is 20 cm* 20 cm. The MITR reactor power was set at 5 MW.
Figure 3.16 141
Comparison of the neutron flux spectra at the patient position generated by the fission converter beams with D_2O-cooled burned MITR-II fuel and the fast neutron filter/moderator designs using 83 cm Al - 17 cm Al_2O_3 (skm451), 71 cm Al - 27 cm AlF_3 (skm308), 80 cm Al - 17 cm $(CF_2)_n$ (skm434) and 96 cm Al - 12 cm C (skm471) shown in a linear scale. The reactor power was set at 5 MW.
Figure 3.17 142
Comparison of the neutron flux spectra at the patient position generated by the fission converter beams with D_2O-cooled burned MITR-II fuel and the fast neutron filter/moderator designs using 83 cm Al - 17 cm Al_2O_3 (skm451), 71 cm Al - 27 cm AlF_3 (skm308), 80 cm Al - 17 cm $(CF_2)_n$ (skm434) and 96 cm Al - 12 cm C (skm471) in a log scale. The reactor power was set at 5 MW.
Figure 3.18 143
Comparison of the neutron flux spectra at the patient position generated by the fission converter beams with D_2O-cooled burned MITR-II fuel and the fast neutron filter/moderator designs using 71 cm Al - 27 cm AlF_3 (skm308), 68 cm AlF_3(70%)/Al(30%) - 2 cm Ti (std473), and 66 cm FLUENTAL $^{w}/_{o}$ LiF (skm439) in a linear scale. The reactor power was set at 5 MW.

Figure 3.19 144
Comparison of the neutron flux spectra at the patient position generated by the fission converter beams with D_2O-cooled burned MITR-II fuel and the fast neutron filter/moderator designs using 71 cm Al - 27 cm AlF_3 (skm308), 68 cm AlF_3(70%)/Al(30%) - 2 cm Ti (std473), and 66 cm FLUENTAL $^{W}/_{O}$ LiF (skm439) in a log scale. The reactor power was set at 5 MW.
Figure 3.20 145
Comparison of dose-depth profiles for unilateral irradiation produced by the fission converter beams with D_2O-cooled burned MITR-II fuel and the fast neutron filter/moderator designs using 71 cm Al - 27 cm AlF_3 (skm308), 68 cm 70% AlF_3/30% Al - 2 cm Ti (std473) and 66 cm FLUENTAL $^{W}/_{O}$ LiF (skm460). Boron uptake was assumed at 40 ppm ^{10}B in tumor with a tumor-to-normal uptake ratio of 3.5:1. The RBE's are 3.2 for neutrons, 1.0 for photons, 3.8 for boron in tumor, 1.35 for boron in normal tissue. The reactor power was set at 5 MW.
Figure 3.21 146
Comparison of the neutron flux spectra at the patient position generated by the fission converter beams with D_2O-cooled burned MITR-II fuel and the fast neutron filter/moderator designs using 71 cm Al - 27 cm AlF_3 (skm308), 71 cm Al - 22 cm AlF_3 (skm454), and 71 cm Al - 17 cm AlF_3 (skm460) in a linear scale. The reactor power was set at 5 MW.
Figure 3.22 147
Comparison of the neutron flux spectra at the patient position generated by the fission converter beams with D_2O-cooled burned MITR-II fuel and the fast neutron filter/moderator designs using 71 cm Al - 27 cm AlF_3 (skm308), 71 cm Al - 22 cm AlF_3 (skm454), and 71 cm Al - 17 cm AlF_3 (skm460) in a log scale. The reactor power was set at 5 MW.
Figure 3.23 148
Comparison of dose-depth profiles for unilateral irradiations using the fission converter beams with D_2O-cooled burned MITR-II fuel and the fast neutron filter/moderator designs composed of 71 cm Al - 27 cm AlF_3 (skm308), 71 cm Al - 22 cm AlF_3 (skm454) and 71 cm Al - 17 cm AlF_3 (skm460). Boron uptake was assumed at 40 ppm ^{10}B in tumor with a tumor-to-normal uptake ratio of 3.5:1. The RBE's are 3.2 for neutrons, 1.0 for photons, 3.8 for boron in tumor, 1.35 for boron in normal tissue. The reactor power was set at 5 MW.

CHAPTER FOUR

Sensitivity Study Of The Collimator Design - Effect Of Beam Directionality And Beam Size

Figure 4.1 163
Schematic view of a tally surface (area A) thorough which the i-th particle is passing with the weight w_i and polar angle θ_i (between the tally surface normal and trajectory of the particle).
Figure 4.2 163
The probability density function for μ, which is uniformly distributed from 1 (= $cos\ 0\ ^{o}$) to $cos\ \theta_{max}$.
Figure 4.3 169
Cross-sectional view of the funnel-shaped collimator design. This type of collimator consists of a four-sided sloped portion lined with 15cm thick lead and a 20 cm long straight portion with the square cross section surrounded by a Li-poly delimiter, which covers the whole beam cross-section except for the beam aperture.

Figure 4.4 170
Cross-sectional view of the truncated pyramid-shaped collimator design. This design has a 15 cm thick lead lining, where the last *t* cm (t =0, 10, 20 and 30) long part of the lining in front of the patient position was replaced with Li-poly.
Figure 4.5 172
Epithermal neutron flux vs. current-to-flux ratio for different collimator designs shown in Table 4.2. The label of each data point denotes Run-ID of each collimator design.
Figure 4.6 173
Normalized neutron current angular distribution at the patient position for different collimator designs described as a function of μ (the cosine of the angle between the particle trajectory and the beam axis). The angular distribution is normalized to one at the maximum tally bin. The funnel-shaped collimator (skm311) has a four-sided sloped potion lined with 15 cm thick lead and a 20 cm long straight portion with the square cross section surrounded by a Li-poly delimiter. The pyramidal collimators of std473 and skm304 are lined with 15 cm thick lead, where the last *t* cm (t = 0 and 10) long part of the lining in front of the patient position are replaced with Li-poly. All of these designs have a 20 cm* 20 cm beam aperture.
Figure 4.7 174
Vertical profiles of neutron flux of all energies centered on the beam axis at the patient position for Designs std473, skm304 and skm311. Design skm311 has a funnel-shaped collimator composed of a four-sided sloped portion with 15 cm thick lead lining and a 20 cm long straight portion with the square cross section surrounded by a Li-poly delimiter. Design std473 and skm304 have pyramidal collimators lined with 15 cm thick lead, where the last t cm (t = 0 and 10) long parts of the lining in front of the patient position are replaced with Li-poly. All of these designs have a 20 cm*20 cm beam aperture.
Figure 4.8 183
Two dimensional dose distributions produced by Designs std473 (solid curve) and skm311 (dashed curve) using the data of actual human head. Each curve denotes the iso-dose contour which represents the locations where the same ratio of tumor dose to the maximum normal tissue dose is achieved. The number besides the color bar denotes the ratio in percent for each color. Design std473 uses a pyramidal collimator with a 15 cm thick lead lining and no Li-poly. Design skm311 has a funnel-shaped collimator with a four-sided sloped portion lined with 15 cm thick lead and a 20 cm long straight portion with the square cross section surrounded by a Li-poly delimiter. Both collimator designs have a 20 cm*20 cm beam aperture.
Figure 4.9 185
Normalized neutron current angular distribution at the patient position for the pyramidal collimator designs with different beam aperture sizes. The angular distribution is described as a function of μ (the cosine of the angle between the particle trajectory and the beam axis). The angular distribution is normalized to one at the maximum tally bin. Both designs use pyramidal collimators lined with 15 cm thick lead and no Li-poly delimiter and have different beam aperture sizes (20 cm*20 cm for std473 and 10 cm*10 cm for skm468).
Figure 4.10 186
Vertical profiles of neutron flux of all energies centered on the beam axis at the patient position for Designs skm468 and std473. Both designs use pyramidal collimators lined with 15 cm thick lead and no Li-poly delimiter and have different beam aperture sizes (20 cm*20 cm for std473 and 10 cm*10 cm for skm468).

Figure 4.11 187
Normalized neutron current angular distribution at the patient position for the different collimator configurations. The angular distribution, which is described as a function of μ (the cosine of the angle between the particle trajectory and the beam axis), is normalized to one at the maximum tally bin. Design skm468 uses a pyramidal collimator lined with 15 cm thick lead and delimiter. Design skm464 has a funnel-shaped collimator composed of a four-sided sloped portion lined with 15 cm thick lead lining and a 20 cm long straight portion with the square cross section surrounded by a Li-poly delimiter. Both designs have the beam aperture with a size of 10 cm*10 cm.
Figure 4.12 188
Vertical profiles of neutron flux of all energies centered on the beam axis at the patient position for Designs skm468 and skm464. Design 468 uses a pyramidal collimator lined with 15 cm thick lead and no Li-poly. Design 464 has a funnel-shaped collimator composed of a four-sided sloped portion lined with 15 cm thick lead and a 20 cm long straight portion with the square cross section surrounded by a Li-poly delimiter. Both designs have the beam aperture with a size of 10 cm*10 cm..
Figure 4.13 189
Profiles of the epithermal and thermal neutron fluxes as a function of depth in the head phantom produced by Designs std473, skm311 and skm464. Design std473 has a pyramidal collimator lined with 15 cm thick lead and no Li-poly delimiter and a 20 cm*20 cm beam aperture. Designs skm311 and skm464 use funnel-shaped collimators with a four-sided sloped portion with 15 cm thick lead lining and a 20 cm long straight portion with the square cross section surrounded by a Li-poly delimiter and different beam aperture sizes (20 cm*20 cm for skm311 and 10 cm*10 cm for skm464). The reactor power was set at 5 MW.
Figure 4.14 190
Thermal neutron profiles as a function of depth in the head phantom produced by Designs std473, skm311 and skm464. The profiles are normalized to one at the peaks. Design std473 has a pyramidal collimator lined with 15 cm thick lead and no Li-poly delimiter and a 20 cm*20 cm beam aperture . Designs skm311 and skm464 use funnel-shaped collimators with a four-sided sloped portion with 15 cm thick lead lining and a 20 cm long straight portion with the square cross section surrounded by a Li-poly delimiter and different beam aperture sizes (20 cm*20 cm for skm311 and 10 cm*10 cm for skm464).
Figure 4.15 191
Comparison of dose-depth profiles for unilateral irradiation produced by Designs std473, skm311 and skm464. Design std473 has a pyramidal collimator lined with 15 cm thick lead and no Li-poly delimiter and a 20 cm*20 cm beam aperture. Designs skm311 and skm464 use funnel-shaped collimators with a four-sided sloped portion with a 15 cm thick lead lining followed by a 20 cm long straight portion with the square cross section surrounded by a Li-poly delimiter and with different beam aperture sizes (20 cm*20 cm for skm311 and 10 cm*10 cm for skm464). The reactor power was set at 5 MW. Boron uptake was assumed at 40 ppm ^{10}B in tumor with a tumor-to-normal uptake ratio of 3.5:1. The RBE's are 3.2 for neutrons, 1.0 for photons, 3.8 for boron in normal tissue. The reactor power was set at 5 MW.

CHAPTER FIVE

Neutronic Calculations Related To The Engineering Considerations On The Fission Converter Beam

Figure 5.1 212
Transverse power profile in a fission converter with eleven fresh MITR-II fuel elements and H_2O or D_2O cooling.
Figure 5.2 213
Vertical power profile for Plate 1 of Element 7, which is the hottest fuel plate, in an H_2O-cooled fission converter using fresh MITR-II fuel. The ordinate shows the height of the centers of the segments.
Figure 5.3 224
Vertical photon dose rate profiles centered on the beam axis at the patient position for the beam designs using heavy concrete. The profile labeled 'Heavy Concrete Voided' is for the beam design with heavy concrete cells voided. The profiles due to photons from particular elements (Fe, Ti, and ^{10}B) are also presented.
Figure 5.4 225
Comparison of vertical photon dose rate profiles for the beam designs using heavy and regular concrete.
Figure 5.5 226
The cross-sectional view of the beam design using regular concrete followed by a 6 cm thick lead photon shield.
Figure 5.6 227
Vertical profiles of photon dose rate centered on the beam axis at the patient position for Design std473, skm304 and skm311.

CHAPTER SIX

Summary And Recommendations For Future Analysis

Figure 6.1 235
Cross-sectional view of a beam design with a removable variable-size beam delimiter at the end of the collimator and neutron and photon shields on the downstream side of the concrete.

APPENDIX

Numerical Results Of The MCNP Calculations For Transverse And Vertical Power Profiles

List of Tables

CHAPTER ONE

Introduction

Table 1.1 29
A comparison of in-air beam performance and materials used for neutron filtration/moderation and photon shielding for MITR-II, BMRR and HFR
Table 1.2 31
Comparison of in-air beam performance and materials used for neutron filtration/moderation and photon shielding of the fission converter-based epithermal neutron beam designed at MITR and BMRR. The number below each figure of merit denotes one standard deviation of each quantity.

CHAPTER TWO

Sensitivity Study Of The Fission Converter Design: Fuel Configuration And Fuel Spacing

Table 2.1 63
Converter power and in-air beam performance for single flat plate type fuel with varying coolant type, enrichment and coolant thickness. In-air figures of merit were calculated at the patient position for a reactor power of 5 MW. The statistical error (one standard deviation) of each quantity is shown immediately below the value. These calculations used a neutron filter/moderator composed of 68 cm 70% AlF_3/30% Al + 2 cm Ti followed by a 0.04 cm Cd thermal neutron filter, an 8 cm thick Bi photon shield and a pyramidal collimator with a 15 cm thick lead lining. The filter/moderator is surrounded by a 10 cm thick lead reflector.
Table 2.2 68
Fission converter power and in-air beam performance for D_2O-cooled single plate fuel fission converters using 20% or 93% enriched fuel with and without aluminum in the fuel meat. The thickness of coolant layers on both sides of the fuel plate is 0.5 cm. These calculations used a filter/moderator composed of 68 cm 70% AlF_3/30% Al + 2 cm Ti followed by an 8 cm thick Bi photon shield and a pyramidal collimator with a 15 cm thick lead lining. The filter/moderator is surrounded by a 10 cm thick lead reflector.
Table 2.3 72
Fission converter power and in-air beam performance for different fuel types and coolants with varying fuel loading, enrichment and coolant thickness. In-air figures of merit were calculated at the patient position for a reactor power of 5MW. The number shown below the coolant type for a single plate fission converter denotes the coolant thickness on both sides of the fuel plate. These calculations used a filter/moderator composed of 68 cm 70% AlF_3/30% Al + 2 cm Ti followed by an 8 cm thick Bi photon shield and a pyramidal collimator with a 15 cm thick lead lining. The filter/moderator is surrounded by a 10 cm thick lead reflector.

Table 2.4 78
Fission converter power and in-air beam performance for burned MITR-II fuel fission converter (312g ^{235}U per element) with H_2O or D_2O cooling and varying spacing between fuel elements. In-air figures of merit were calculated at the patient position for a reactor power of 5 MW. The statistical error (one standard deviation) of each quantity is shown immediately below the value. These calculations used a neutron filter/moderator composed of 68 cm 70% AlF_3/30% Al + 2cm Ti followed by a 0.04 cm Cd thermal neutron filter, an 8 cm thick Bi photon shield and a pyramidal collimator with a 15 cm thick lead lining. The filter/moderator is surrounded by a 10 cm thick lead reflector.
Table 2.5 83
Comparison of in-air and in-phantom figures of merit for H_2O- and D_2O-cooled fission converters. These calculations used a fission converter composed of eleven burned MITR-II fuel elements (312 g ^{235}U per element) followed by a fast neutron filter/moderator of 68 cm 70% AlF_3/30% Al - 2cm Ti, a 0.04 cm Cd thermal neutron filter, an 8 cm Bi photon shield and a pyramidal collimator with 15 cm thick lead lining. The filter/moderator is surrounded by a 10 cm thick leaf. The reactor power was set at 5 MW.

CHAPTER THREE

Sensitivity Study Of The Neutron Filter Design- Effect Of Variation Of The Neutron Spectrum

Table 3.1 96
In-air beam performance for the fast neutron filter/moderator composed of 71 cm thick Al and 27 cm thick AlF_3 (2115 kg Al and 858 kg AlF_3) with varying arrangement. For the mixture of these materials, 100% theoretical density is assumed. The material listed on the left hand side is adjacent to the fission converter. These calculations used a fission converter composed of eleven burned MITR-II fuel elements (312g ^{235}U per element) with D_2O cooling. The fast neutron filter/moderator is followed by a 0.04 cm Cd thermal neutron filter, an 8 cm Bi photon shield and a pyramidal collimator with a 15 cm thick lead lining, and is surrounded by a 10 cm thick lead reflector. The reactor power was set at 5 MW.
Table 3.2 97
In-air beam performance for the fast neutron filter/moderator composed of 83 cm thick Al and 19 cm thick Al_2O_3 (2473 kg Al and 831 kg Al_2O_3) with varying arrangement. For the mixture of these materials, 100% theoretical density is assumed. The material listed on the left hand side is adjacent to the fission converter. These calculations used a fission converter composed of eleven burned MITR-II fuel elements (312g ^{235}U per element) with D_2O cooling. The fast neutron filter/moderator is followed by a 0.04 cm Cd thermal neutron filter, an 8 cm Bi photon shield and a pyramidal collimator with a 15 cm thick lead lining, and is surrounded by a 10 cm thick lead reflector. The reactor power was set at 5 MW.
Table 3.3 100
Macroscopic total cross sections of AlF_3 and Al_2O_3 averaged with the spectrum of the fission converter beam. Microscopic total cross sections from Reference 5 were used. Thermal cross sections are for 0.025 eV and epithermal and fast cross sections are averaged over the ranges of 1 eV to 10 keV and 10 keV to 5 MeV, respectively.

Table 3.4 109
In-air beam performance for the fast neutron filter/moderator composed of an Al block followed by an Al_2O_3 block while varying their thicknesses. These calculations used a fission converter composed of eleven burned MITR-II fuel elements (312g ^{235}U per element) with D_2O cooling. The fast neutron filter/moderator is followed by a 0.04 cm Cd thermal neutron filter, an 8 cm Bi photon shield and a pyramidal collimator with a 15 cm thick lead lining, and is surrounded by a 10 cm thick lead reflector. The materials listed on the left hand side of column 2 are closest to the fission converter. The reactor power was set at 5 MW. D_{epi} and D_{fast} denote epithermal and fast components of the fast neutron dose rate (D_{fn}).
Table 3.5 111
In-air beam performance for the fast neutron filter/moderator composed of an Al block followed by an AlF_3 block while varying their thicknesses. These calculations used a fission converter composed of eleven burned MITR-II fuel elements (312g ^{235}U per element) with D_2O cooling. The fast neutron filter/moderator is followed by a 0.04 cm Cd thermal neutron filter, an 8 cm Bi photon shield and a pyramidal collimator with 15 cm thick lead lining, and is surrounded by a 10 cm thick lead reflector. Column 2 lists the filter/moderator materials starting at the fission converter. The reactor power was set at 5 MW. D_{epi} and D_{fast} denote epithermal and fast components of the fast neutron dose rate (D_{fn}).
Table 3.6 112
In-air beam performance for the fast neutron filter/moderator composed of an Al block followed by an Teflon [$(CF_2)_n$] block while varying their thicknesses. These calculations used a fission converter composed of eleven burned MITR-II fuel elements (312g ^{235}U per element) with D_2O cooling. The fast neutron filter/moderator is followed by a 0.04 cm Cd thermal neutron filter, an 8 cm Bi photon shield and a pyramidal collimator with a 15 cm thick lead lining, and is surrounded by a 10 cm thick lead reflector. The reactor power was set at 5 MW. D_{epi} and D_{fast} denote epithermal and fast components of the fast neutron dose rate (D_{fn}).
Table 3.7 122
In-air beam performance for the filter/moderator designs composed of Al1100-$(CF_2)_n$-[Al+2% Li(natural)]-$(CF_2)_n$-Al1100 (INEL Design) where carbon in Teflon [$(CF_2)_n$] was kept or removed. These calculations used a fission converter composed of eleven burned MITR-II fuel elements (312g ^{235}U per element) with D_2O cooling. The fast neutron filter/moderator is followed by a 0.04 cm Cd thermal neutron filter, a Pb photon shield with different thicknesses and a pyramidal collimator with a 15 cm thick lead lining, and is surrounded by a 10 cm thick lead reflector. The reactor power was set at 5 MW.
Table 3.8 122
In-air beam performance for the filter/moderator composed of an Al block followed by an graphite block with varying their thicknesses. These calculations used a fission converter composed of eleven burned MITR-II fuel elements (312g ^{235}U per element) with D_2O cooling. The fast neutron filter/moderator is followed by a 0.04 cm Cd thermal neutron filter, an 8 cm Bi photon shield and a pyramidal collimator with a 15 cm thick lead lining, and is surrounded by a 10 cm thick lead reflector. The reactor power was set at 5 MW.

Table 3.9 125
Summary of in-air beam performance for the fast neutron filter/moderator designs using the combinations of Al-Al_2O_3, Al-AlF_3, Al-$(CF_2)_n$ and Al-C. These calculations used a fission converter composed of eleven burned MITR-II fuel elements (312g ^{235}U per element) with D_2O cooling. The fast neutron filter/moderator is followed by a 0.04 cm Cd thermal neutron filter, an 8 cm Bi photon shield and a pyramidal collimator with a 15 cm thick lead lining, and is surrounded by a 10 cm thick lead reflector. The MITR reactor power was assumed to be 5 MW. D_{epi} and D_{fast} denote epithermal and fast components of the fast neutron dose rate (D_{fn}).
Table 3.10 129
Comparison of in-air beam performance of the beam designs with and without a PbF_2 photon shield. These calculations used a fission converter composed of eleven burned MITR-II fuel elements (312g ^{235}U per element) with D_2O cooling. The fast neutron filter/moderator is followed by a 0.04 cm Cd thermal neutron filter, a PbF_2 or Bi photon shield and a rectangular collimator with 15 cm thick lead lining, and is surrounded by a 10 cm thick lead reflector. The reactor power was set at 5 MW.
Table 3.11 137
In-phantom beam performance for different fast neutron filter/moderator designs. Boron uptake was assumed at 40 ppm ^{10}B in tumor with a tumor-to-normal uptake ratio of 3.5:1. The RBE's are 3.2 for neutrons, 1.0 for photons, 3.8 for boron in tumor, 1.35 for boron in normal tissue. These calculations used a D_2O cooled fission converter composed of eleven burned MITR-II fuel elements (fuel loading is 312 g-^{235}U per element) at the MITR reactor power of 5 MW. The fast neutron filter/moderator is surrounded by a 10 cm thick lead reflector. It is followed by a 0.04 cm Cd thermal neutron filter, an 8 cm Bi photon shield and a pyramidal collimator with a 15 cm thick lead lining and beam aperture size of 20 cm*20 cm.
Table 3.12 151
In-air beam performance for beam designs using different thermal neutron filters, ^6Li or Cd. These calculations used LiF which was uniformly distributed in FLUENTAL or a 0.04 cm Cd sheet which was located downstream of the fast neutron filter/moderator and in front of the photon shield. The materials used for the fast neutron filter/moderator are FLUENTAL and Titanium. The fission converter consists of eleven burned MITR-II fuel elements (312g ^{235}U per element) with D_2O cooling. The neutron filters are followed by an 8 cm Bi photon shield and a pyramidal collimator with 15 cm thick lead lining, and is surrounded by a 10 cm thick lead reflector. The reactor power was assumed to be 5 MW.
Table 3.13 151
In-air beam performance for beam designs using different configurations of the Cd thermal neutron filter. Design skm436 used two 0.02 cm thick Cd sheets; one was located in the middle of the fast neutron filter/moderator composed of 71 cm Al - 27 cm AlF_3 and the other was placed at the original location (i.e., downstream of the filter/moderator and in front of the photon shield). Design skm308 had one 0.04 cm thick Cd sheet behind the filter/moderator. The fission converter consists of eleven burned MITR-II fuel elements (312g ^{235}U per element) with D_2O cooling. The neutron filters are followed by an 8 cm Bi photon shield and a pyramidal collimator with a 15 cm thick lead lining, and is surrounded by a 10 cm thick lead reflector. The reactor power was assumed to be 5 MW.

CHAPTER FOUR

Sensitivity Study Of The Collimator Design - Effect Of Beam Directionality And Beam Size

Table 4.1 164

J/Φ with varying θ_{max} calculated by the analytical solution. It was confirmed that these results agree completely with those from the MCNP calculation using the geometry and the angular distribution illustrated in Figures 4.1 and Figure 4.2.

Table 4.2 171

In-air beam performance for different collimator designs. The funnel-shaped collimator consists of a four-sided sloped portion lined with a 15 cm thick lead lining and a 20 cm long straight portion with the square cross section surrounded by a Li-poly delimiter which covers the whole beam cross-section except for the beam aperture. The pyramidal collimator is lined with 15 cm thick lead, where the last *t* cm (t = 10, 20 and 30) long part of the lining in front of the patient position was replaced with Li-poly. These calculations used a fission converter composed of eleven burned MITR-II fuel elements (312g ^{235}U per element) with D_2O cooling, which is followed by a fast neutron filter/moderator composed of 68 cm 70% AlF_3/30% Al - 2 cm Ti, a 0.04 cm Cd thermal neutron filter and an 8 cm Bi photon shield. The filter/moderator is surrounded by a 10 cm thick lead reflector.

Table 4.3 181

Comparison of in-phantom figures of merit produced by different collimator designs. The funnel-shaped collimator consists of a four-sided sloped portion with 15 cm thick lead lining and a 20 cm long straight portion with the square cross section surrounded by a Li-poly delimiter, which covers the whole beam cross-section except for the beam aperture. The pyramidal collimator is lined with 15cm thick lead, where the last *t* cm (t = 0 for std473, skm468 and 10 for skm304) long part of the lining in front of the patient position was replaced with Li-poly. These calculations used a fission converter composed of eleven burned MITR-II fuel elements (312g ^{235}U per element) with D_2O cooling, which is followed by a fast neutron filter/moderator composed of 68 cm 70% AlF_3/30% Al - 2 cm Ti, a 0.04 cm Cd thermal neutron filter and an 8 cm Bi photon shield. The filter/moderator is surrounded by a 10 cm thick lead reflector.

CHAPTER FIVE

Neutronic Calculations Related To The Engineering Considerations On The Fission Converter Beam

Table 5.1 198

Comparison of in-air beam performance of the beam designs using fast neutron filter/moderators with different cross-sectional areas. These calculations used a fission converter composed of eleven burned MITR-II fuel elements (312 g ^{235}U per element) with D_2O cooling, which is followed by a fast neutron filter/moderator composed of 68 cm 70% AlF_3/30% Al - 2 cm Ti, a 0.04 cm Cd thermal neutron filter, an 8 cm Bi photon shield and a pyramidal collimator with a 15 cm thick lead lining. The filter/moderator is surrounded by a 10 cm thick lead reflector. The reactor power was set at 5 MW. The statistical error (one standard deviation) of each result is listed below the value.

Table 5.2 200

Linear attenuation coefficients for 2 MeV photons and thicknesses of the materials which intervene between the core and the patient position. The mass attenuation coefficient data were obtained from Reference 3.

Table 5.3 201
Photon dose rate at the patient position due to photons generated in the MITR-II reactor region (core gamma rays). The MCNP calculations used a fission converter composed of eleven burned MITR-II fuel elements (312 g ^{235}U per element) with D_2O cooling, which is followed by a fast neutron filter/moderator composed of 68 cm 70% AlF_3/30% Al - 2 cm Ti, a 0.04 cm Cd thermal neutron filter, an 8 cm Bi photon shield and a pyramidal collimator with a 15 cm thick lead lining. The filter/moderator is surrounded by a 10 cm thick lead reflector. The statistical error (one standard deviation) of each MCNP calculation is listed below the value. The reactor power was assumed to be 5MW. The fission converter power obtained in the calculation is 78 kW.
Table 5.4 204
The multiplication factors and fission converter powers calculated using the coupled core-fission converter model. The fission converter power for each case is compared with that from the fixed-source run using the same fission converter model. The Cd shutter was incorporated in the model. The error denotes one standard deviation of each value. The reactor power was assumed to be 5 MW.
Table 5.5 205
MCNP calculations of tritium production rate in a fission converter when the Cd shutter is open or closed. These calculations used a fission converter with D_2O-cooled eleven burned MITR-II fuel elements (312 g U-235 per element). The statistical error (one standard deviation) is listed immediately below each value. The reactor power was assumed to be 5 MW.
Table 5.6 209
Energy deposition in the fuel elements of the fission converter. The calculation used a coupled core-fission converter model where the fission converter consists of eleven fresh MITR-II fuel elements (510 g U-235 per element) cooled with H_2O. The statistical error (one standard deviation) is listed immediately below each value. The reactor power was assumed to be 5 MW.
Table 5.7 210
Energy deposition in the coolant (H_2O) and the structural material (aluminum) of the H_2O-cooled fission converter with eleven fresh fuel elements. The components which contain most of the aluminum considered here are the converter tank walls.
Table 5.8 215
Chemical requirements for A11100, A16061 and common lead in weight percent from ASTM standards.[8] The limit described by a single value denotes weight percent maximum unless stated otherwise.
Table 5.9 216
The compositions of A11100 and A16061 used in the MCNP model (in weight percent).
Table 5.10 216
In-air beam performance for filter/moderator designs composed of 71 cm Al - 27 cm AlF_3 where pure aluminum, A11100 or A16061 is used as the Al block. These calculations used a fission converter composed of eleven burned MITR-II fuel elements (312 g U-235 per element) cooled with D_2O. The filter/moderator is followed by a thermal neutron filter (0.04 cm Cd), a photon shield (8 cm Bi) and a pyramidal collimator with a 15 cm thick lead lining. The statistical error (one standard deviation) is listed immediately below each value. The reactor power was set at 5 MW.
Table 5.11 218
The compositions of common lead used in the MCNP model (in weight percent).

Table 5.12 219
In-air beam performance for collimator designs using pure lead or common lead for the lining. These calculations used a fission converter composed of eleven burned MITR-II fuel elements (312 g U-235 per element) cooled with D_2O followed by a filter/moderator (68 cm 70% AlF_3/30% Al - 2 cm Ti), a thermal neutron filter (0.04 cm Cd), a photon shield (8 cm Bi) and a pyramidal collimator with a 15 cm thick lead lining. The statistical error (one standard deviation) is listed immediately below each value. The reactor power was assumed to be 5 MW.
Table 5.13 222
Compositions of heavy concrete and regular concrete in weight percent. The data of heavy concrete is that used in the study of Reference 1. Regular concrete used here is LOS ALAMOS (MCNP) Mix from Reference 9.

CHAPTER SIX

Summary And Recommendations For Future Analysis

APPENDIX

Numerical Results Of The MCNP Calculations For Transverse And Vertical Power Profiles

Table A.1 240
Power generation for each fuel plate in a H_2O-cooled fresh fuel fission converter. The reactor power was assumed to be 5 MW
Table A.2 243
Power generation for each fuel plate in a D_2O-cooled fresh fuel fission converter. The reactor power was assumed to be 5 MW
Table A.3 246
Axial power distribution of Plate 1 of Element 7 (fresh fuel) with H_2O cooling.

Preface

It may be helpful to provide a few explanations about the presentation of the results from the Monte Carlo Calculations. To express the statistical uncertainty of the computational result, one standard deviation is always used in this thesis; in tables of the results, one standard deviation is shown as a percent immediately below the value. Also, all error bars in figures denote statistical uncertainties of one standard deviation.

CHAPTER ONE

Introduction

1.1 Background

Cancer is ranked as the second leading cause of death in the United States; in 1997, deaths due to this disease were estimated at 560,000, more than 1,500 per day.[1] Although, nowadays, early detection and modern modalities of treatment have increased the possibility of cure significantly, there are several types of tumors, such as glioblastoma multiforme, for which no effective therapy has been established yet.

Boron neutron capture therapy (BNCT) is a therapy which may be effective in the treatment of cancers that cannot be cured by conventional modalities. BNCT consists of two components: a drug containing non-radioactive ^{10}B and a neutron beam. A boron-containing drug is developed which is selectively taken up by tumor tissue. When a neutron is absorbed by ^{10}B, it causes a fission reaction and emits an α particle and a ^{7}Li ion. These heavy charged particles carry 2.310 MeV of energy (94% of reactions where the ^{7}Li nucleus is in the excited state) or 2.792 MeV (6% of reactions where the ^{7}Li nucleus is in the ground state). In the former case, an α particle and a ^{7}Li ion have 1.47 MeV and 0.84 MeV, respectively[2]. Then, they deposit their energies within 12-14 microns, which is within the range of the size of most cells. As a result, the lethal damage is highly localized to tumor cells, while sparing normal cells.

BNCT was first performed in the 1950s. Unfortunately, the early trials failed mainly for two reasons[3]: 1) lack of proper boron-containing drugs which effectively concentrate in tumor cells and

2) use of thermal neutron beams which attenuate very rapidly in the tissue and which produces maximum normal tissue dose at the surface.

The first problem has been addressed by using more sophisticated carrier molecules which can achieve a significant tumor-to-normal tissue uptake ratio. The latter problem can be solved by using an epithermal neutron beam. Epithermal neutrons, whose energies range from 1 eV -10 keV, penetrate tissues more deeply than thermal neutrons and do not damage normal tissues at the surface as much as thermal neutrons do. Epithermal neutrons lose energy while scattering off tissue nuclei, primarily hydrogen, and achieve peak thermal fluxes at a depth greater than a few centimeters. The thermal neutrons are captured by ^{10}B and produce the resulting (n,α) reactions which is the basis for BNCT.

Researchers in Japan have made special efforts to develop BNCT since Dr. Hiroshi Hatanaka implemented their first BNCT treatment in 1968. By 1994, Dr. Hatanaka's group treated around 150 patients with malignant brain tumors using thermal neutron beams.[4] The encouraging results in Japan and the recent development of improved boron-compounds such as l-boronophenylalanine-fructose (BPA-f) and epithermal neutron beams have led to renewed interest in BNCT in the USA. As a result, clinical studies were revived at both the Brookhaven Medical Research Reactor (BMRR) and the Massachusetts Institute of Technology Reactor (MITR-II) in 1994. The protocols executed at these facilities are designed to examine normal tissue toxicity and evaluate a tolerance dose for BNCT using an epithermal neutron beam and BPA-f for glioblastoma (BMRR and MITR) and melanoma (MITR)[5,6]. At MITR, four human subjects with melanoma of the extremities and eight subjects with brain tumors (seven with glioblastoma and one with melanoma) were treated between September 1994 and April 1997 in the Phase I clinical trials. A clinical follow-up of the subjects with melanoma of the extremities irradiated at MITR shows that none of them has suffered any significant normal tissue reaction, either acute or chronic, up to a

blood dose level of 12.5 RBE-Gy; moreover, all evaluable subjects experienced at least a partial response[6]. The follow-up study of 15 human subjects who received BNCT at BMRR also shows no acute adverse effects on normal brain tissue[7].

In addition to MITR and BMRR, the High Flux Reactor at Petten in the Netherlands has been prepared for BNCT and will be the next facility to irradiate human subjects with an epithermal neutron beam[3]. The beam performance and the materials used for neutron filtration/moderation and photon shielding for these three facilities are summarized in Table 1.1[3,8,9,18,19]. In-air figures of merit used to compare beam performance are epithermal neutron flux(Φ_{epi}), absorbed dose rate due to fast neutrons per epithermal neutron flux or specific fast neutron dose (D_{fn}/Φ_{epi}) and absorbed dose rate due to gamma rays per epithermal neutron flux or specific photon dose (D_{γ}/Φ_{epi}) which are indicative of intensity and fast neutron and photon contamination of the beam, respectively.

Table 1.1 A comparison of in-air beam performance and materials used for neutron filtration/moderation and photon shielding for MITR-II, BMRR and HFR

Facility	Reactor Power MW	Neutron Filter/moderator	Photon shield	Φ_{epi} n/cm^{2}s	D_{fn}/Φ_{epi} cGy cm^2/n	D_{γ}/Φ_{epi} cGy cm^2/n
MITR-II (M67)[8]	5	Al,S,Cd	Bi	$2.1*10^{8}$	$8.6*10^{-11}$	$1.3*10^{-10}$
BMRR[9,18]	3	Al,Al_2O_3,Cd	Bi	$1.8*10^{9}$	$4.3*10^{-11}$	$1.3*10^{-11}$
HFR[3,19]	45	Al,S,Ti,Cd	Ar	$3.3*10^{8}$	$8.6*10^{-11}$	$1.03*10^{-10}$

1.2 Previous Work on the Fission Converter

If the clinical trials can prove the efficacy of BNCT, routine treatment with BNCT will be initiated. For this purpose, a high-intensity epithermal neutron beam is required to irradiate each patient with enough fluence of epithermal neutrons in a reasonably short time. It is also important to mitigate the discomfort that patients would experience during the treatment as a result of maintaining a fixed position on a couch for a long time (in the case of the MIT M67 beam, several hours are currently required to finish a bilateral irradiation based on the Phase I protocol). Rief *et al.*[10] have proposed using a fission converter in the thermal column of a low-power reactor to produce an epithermal neutron beam. The principle of the fission converter is to use ^{235}U fission plates (or fuel elements) to convert thermal neutrons from the reactor core to fast neutrons, which are then moderated and filtered into the desired energy range for BNCT by using filter/moderator materials. It should be emphasized that the fission-converter concept could enable many small research reactors with thermal columns or other thermal neutron sources to generate high-quality and high-intensity epithermal neutron beams which adequately meet medical requirements. In the USA, it is estimated that there are more than 15 potentially suitable reactors[11].

Stimulated by Rief's work, design studies of fission converter-based epithermal neutron beams have been conducted at both MITR and BMRR in the USA.[11,12,13] The beam performance of both designs are compared in Table 1.2. In this table, current-to-flux ratio, which is indicative of beam directionality (i.e., collimation) is presented in addition to other three in-air figures of merit (Φ_{epi}, D_{fn}/Φ_{epi} and D_{γ}/Φ_{epi}).

Table 1.2 Comparison of in-air beam performance and materials used for neutron filtration/moderation and photon shielding of the fission converter-based epithermal neutron beam designed at MITR and BMRR. The number below each figure of merit denotes one standard deviation of each quantity.

Facility	Fission Plate	Coolant	Neutron Filter/moderator	Photon shield	Φ_{epi} n/cm^{2}s	D_{fn}/Φ_{epi} cGy cm^2/n	D_γ/Φ_{epi} cGy cm^2/n	J/Φ
MITR-II[12]	MITR-II Fuel (Burned)	D_2O	Al/AlF_3 (Mix.), Ti, Cd	Bi	$1.3*10^{10}$ 1%	$1.3*10^{-11}$ 2%	$1.0*10^{-11}$ 2%	0.67 2%
MITR-II[12]	MITR-II Fuel (Fresh)	D_2O	Al/AlF_3 (Mix.), Ti, Cd	Bi	$1.7*10^{10}$ 1%	$1.3*10^{-11}$ 2%	$9.7*10^{-12}$ 2%	0.66 2%
BMRR[9,13]	ANL Janus Reactor Fuel	D_2O	Al,Al_2O_3,Cd	Bi	$1.2*10^{10}$ 3%	$2.8*10^{-11}$ 6%	$<1*10^{-11}$ N.A.	0.78 N.A.

The studies that have been performed at MITR consist of neutronic and engineering designs of the fission-converter beam, which is to be installed in the thermal column and hohlraum of the MITR-II. The current facilities of the MITR-II, especially the thermal column and hohlraum, and the modifications in them which would be necessary to construct a medical irradiation facility with the fission converter beam are discussed elsewhere[12, 20, 21,22]. The isometric view of MITR-II is shown in Figure 1.1. A fission converter is to be located in a vertical duct between the graphite reflector and thermal column, where two main coolant pipes of the MITR-II run vertically to connect to the core tank. This is illustrated in Figure 1.2. The components of the beam such as the filter/moderator, reflector, photon shield, and collimator are to be placed in the thermal column region. The hohlraum will be reconfigured as a medical irradiation room, where a patient can take any position, reclining or sitting during irradiation. The conceptual design of the entire medical irradiation facility is depicted in Figure 1.3. Since there is significant distance between the fission converter and hohlraum, beam intensity would be increased if the patient were positioned closer to the fission converter, namely, in the thermal column region. However, flexibility of positioning

would be substantially limited in the thermal column due to lack of space. Therefore, it was decided to locate the patient position inside the hohlraum.

The previous neutronic design study in Reference 12 is composed of three major sections: the development of a methodology for the efficient neutronic calculation of the beam design using the general purpose Monte Carlo radiation transport code MCNP (Monte Carlo N-Particle)[14]; the validation of the MCNP model of MITR-II by comparing computational results with measurement; and design calculations of various components of the beam. These works sought to achieve the design goal in terms of beam performance; that is, high intensity (Φ_{epi} of about $1*10^{10}$ n/cm^2 s) to allow completion of an irradiation in a few minutes, and very low or negligible fast neutron and photon contamination (D/Φ_{epi} not greater than $2*10^{-11}$ cGycm^2/n) compared to the inherent background contamination due to radiative capture of hydrogen (the peak dose from this component is ~ $2*10^{-10}$ cGycm^2/n), which would be the dominant component of background contamination if normal tissue ^{10}B dose becomes very small due to significant improvement of tumor-to-normal tissue uptake ratio with advanced compounds.

As for the beam design, neutrons exiting from the fission converter have a slightly moderated fission spectrum and are accompanied by a significant amount of gamma rays. This beam has to be tailored into a clean epithermal neutron beam by filtering out contaminants which can cause healthy tissue dose: fast neutrons, thermal neutrons and gamma rays. Thermal and fast neutrons can be removed by utilizing the nuclear characteristics of certain materials, so-called filter/moderators, by which fast neutrons are moderated into the desired energy range or scattered out of the beam and thermal neutrons are captured, allowing only epithermal neutrons to pass through the beam unimpeded. Gamma rays can be attenuated by using appropriate high-Z materials. The lateral leakage of useful neutrons from the beam can be reduced by reflector and the resulting epithermal neutron beam will be guided to the patient position by a collimator.

Reference 12 reported a extensive series of parametric studies for these components of the epithermal neutron beam. As a result of various optimizations, a beam design was proposed in Reference 12, which is shown in Figure. 1.4. This design incorporates a fission converter with 11 MITR-II fuel elements, each of which has 15 finned fuel plates of 93% enriched uranium in the form of U-Al_x cermet clad with aluminum. The fission converter is enclosed in a trapezoidal tank with double aluminum walls and is cooled by H_2O or D_2O. It is irradiated with thermal neutrons from the MITR-II core and generates fission neutrons. These fission neutrons are moderated and filtered while passing through a filter/moderator composed of 68 cm thick 70% AlF_3/30% Al (by volume) and 2 cm thick Ti layers. Then, they are guided to the patient position, i.e. the target position at the end of the beam by a pyramidal collimator lined with 15 cm thick lead. Thermal neutrons and gamma rays are removed from the beam by a 0.04 cm thick Cd sheet and an 8 cm thick Bi photon shield. Photons outside the beam aperture are shielded by the lead collimator lining. The filter/moderator is surrounded by a 10 cm thick lead reflector.

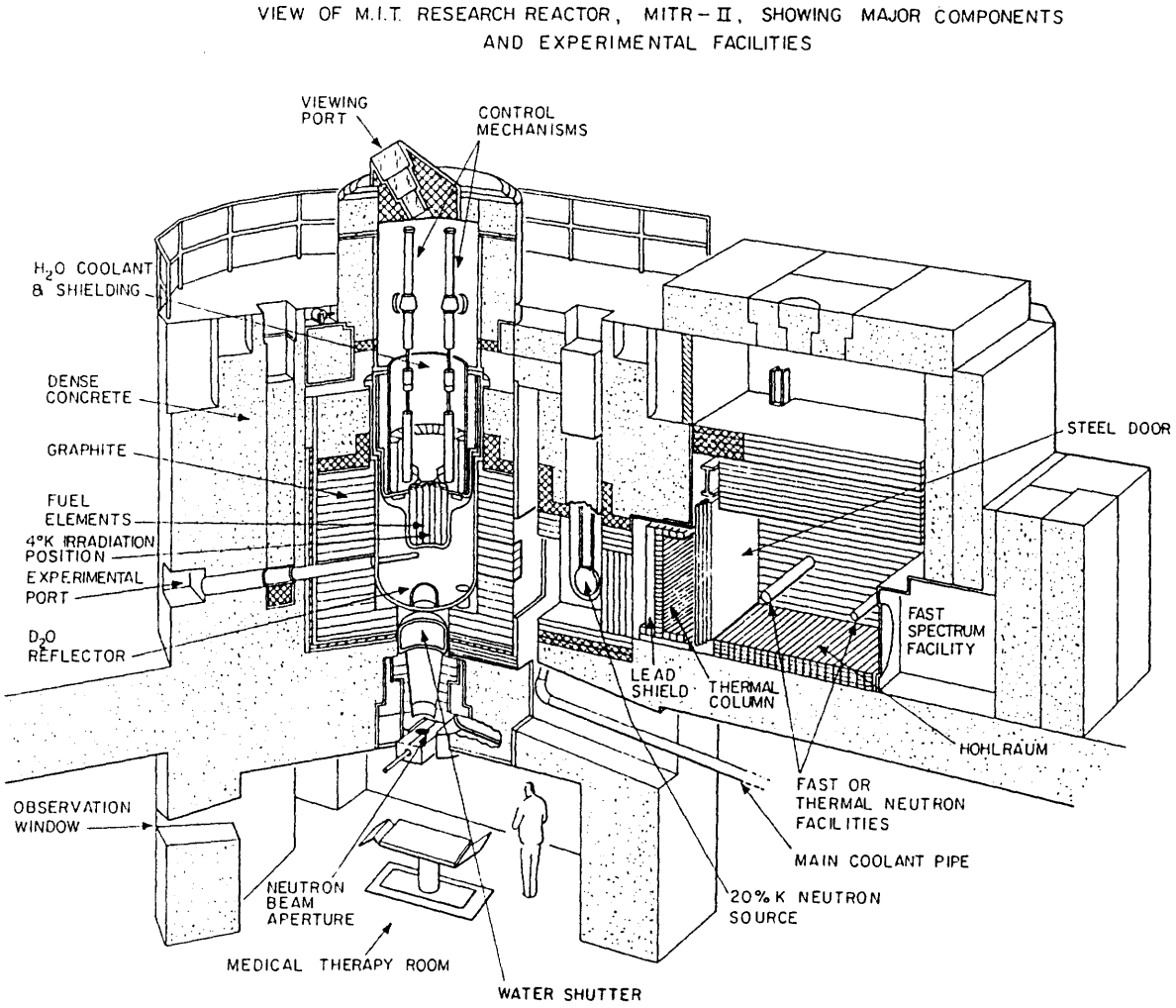

Figure 1.1 Isometric view of MITR-II showing major components and experimental facilities.

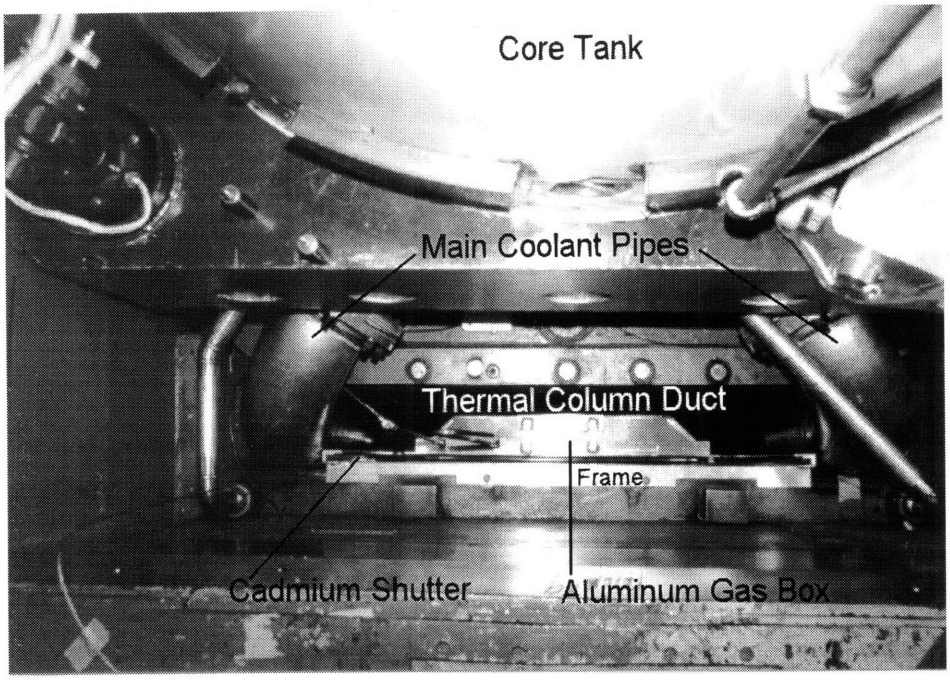

Figure 1.2 The thermal column duct with the aluminum gas box during reactor renovation in 1974-75. The main coolant pipes curve over the top of the duct where they connect to the core tank. The duct is the future location of the fission converter (Courtesy of W. S. Kiger).

This is the back side of Figure 1.2.

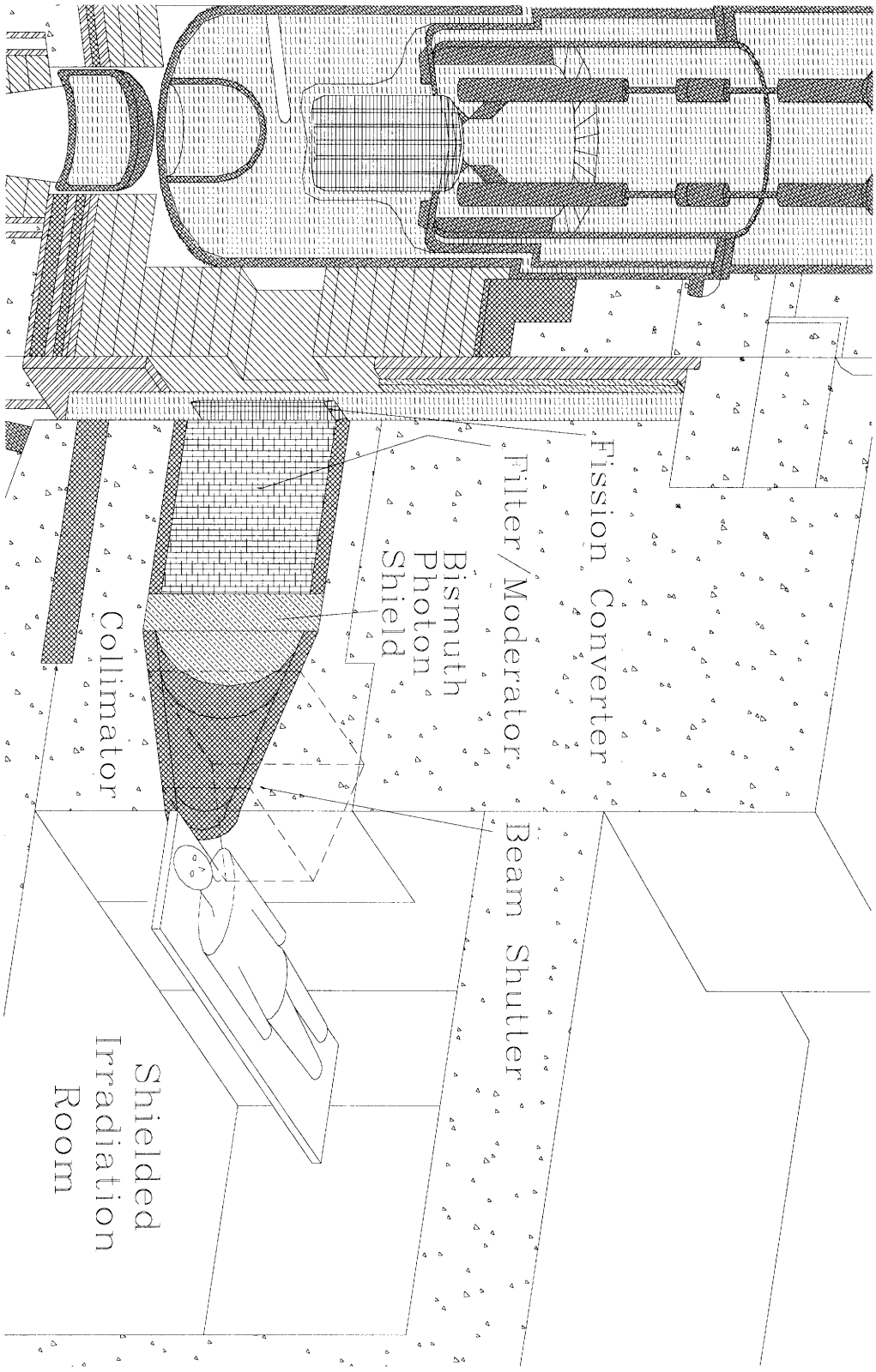

Figure 1.3 Isometric view of MIT fission converter beam and medical irradiation facility. Drawing is roughly to scale (Courtesy of W. S. Kiger).

This is the back side of Figure 1.3.

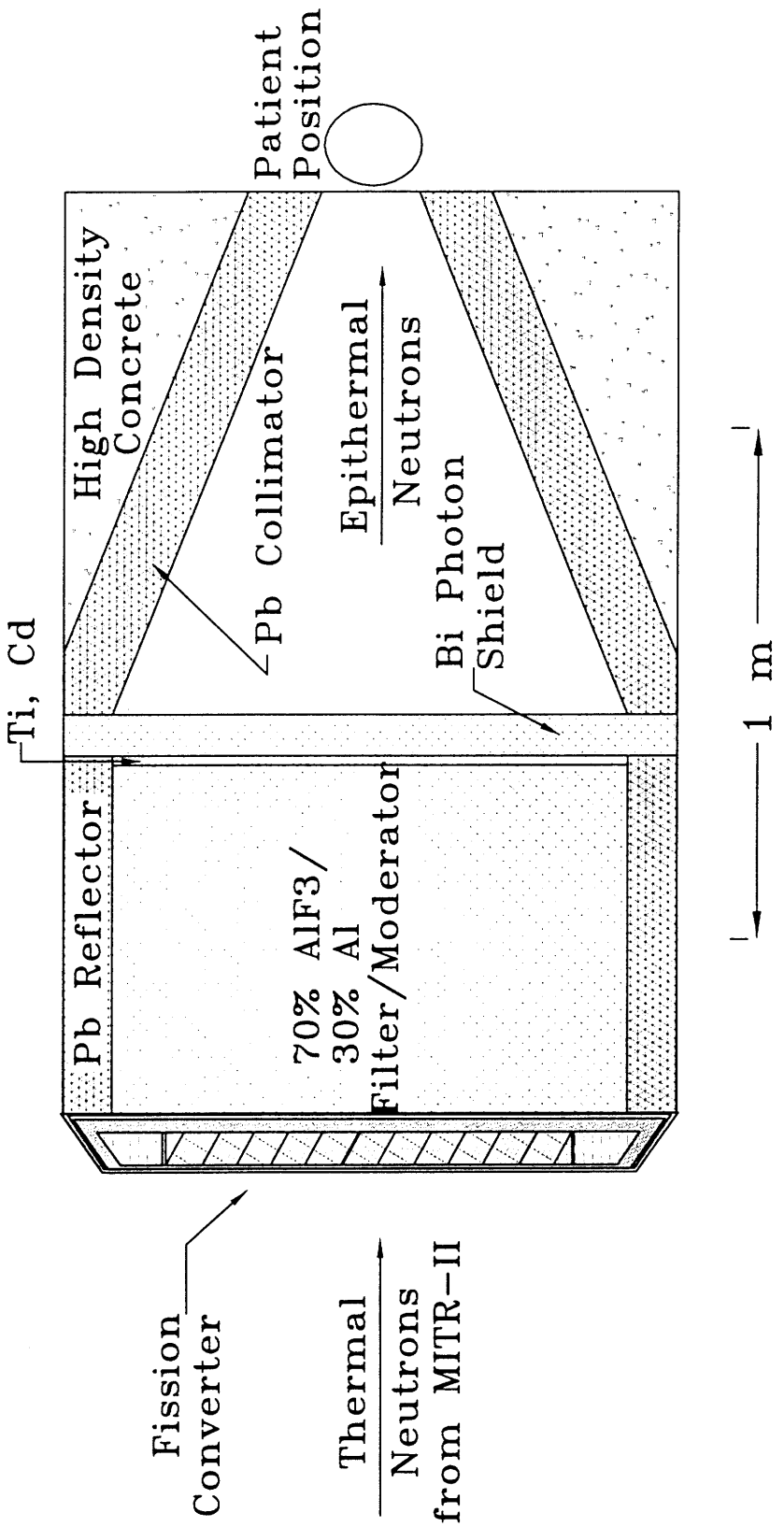

Figure 1.4 Plan view of the fission converter beam design proposed by Reference 12 (Courtesy of W. S. Kiger)

It was shown that the current beam design surpasses its design goals and provides excellent performance for the treatment of brain tumors by BNCT. With D_2O-cooled spent MITR-II fuel (fuel loading of 312 g ^{235}U per element) at 5 MW reactor power, this beam design produces an epithermal neutron flux of $1.3*10^{10}$ n/cm^{2}s and specific fast neutron and photon doses of $1.3*10^{-11}$ cGy cm^2/n and $1.0*10^{-11}$ cGy cm^2/n. The epithermal neutron flux can be increased by 30% (for D_2O cooling) by using fresh fuel (fuel loading of 510 g ^{235}U per element) instead of burned fuel without increasing fast neutron and photon contamination. By examining Tables 1.1 and 1.2, one can see that this design is far superior to the current MIT medical beam (increase in beam intensity by a factor of ~60-80 and decrease in fast neutron and photon contamination by a factor of ~10). It is also superior in intensity and low background to all other existing or planned facilities. Using reasonable assumptions of boron concentration in tumors, tumor-to-normal tissue uptake ratio and RBE values, excellent in-phantom figures of merits were obtained: advantage depth of 9.5 cm, advantage ratio of 4.9, and advantage depth dose rate of 435 cGy/min (the explanation of these in-phantom figures of merit will be given in the following section). For a bilateral irradiation, an advantage ratio of 4.7 is obtained. This beam will enable us to complete a treatment in only 2.3 minutes, assuming a normal tissue tolerance dose of 1000 RBE cGy, with a high therapeutic ratio and deep beam penetration. An engineering design of the facility including thermal hydraulics and mechanics of the fission converter, shutter and medical room design has been performed by Balendra Sutharshan, a Ph.D. candidate in the Nuclear Engineering Department[20,21,22].

1.3 Objective

Although the epithermal neutron beam design proposed in Reference 12 is very promising, several approaches are expected to further improve the performance of the beam. These should provide a better therapeutic ratio and other figures of merit, lower cost, enhanced safety, flexibility, engineering advantages and the environmental compatibility of the facility. A main objective of this thesis is to perform neutronic sensitivity analyses for optimization of the fission converter beam by studying several important aspects of the facility, including:

(1) Identification of the best configuration of multi-plate reactor type fuel elements (MITR-II fuel) or use of a single fission plate designed specifically for the fission converter beam

(2) Selection of the best materials and configuration for the neutron filters (i.e., the fast neutron filter/moderator and the thermal neutron filter)

(3) Improvement of the collimator design in terms of directionality and beam aperture size

In addition to these analyses, several other factors relevant to neutronic performance are to be analyzed for detailed engineering design and safety of the fission converter beam facility, such as reactivity insertion due to the fission converter, the effect of impurities in the materials and heat generation in the fission converter. These analyses are also within the scope of this thesis. In conclusion, this thesis is intended to provide detailed analyses of the various components of the fission-converter beam which are required to complete the engineering design work.

This thesis will present the sensitivity analyses for the main components of the beam, the fission converter, the neutron filters and the collimator in Chapter 2, 3 and 4, respectively. The neutronic analyses required for detailed engineering design and safety will be presented in Chapter 5. Finally, the summary of this study and recommendations for future analysis will be provided in

Chapter 6.

1.4 Methodology of the Analysis

A methodology for the neutronic analysis of a fission converter beam was developed in Reference 12. It utilizes the general purpose Monte Carlo radiation transport code MCNP (Monte Carlo N-Particle) developed at Los Alamos National Laboratory[14]. This code can be used for neutron, photon, electron, or coupled neutron/photon/electron transport calculations. It was selected because of its excellent features for this kind of study, which include its ability to treat an arbitrary three-dimensional geometry and pointwise cross-sectional data, and high confidence in its performance based on an extensive series of benchmark calculations. However, the Monte Carlo technique requires a large amount of computer time, which restricts its use. Fortunately, new high-speed computers with 200 MHz Intel Pentium Pro introduced in the course of the current study, which are 10 times faster than the computers used in Reference 12, have mitigated this problem significantly[24]. In addition, several approaches have been developed to improve the efficiency of the calculations including the decoupling of the MITR-II core model, the fission converter beam model and the head phantom model, and the use of variance reduction techniques. For the latter, the weight window is used; this technique uses space-energy-dependent splitting and Roussian roulette to control the number of samples (i.e., many samples with low weight in important regions of phase space and few samples with high weight in unimportant regions) without biasing the solution.

The computational scheme consists of three steps: 1) a criticality calculation of the MITR-II model to create a surface neutron source at the edge of the graphite reflector (facing the thermal column vertical duct); 2) a fixed source calculation for neutrons and induced photons from the edge of the graphite reflector through the fission converter beam to generate a subsequent surface source

at the patient position; and 3) transport of the final surface source through a head phantom to create dose-depth profiles. The outline of the original computational method is depicted schematically in Figure 1.5. In the current study, as will be explained later, the third step was improved so that one can reduce the number of transport calculations through the fission converter beam. The modified method is depicted in Figure 1.6. Each step of the scheme is briefly reviewed below, where some improvements or changes made in the current study are also described. However, for detailed explanations of the method and computational models, the reader should consult Reference 12.

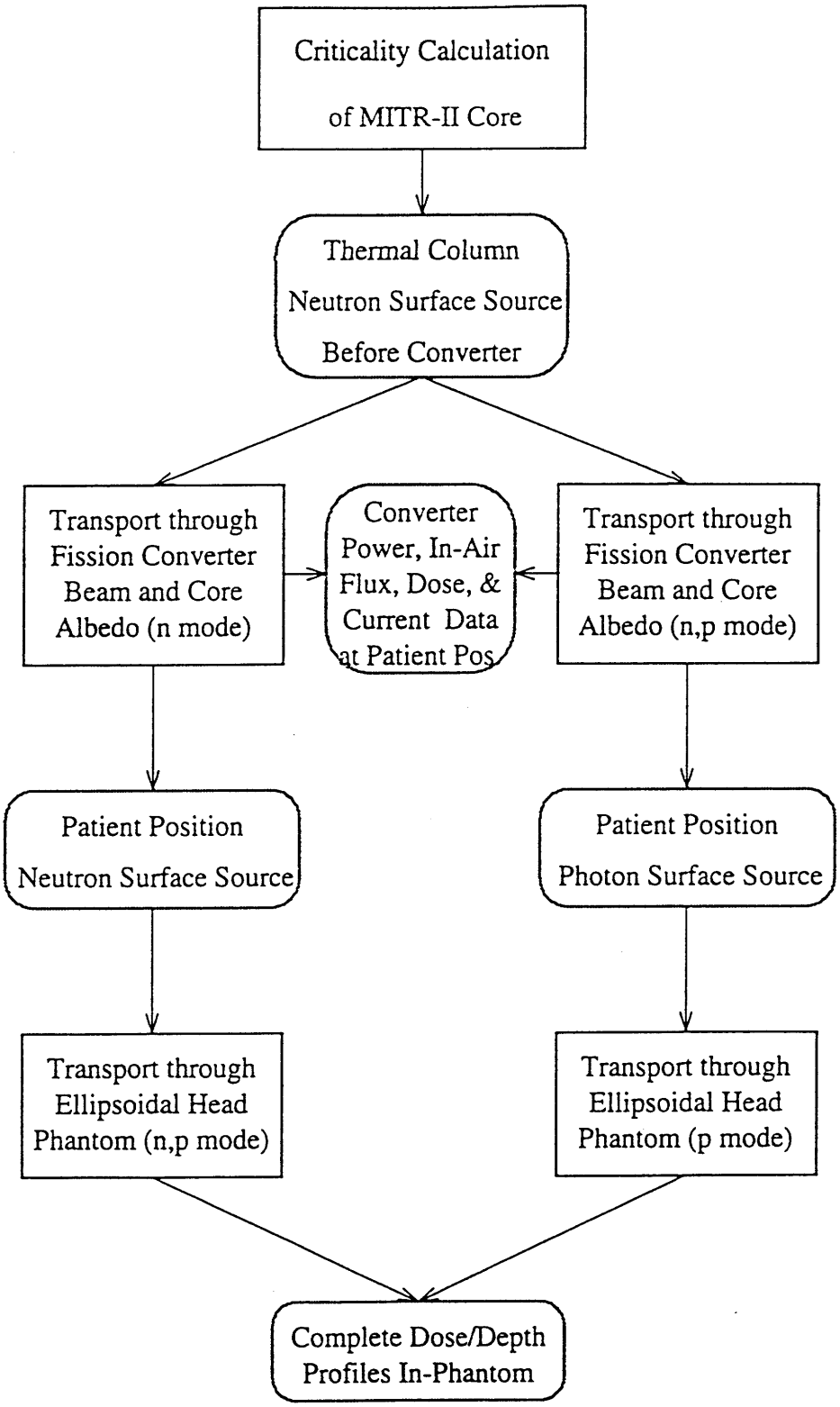

Figure 1.5 Previous methodology for MCNP calculations (Courtesy of W.S. Kiger)

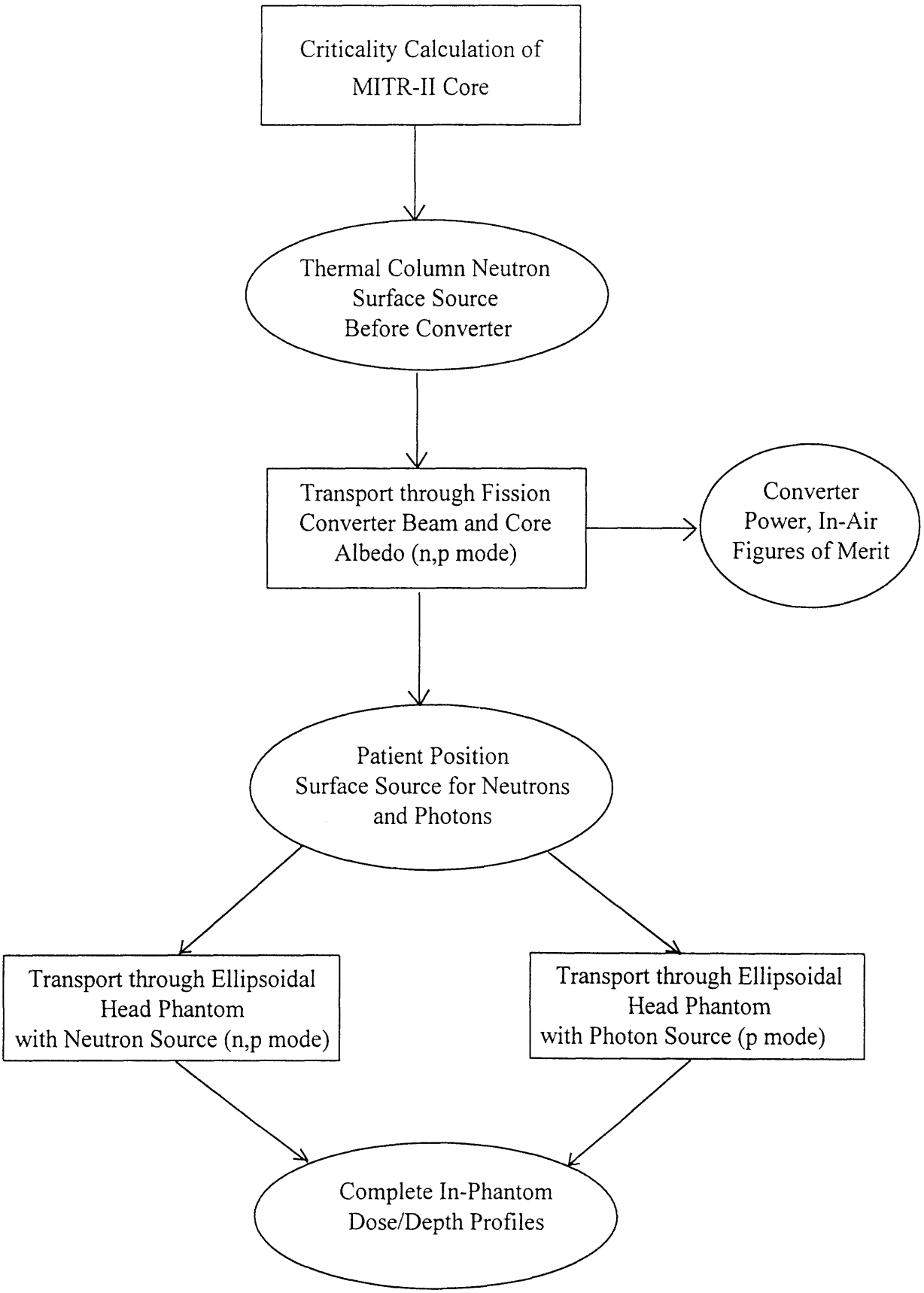

Figure 1.6 Modified methodology of MCNP calculations for the fission converter beam design

1.4.1 Criticality Calculation to Create the Thermal Column Surface Source

The MITR-II core drives the fission converter as a neutron source; they form a coupled system. However, for doing detailed design calculations of the fission converter beam without rerunning the model of the entire system, the reactor model should be decoupled from the fission converter model. For this purpose, a criticality calculation for the reactor-only model is performed to transport neutrons from the core to the edge of the graphite reflector, where the model is truncated; when neutron histories reach the edge of the graphite reflector, they are terminated and stored in the surface source file. The decoupling of the core and the fission converter is justified by the fact that the feedback from the fission converter to the core is very small due to many mean free paths of D_2O and graphite between them. Only neutrons are stored in the surface source because it is uneconomical to keep a large number of photons from the reactor at the expense of a large amount of disk space required for their storage (> 100 MB) as they have a very small effect on beam performance. Energy independent weight windows generated by Everett Redmond II[15] are used to enhance the transport from the core to the graphite edge. The calculation using these techniques permits the accuracy of the coupled neutron-photon run for the entire model to be retained while spending a reasonable amount of computer time.

The MCNP model of MITR-II used in the calculation was originally developed in the study of Reference 15. This model has been fully validated in the core[15] and thermal column region[12] by experiments; it has therefore been used as a basis for neutronic design of the fission converter beams with high confidence.

It is assumed that the content of the 14 inch window, which would reduce the intensity of thermal neutrons from the MITR-II core by a factor of ~2, will be removed during the construction of the fission converter beam facility. Therefore, this study uses the reactor model with the 14 inch

window empty as Reference 12 did.

1.4.2 Fixed-Source Calculation to Generate a Surface Source at the Patient Position

In the next step, a coupled neutron-photon transport calculation is performed for the fission converter beam model with the MITR-II core albedo, which permits the backscattering of particles in the reflector of the MITR-II to be taken into account. Neutrons in the thermal column surface source impinge on the fission converter and cause fissions. The resulting neutrons and photons are transported through the beam and reach the patient position, where in-air figures of merits are calculated and a neutron-photon surface source is created for subsequent in-phantom analyses.

While passing through the beam, neutrons in different energy ranges undergo significantly different attenuation because of resonance scattering in the fast neutron filter/moderator. In order to have a adequate number of neutrons at the patient position for all energy regions, energy dependent weight windows (five energy intervals) are used for neutron transport. However, energy-independent weight windows are used for photons. Sensitivity analyses require frequent and significant changes in the beam design. When necessary, a new set of weight windows is generated using the weight window generator option of MCNP to allow for changes in the physical characteristics of the beam components.

As an output of the transport calculation through the beam, in-air figures of merit, i.e. epithermal neutron flux(Φ_{epi}), specific fast neutron dose (D_{fn}/Φ_{epi}), specific photon dose (D_{γ}/Φ_{epi}) and current-to-flux ratio (J/Φ), are obtained using 3 energy groups, i.e., thermal energy range of 0 to 1 eV, epithermal range of 1 eV to 10 keV, and fast range of 10 keV to 20 MeV. One should note that D_{fn} is defined as the absorbed dose rate due to both epithermal and fast neutrons (i.e., neutrons with energies within 1 eV - 20 MeV). KERMA factors for brain tissue are used to

calculate neutron and photon dose rates, which are from Reference 16. These in-air parameters provide a quick way to estimate and compare beam performance although in-phantom figures of merit, which reflect realistic therapeutic conditions, are the bottom-line for analyzing beam performance.

1.4.3 Dose-Depth Profile Calculation in a Head Phantom

Again, for the efficiency of the calculation, the head phantom model was decoupled from the fission converter beam model; the effect of neglecting neutrons backscattered from the head phantom to the collimator and scattered back to the phantom is considered to be very small due to existence of a large open space in the collimator. The water-filled ellipsoidal head phantom model represented by the following equation[23], which was used in the previous study, is also employed for all the calculations of the in-phantom analyses in the current study:

$$(x/7)^2 + (y/10)^2 + (z/8.5)^2 \leq 1$$

where the denominators are the ellipsoid semi-axes in cm. In this phantom, a 1.27 cm diameter cylinder along the lateral axis (i.e., x axis or central axis) of the phantom is segmented every 0.5 cm. The neutrons and photons stored in the patient position surface source are transported separately through the phantom, which is located 1 cm from the source plane. Then, RBE-weighted, volume-averaged ^{10}B, neutron and photon doses are tallied in every segment and all dose components are summed up to construct one-dimensional central axis dose-depth profiles. KERMA factors for ^{10}B dose are to be found in Reference 16.

In the previous study, two different fixed-source calculations through the beam were run before this dose-depth profile calculation, one in neutron-only mode and the other in coupled neutron-photon mode, to create a neutron surface source and photon surface source separately at

the patient position. This separation was done in order to distinguish the contribution in the dose-depth profile of incident photons from that of photons induced in the phantom. However, in the current study, this approach was modified so that one neutron-photon surface source can be used to sample neutrons and photons separately; that is, to transport only neutrons, photons on the patient position surface source are killed just after they exit from the surface source in an in-phantom run in coupled neutron-photon mode. By adopting this approach, one can eliminate one neutron-only run throughout the beam and save a significant amount of computer time.

To have better statistics of in-phantom tallies than those of the previous study, the number of independent histories stored in both the thermal column surface source and the patient position surface source were increased substantially. The neutron source at the patient position is sampled up to one hundred times, while the photon source is sampled only once because multiple sampling is unnecessary due to weak photon scattering in the phantom.[12]

Three in-phantom figures of merit, i.e., the advantage depth (AD), advantage ratio (AR) and advantage-depth dose rate (ADDR), are calculated in this step from the dose-depth profile. Definitions of these figures of merit are as follows.[17] Advantage depth is the depth in a given material (e.g. brain tissue) at which the total therapeutic dose to the material is equal to the maximum total background dose (neutron and photon doses + ^{10}B dose in normal tissue), where the therapeutic dose is the sum of the total background dose from neutrons and gammas and the ^{10}B dose in tumor. The AD indicates the depth of effective beam penetration over which therapeutic gain is realized. The advantage ratio is the ratio of the integral of the total therapeutic dose to the integral of the total background dose over a given depth in the material (usually AD), which indicates the magnitude of the therapeutic gain. While these two figures of merit provide measures of beam quality, the advantage depth dose rate - the total therapeutic dose rate at the advantage depth - is indicative of beam intensity. These three in-phantom parameters constitute the

basis for comparison of beam performance of different designs in terms of expected therapeutic effect.

1.5 References

1. *Cancer Facts & Figures - 1997*, American Cancer Society, Inc., 1997.
2. G. F. Knoll, *Radiation Detection and Measurement*, John Wiley & Sons, New York, 1989.
3. R. L. Moss, O. Aizawa, D. Beynon, R. Brugger, G. Constantine, O. Harling, H. B. Liu, and P. Watkins, "The Requirements and Development of Neutron Beams for Neutron Capture Therapy of Brain Cancer," *Journal of Neuro-oncology*, to be published.
4. Y. Nakagawa and H. Hatanaka, "Recent Study of Boron Neutron Capture Therapy for Malignant Brain Tumor in Japan" in *Cancer Neutron Capture Therapy*, edited by Mishima, Plenum Press, New York, 1996.
5. R. G. Zamenhof, "Procedures for Phase-I Study of Boron Neutron Capture Therapy for Glioblastoma Multiforme & Intracranial Melanoma at the New England Deaconess Hospital & the Massachusetts Institute of Technology", Protocol IND No. 46,176/No. 5, original submitted to FDA on Nov. 8, 1995.
6. P. Busse, R. Zamenhof, H. Madoc-Jones, G. Solares, S. Kiger, K. Riley, C. Chuang, G. Rogers, O. Harling, "Clinical Follow-up of Patients with Melanoma of the Extremity Treated in a Phase-I Boron Neutron Capture Therapy Protocol", Proc. 7th Int. Symp. on Neutron Capture Therapy for Cancer, held in Zurich, Switzerland, Sep. 4-7, 1996 (in press).
7. L. Wielopolski, J. A. Coderre, A. D. Chanana, J. Capara, E. H. Elowitz, M. Shady, M. Chadha, A. Z. Diaz, J. Iwai, D. D. Joel, D. N. Slatkin, "Clinical Trial of BNCT for Glioblastoma Multiforme", Transactions of ANS, Vol. 75, Nov. 1996.
8. R. D. Rogus, *Design and Dosimetry of Epithemal Neutron Beam for Clinical Trials of Boron Neutron Capture Therapy at the MITR-II Reactor*, Ph.D. Thesis, Massachusetts Institute of Technology, 1994.

9. H. B. Liu, R. M. Brugger, "Conceptual Designs of Epithermal Neutron Beams for Boron Neutron Capture Therapy from Low-power Reactors", *Nuclear Technology*, Vol.108, pp 151-156, Nov. 1994.

10. H. Rief, R. Van Heusden, and G. Perlini. "Generating Epithermal Neutron Beams for Neutron Capture Therapy in TRIGA Reactors" in *Advances in Neutron Capture Therapy*, edited by A. H. Soloway *et. al.*, Plenum Press, New York, 1993

11. O. K. Harling and W. S. Kiger, III, "High-Intensity Fission-Converter Based Epithermal Neutron Beam for Neutron Capture Therapy," in *Cancer Neutron Capture Therapy*, edited by Mishima, Plenum Press, New York, 1996.

12. W.S. Kiger III, *Neutronic Design of a Fission Converter-Based Epithermal Beam for Neutron Capture Therapy*, Nucl. E. Thesis, Massachusetts Institute of Technology, 1996

13. H. B. Liu, R. M. Brugger, D. C. Rorer, P. R. Tichler and J. P. Hu, "Design of a high-flux epithermal beam using ^{235}U fission plates at the Brookhaven Medical Research Reactor," *Medical physics*, 21(10), October 1994.

14. J. F. Briesmeister, Ed., *MCNP - A General Monte Carlo N-Particle Transport Code, Version 4A*, LA-12625-M, Los Alamos National Laboratory, 1993.

15. E. L. Redmond II, J. C. Yanch, O. K. Harling, "Monte Carlo Simulation of the Massachusetts Institute of Technology Research Reactor", *Nuclear Technology*, Vol.106, Apr. 1994.

16. R. G. Zamenhof, S. D. Clement, O. K. Harling, J. F. Brenner, D. E. Wazer, H. Madoc-Jones, and J.C. Yanch, "Monte Carlo Based Dosimetry and Treatment Planning for Neutron Capture Therapy of Brain Tumors", *Neutron Beam Design, Development, and Performance for Neutron Capture Therapy*, edited by O.K. Harling *et al.*, Plenum Press, New York, 1990.

17. S. D. Clement, J. R. Choi, R. G. Zamenhof, J. C. Yanch and O. K. Harling, "Monte Carlo Methods of Neutron Beam Design for Neutron Capture Therapy at the MIT Research Reactor

(MITR-II)", *Neutron Beam Design, Development, and Performance for Neutron Capture Therapy*, edited by O.K. Harling *et al.*, Plenum Press, New York, 1990.

18. H. B. Liu, R. M. Brugger, D. D. Greenberg, D. C. Rorer, J. P. Hu and H. M. Hauptman, "Enhancement of the Epithermal Neutron Beam Used for Boron Neutron Capture Therapy", *Int. J. Radiat. Onc. Biol. Phys,* 28(5), 1994.
19. R. L. Moss, "Review of Reactor-Based Neutron Beam Development for BNCT Applications", *Advances in Neutron Capture Therapy*, edited by A. H. Soloway *et. al.*, Plenum Press, New York, 1993.
20. B. Sutharshan, Ph.D. Thesis, Massachusetts Institute of Technology (to be published in 1997).
21. B. Sutharshan, N. E. Todreas and O. K. Harling, "Fission Converter Heat Removal and Safety under Accident Conditions", Transactions of ANS, Vol. 75, Nov. 1996
22. B. Sutharshan, N. E. Todreas and O. K. Harling, "Fission Converter Based Epithermal Beam - Heat Removal and Safety under Accident Conditions", Proc. 7th Int. Symp. on Neutron Capture Therapy for Cancer, held in Zurich, Switzerland, Sep. 4-7, 1996 (in press).
23. O. K. Harling, K. A. Roberts, D. J. Moulin and R. D. Rogus, "Head Phantoms for Neutron Capture Therapy", *Medical Physics*, 22(5), May 1995
24. Personal Communication from W. S. Kiger

CHAPTER TWO

Sensitivity Study of the Fission Converter Design: Fuel Configuration and Fuel Spacing

2.1 Introduction

A series of sensitivity analyses has been performed for the fission converter design using MITR-II fuel elements (see Reference 1). The parameters of the analyses included: fuel loading, coolant type, coolant thickness on the upstream side (i.e., the reactor-core side) and downstream side (i.e., the patient-position side), and aluminum tank thickness. In addition, the use of front reflectors (graphite or bismuth), of aluminum spacers above and below the fuel, and of side reflectors (aluminum or graphite) was also examined. The analyses of thermal hydraulics and structural mechanics[2,3,6] have also influenced the design of the fission converter. As a result of these analyses, the fission converter design shown in Figure 2.1 and Figure 2.2 was proposed. In this design, the fission converter composed of eleven MITR-II fuel elements is contained in a trapezoidal tank with double aluminum walls. There are flow channels, i.e., downcomers, at both ends of the fission converter tank, where the coolant goes down to the lower plenum. In the fuel region, the coolant flows upward and this flow path is separated from the downcomers by 0.635 cm aluminum plates. The tank thickness is carefully designed to minimize attenuation of incident thermal neutrons by reducing the tank-wall thickness on the upstream side while maintaining mechanical strength. The double-wall tank design makes a loss-of-coolant accident extremely unlikely. Its trapezoidal shape fits well into the space between the main coolant pipes in the thermal column vertical duct, and provides enough area for coolant channels and reduces radiation

streaming through vacant space in the vertical duct. The thermal-hydraulic study[2,3,6] of the fission converter has demonstrated that in all credible accident scenarios and bounding cases, the fission converter can be maintained in a safe situation without any fuel disruption. In fact, these analyses have shown that the fuel will not reach its softening temperature even if all the water cooling is rapidly lost. Therefore, in the latest fuel tank design, a single-walled tank has been proposed[5].

Although this design of the fission converter was shown to produce an epithermal neutron beam with high intensity and high quality[1], there are two important aspects to be further investigated for improvement in neutron generation of the fission converter: use of a fuel with different configuration (i.e., multi-plate reactor type fuel vs. single flat plate type fuel) and variation of fuel spacing. The analyses of these aspects are discussed in Sections 3.2 and 3.3, respectively. In addition, the effect of using different types of coolant (H_2O vs.D_2O) on in-phantom figures of merit will be presented in Section 3.4.

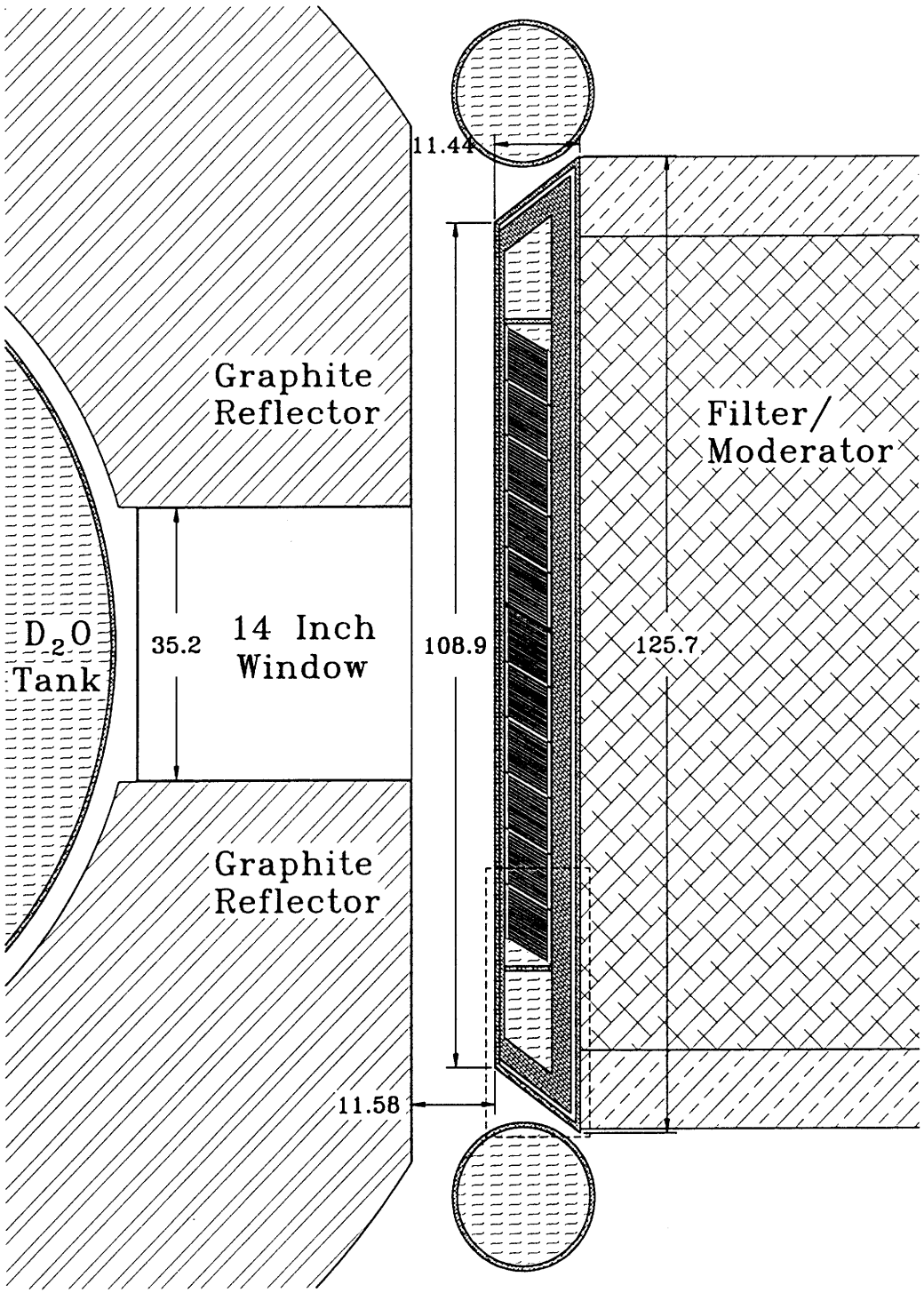

Figure 2.1 Plan view of the fission converter design proposed as the 'final design' in Reference 1. The area enclosed by the dashed rectangle is enlarged in Figure 2.2. All dimensions in cm. (Courtesy of W. S. Kiger)

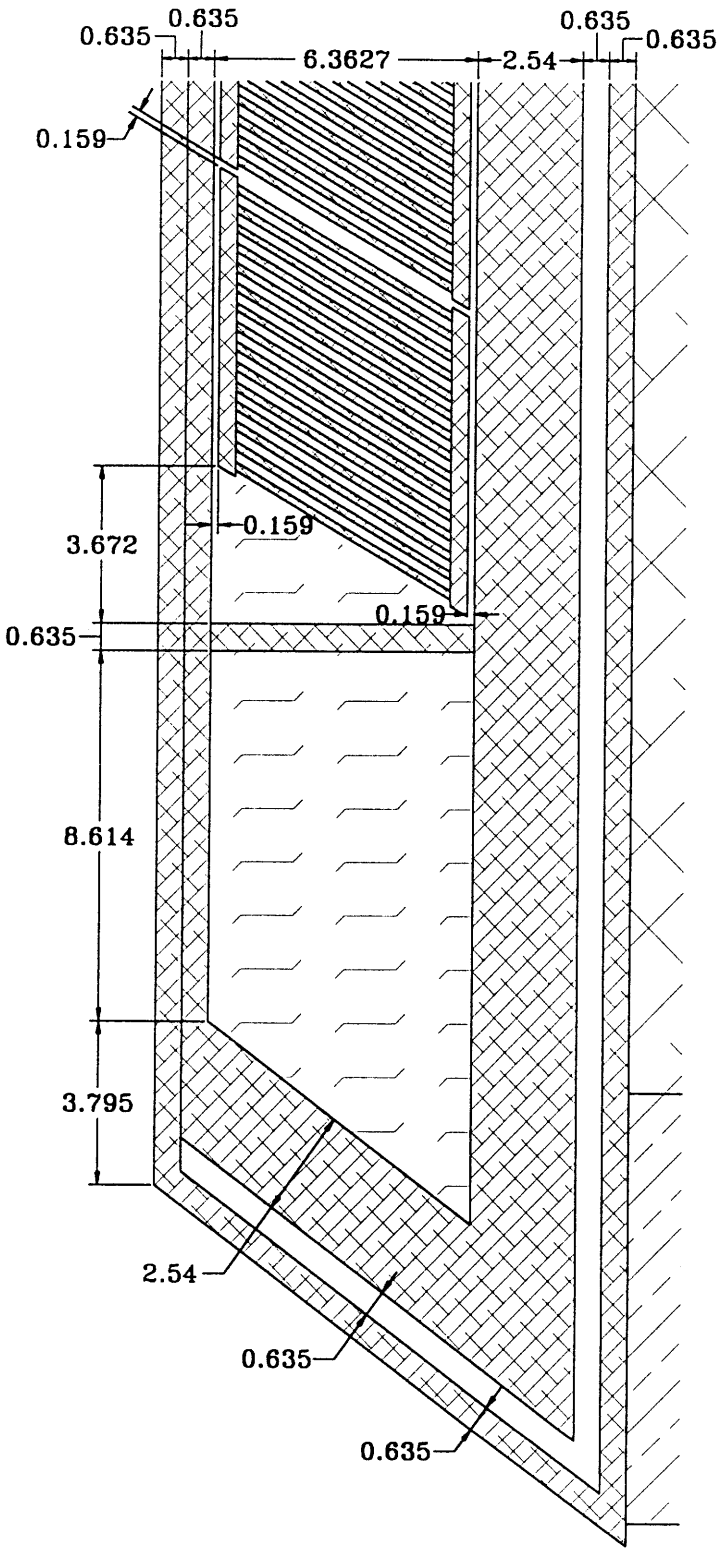

Figure 2.2 Close-up view of the fission converter design proposed as the 'final design' in Reference 1. All dimensions in cm (Courtesy of W. S. Kiger).

2.2 Fuel Configuration - Multi-Plate Reactor Type Fuel vs. Single Flat Plate Type Fuel

The study of coolant type (H_2O vs. D_2O) in Reference 1 showed that, a fission converter using MITR-II multi-plate reactor type fuel elements produces significantly higher beam intensity and lower fast neutron contamination with D_2O coolant than with H_2O coolant. It was suggested that hydrogen in the H_2O coolant overmoderates the useful portion of the neutron spectrum (especially, above 100 eV), the slowing down source for the epithermal neutron range, without commensurate reduction of fast neutrons because of hydrogen's higher scattering cross section in the slowing down region and its lighter mass relative to deuterium. Thus, the fission converter with D_2O coolant generates a harder spectrum that leads to higher epithermal neutron flux without a proportionate increase in the fast neutron dose. As a consequence, the use of D_2O as the coolant was recommended[1].

However, there still exists a strong incentive to pursue the use of H_2O because it is much cheaper and easier to handle than D_2O. It should be noted that the amount of the coolant would be an important factor as well as the nuclear properties of the coolant in terms of neutron moderation. Unfortunately, the large volume fraction of coolant in a MITR-II fuel element (~ 50%) cannot be reduced because of its multi-plate type structure. However, one can control the amount of coolant in a fission converter using single plate type fuel as long as one maintains sound engineering properties of the design (e.g. adequate cooling of the fuel). It was expected that the reduction of the volume fraction of the coolant in the single plate fuel fission converter relative to a converter using multi-plate type MITR-II fuel might offset the disadvantage of the overmoderation of H_2O coolant. Therefore, a single flat plate type fuel was considered as an alternative fuel option.

The performance of the fission converters using single flat plate fuel was studied with varying coolant thickness (0.16 to 1.0 cm) on both sides of the fuel. The minimum coolant thickness was set to 0.16 cm because it is considered to be a practical minimum from engineering considerations. The horizontal cross section of this design is depicted in Figure 2.3. The single flat plate fuel uses uranium of different fuel enrichments (20% or 93%) in the form of U-Al_x cermet (44% U and 56% Al by weight). The weight fractions of U and Al in the U-Alx cermet fuel are the same as used in the fresh MITR-II fuel element in the MCNP model. This fuel plate is clad with 0.0518 cm thick aluminum, equal to that of fuel plates in the MITR-II fuel element[4]. The size of the single plate fuel used in this design was determined by the following considerations:

Height: 56.83 cm, which is equal to the active fuel length of an MITR-II fuel element in the MCNP model.

Width: 78.51 cm, which is equal to the width of the fission converter composed of 11 MITR-II fuel elements; i.e., {6.9921(fuel element)*11+0.16(coolant thickness)*10} cm.

Fuel Meat Thickness: 5.3 cm for 20% EU and 1.1 cm for 93% EU to assure the absorption of thermal neutrons (0.025 eV) by uranium in the fuel meat with a probability of more than 95%.

The resulting single plate fuel has a fuel loading of 7.5 kg of ^{235}U for 20% EU and 7.7 kg of ^{235}U for 93% EU.

The results of the calculations using single plate fuel are given in Table 2.1, which shows the fission converter power and in-air beam performance with varying coolant type (H_2O vs. D_2O), enrichment (20% and 93%) and coolant thickness. The plots of epithermal neutron flux (ϕ_{epi}) vs. coolant thickness and specific fast neutron dose (D_{fn}/ϕ_{epi}) vs. coolant thickness are shown in Figures 2.4 and 2.5, respectively. These calculations used a fast neutron filter/moderator composed of 68 cm 70% AlF_3/30% Al - 2 cm Ti surrounded by a 10 cm thick lead reflector, a 0.04 cm Cd

thermal neutron filter, an 8 cm thick Bi photon shield and a pyramidal collimator with a 15 cm thick lead lining. The performance of single plate fuel fission converters will be discussed first in the Section 3.2.1. Then, in Section 3.2.2, a comparison between single plate type fuel and multi-plate reactor type MITR-II fuel will be made.

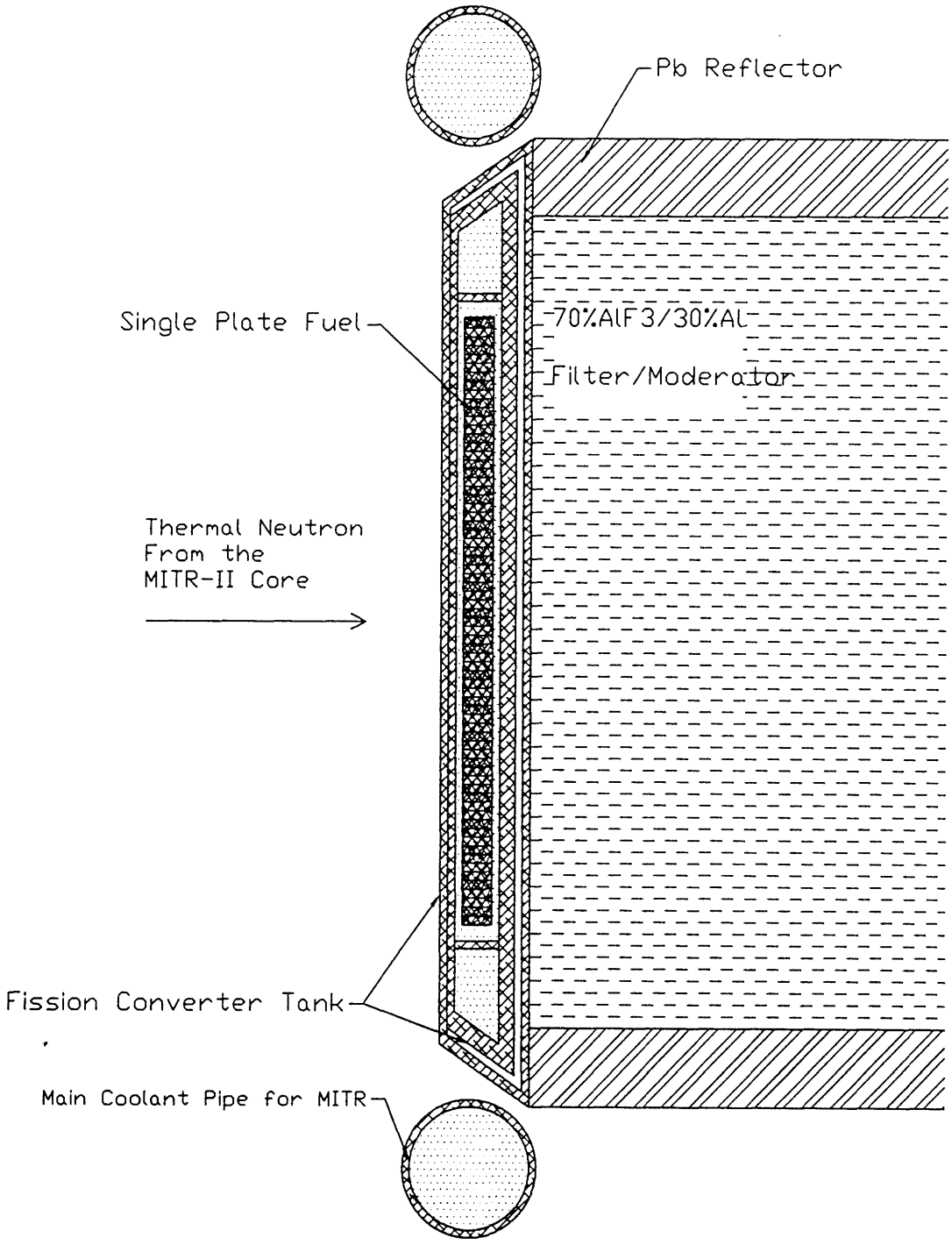

Figure 2.3 Cross-sectional view of a fission converter design using a single flat plate fuel. The fuel meat of the single plate fuel has a thickness 5.3 cm for 20% EU and 1.1 cm for 93% EU. The coolant thickness on both sides of the fuel is varied from 0.16 cm to 1.0 cm.

Table 2.1 Converter power and in-air beam performance for single flat plate type fuel with varying coolant type, enrichment and coolant thickness. In-air figures of merit were calculated at the patient position for a reactor power of 5 MW. The statistical error (one standard deviation) of each quantity is shown immediately below the value. These calculations used a neutron filter/moderator composed of 68 cm 70% AlF_3/30% Al + 2cm Ti followed by a 0.04 cm Cd thermal neutron filter, an 8 cm thick Bi photon shield and a pyramidal collimator with a 15 cm thick lead lining. The filter/moderator is surrounded by a 10 cm thick lead reflector.

Enrichment %	Run ID	Coolant	Coolant thickness cm	Power kW	Φ_{th} n/cm^{2}s	Φ_{epi} n/cm^{2}s	Φ_f n/cm^{2}s	Φ_{epi}/P n/cm^{2}kJ	J_{th}/Φ_{th}	J_{epi}/Φ_{epi}	J_f/Φ_f	D_{fn} cGy/min	D_{fn}/Φ_{epi} cGycm^2/n
20	uallw5	H_2O	0.16	95.1	8.23E+08	1.42E+10	1.63E+08	1.50E+08	0.64	0.66	0.67	14.1	1.66E-11
				0.63%	2.0%	1.3%	2.4%	1.4%	2.7%	1.7%	3.2%	1.4%	1.8%
	uallw1	H_2O	0.5	79.4	6.33E+08	1.05E+10	1.24E+08	1.33E+08	0.66	0.66	0.66	10.5	1.65E-11
				0.70%	2.2%	1.5%	3.2%	1.6%	3.0%	1.9%	4.1%	1.6%	2.1%
	uallw6	H_2O	1	67.7	5.24E+08	7.93E+09	9.30E+07	1.17E+08	0.64	0.66	0.69	8.1	1.69E-11
				0.67%	1.9%	1.3%	2.2%	1.4%	2.5%	1.7%	3.0%	1.2%	1.8%
	ualhw9	D_2O	0.16	105.2	1.15E+09	1.84E+10	1.83E+08	1.75E+08	0.64	0.67	0.67	16.0	1.44E-11
				0.60%	1.7%	1.1%	2.9%	1.3%	2.3%	1.5%	3.6%	1.2%	1.7%
	ualhw1	D_2O	0.5	104.3	1.14E+09	1.78E+10	1.62E+08	1.70E+08	0.63	0.66	0.68	14.4	1.35E-11
				0.61%	1.8%	1.2%	2.6%	1.3%	2.3%	1.6%	3.4%	1.3%	1.7%
	ualhw6	D_2O	1	102.4	1.16E+09	1.69E+10	1.44E+08	1.65E+08	0.64	0.66	0.70	13.4	1.32E-11
				0.63%	1.7%	1.2%	2.3%	1.3%	2.3%	1.6%	3.2%	1.3%	1.8%

Table 2.1 (Continued)

Enrichment	Run ID	Coolant	Coolant thickness	Power	Φ_{th}	Φ_{epi}	Φ_f	Φ_{epi}/P	J_{th}/Φ_{th}	J_{epi}/Φ_{epi}	J_f/Φ_f	D_{fn}	D_{fn}/Φ_{epi}
%			cm	kW	n/cm^{2}s	n/cm^{2}s	n/cm^{2}s	n/cm^{2}kJ				cGy/min	cGycm^2/n
93	uallw3	H_2O	0.16	86.1	8.51E+08	1.47E+10	1.88E+08	1.70E+08	0.64	0.66	0.66	15.2	1.72E-11
				0.63%	2.1%	1.2%	2.7%	1.4%	2.7%	1.7%	3.4%	1.3%	1.8%
	uallw4	H_2O	0.5	71.8	6.85E+08	1.14E+10	1.40E+08	1.59E+08	0.63	0.66	0.68	11.8	1.72E-11
				0.71%	2.3%	1.4%	2.9%	1.6%	3.0%	1.9%	3.8%	1.4%	2.0%
	uallw7	H_2O	1	61.2	5.16E+08	8.06E+09	1.08E+08	1.32E+08	0.65	0.66	0.70	8.9	1.83E-11
				0.80%	2.5%	1.7%	2.8%	1.8%	3.3%	2.2%	3.8%	1.6%	2.3%
	ualh10	D_2O	0.16	92.7	9.87E+08	1.72E+10	2.04E+08	1.86E+08	0.65	0.67	0.66	16.9	1.64E-11
				0.61%	1.8%	1.1%	2.8%	1.3%	2.4%	1.5%	3.5%	1.2%	1.7%
	ualhw4	D_2O	0.5	91.3	1.01E+09	1.72E+10	1.83E+08	1.88E+08	0.65	0.66	0.68	15.9	1.54E-11
				0.62%	1.8%	1.2%	2.2%	1.3%	2.4%	1.6%	3.0%	1.2%	1.7%
	ualhw5	D_2O	1	90.4	1.02E+09	1.67E+10	1.71E+08	1.85E+08	0.66	0.66	0.68	14.9	1.48E-11
				0.63%	1.8%	1.2%	2.4%	1.4%	2.4%	1.6%	3.2%	1.3%	1.8%

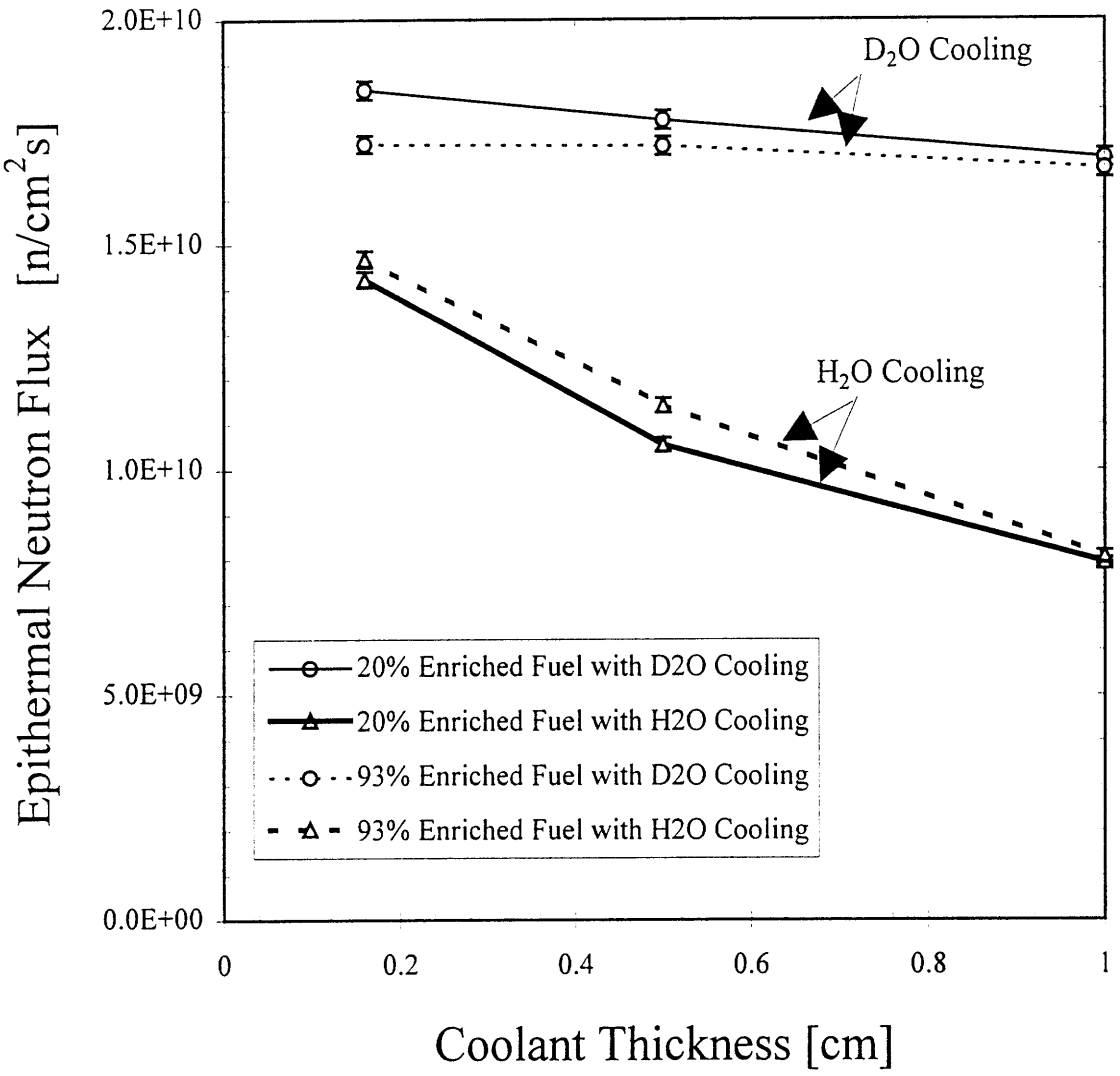

Figure 2.4 Epithermal neutron flux as a function of coolant thickness, coolant type and fuel enrichment for single plate fission converters. These calculations used a fast neutron filter/moderator composed of 68 cm 70% AlF_3/30% Al - 2cm Ti followed by a 0.04 cm Cd thermal neutron filter, an 8 cm thick Bi photon shield and a pyramidal collimator with a 15 cm thick lead lining. The filter/moderator is surrounded by a 10 cm thick lead reflector.

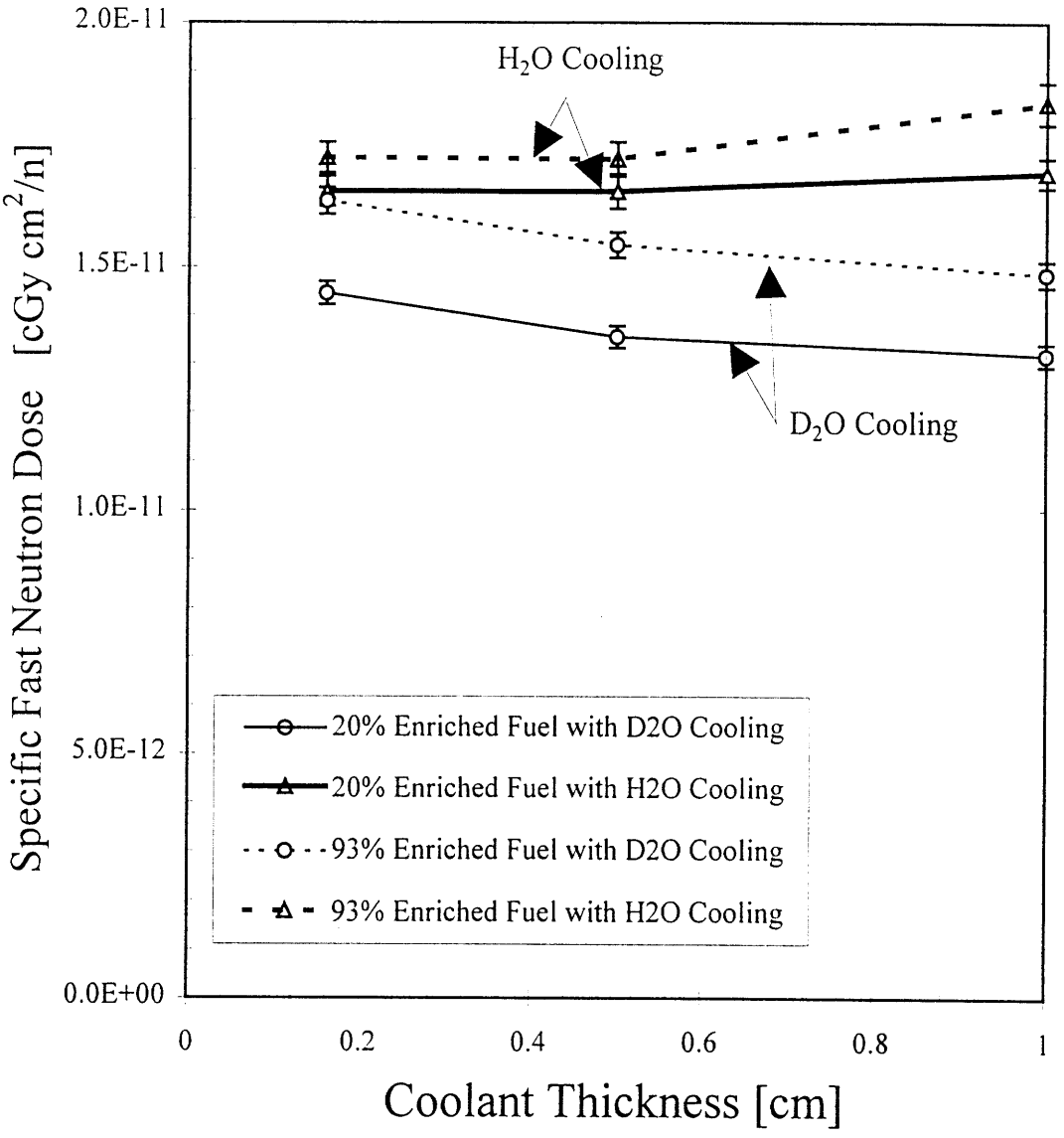

Figure 2.5 Specific fast neutron dose as a function of coolant thickness, coolant type and fuel enrichment for single plate fission converters. These calculations used a fast neutron filter/moderator composed of 68 cm 70% AlF_3/30% Al + 2cm Ti followed by a 0.04 cm Cd thermal neutron filter, an 8 cm thick Bi photon shield, and a pyramidal collimator with a 15 cm thick lead lining. The filter/moderator is surrounded by a 10 cm thick lead reflector.

2.2.1 Performance of Single Plate Fuel Fission Converters

Table 2.1 and Figure 2.4 show that, for both 20% enriched and 93% enriched fuel with H_2O cooling, epithermal neutron flux increases significantly as coolant thickness decreases from 1.0 to 0.16 cm. On the other hand, it increases slightly or does not increase with decreasing coolant thickness for D_2O cooling. This difference in the effect of decreasing coolant thickness on beam intensity between H_2O and D_2O is due to different neutronic properties of these coolants for neutron moderation; i.e., far more rapid moderation is obtained by H_2O than D_2O. The highest epithermal neutron flux for 20% enriched fuel is $1.42*10^{10}$ n/cm^{2}s for H_2O cooling and $1.84*10^{10}$ n/cm^{2}s for D_2O cooling, while for 93% enriched fuel is $1.47*10^{10}$ n/cm^{2}s for H_2O cooling and $1.72*10^{10}$ n/cm^{2}s for D_2O cooling. In Figures 2.4 and 2.5, one can see that D_2O cooling provides significantly higher epithermal neutron flux and somewhat lower specific fast neutron dose than H_2O cooling for single plate fuel as for MITR-II fuel. However, the specific fast neutron dose is very low ($< 2*10^{-11}$ cGycm^2/n), essentially unimportant for either H_2O or D_2O cooling. The differences in epithermal neutron flux and specific fast neutron dose between these two coolants become smaller as coolant thickness is decreased from 1.0 cm to 0.16 cm, which is expected because the effect of moderation of the coolant becomes smaller as its thickness is reduced. It should be noted that single plate fuel with low-enriched or high-enriched uranium gives comparable performance for both H_2O and D_2O cooling, which is an interesting result considering the advantages of using of low-enriched fuel because of security concerns.

Two explanations are meaningful regarding the results. The first one is that Figure 2.5 shows a slightly lower specific fast neutron dose for 20% enriched fuel than for 93 % enriched fuel for D_2O cooling (by around 14%) while showing very small differences between these fuels for H_2O cooling. This effect is related to the difference in the amount of Al in the fuel meat between 20%

enriched fuel and 93 % enriched fuel. Because the amount of Al contained in the fuel meat is larger for the 20% enriched fuel, its effect on fast neutron moderation also is greater for 20% enriched fuel than for 93% enriched fuel; this difference in the effect of Al on fast neutron moderation appears clearly in the case of D_2O cooling. However, in the case of H_2O cooling, this difference is not prominent because H_2O moderates neutrons much more efficiently than Al. This conclusion is supported by the results of the calculations, shown in Table 2.2 using D_2O-cooled 20% or 93% enriched single plate fuel where Al in the fuel meat is removed. For comparison, the results for single plate fuel including aluminum in the fuel meat are also shown in Table 2.2.

Table 2.2 Fission converter power and in-air beam performance for D_2O-cooled single plate fuel fission converters using 20% or 93% enriched fuel with and without aluminum in the fuel meat. The thickness of coolant layers on both sides of the fuel plate is 0.5 cm. These calculations used a filter/moderator composed of 68 cm 70% AlF_3/30% Al + 2 cm Ti followed by an 8 cm thick Bi photon shield and a pyramidal collimator with a 15 cm thick lead lining. The filter/moderator is surrounded by a 10 cm thick lead reflector.

Run ID	Al in the fuel meat*	Enrichment %	Coolant thickness cm	Power kW	Φ_{epi} n/cm^{2}s	Φ_{epi}/P n/cm^{2}kJ	D_{fn} cGy/min	D_{fn}/Φ_{epi} cGycm^2/n
ualhw1	y	20	0.5	104.3 0.6%	1.78E+10 1.2%	1.70E+08 1.3%	14.4 1.3%	1.35E-11 1.7%
ualh7m	n	20	0.5	107.1 0.6%	1.86E+10 1.1%	1.74E+08 1.3%	17.3 1.2%	1.55E-11 1.6%
ualhw4	y	93	0.5	91.3 0.62%	1.72E+10 1.2%	1.88E+08 1.3%	15.9 1.2%	1.54E-11 1.7%
ualh8m	n	93	0.5	92.9 0.6%	1.72E+10 1.2%	1.85E+08 1.3%	16.5 1.2%	1.60E-11 1.7%

* 'y' or 'n' means that Al is contained or not contained in the fuel meat.

In Table 2.2, it is noted that the removal of Al in the fuel meat increases specific fast neutron dose by 15% for 20% enriched fuel while there is only a small change for 93% enriched fuel. As a

result, with Al removed, the specific fast neutron doses for both enrichments become almost equal. This result suggests that Al in the fuel meat of 20% enriched fuel has significant impact on moderation of fast neutrons in the case of D_2O cooling for the beam design used here.

The second thing is that, for the same coolant thickness, the fission converter power of 93% enriched fuel is slightly less than that of 20% enriched fuel although the effect of neutron absorption due to Al and ^{238}U in the fuel meat is expected to be less in 93% enriched fuel. In fact, by comparing the powers of fission converters with and without Al in the fuel meat shown in Table 2.2, it is seen that the existence of Al decreases the fission converter power because of its neutron absorption; therefore, reduction of Al in the fuel meat is expected to increase the fission converter power. The effect which offsets neutron absorption due to Al and ^{238}U and causes higher power for 20% enriched fuel is the increase in the number of thermal neutrons that enter into the fission converter for 20% enriched fuel relative to that for 93% enriched fuel. This is caused by the difference in thickness between 20% and 93% enriched fuel plates; the former is much thicker (5.3 cm) than the latter (1.1 cm). Since the location of the plane between the rear outer-tank wall and the neutron filter/moderator is fixed to keep patient position unchanged, the front surface of the outer tank of a 20% enriched plate fuel fission converter is located 4.2 cm closer to the thermal column than the 93% enriched plate fuel fission converter; therefore, the number of thermal neutrons that impinge on the fission converter is larger for 20% enriched fuel than for 93% enriched fuel. This point was verified by computational results: the thermal neutron current in the direction of the patient position tallied at the front surface of the outer tank is 13% lower for 93% enriched fuel than for 20% enriched fuel. Also, increased neutron leakage from the fuel region for the 93% enriched fuel plate due to its flatter geometry (i.e., larger buckling) might contribute to the power decrease.

2.2.2 Comparison of MITR-II Fuel and Single Plate Fuel Fission Converters

For better comparison of beam performance produced by single flat plate type fuel and multi-plate reactor type MITR-II fuel, the computational results for both types of fuels are summarized in Table 2.3 and in the plot of epithermal neutron flux (ϕ_{epi}) vs. specific fast neutron dose (D_{fn}/ϕ_{epi}) shown in Figure 2.6.

The analysis of a single plate type fission converter with about 7.5 kg of ^{235}U, which is considerably more than 5.6 kg or 3.4 kg of ^{235}U in fresh or burned MITR-II fuel, indicated that the single plate fuel provides an advantage over a fission converter using burned MITR-II fuel for the same coolant because it increases epithermal neutron flux without substantial increases in the specific fast neutron dose for most coolant thicknesses. However, it was also shown that, using the same coolant, the single plate fuel does not improve beam performance relative to the fresh MITR-II fuel because it provides comparable or lower epithermal neutron flux without decreasing the specific fast neutron dose. Moreover, compared with a burned MITR-II fuel fission converter with D_2O cooling, a single plate fission converter with the minimum thickness of H_2O coolant (0.16 cm) increases fast neutron contamination without a commensurate improvement of beam intensity. This result suggests that, even with the minimum thickness, H_2O coolant in a single plate fission converter overmoderates the neutron spectrum relative to D_2O coolant in the MITR-II fuel fission converter; this point is demonstrated clearly by Figure 2.7, which depicts partial neutron current spectra at the interface between the converter coolant and the rear inner tank wall in the direction of the patient position for an H_2O-cooled single plate fuel fission converter with 0.16 cm thick coolant layers and H_2O- or D_2O-cooled burned MITR-II fuel fission converters. It should be noted that, compared with D_2O coolant in the MITR-II fuel fission converter, a very thin layer of H_2O in a single plate fuel fission converter significantly reduces the useful portion of the spectrum

(from the epithermal energy range up to ~100 keV). On the other hand, this single plate fission converter provides an slight advantage of improved beam intensity over an H_2O-cooled burned MITR-II fuel fission converter by increasing the portion of the spectrum above 3 keV.

In Table 2.3, it is noted that, for the same coolant, the single fuel plate fission converter does not increase the power appreciably relative to the fission converter using the fresh MITR-II fuel although the former has significantly more fuel loading than the latter. This is because the latter has enhanced moderation of neutrons relative to the former because of its larger volume fraction of coolant. However, the power of the single plate fuel fission converter decreases as the thickness of the coolant increases. This is likely because the loss of neutrons due to increased absorption in the coolant layer on the upstream side outweighs enhanced neutron moderation caused by increased coolant thickness.

The performance data for the different fuel configurations presented in Table 2.3 and Figure 2.6 indicate the clear superiority of D_2O coolant in terms of beam intensity. Heavy water cooling also provides lower specific fast neutron doses; however, acceptably low fast neutron contamination is also achieved with H_2O coolant.

Table 2.3 Fission converter power and in-air beam performance for different fuel types and coolants with varying fuel loading, enrichment and coolant thickness. In-air figures of merit were calculated at the patient position for a reactor power of 5 MW. The number shown below the coolant type for a single plate fission converter denotes the coolant thickness on both sides of the fuel plate. These calculations used a filter/moderator composed of 68 cm 70% AlF_3/30% Al + 2 cm Ti followed by an 8 cm thick Bi photon shield and a pyramidal collimator with a 15 cm thick lead lining. The filter/moderator is surrounded by a 10 cm thick lead reflector.

Fuel Type	Fuel Loading kg ^{235}U-Total	Coolant	Power kW	ϕ_{epi} n/cm^2·s	D_{fn}/ϕ_{epi} cGy·cm^2/n	ϕ_{epi}/P n/cm^2·kJ
MITR-II fuel elements 93 % Enriched	3.4 Burned Fuel	D_2O	78.1 0.2%	1.3E+10 1%	1.3E-11 2%	1.7E+08 1%
		H_2O	83.1 0.2%	8.5E+09 2%	1.8E-11 2%	1.0E+08 2%
	5.6 Fresh Fuel	D_2O	102.9 0.2%	1.7E+10 1%	1.3E-11 2%	1.6E+08 1%
		H_2O	124.9 0.2%	1.3E+10 1%	1.7E-11 2%	1.0E+08 1%
Single Plate 20% Enriched	7.5	D_2O 0.16 cm	105.2 0.6%	1.8E+10 1%	1.4E-11 2%	1.8E+08 1%
		D_2O 1 cm	102.4 0.6%	1.7E+10 1%	1.3E-11 2%	1.7E+08 1%
		H_2O 0.16 cm	95.1 0.6%	1.4E+10 1%	1.7E-11 2%	1.5E+08 1%
		H_2O 1 cm	67.7 0.7%	7.9E+09 1%	1.7E-11 2%	1.2E+08 1%
Single Plate 93% Enriched	7.7	D_2O 0.16 cm	92.7 0.6%	1.7E+10 1%	1.6E-11 2%	1.9E+08 1%
		D_2O 1 cm	90.4 0.6%	1.7E+10 1%	1.5E-11 2%	1.9E+08 1%
		H_2O 0.16 cm	86.1 0.6%	1.5E+10 1%	1.7E-11 2%	1.7E+08 1%
		H_2O 1 cm	61.2 0.8%	8.1E+09 2%	1.8E-11 2%	1.3E+08 2%

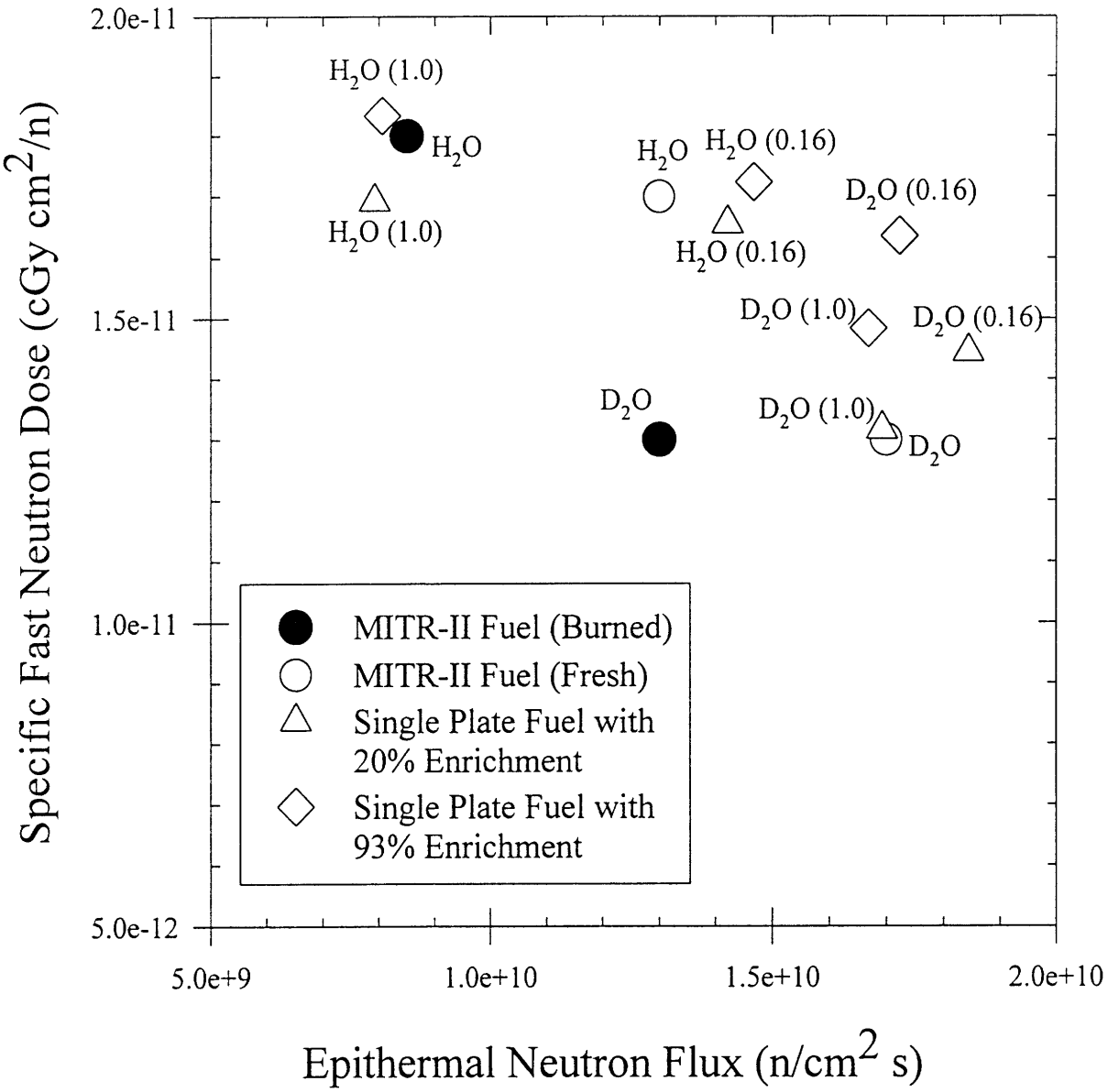

Figure 2.6 Epithermal neutron flux vs. specific fast neutron dose at the patient position for different fuel configurations and coolants. Data labels denote coolant types and, for single plate fuel, coolant thicknesses on both sides of the plate are in parentheses. Statistical uncertainties are less than the size of the data points.

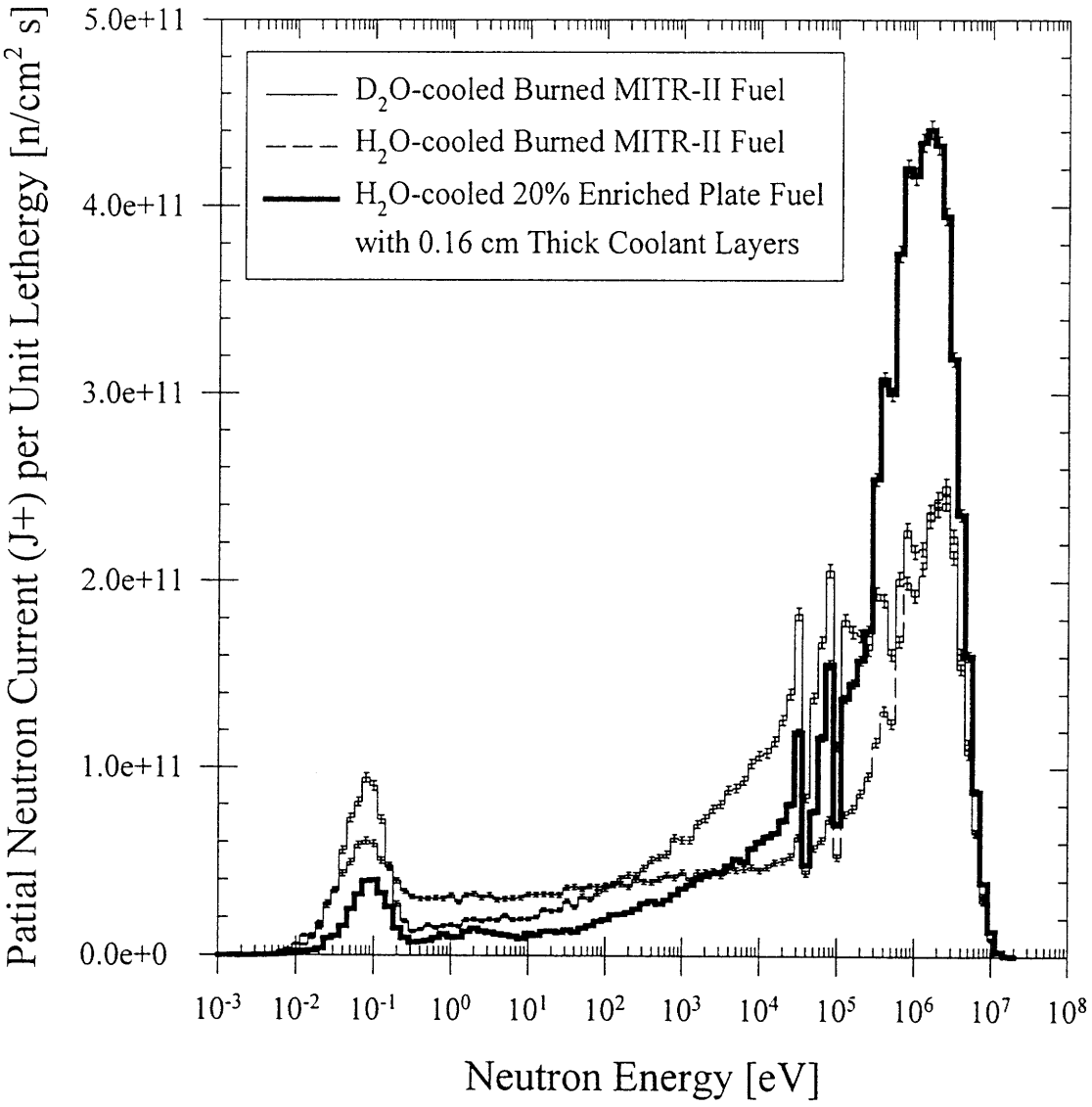

Figure 2.7 Partial neutron current spectra in the direction of the patient position at the interface between the coolant and the inner tank for fission converters using H_2O-cooled 20% enriched single plate fuel with 0.16 cm thick coolant layers, or eleven H_2O- or D_2O-cooled burned MITR-II fuel elements.

2.3 Fuel Spacing in the MITR-II Fuel Fission Converter

Increasing the coolant thickness surrounding the fuel is expected to have the following effects on the neutron spectrum and on power generation in the fission converter: 1) enhanced moderation of high energy neutrons which would soften the neutron spectrum exiting from the fission converter and increase power, 2) reduction of neutron leakage from the fission converter which increases power, 3) greater neutron absorption by the coolant which would result in a power decrease and lower beam intensity. Reference 1 examined the effect of varying D_2O coolant thickness in front of and behind the row of fuel elements. It showed that the epithermal neutron flux decreases approximately in proportion to the fission converter power and the specific fast neutron dose is unchanged as the front layer thickness increases, which is because the absorption of the incident thermal neutrons outweighs enhanced moderation and reduced neutron leakage. Reference 1 also demonstrated that, as the thickness of the back D_2O layer is increased, power increases but epithermal neutron flux decreases rapidly, while the specific fast neutron dose decreases only slowly. This result suggests that with increasing the back layer thickness, enhanced moderation and/or increased absorption reduces the neutron intensity, especially in the slowing down region, and causes a decrease in the epithermal neutron flux at the patient position. As a result, Reference 1 concluded that increases in coolant thickness in front of and behind the fuel elements provide very little improvement in beam performance. However, a significant increase in power per element was observed when the spacing between fuel elements was increased from 0.0998 cm to 0.159 cm in the course of development of the fission converter design, and further study of the effect of fuel spacing was suggested. Therefore, a detailed analysis of fuel spacing was performed in the current study.

A series of calculations was performed using burned MITR-II fuel elements (312 g ^{235}U per element) with varying spacing between fuel elements and varying the number of elements for both D_2O and H_2O cooling. Because the space available for the fuel elements in the fission converter tank is limited, the number of fuel elements was decreased when fuel spacing became large. (One should note that, as the size of the fuel region increases, the space for coolant channels on the sides of the fission converter (i.e., downcomers) has to be reduced, which might not assure enough coolant flow for heat removal.) These calculations employed a fast neutron filter/moderator composed of 68 cm 70% AlF_3/30% Al - 2 cm Ti surrounded a 10 cm thick lead reflector, a 0.04 cm Cd thermal neutron filter, an 8 cm thick Bi photon shield and a pyramidal collimator with a 15 cm thick lead lining. The results of these calculations are shown in Table 2.4 for both D_2O and H_2O cooling. As seen in the table, for both coolants, power of the fission converter using the same number of fuel elements increases as the space between elements increases. This is because enhanced neutron moderation due to increased coolant layer thickness between fuel elements leads to increases in power per element except for the elements at the edges of the fission converter, where the effect of increased loss of neutrons from other fuel elements due to increased fuel spacing outweighs the effect of enhanced moderation. This point is illustrated in Figure 2.8, the plot of power distribution of D_2O-cooled fission converters with 0.16 cm or 1.6 cm spacing between fuel elements. Moreover, from Table 2.4, one can see that power per element increases as the number of elements decreases except for the case of the fission converter using 8 fuel elements with 3.5 cm spacing. As a result, the fission converter power decreases more slowly than the fuel loading as the number of fuel elements is reduced. For example, by comparing the power for 11 fuel elements with 0.16 cm spacing and that for 9 elements with 2 cm spacing, which have comparable size of the fuel region (i.e. almost the same distance between the elements at both edges of the fission converter), it is seen that the fission converter power for the 9 fuel elements is

smaller by 8% for D_2O cooling and by 12% for H_2O cooling relative to that for the 11 fuel elements although the fuel loading is decreased by 18 %. This result is consistent with what was observed in Reference 1 and considered to be due to enhanced neutron moderation and increased fraction of fuel elements illuminated with high thermal flux in the central region of the converter with increasing fuel spacing and decreasing the number of fuel elements.

However, it is seen that increasing fuel spacing does not increase beam intensity although it increases the power per element. Figure 2.9, which depicts the partial neutron current spectra at the interface between the D_2O coolant and the rear inner tank wall in the direction of the patient position for eleven burned MITR-II fuel elements with varying fuel spacing, shows that increasing fuel spacing softens the neutron spectrum exiting from the fission converter; that is, it slightly decreases the slowing down region of the spectrum (above ~ 10 keV) and increases flux in the thermal range. Therefore, it is considered that the effect of softening the spectrum due to enhanced neutron moderation balances the increased neutron generation and leaves beam intensity unchanged. Since increasing the fuel spacing does not improve the beam performance, it was decided to keep the spacing as tight as possible (i.e., 0.16 cm).

Table 2.4 Fission converter power and in-air beam performance for a burned MITR-II fuel fission converter (312 g ^{235}U per element) with H_2O or D_2O cooling and varying spacing between fuel elements. In-air figures of merit were calculated at the patient position for a reactor power of 5 MW. The statistical error (one standard deviation) of each quantity is shown immediately below the value. These calculations used a neutron filter/moderator composed of 68 cm 70% AlF_3/30% Al + 2cm Ti followed by a 0.04 cm Cd thermal neutron filter, an 8 cm thick Bi photon shield and a pyramidal collimator with a 15 cm thick lead lining. The filter/moderator is surrounded by a 10 cm thick lead reflector.

D_2O Cooling

Run ID	# of Fuel Element	Space (cm)	Flow Chan. Area (cm^2)	Power (kW)	Pow. per Ele. (kW)	Φ_{th} (n/cm^2s)	Φ_{epi} (n/cm^2s)	Φ_f (n/cm^2s)	Φ_{epi}/P (n/cm^2kJ)	J_{th}/Φ_{th}	J_{epi}/Φ_{epi}	J_f/Φ_f	D_{fn} (cGy/min)	D_{fn}/Φ_{epi} ($cGycm^2/n$)
spa1016	11	0.16	69.7	78.6	7.15	9.35E+08	1.31E+10	1.13E+08	1.66E+08	0.66	0.66	0.68	10.2	1.30E-11
				0.2%	0.2%	2%	1%	3%	1%	2%	2%	4%	2%	2%
spa1048	11	0.48	59.5	78.9	7.17	9.51E+08	1.31E+10	1.15E+08	1.66E+08	0.65	0.66	0.66	10.3	1.31E-11
				0.2%	0.2%	2%	1%	4%	1%	2%	2%	5%	2%	2%
spa1079	11	0.79	49.4	79.2	7.20	9.53E+08	1.31E+10	1.05E+08	1.65E+08	0.64	0.66	0.70	9.9	1.26E-11
				0.2%	0.2%	2%	1%	3%	1%	2%	2%	4%	2%	2%
spa1159	11	1.59	24.2	79.3	7.21	9.57E+08	1.29E+10	1.05E+08	1.62E+08	0.65	0.66	0.69	9.9	1.28E-11
				0.2%	0.2%	2%	1%	3%	1%	2%	2%	4%	2%	2%
spa0238	10	2.38	28.7	75.3	7.53	9.00E+08	1.21E+10	1.03E+08	1.61E+08	0.64	0.66	0.68	9.4	1.29E-11
				0.2%	0.2%	2%	1%	4%	1%	3%	2%	4%	2%	2%
spa920	9	2	68.3	72.2	8.02	8.80E+08	1.15E+10	9.36E+07	1.60E+08	0.64	0.66	0.69	9.0	1.30E-11
				0.2%	0.2%	2%	1%	3%	1%	3%	2%	4%	2%	2%
spa820	8	2	96.9	67.5	8.44	8.32E+08	1.12E+10	1.02E+08	1.66E+08	0.65	0.66	0.66	8.6	1.29E-11
				0.2%	0.2%	2%	1%	5%	1%	3%	2%	6%	2%	2%
spa835	8	3.5	63.5	67.2	8.40	8.30E+08	1.09E+10	9.88E+07	1.62E+08	0.64	0.66	0.68	8.5	1.29E-11
				0.2%	0.2%	2%	1%	4%	1%	3%	2%	5%	2%	2%

Table 2.4 (Continued)

H_2O Cooling

Run ID	# of Fuel Element	Space (cm)	Flow Chan. Area (cm^2)	Power kW	Pow. per Ele. (kW)	Φ_{th} (n/cm^2s)	Φ_{epi} (n/cm^2s)	Φ_f (n/cm^2s)	Φ_{epi}/P (n/cm^2kJ)	J_{th}/Φ_{th}	J_{epi}/Φ_{epi}	J_f/Φ_f	D_{fn} (cGy/min)	D_{fn}/Φ_{epi} ($cGycm^2/n$)
H2O1016	11	0.16	69.7	82.5 0.2%	7.50 0.2%	5.93E+08 2%	8.39E+09 2%	1.03E+08 3%	1.02E+08 2%	0.63 3%	0.66 2%	0.70 4%	8.5 2%	1.69E-11 2%
H2O1079	11	0.79	49.4	84.7 0.2%	7.70 0.2%	5.72E+08 3%	8.35E+09 2%	1.08E+08 3%	9.87E+07 2%	0.63 3%	0.65 2%	0.69 4%	9.0 2%	1.79E-11 2%
H2O1159	11	1.59	24.2	85.4 0.2%	7.76 0.2%	5.51E+08 2%	7.97E+09 2%	1.10E+08 4%	9.34E+07 2%	0.66 3%	0.67 2%	0.67 5%	8.9 2%	1.85E-11 2%
H2O0238	10	2.38	28.7	77.3 0.2%	7.73 0.2%	5.72E+08 3%	8.35E+09 2%	1.08E+08 3%	1.08E+08 2%	0.63 3%	0.65 2%	0.69 4%	9.0 2%	1.79E-11 2%
H2O920	9	2	68.3	72.7 0.2%	8.08 0.2%	4.80E+08 3%	7.01E+09 2%	8.67E+07 3%	9.64E+07 2%	0.65 3%	0.65 2%	0.69 4%	7.6 2%	1.80E-11 2%
H2O820	8	2	96.9	66.1 0.2%	8.27 0.2%	4.38E+08 3%	6.54E+09 2%	8.46E+07 3%	9.89E+07 2%	0.64 4%	0.65 2%	0.68 4%	7.0 2%	1.79E-11 3%
H2O835	8	3.5	63.5	62.0 0.3%	7.75 0.3%	4.05E+08 3%	5.52E+09 2%	7.72E+07 4%	8.90E+07 2%	0.64 4%	0.67 2%	0.68 5%	6.3 2%	1.91E-11 3%

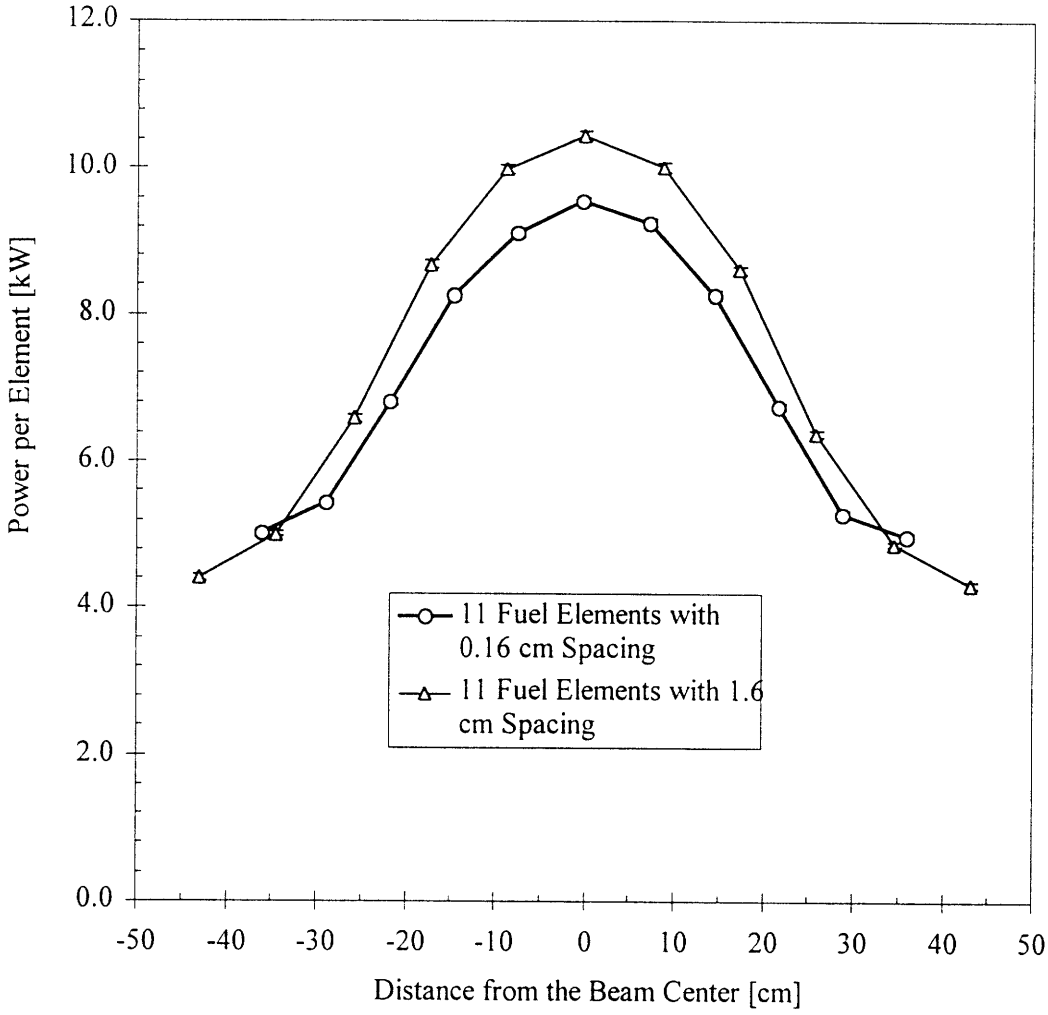

Figure 2.8 Power generation in the D_2O-cooled fission converters composed of eleven burned MITR-II fuel elements with varying fuel spacing. These calculations used a neutron filter/moderator composed of 68 cm 70% AlF_3/30% Al + 2cm Ti followed by a 0.04 cm Cd thermal neutron filter, an 8 cm thick Bi photon shield and a pyramidal collimator with a 15 cm thick lead lining. The filter/moderator is surrounded by a 10 cm thick lead reflector.

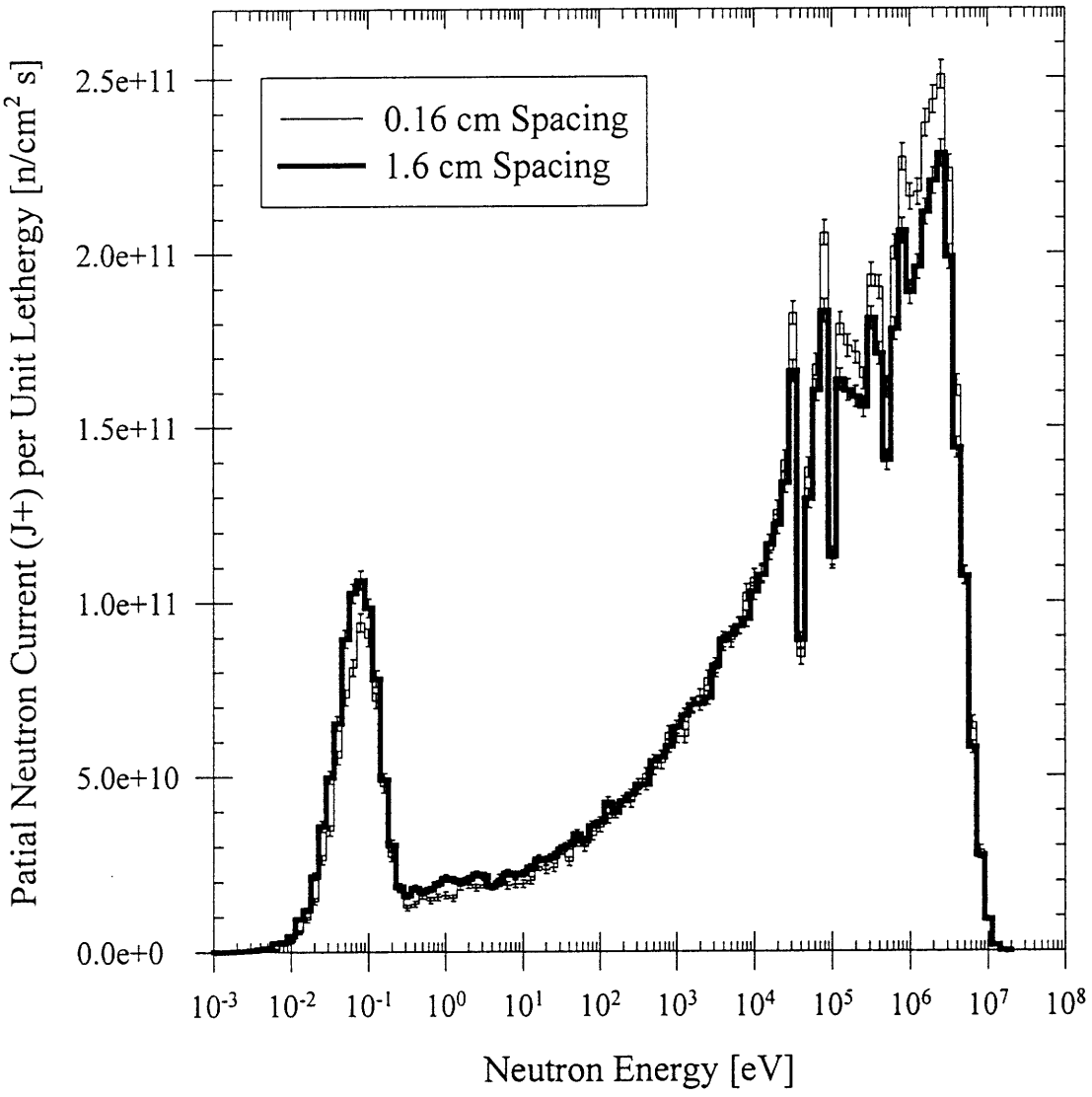

Figure 2.9 Partial neutron current spectra in the direction of the patient position at the interface between the coolant and the rear inner tank wall for fission converters using D_2O-cooled eleven burned MITR-II fuel elements with varying fuel spacing.

2.4 Comparison of In-Phantom Beam Performance for H_2O and D_2O Cooling

Reference 1 showed that the type of coolant affects the neutron spectrum exiting from the fission converter significantly, which results in variations of the epithermal neutron flux, and the specific fast neutron and photon doses at the patient position. It was expected that the type of coolant might affect in-phantom beam performance. Therefore, in-phantom analysis was performed using a fission converter with H_2O cooling and its result was compared with that for D_2O cooling. These calculations used a fission converter composed of eleven burned MITR-II fuel elements (312 g ^{235}U per element) followed by a fast neutron filter/moderator of 68 cm 70% AlF_3/30% Al - 2cm Ti, a 0.04 cm Cd thermal neutron filter, an 8 cm Bi photon shield and a rectangular collimator with a 15 cm thick lead lining. The filter/moderator is surrounded by a 10 cm thick lead reflector. The reactor power was assumed to be 5 MW. The model used here (Run ID - skm314) is identical to that of std475 in Reference 1.

In-air and in-phantom figures of merit for H_2O cooling are compared with those for D_2O cooling in Table 2.5. From this table, it is noted that the ADDR is reduced approximately in proportion to the epithermal neutron flux while AD and AR are unchanged. The trend of the in-phantom figures of merit for different coolants is explained as follows. Figures 2.10 and 2.11 compare the normalized neutron flux spectra at the patient position for H_2O and D_2O cooling in linear and log scales, respectively. These two different scales were used to present the spectra because they emphasize different energy regions. The linear scale accentuates the epithermal energy region and the log scale accentuates the thermal and fast energy regions, where there is a large variation in the flux. The spectra are normalized to one at the maximum tally bin to compare

those shapes. These figures show that the fission converter with H_2O cooling slightly increases the high energy portion of the epithermal energy region and the fast energy region relative to D_2O cooling. However, the specific fast neutron dose for H_2O cooling is still below the design goal. Since this level of fast neutron contamination is negligible compared to the inherent background due to hydrogen and nitrogen capture, beam quality parameters (AD and AR) are unchanged while ADDR is reduced in proportion to beam intensity at the patient position.

Table 2.5 Comparison of in-air and in-phantom figures of merit for H_2O and D_2O-cooled fission converters. These calculations used a fission converter composed of eleven burned MITR-II fuel elements (312 g ^{235}U per element) followed by a fast neutron filter/moderator of 68 cm 70% AlF_3/30% Al - 2cm Ti, a 0.04 cm Cd thermal neutron filter, an 8 cm Bi photon shield and a pyramidal collimator with a 15 cm thick lead lining. The filter/moderator is surrounded by a 10 cm thick lead reflector. The reactor power was set at 5 MW.

Run ID	Coolant Type	Φ_{epi} n/cm^{2}s	J_{epi}/Φ_{epi}	D_{fn}/Φ_{epi} cGycm^2/n	D_γ/Φ_{epi} cGycm^2/n	AD cm	ADDR RBEcGy/min	AR	ADDR/Φepi RBEcGycm^2/n
std473	D_2O	1.30E+10	0.67	1.33E-11	1.02E-11	9.5	435	4.9	5.59E-10
		1.3%	1.7%	1.9%	2.0%				
skm314 (std475)	H_2O	8.51E+09	0.66	1.76E-11	1.06E-11	9.5	282	4.9	5.52E-10
		0.5%	0.7%	0.8%	0.9%				

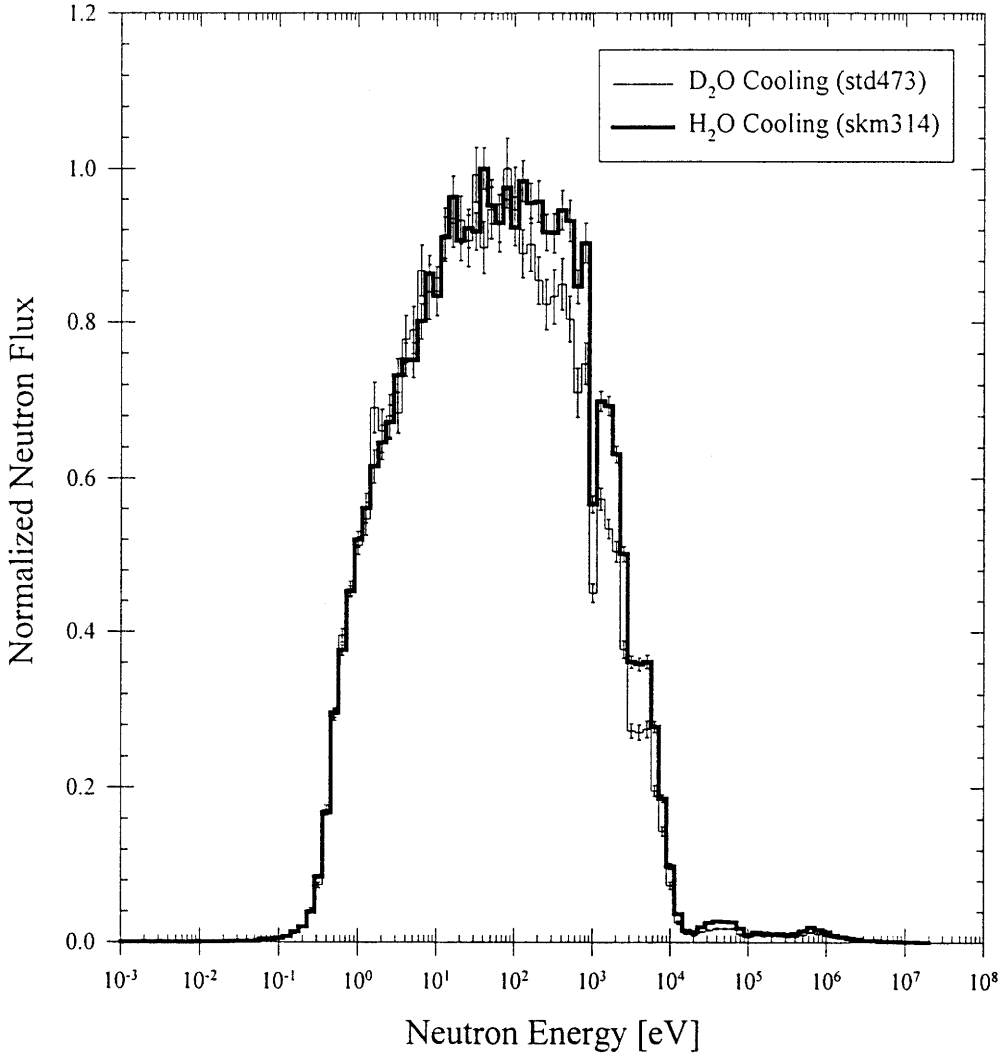

Figure 2.10 Normalized neutron flux spectra at the patient position for H_2O and D_2O cooling in linear scale. These calculations used a fission converter composed of eleven burned MITR-II fuel elements (312 g ^{235}U per element) followed by a fast neutron filter/moderator of 68 cm 70% AlF_3/30% Al - 2 cm Ti, a 0.04 cm Cd thermal neutron filter, an 8 cm Bi photon shield and a pyramidal collimator with a 15 cm thick lead lining. The filter/moderator is surrounded by a 10 cm thick lead reflector. The reactor power was set at 5 MW.

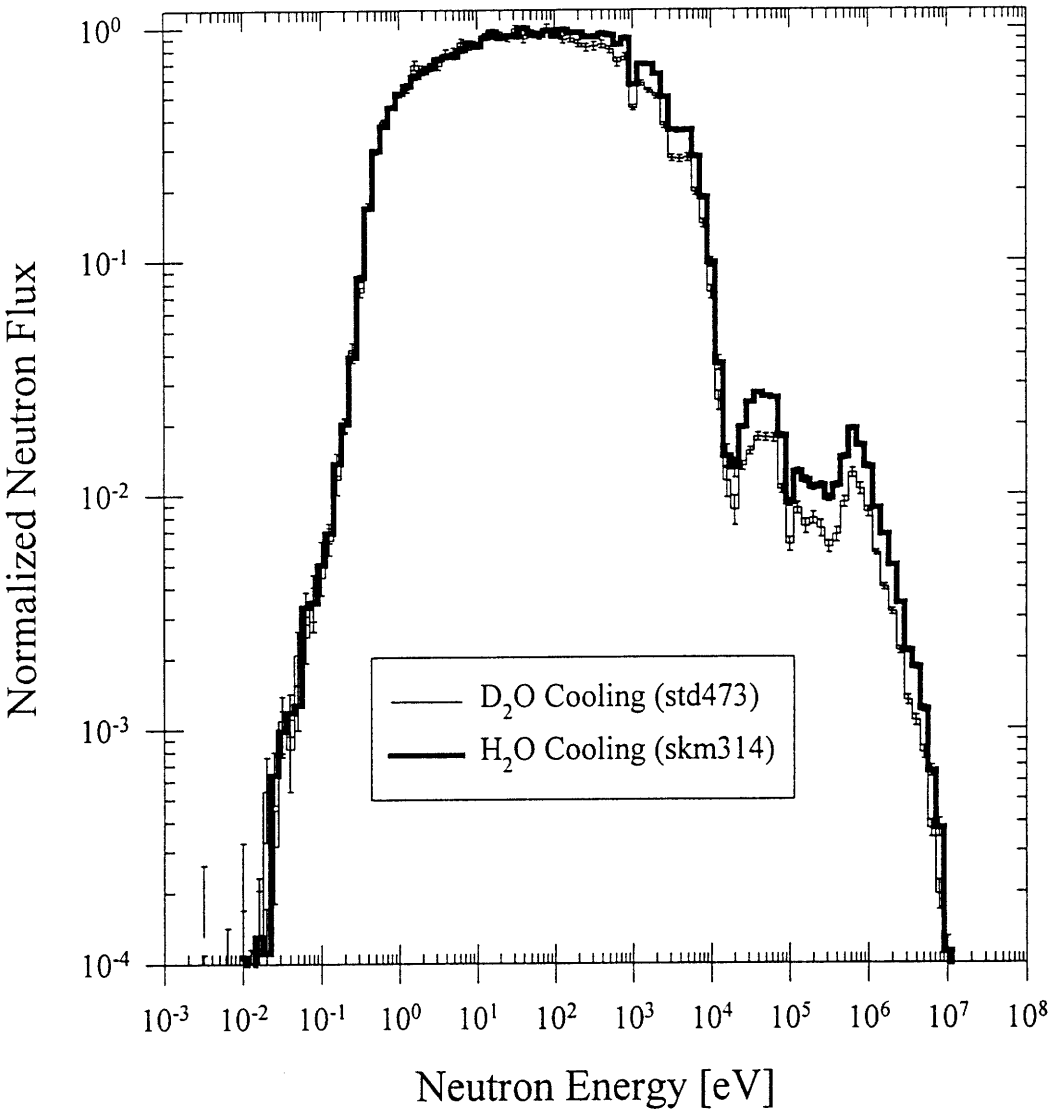

Figure 2.11 Normalized neutron flux spectra at the patient position for H_2O and D_2O cooling in log scale. These calculations used a fission converter composed of eleven burned MITR-II fuel elements (312 g ^{235}U per element) followed by a fast neutron filter/moderator of 68 cm 70% AlF_3/30% Al - 2 cm Ti, a 0.04 cm Cd thermal neutron filter, an 8 cm Bi photon shield and a pyramidal collimator with a 15 cm thick lead lining. The filter/moderator is surrounded by a 10 cm thick lead reflector. The reactor power was set at 5 MW.

2.5 Conclusion

A sensitivity study of the fission converter design was performed using different fuel configurations (multi-plate reactor type MITR-II fuel vs. single flat plate type fuel) and varying fuel spacing for MITR-II fuel fission converters. The analysis of fuel configuration showed that H_2O- or D_2O-cooled single plate fuel fission converters, which have considerably more ^{235}U fuel loading than the MITR-II fuel, do not improve beam performance relative to the fresh MITR-II fuel for the same coolant because it provides comparable or lower epithermal neutron flux without decreasing the specific fast neutron dose. However, it provides an advantage over a burned MITR-II fuel fission converter for most coolant thicknesses. Moreover, in spite of its much lower volume fraction of coolant, an H_2O-cooled single plate fission converter with the minimum coolant thickness (0.16 cm) does not improve beam performance substantially relative to a D_2O-cooled burned MITR-II fuel fission converter. Therefore, it is concluded that both burned and fresh MITR-II fuels are as efficient generators of epithermal neutron beams, especially with D_2O coolant, as the single plate fuel. The studies of the single plate fission converters with low enriched and high enriched uranium indicated comparable performance for both D_2O and H_2O cooling.

The study of the fuel spacing effect showed that increasing spacing between the fuel elements causes power to increase without affecting the epithermal neutron flux and the specific fast neutron dose at the patient position. Considering the effect of varying D_2O coolant thickness on the upstream and downstream sides of the fuel elements analyzed in Reference 1, it is concluded that, because the MITR-II fuel already has a large coolant volume fraction, increases in the thickness of the coolant layers surrounding the fuel elements does not reduce fast neutron contamination enough to offset loss of beam intensity. Therefore, it is not recommended to

increase fuel spacing because it would require additional engineering considerations to avoid bypass flow between the fuel elements without any benefit in terms of beam performance.

The effect of using H_2O coolant on in-phantom figures of merit was also examined in the current study. The result showed that it does not affect AD and AR but does reduce ADDR in proportion to the epithermal neutron flux.

The next chapter will present the results of the sensitivity analyses of the fast neutron filter/moderator and the thermal neutron filter designs, where the effect of varying materials and configurations on in-air and/or in-phantom beam performance will be discussed.

2.6 References

1. W. S. Kiger III, *Neutronic Design of a Fission Converter-Based Epithermal Beam for Neutron Capture Therapy*, Nucl. E. Thesis, Massachusetts Institute of Technology, 1996.
2. B. Sutharshan, Ph. D. Thesis, Massachusetts Institute of Technology, to be published.
3. B. Sutharshan, N. E. Todreas, O. K. Harling, "Fission Converter Heat Removal and Safety Under Accident Conditions", Transactions of ANS, Vol. 75, Nov. 1996.
4. *Reactor Systems Manual*, MITNRL-004, Massachusetts Institute of Technology, 1980.
5. Personal Communication from B. Sutharshan.
6. B. Sutharshan, N. E. Todreas and O. K. Harling, "Fission Converter Based Epithermal Beam - Heat Removal and Safety under Accident Conditions", Proc. 7th Int. Symp. on Neutron Capture Therapy for Cancer, held in Zurich, Switzerland, Sep. 4-7, 1996 (in press).
7. S. Sakamoto, W. S. Kiger, III, O. K. Harling, "Parametric Studies of Coolant, Fuel Configuration, and Enrichment for the MIT Fission Converter-Based Epithermal Neutron Beam", Transactions of ANS, Vol. 75, Nov. 1996.
6. S. Sakamoto, W. S. Kiger, III, O. K. Harling, "Optimization of the Neutronic Design of the MIT Fission Converter Beam", Proc. 7th Int. Symp. on Neutron Capture Therapy for Cancer, held in Zurich, Switzerland, Sep. 4-7, 1996 (in press).

CHAPTER THREE

Sensitivity Study of the Neutron Filter Design - Effect of Variation of the Neutron Spectrum

3.1 Introduction

Among various components of the epithermal neutron beam, the neutron filters (i.e., the fast neutron filter/moderator and the thermal neutron filter) are the ones which require much effort to optimize their designs. There are a number of factors to be considered in selecting the materials and optimizing the configuration of the neutron filters. In terms of neutronics, the fast neutron filter/moderator must have a high resonance scattering cross sections in the fast energy range and a low cross section in the epithermal range to provide windows allowing epithermal neutrons to pass through the filter. Light elements are preferable because of the forward-oriented angular distribution of scattered neutrons in the laboratory frame of reference and greater energy loss per collision relative to heavy elements. The thermal neutron filter should absorb thermal neutrons efficiently while transmitting epithermal neutrons with little attenuation. For both types of filters, production of gamma rays has to be minimized. Desirable engineering characteristics for the filter/moderator materials are that they do not undergo phase changes, decompose, or emit toxic substances in the high radiation field and potentially elevated temperature environment. Materials which accumulate long-term radioactivity should be avoided because they may cause difficulty in beam modifications and decommissioning. The effect of impurities or hydration of the commercially available materials on the beam performance should be taken into account.

Furthermore, the cost of materials and component fabrication is also an important factor in actual planning of the beam construction. The physical form (i.e., single, combination or mixture), dimension and arrangement (i.e., order) of the materials are also to be optimized, depending on the neutronic and engineering characteristics of the selected materials.

For the fast neutron filter/moderator, various materials and their combinations/mixtures have been extensively examined (for example, see References 1, 2 ,3 and 4). In Reference 5, several materials including Al, D_2O, Ti, Al_2O_3, AlF_3, S, Al_2S_3 were selected for detailed analysis based on the experience of the epithermal beam development at MIT, the knowledge of the previous studies and the survey of neutronic and engineering properties of various candidate materials. Beam performance of filter/moderator designs using single materials and combinations/mixtures of these materials were examined using in-air figures of merit, i.e., epithermal neutron flux (Φ_{epi}), specific fast neutron and photon doses (D_{fn}/Φ_{epi} and D_{γ}/Φ_{epi}) at the patient position. As a result of these analyses, Reference 5 proposed the design of the fast neutron filter/moderator shown in Figure 1.4, which consists of a homogeneous mixture of 70% AlF_3 /30% Al (by volume, where 96% theoretical density is assumed) with a thickness of 68 cm and 2 cm thick Ti. As mentioned in Chapter 1, this design provides an epithermal neutron beam with high intensity and high quality in terms of both in-air and in-phantom beam performance.

It is expected that the neutron spectrum is significantly affected by the filter/moderator design. Different filter/moderator materials, compositions and arrangements vary in-phantom figures of merit, as suggested by the previous studies.[2,9] The effect of different neutron energies on in-phantom beam performance has been examined using ideal beams;[3,6] these studies provide insight to estimate the effect of variation of neutron spectrum on in-phantom beam performance. Based on these considerations, it is desirable to optimize the design of the fast neutron filter/moderator by examining the variation of the neutron spectrum for different designs and its effect on in-phantom

beam performance.

The current study performed a series of sensitivity analyses of the fast neutron filter/moderator making use of this approach. These analyses first examined the filter/moderator designs using the combinations of Al and Al_2O_3 or Al and AlF_3. These were selected due to their excellent neutronic behavior and/or stability in the high radiation field and high temperature environment. In addition to these materials, new candidate materials, i.e. polytetrafluoroethene - Teflon, $(CF_2)_n$[7], carbon and lead fluoride, PbF_2[8], were included in the scope of the analyses. Ti was also used in some calculations. Following parametric studies of different combinations of the materials based on in-air figures of merit, some promising designs of the fast neutron filter/moderator were selected and further analyzed in terms of in-phantom beam performance while paying attention to the variation of the neutron spectrum. Moreover, the thermal neutron filter design was also studied to examine alternative designs which could result in reduction or elimination of photon contamination due to radiative capture by Cd.

The parametric studies of the fast neutron filter/moderator designs based on in-air beam performance will be discussed in Section 3.2. Section 3.3 will present the results of the in-phantom analyses for selected filter/moderator designs. In Section 3.4, the alternative designs for the thermal neutron filter using Li and Cd will be discussed. All the calculations used a fission converter composed of eleven burned MITR-II fuel elements (312 g ^{235}U per element) with D_2O cooling in a double-walled aluminum tank (illustrated in Figure 2.1 and 2.2), a 10 cm thick lead reflector surrounding the fast neutron filter/moderator and a pyramidal collimator with a 15 cm thick lead lining. An 8 cm thick Bi photon shield was used unless it is specifically noted that a different one was used. The theoretical density of the filter/moderator materials used here was assumed to be 100% unless stated otherwise. The reactor power was set at 5 MW. The schematic view of the beam showing the components to be varied in this chapter is presented in Figure 3.1. The patient

position was fixed at the entrance of the hohlraum (i.e., the edge of the permanent reactor shielding block), 303 cm from the center of the reactor core, to assure adequate flexibility of patient positioning.

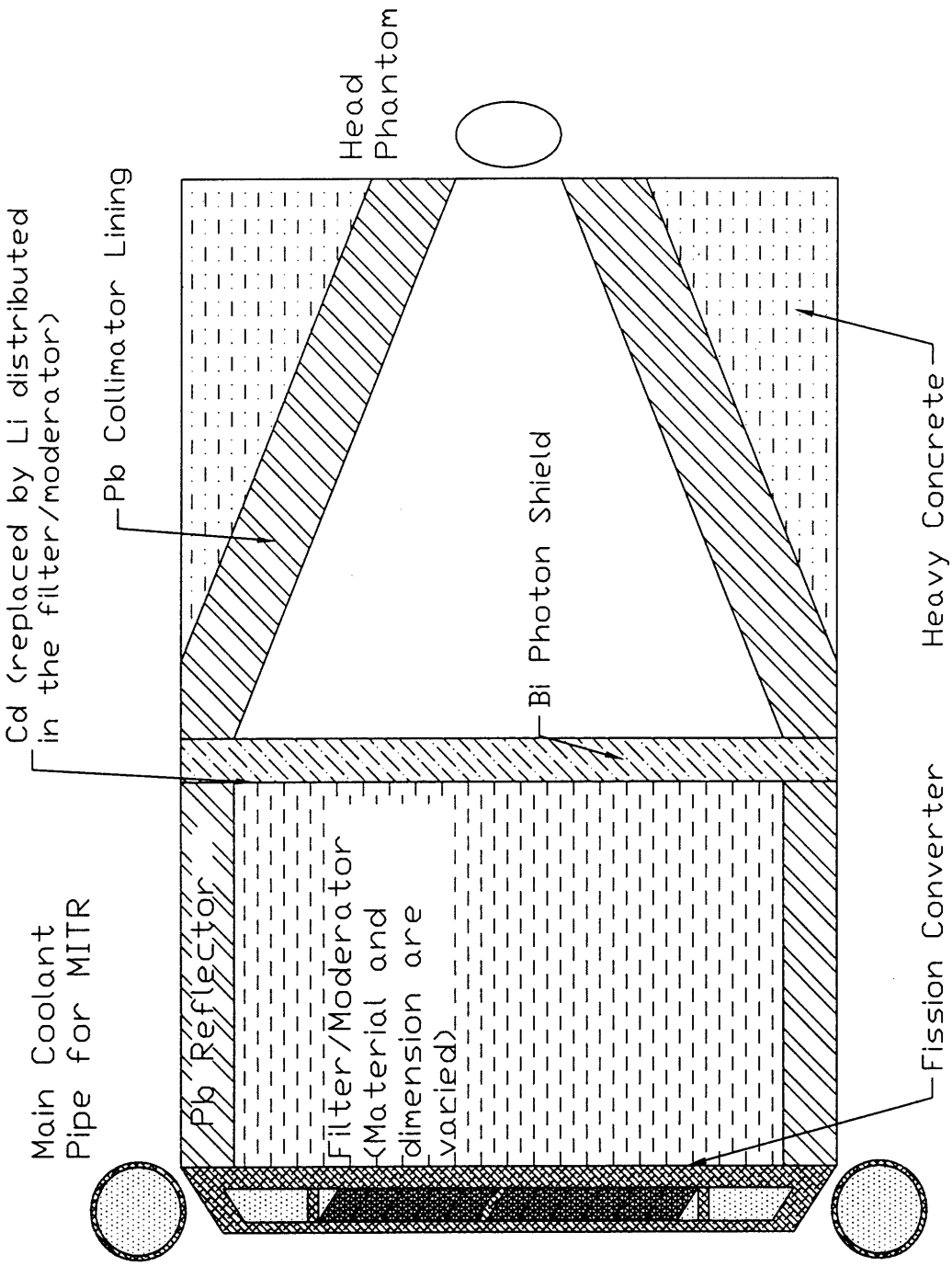

Figure 3.1 Schematic view of the fission converter beam design used in the sensitivity analysis of the neutron filter design, where the components to be varied are shown.

3.2 Analysis of the Fast Neutron Filter/Moderator

In this section, the effect of arrangement (i.e. order) of filter/moderator materials on beam performance will be discussed first. Then, the results of sensitivity analyses for different combinations of the selected filter/moderator materials (aluminum, aluminum oxide, aluminum fluoride, Teflon, carbon, and lead fluoride) based on in-air beam performance will be presented.

3.2.1 Effect of the Arrangement or Ordering of Filter/Moderator Materials

There are two physical forms for multiple filter/moderator materials to be arranged in a fast neutron filter/moderator; i.e., mixtures vs. separate blocks. For the latter form, the order of the materials is a parameter to be optimized in the filter/moderator design. Auterinen *et.al.* analyzed fast neutron filter/moderators composed of single and mixtures of the materials.[2,9] Idaho National Engineering Laboratory (INEL) proposed a fast neutron filter/moderator model which is equivalent to a homogeneous mixture of aluminum, lithiated aluminum and Teflon.[7] On the other hand, Brookhaven National Laboratory (BNL) studied the fast neutron filter/moderator designs using single or combinations of D_2O, Al, and Al_2O_3 for an epithermal neutron beam with ^{235}U fission plates; they found that a 48 cm thick Al block followed by a 24 cm Al_2O_3 block was an optimum combination[11]. Although these papers proposed various types of materials and their arrangements for the filter/moderator design, they have not discussed the effect of the arrangement (i.e. order) of the materials on beam performance, which would affect the process of optimization of the design in terms of neutronics and engineering. Therefore, this effect was analyzed by examining the change of in-air beam performance and neutron spectrum for different arrangements using the combinations of Al-Al_2O_3 and Al-AlF_3.

As presented below, the results of this analysis indicated that, using the same amount of aluminum and fluorine or oxygen, the relative location or ordering of these components significantly affects the neutron spectrum exiting from the fast neutron filter/moderator. Figure 3.2 depicts the partial neutron current spectra in the direction of the patient position at the interface between the Cd thermal neutron filter and a fast neutron filter/moderator composed of 71 cm thick Al and 27 cm thick AlF_3 (2115 kg Al and 858 kg AlF_3) with varying arrangement, i.e., varying the form (homogeneous mixture vs. separate blocks) and the order of Al and AlF_3. The in-air figures of merit for these filter/moderator designs are given in Table 3.1. It is noted that the neutron spectrum becomes harder as fluorine nuclei are moved upstream (i.e. toward the fission converter), which results in higher epithermal neutron flux and specific fast neutron dose at the patient position; when the AlF_3 block is located on the upstream side and followed by the Al block, the spectra show peaks around energies which correspond to the dips of the resonance peaks of Al (e.g. 25 keV). The same trend is seen in Figure 3.3, which depicts the partial neutron current spectra produced by the filter/moderator designs using 83 cm thick Al and 19 cm thick Al_2O_3 (2473 kg Al and 831 kg Al_2O_3) with varying arrangement (the in-air figures of merit for these designs are presented in Table 3.2). These results suggest that neutrons passing through the dips of resonance peaks of aluminum are moderated more efficiently when more fluorine or oxygen nuclei are located behind or downstream of the aluminum. In other words, in terms of fast neutron moderation, fluorine or oxygen nuclei can be used more efficiently by locating them on the downstream side (i.e. on the side of the patient). Also, they indicate that fluorine and oxygen have a significant effect on neutron moderation; therefore, to some extent, we can adjust the shape of the neutron spectrum by varying the amount of these complementary elements. From engineering considerations, the arrangement locating fluorine-containing materials (e.g. AlF_3) downstream of the aluminum provides an advantage. Because the fluorine-containing material is shielded and

insulated from the fission converter by a large amount of aluminum, the radiation level and temperature would be significantly lower in the fluorine-containing material where decomposition of the material and resulting release of very active fluorine have to be avoided. In addition, compared to a homogeneous mixture or a structure equivalent to it (e.g., assembly of many thin layers), the design using separate blocks might save fabrication cost by eliminating the need for mixing different types of materials (e.g., metal and ceramic in the case of Al and Al_2O_3) or save the labor required to assemble a number of thin layers of different materials. Based on these considerations, the arrangement which has an aluminum block followed by materials containing complementary elements (fluorine, oxygen or carbon) was selected for the following analyses of the fast neutron filter/moderator.

Table 3.1 In-air beam performance for the fast neutron filter/moderator composed of 71 cm thick Al and 27 cm thick AlF_3 (2115 kg Al and 858 kg AlF_3) with varying arrangement. For the mixture of these materials, 100% theoretical density is assumed. The material listed on the left hand side is adjacent to the fission converter. These calculations used a fission converter composed of eleven burned MITR-II fuel elements (312 g ^{235}U per element) with D_2O cooling. The fast neutron filter/moderator is followed by a 0.04 cm Cd thermal neutron filter, an 8 cm Bi photon shield and a pyramidal collimator with a 15 cm thick lead lining, and is surrounded by a 10 cm thick lead reflector. The reactor power was set at 5 MW.

Run ID	Filter/Moderator Arrangement	Power kW	Φ_{th} n/cm²s	Φ_{epi} n/cm²s	Φ_f n/cm²s	J_{th}/Φ_{th}	J_{epi}/Φ_{epi}	J_f/Φ_f	D_{fn} cGy/min	D_{fn}/Φ_{epi} cGycm²/n
skm308	71cm Al - 27cm AlF_3	70.3	9.76E+08	1.30E+10	2.36E+08	0.61	0.63	0.64	9.3	1.19E-11
		0.1%	2.5%	1.4%	4.2%	3.0%	1.9%	5.4%	1.8%	2.3%
skm448	98cm Al(72%)/AlF_3(28%)	74.0	8.30E+08	1.40E+10	3.32E+08	0.63	0.64	0.66	11.0	1.31E-11
		0.2%	2.2%	1.4%	3.5%	3.0%	1.8%	4.5%	1.6%	2.1%
skm449	27cm AlF_3 - 71cm Al	80.9	7.93E+08	1.60E+10	9.74E+08	0.63	0.64	0.65	22.2	2.30E-11
		0.2%	2.4%	1.3%	2.5%	3.3%	1.7%	3.4%	1.8%	2.2%

Table 3.2 In-air beam performance for the fast neutron filter/moderator composed of 83 cm thick Al and 19 cm thick Al_2O_3 (2473 kg Al and 831 kg Al_2O_3) with varying arrangement. For the mixture of these materials, 100% theoretical density is assumed. The material listed on the left hand side is adjacent to the fission converter. These calculations used a fission converter composed of eleven burned MITR-II fuel elements (312g ^{235}U per element) with D_2O cooling. The fast neutron filter/moderator is followed by a 0.04 cm Cd thermal neutron filter, an 8 cm Bi photon shield and a pyramidal collimator with a 15 cm thick lead lining, and is surrounded by a 10 cm thick lead reflector. The reactor power was set at 5 MW.

Run ID	Filter/Moderator Arrangement	Power kW	Φ_{th} n/cm²s	Φ_{epi} n/cm²s	Φ_f n/cm²s	J_{th}/Φ_{th}	J_{epi}/Φ_{epi}	J_f/Φ_f	D_{fn} cGy/min	D_{fn}/Φ_{epi} cGycm²/n
AlO27	83cm Al - 19cm Al_2O_3	70.6	8.99E+08	1.17E+10	2.90E+08	0.62	0.64	0.66	9.7	1.39E-11
		0.2%	2.1%	1.4%	3.6%	2.7%	1.9%	4.6%	1.9%	2.4%
AlO28	102cm Al(81%)/Al_2O_3(19%)	73.2	7.54E+08	1.32E+10	5.26E+08	0.62	0.63	0.65	14.2	1.80E-11
		0.2%	2.4%	1.4%	2.9%	3.1%	1.8%	3.7%	1.8%	2.3%
AlO26	19cm Al_2O_3 -83cm Al	79.9	6.37E+08	1.41E+10	1.59E+09	0.64	0.64	0.65	30.7	3.63E-11
		0.2%	2.5%	1.3%	2.0%	3.3%	1.8%	2.7%	1.5%	2.0%

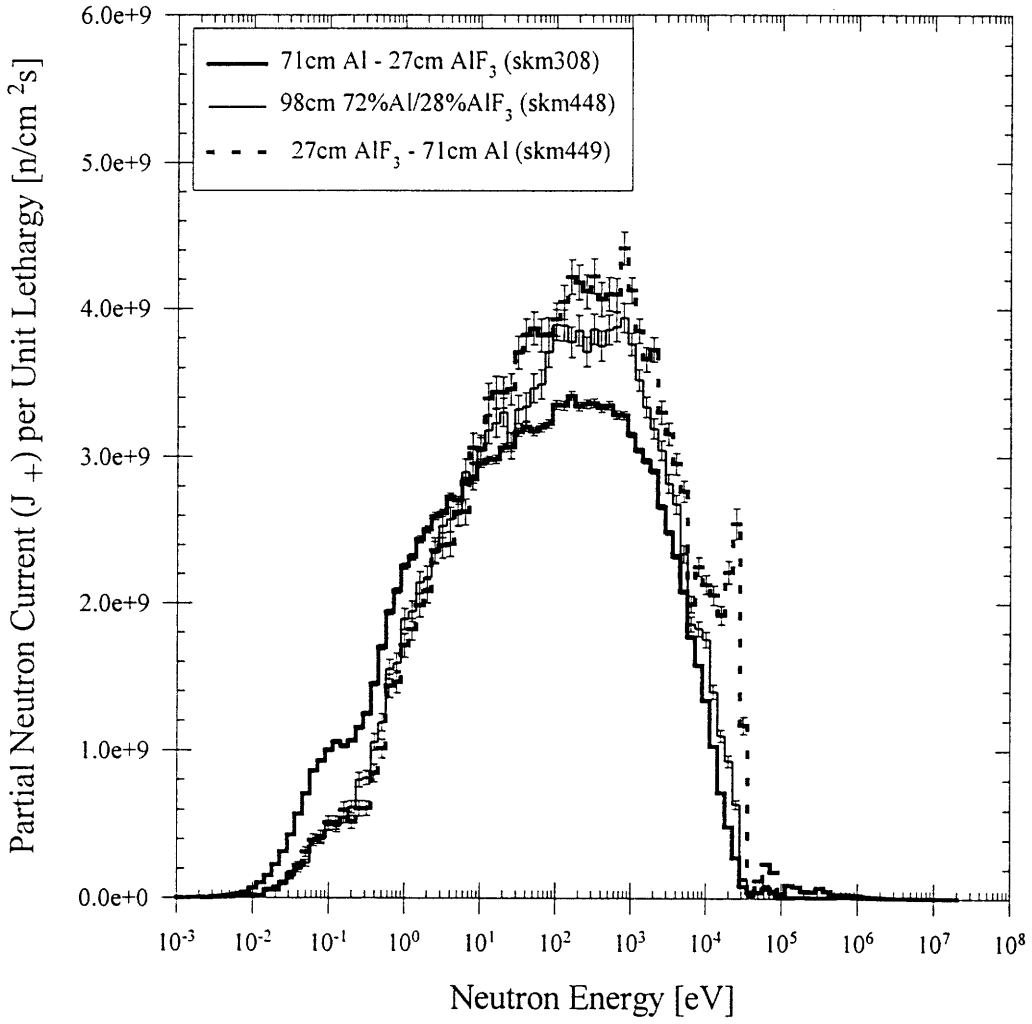

Figure 3.2 Partial neutron current spectra in the direction of the patient position at the interface between the fast neutron filter/moderator and the Cd thermal neutron filter. The fast neutron filter/moderator is composed of 71 cm thick Al and 27 cm thick AlF_3 (2115 kg Al and 858 kg AlF_3) with varying arrangements or ordering.

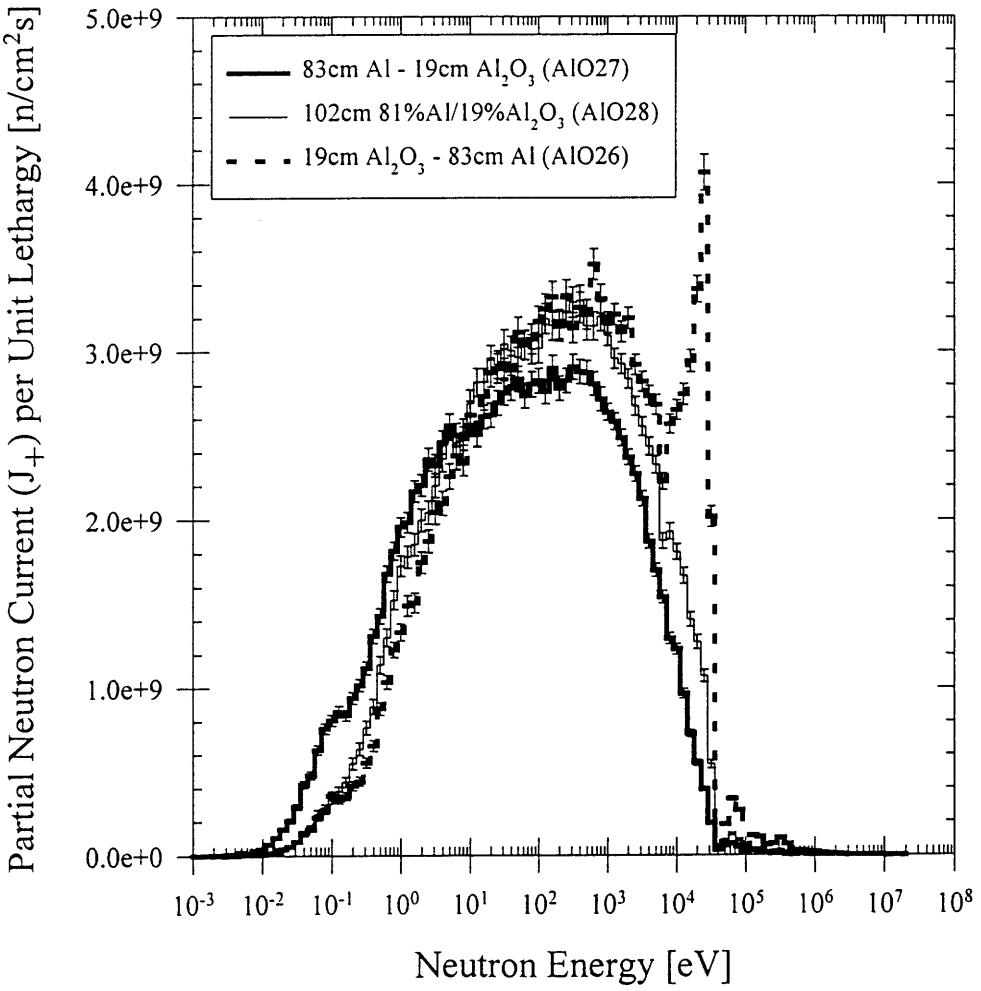

Figure 3.3 Partial neutron current spectra in the direction of the patient position at the interface between the fast neutron filter/moderator and the Cd thermal neutron filter. The fast neutron filter/moderator is composed of 83 cm thick Al and 19 cm thick AlF_3 (2473 kg Al and 831 kg AlF_3) with varying arrangements or ordering.

There is one more thing to be mentioned about the analysis of different arrangements. Tables 3.1 and 3.2 show that the fission converter power increases as AlF_3 or Al_2O_3 is moved upstream toward the fuel. This is due to increased reflection of neutrons back to the fission converter by the filter/moderator with AlF_3 or Al_2O_3 adjacent to the fission converter. As shown in Table 3.3, the macroscopic total cross sections of AlF_3 and Al_2O_3 averaged over different energy ranges (thermal, epithermal and fast ranges) with the spectrum of the fission converter beam[5] are greater than that of Al. Therefore, neutron reflection from the filter/moderator is increased as AlF_3 or Al_2O_3 is moved toward the fission converter. This point is clearly illustrated in Figure 3.4, which depicts the partial neutron current spectra in the upstream (i.e. backward) direction at the interface between the converter coolant (D_2O) and the rear inner tank wall for the fast neutron filter/moderator designs using 83 cm Al + 19 cm Al_2O_3 with varying arrangement.

Table 3.3 Macroscopic total cross sections of AlF_3 and Al_2O_3 averaged with the spectrum of the fission converter beam. Microscopic total cross sections from Reference 5 were used. Thermal cross sections are for 0.025 eV and epithermal and fast cross sections are averaged over the ranges of 1 eV to 10 keV and 10 keV to 5 MeV, respectively.

	Thermal (0.025eV) 1/cm	Epithermal 1/cm	Fast 1/cm
Al	0.099	0.093	0.18
AlF_3	0.28	0.26	0.26
Al_2O_3	0.37	0.34	0.32

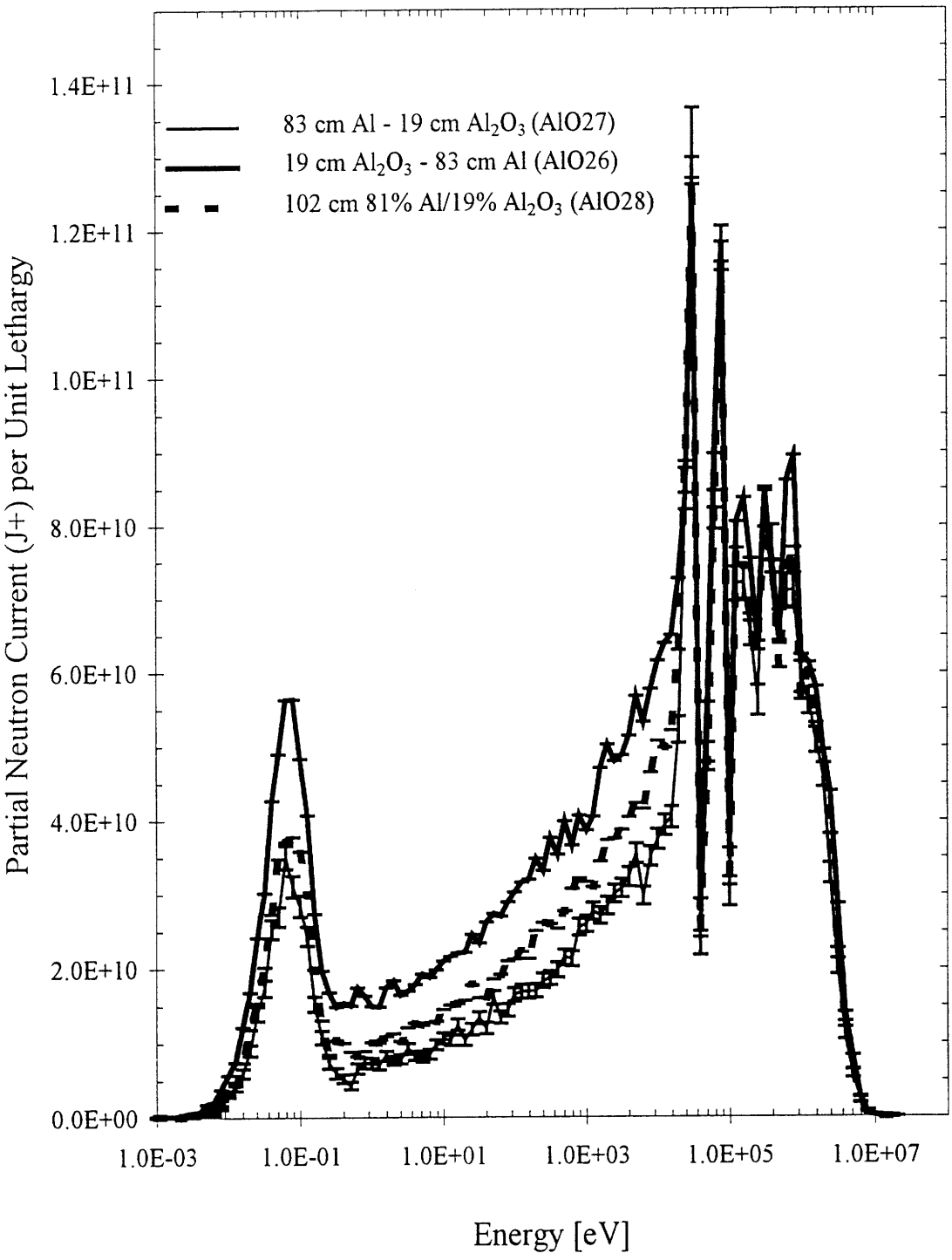

Figure 3.4 Partial neutron current spectra at the interface between the converter coolant (D_2O) and the rear inner tank wall in the upstream (i.e. backward) direction for the fast neutron filter/moderators composed of 83 cm Al + 19 cm Al_2O_3 with varying arrangements.

3.2.2 Sensitivity Analysis of the Fast Neutron Filter/Moderator Using Combinations of Aluminum and Fluorine or Oxygen Containing Materials or Carbon

Section 3.2.1 identified the arrangement of the filter/moderator materials composed of an aluminum block followed by the materials containing complementary elements (F, O or C) as the one to be primarily investigated. This section will discuss the results of parametric studies of the fast neutron filter/moderator design using this arrangement in terms of in-air beam performance. The parameters examined in this analysis are the type and the dimension of the filter/moderator materials. One should note that, in the case of the MIT fission converter beam, the total thickness of the fast neutron filter/moderator can be varied significantly as well as the thickness of each material block because of the large space available between the fission converter and the patient position (180 cm).

Four basic combinations of the selected filter/moderator materials were considered in this analysis; that is, Al - Al_2O_3, Al - AlF_3 and Al - $(CF_2)_n$ and Al - C. In addition, designs which replace a part of fluorine containing materials (AlF_3 or $(CF_2)_n$) with PbF_2 were also examined. In these designs, the 8 cm thick Bi photon shield was also replaced with PbF_2 because it can be used as the photon shield. The following is the consideration regarding the features of the selected materials.

(1) Combination of Al and Al_2O_3

The combination of Al and Al_2O_3 has been investigated as a fast neutron filter/moderator for many years.[4,12] In Reference 4, Al_2O_3 was identified as a good fast neutron filter/moderator because of its well-known engineering properties, reasonable price with high purity, physical and chemical stability in the high temperature and high level radiation environment as well as good neutronic performance. The environmental compatibility of Al_2O_3 primarily motivated the study

of this combination.

(2) Combination of Al and AlF_3

Auterinen *et.al*[2,9] examined almost all elements with reasonably low thermal neutron absorption (16 elements) and many of their mutual compounds. Among the tested materials, they identified the fluorine-containing materials, i.e., AlF_3, PbF_2, CaF_2, $CaSiF_6$, MgF_2, as the best candidates. Moreover, they found that the optimized mixture of Al and AlF_3 is superior to other tested materials. As a result of their extensive study, they developed a metal/ceramic composite which consists of a mixture of Al and AlF_3 called FLUENTAL as a commercial product for a fast neutron filter/moderator material; it is patented in Finland and an international patent for it is pending.[10] The superiority of the fast neutron filter/moderator composed of a combination of Al and AlF_3 to that composed of a combination of Al and Al_2O_3 has also been indicated by Liu.[8]

Although Auterinen *et. al.* claimed that FLUENTAL has adequate mechanical strength and high resistance to irradiation for long-term use under very demanding conditions,[10] it is desirable to place AlF_3 as far from the neutron source as possible and have other chemically stable materials between them to reduce the radiation level in AlF_3 for avoiding its decomposition and emission of fluorine. The arrangement of an Al block followed by an AlF_3 block meets this goal and potentially reduces fabrication cost as discussed in Section 3.2.1. As for the commercial product of AlF_3 such as is used in the aluminum industry, one should be aware of the problem of its hydration. To avoid degradation of beam performance, H_2O contained in AlF_3 has to be removed by a method such as heating before fabrication.

(3) Combination of Al and $(CF_2)_n$

The use of Teflon, $(CF_2)_n$, was proposed by INEL for the design of the Washington State

University (WSU) epithermal neutron beam extraction facility for BNCT.[7] This study considered a filter/moderator design composed of thin plates of aluminum, lithiated aluminum and Teflon (0.635 cm each), which is neutronically equivalent to the homogeneous mixture of these materials.[7] Teflon has a significant advantage as a filter/moderator material because it is available for a relatively low price with high purity. If it provides adequate beam performance, it would be a promising candidate.

However, Teflon has a big disadvantage too; that is, Teflon is vulnerable to radiation damage, which results in decomposition and release of fluorine. To avoid the release of fluorine, INEL proposed to sandwich a Teflon plate with two aluminum plates so that gaseous fluorine emitted from Teflon will be bond immediately to the adjacent aluminum plates. Although this idea is expected to work, an arrangement with a Teflon block located behind a thick aluminum block would provide an additional safety measure to mitigate the problem.

(4) Combination of Al and carbon

Carbon was selected as a result of the study of the combination of Al - $(CF_2)_n$, where it was shown that carbon in $(CF_2)_n$ contributes to reduction of fast neutron contamination. This combination is very attractive for two reasons: first, carbon is a very stable material and its physical and chemical properties are well-known; second, high-purity reactor grade graphite is available at the MIT Nuclear Reactor Laboratory so that this combination would allow significant reduction of the cost for the filter/moderator.

The results of the calculations for fast neutron filter/moderator designs using the first three combinations of materials are summarized in Table 3.4 for Al-Al_2O_3, Table 3.5 for Al-AlF_3, and Table 3.6 for Al-$(CF_2)_n$. For these combinations, the plots of epithermal neutron flux (Φ_{epi}) vs.

specific fast neutron dose (D_{fn}/Φ_{epi}) are also shown in Figure 3.5 (Al - Al_2O_3), Figure 3.6 (Al - AlF_3) and Figure 3.7 (Al - $(CF_2)_n$) . In the tables and figures, the in-air beam performance for the 'final' beam design (std473) proposed in Reference 5, which uses the fast neutron filter/moderator composed of 68cm 70% AlF_3/30% Al (96% theoretical density) and 2 cm Ti, is also included for comparison.

These results show that Al_2O_3, AlF_3, $(CF_2)_n$ are very powerful filter/moderator materials. For example, comparing the result for 72 cm Al (Run ID - AlO12) with that for 48 cm Al - 24 cm Al_2O_3 (Run ID - AlO2), the replacement of 24 cm Al with the same thickness of Al_2O_3 reduces the specific fast neutron dose by a factor of ~7 while decreasing the epithermal neutron flux only by a factor of 2. The comparison between the results for 72 cm Al (AlO12) and 41cm Al - 27 cm AlF_3 (Run ID - AlFTi8) also shows a great reduction of fast neutron contamination by a factor of ~ 6 while decreasing the epithermal neutron flux by only ~ 20% when 31 cm Al was replaced with 27 cm AlF_3. In addition, by replacing 32.6 cm of 72cm Al with 39.6 cm $(CF_2)_n$ to make a filter/moderator composed of 39.4 cm Al - 39.6 cm $(CF_2)_n$ (Run ID - skm430), the specific fast neutron dose is decreased by a factor of ~ 10 while beam intensity is decreased by a factor of 4. Using these materials, one can make many designs of the fast neutron filter/moderator which meet design goals of beam intensity and fast neutron contamination as shown in the tables. Although the specific photon doses were not calculated for all the designs, the results for some of the designs suggests that most of these designs produce photon contamination less than $2*10^{-11}$ $cGycm^2/n$ (Table 3.9 which will be presented below shows the specific photon doses for several designs). However, the results also show a clear trade-off between beam intensity and fast neutron contamination for all the combinations; that is, as the specific fast neutron dose is reduced, the epithermal neutron flux is also decreased. The comparison of the results for 48 cm Al - 24 cm

Al_2O_3 (AlO2) and 48 cm Al - 29 cm Al_2O_3 (Run ID - AlO5) shows that the addition of a 5 cm Al_2O_3 block to 48 cm Al - 24 cm Al_2O_3 reduces both the epithermal neutron flux and the fast neutron dose by ~30%. Compared to 41cm Al - 27 cm AlF_3 (AlFTi8), 41 cm Al - 32 cm AlF_3 (Run ID - skm457), which has a 5 cm thicker AlF_3 block, reduces the epithermal neutron flux by 20% while decreasing the specific fast neutron dose by 30%. Therefore, it is considered that an Al_2O_3 or AlF_3 block which is thicker than ~ 25 cm would decrease fast neutron contamination with commensurate reduction of beam intensity.

By examining the results carefully, it is also noted that the filter/moderator designs using different dimensions of the filter/moderator materials (i.e., different thicknesses of Al and the other material) produce almost the same levels of the epithermal neutron flux and the specific fast neutron dose with different neutron spectrum shapes at the patient position. For example, comparing the result of 41 cm Al - 32 cm AlF_3 (skm457) and that of 71 cm Al - 22 cm AlF_3 (Run ID - skm454) shown in Table 3.5, which produce almost the same epithermal neutron flux and specific fast neutron dose, the thermal neutron flux is higher and the fast neutron flux is lower for the former design (note that Design skm457 has more AlF_3 and less Al than Design skm454). On the other hand, in terms of the fast neutron dose rate at the patient position, Design skm457 has a smaller epithermal energy component and a larger fast energy component than Design skm454. The same trend is observed in comparing the in-air beam performances of the designs using 58 cm Al - 24 cm Al_2O_3 (Run ID - skm463) and 83 cm Al - 17 cm Al_2O_3 (Run ID - skm451), where the former design has more Al_2O_3 and less Al than the latter. Although these results seem contradictory, they can be explained by examining the neutron spectrum. Figure 3.8 and Figure 3.9 depict the neutron flux spectra at the patient position for the filter/moderator designs using 41 cm Al - 32 cm AlF_3 (skm457) and 71 cm Al - 22 cm AlF_3 (skm454) in linear and log scales, respectively. From Figure 3.8, it is seen that Design skm457 (41 cm Al - 32 cm AlF_3) increases the

spectrum within the thermal region and the low energy portion of the epithermal region while decreasing its high energy portion relative to Design skm454 (71 cm Al - 22 cm AlF_3), which is caused by a larger amount of the complementary element (i.e., fluorine) in Design skm457. Moreover, Figure 3.9 shows that Design skm457 decreases the lower energy portion of the fast region (especially, the range from 10 keV to 25 keV, which accounts for 60-80 % of the fast neutron flux) and increases the higher energy portion (where the flux is very low) relative to Design skm454, which is likely because Design skm457 contains less Al. As a result, Design skm457 produces a higher thermal flux and lower fast flux. On the other hand, the neutron KERMA factor for the brain becomes minimum around 20 eV before increasing very rapidly at higher energies. For the epithermal region, Design skm457 (41 cm Al - 32 cm AlF_3) increases the spectrum in the low energy portion where the KERMA factor is small and decreases that in the high energy portion relative to Design skm454 (71 cm Al - 22 cm AlF_3). For the fast region, Design skm457 decreases the spectrum in the low energy portion and increases that in the high energy portion where the neutron KERMA becomes very large. As a result, Design skm457 provides a lower epithermal energy component and higher fast energy component of the fast neutron dose rate (one should remember that the fast neutron dose is the dose due to neutrons within both epithermal and fast energy regions). Again, the same trend is observed in comparing the neutron spectra of Design skm463 (58 cm Al - 24 cm Al_2O_3) and Design skm451 (83 cm Al - 17 cm Al_2O_3) which are shown in Figures 3.10 (linear scale) and 3.11 (log scale). These results indicate that, for the filter/moderator designs examined in this analysis, aluminum plays a major role to moderate or filter out the fast neutrons with energies above ~ 30 keV where aluminum has large resonance peaks. On the other hand, the complementary elements (fluorine and oxygen) moderate neutrons with energies below ~ 30 keV more efficiently than aluminum. Since the previous ideal beam studys[3,6] show that neutrons within the high energy portion of the epithermal

range would maximize effective beam penetration in phantom, it would be beneficial to increase the amount of Al and decrease the amount of the complementary element to reduce fast neutron contamination and simultaneously minimize moderation in the epithermal region. However, as discussed before, a certain amount of the complementary elements is also necessary to attenuate fast neutrons efficiently. The optimization of the fast neutron filter/moderator has to be performed taking these factors into account.

Table 3.5 includes the result for the filter/moderator design composed of 71 cm Al - 36 cm AlF_3 (Run ID - skm431), which contains the same mass of Al and AlF_3 as in the design using 71 cm Al - 27 cm AlF_3 (Run ID - skm308), but the density of AlF_3 is reduced to 75% of theoretical density. This design was considered to examine the effect of reducing the density of AlF_3 on beam performance because commercially available aluminum fluoride would be provided in the form of powder and would need to be fabricated by compressing it. The comparison of the results of these filter/moderator designs show that the reduction of the AlF_3 density does not affect beam performance at all.

Table 3.4 In-air beam performance for the fast neutron filter/moderator composed of an Al block followed by an Al_2O_3 block while varying their thicknesses. These calculations used a fission converter composed of eleven burned MITR-II fuel elements (312 g ^{235}U per element) with D_2O cooling. The fast neutron filter/moderator is followed by a 0.04 cm Cd thermal neutron filter, an 8 cm Bi photon shield and a pyramidal collimator with a 15 cm thick lead lining, and is surrounded by a 10 cm thick lead reflector. The materials listed on the left hand side of column 2 are closest to the fission converter. The reactor power was set at 5 MW. D_{epi} and D_{fast} denote epithermal and fast components of the fast neutron dose rate (D_{fn}).

Run ID	Filter/moderator	Φ_{th} n/cm^{2}s	Φ_{epi} n/cm^{2}s	Φ_f n/cm^{2}s	J_{th}/Φ_{th}	J_{epi}/Φ_{epi}	J_f/Φ_f	D_{epi} cGy/min	D_{fast} cGy/min	D_{fn} cGy/min	D_{fn}/Φ_{epi} cGycm^2/n
AlO2	48cm Al - 24cm Al_2O_3#	1.25E+09	1.42E+10	5.34E+08	0.64	0.66	0.67	6.51	13.36	19.9	2.33E-11
		1.7%	1.2%	2.2%	2.2%	1.6%	2.8%	1.4%	1.5%	1.1%	1.6%
AlO5	48cm Al - 29cm Al_2O_3	1.10E+09	1.02E+10	2.56E+08	0.64	0.66	0.66	3.70	6.67	10.4	1.69E-11
		1.7%	1.3%	3.2%	2.2%	1.8%	4.0%	1.7%	1.8%	1.3%	1.9%
AlO7	53cm Al - 24cm Al_2O_3	1.17E+09	1.34E+10	4.10E+08	0.65	0.65	0.69	5.73	9.53	15.3	1.90E-11
		1.6%	1.2%	2.3%	2.1%	1.6%	3.1%	1.4%	1.6%	1.1%	1.7%
AlO10	58cm Al - 19cm Al_2O_3	1.15E+09	1.65E+10	7.58E+08	0.65	0.65	0.68	9.09	15.80	24.9	2.51E-11
		1.6%	1.1%	1.8%	2.1%	1.5%	2.4%	1.3%	1.4%	1.0%	1.5%
skm463	58cm Al - 24cm Al_2O_3	1.10E+09	1.25E+10	3.33E+08	0.64	0.65	0.68	5.33	7.22	12.6	1.68E-11
(AlO8)		0.9%	0.7%	1.5%	1.2%	0.9%	1.9%	0.8%	1.0%	0.7%	1.0%
AlO9	63cm Al - 19cm Al_2O_3	1.10E+09	1.53E+10	6.32E+08	0.63	0.66	0.67	8.49	11.86	20.3	2.22E-11
		1.7%	1.1%	2.2%	2.2%	1.5%	2.8%	1.3%	1.5%	1.1%	1.6%
AlOTi4	63cm Al - 19cm Al_2O_3	6.85E+08	1.36E+10	2.10E+08	0.65	0.65	0.68	6.28	7.30	13.6	1.67E-11
	- 2cm Ti	2.0%	1.2%	2.2%	2.6%	1.6%	3.1%	1.4%	1.7%	1.1%	1.7%
AlO12	72cm Al	6.94E+08	2.57E+10	1.11E+10	0.61	0.65	0.67	32.71	202.74	235.4	1.52E-10
		3.6%	1.4%	1.7%	4.3%	1.8%	2.2%	2.1%	1.6%	1.4%	2.0%
AlO14	73cm Al - 19cm Al_2O_3	1.05E+09	1.35E+10	4.07E+08	0.62	0.64	0.67	6.93	6.66	13.6	1.68E-11
		2.0%	1.4%	2.8%	2.6%	1.8%	3.7%	1.5%	3.0%	1.6%	2.1%
AlO18	73cm Al - 19cm Al_2O_3	7.75E+08	1.24E+10	1.96E+08	0.63	0.65	0.65	6.18	4.67	10.8	1.45E-11
	- 1cm Ti	2.2%	1.4%	4.5%	2.9%	1.8%	5.5%	1.6%	4.3%	2.1%	2.5%
AlO16	73cm Al - 19cm Al_2O_3	6.23E+08	1.18E+10	1.29E+08	0.63	0.65	0.63	5.20	4.07	9.3	1.31E-11
	- 2cm Ti	2.4%	1.4%	5.4%	3.2%	1.8%	6.5%	1.5%	7.9%	3.6%	3.8%
AlO17	78cm Al - 19cm Al_2O_3	9.34E+08	1.25E+10	3.60E+08	0.63	0.64	0.66	6.27	5.29	11.6	1.54E-11
		2.0%	1.4%	3.5%	2.6%	1.8%	4.3%	1.5%	3.5%	1.8%	2.3%
AlO15	83cm Al - 14cm Al_2O_3	8.78E+08	1.56E+10	7.53E+08	0.63	0.63	0.64	10.13	10.16	20.3	2.17E-11
		2.0%	1.3%	2.4%	2.7%	1.7%	3.1%	1.4%	2.5%	1.4%	1.9%
AlO21	83cm Al - 16cm Al_2O_3	8.95E+08	1.41E+10	4.99E+08	0.63	0.64	0.67	8.11	6.78	14.9	1.75E-11
		2.0%	1.4%	2.6%	2.7%	1.8%	3.5%	1.5%	2.7%	1.5%	2.0%
AlO24	83cm Al - 16cm Al_2O_3	5.70E+08	1.20E+10	1.24E+08	0.62	0.64	0.68	6.04	3.23	9.3	1.28E-11
	- 2cm Ti	2.6%	1.4%	4.1%	3.5%	1.8%	5.6%	1.5%	4.9%	2.0%	2.4%
skm451	83cm Al - 17cm Al_2O_3	9.28E+08	1.32E+10	4.28E+08	0.62	0.65	0.65	7.30	6.02	13.3	1.69E-11
(AlO22)		2.1%	1.3%	3.2%	2.7%	1.8%	4.0%	1.6%	3.4%	1.8%	2.2%

Table 3.4 (Continued)

Run ID	Filter/moderator	Φ_{th} n/cm^{2}s	Φ_{epi} n/cm^{2}s	Φ_f n/cm^{2}s	J_{th}/Φ_{th}	J_{epi}/Φ_{epi}	J_f/Φ_f	D_{epi} cGy/min	D_{fast} cGy/min	D_{fn} cGy/min	D_{fn}/Φ_{epi} cGycm^2/n
AlO27	83cm Al - 19cm Al_2O_3	8.99E+08	1.17E+10	2.90E+08	0.62	0.64	0.66	5.71	4.03	9.7	1.39E-11
		2.1%	1.4%	3.6%	2.7%	1.9%	4.6%	1.6%	4.0%	1.9%	2.4%
AlO19	93cm Al - 9cm Al_2O_3	7.28E+08	1.73E+10	1.40E+09	0.62	0.63	0.66	14.54	17.07	31.6	3.05E-11
		2.2%	1.2%	1.8%	3.0%	1.6%	2.4%	1.3%	1.9%	1.2%	1.7%
AlO20	93cm Al - 14cm Al_2O_3	7.87E+08	1.37E+10	5.38E+08	0.62	0.63	0.64	8.54	6.66	15.2	1.85E-11
		2.2%	1.3%	2.7%	2.9%	1.8%	3.5%	1.5%	3.2%	1.6%	2.1%
std473	68cm AlF_3(70%)/Al(30%) - 2cm Ti	9.13E+08	1.30E+10	1.16E+08	0.66	0.67	0.68	4.02	6.35	10.4	1.33E-11
		1.8%	1.3%	3.0%	2.4%	1.7%	4.0%	1.6%	2.2%	1.5%	1.9%

The same thicknesses of Al and Al_2O_3 blocks as proposed in the BNL epithermal neutron beam design using ^{235}U fission plates.[11]

Table 3.5 In-air beam performance for the fast neutron filter/moderator composed of an Al block followed by an AlF_3 block while varying their thicknesses. These calculations used a fission converter composed of eleven burned MITR-II fuel elements (312 g ^{235}U per element) with D_2O cooling. The fast neutron filter/moderator is followed by a 0.04 cm Cd thermal neutron filter, an 8 cm Bi photon shield and a pyramidal collimator with 15 cm thick lead lining, and is surrounded by a 10 cm thick lead reflector. Column 2 lists the filter/moderator materials starting at the fission converter. The reactor power was set at 5 MW. D_{epi} and D_{fast} denote epithermal and fast components of the fast neutron dose rate (D_{fn}).

Run ID	Filter/moderator	Φ_{th} n/cm²s	Φ_{epi} n/cm²s	Φ_f n/cm²s	J_{th}/Φ_{th}	J_{epi}/Φ_{epi}	J_f/Φ_f	D_{epi} cGy/min	D_{fast} cGy/min	D_{fn} cGy/min	D_{fn}/Φ_{epi} cGycm²/n
AlFT10	19.6cm Al - 45.7cm AlF_3 - 2cm Ti	8.96E+08 2.0%	1.06E+10 1.4%	8.83E+07 3.0%	0.64 2.6%	0.66 1.8%	0.69 4.1%	2.99 1.7%	5.08 2.4%	8.1 1.7%	1.27E-11 2.1%
skm427	22.4cm Al - 49.6cm AlF_3	1.25E+09 1.6%	9.64E+09 1.4%	1.09E+08 4.5%	0.64 2.1%	0.66 1.8%	0.69 5.8%	2.65 2.0%	3.30 2.7%	6.0 1.7%	1.03E-11 2.2%
AlFTi8	41cm Al - 27cm AlF_3	1.31E+09 1.7%	1.95E+10 1.2%	7.61E+08 2.2%	0.65 2.2%	0.66 1.6%	0.68 2.8%	11.47 1.3%	16.93 1.5%	28.4 1.0%	2.43E-11 1.6%
skm457 (AlF2)	41cm Al - 32cm AlF_3	1.29E+09 0.6%	1.59E+10 0.4%	3.78E+08 0.9%	0.64 0.7%	0.66 0.5%	0.69 1.2%	7.36 0.5%	8.50 0.6%	15.9 0.4%	1.66E-11 0.6%
AlF6	61cm Al - 22cm AlF_3	1.08E+09 1.9%	1.79E+10 1.2%	6.76E+08 2.2%	0.63 2.4%	0.65 1.6%	0.68 2.9%	11.23 1.3%	10.76 1.7%	22.0 1.1%	2.05E-11 1.6%
AlF1	61cm Al - 27cm AlF_3	1.09E+09 2.1%	1.49E+10 1.4%	3.42E+08 3.7%	0.64 2.8%	0.64 1.9%	0.66 4.7%	7.49 1.6%	5.67 4.4%	13.2 2.1%	1.48E-11 2.5%
AlF3	61cm Al - 32cm AlF_3	1.03E+09 2.0%	1.18E+10 1.4%	1.48E+08 4.7%	0.62 2.6%	0.64 1.9%	0.68 6.1%	4.65 1.6%	2.42 4.6%	7.1 1.9%	1.00E-11 2.4%
skm460	71cm Al - 17cm AlF_3	9.42E+08 0.7%	1.91E+10 0.4%	1.00E+09 0.7%	0.63 1.0%	0.64 0.5%	0.67 0.9%	14.56 0.4%	13.71 0.8%	28.3 0.5%	2.46E-11 0.6%
skm454	71cm Al - 22cm AlF_3	9.79E+08 0.7%	1.60E+10 0.4%	4.70E+08 1.0%	0.62 0.9%	0.64 0.6%	0.67 1.3%	9.55 0.5%	6.29 1.1%	15.8 0.5%	1.65E-11 0.7%
skm308 (AlF4m)	71cm Al - 27cm AlF_3	9.70E+08 0.7%	1.28E+10 0.5%	2.20E+08 1.4%	0.62 0.9%	0.64 0.6%	0.66 1.8%	6.06 0.5%	2.89 1.6%	9.0 0.6%	1.16E-11 0.8%
AlF5	76cm Al - 22cm AlF_3	9.20E+08 2.0%	1.49E+10 1.3%	4.04E+08 3.1%	0.64 2.6%	0.64 1.7%	0.67 4.0%	8.64 1.4%	5.05 3.0%	13.7 1.4%	1.53E-11 1.9%
skm439	66 cm FLUENTAL# w/o LiF	1.45E+09 0.6%	1.31E+10 0.5%	1.88E+08 1.3%	0.65 0.8%	0.66 0.6%	0.69 1.7%	4.04 0.6%	5.19 0.8%	9.2 0.5%	1.17E-11 0.7%
skm426	68 cm FLUENTAL w/o LiF	1.39E+09 1.6%	1.19E+10 1.3%	1.62E+08 4.9%	0.65 2.2%	0.67 1.8%	0.68 6.0%	3.52 1.8%	4.35 2.8%	7.9 1.7%	1.10E-11 2.2%
skm403	68 cm FLUENTAL w/o LiF - 2cm Ti	8.77E+08 1.9%	1.04E+10 1.4%	5.54E+07 3.7%	0.64 2.5%	0.66 1.9%	0.68 5.0%	2.61 1.8%	3.03 3.0%	5.6 1.8%	9.07E-12 2.3%
skm431	71cm Al - 36cm AlF_3 (AlF_3 - 75% density)	9.13E+08 2.2%	1.30E+10 1.4%	2.29E+08 4.1%	0.61 2.8%	0.63 1.8%	0.65 5.2%	6.37 1.6%	2.89 3.7%	9.3 1.6%	1.19E-11 2.1%
std473	68cm AlF_3(70%)/Al(30%) - 2cm Ti	9.13E+08 1.8%	1.30E+10 1.3%	1.16E+08 3.0%	0.66 2.4%	0.67 1.7%	0.68 4.0%	4.02 1.6%	6.35 2.2%	10.4 1.5%	1.33E-11 1.9%

The metal/ceramic composite made from Al and AlF_3 mixture developed by VTT Chemical Technology in Finland.[10] The atomic densities of the main elements in FLUENTAL are: Al $3.49*10^{22}$ cm^{-3} and F $4.52*10^{22}$ cm^{-3}. Li (natural) can be added in the form of LiF as an optional absorber (Density: $7.0*10^{20}cm^{-3}$)

Table 3.6 In-air beam performance for the fast neutron filter/moderator composed of an Al block followed by an Teflon [$(CF_2)_n$] block while varying their thicknesses. These calculations used a fission converter composed of eleven burned MITR-II fuel elements (312g ^{235}U per element) with D_2O cooling. The fast neutron filter/moderator is followed by a 0.04 cm Cd thermal neutron filter, an 8 cm Bi photon shield and a pyramidal collimator with a 15 cm thick lead lining, and is surrounded by a 10 cm thick lead reflector. The reactor power was set at 5 MW. D_{epi} and D_{fast} denote epithermal and fast components of the fast neutron dose rate (D_{fn}).

Run ID	Filter/moderator	Φ_{th} n/cm^{2}s	Φ_{epi} n/cm^{2}s	Φ_f n/cm^{2}s	J_{th}/Φ_{th}	J_{epi}/Φ_{epi}	J_f/Φ_f	D_{epi} cGy/min	D_{fast} cGy/min	D_{fn} cGy/min	D_{fn}/Φ_{epi} cGycm^2/n
skm433	69.85 cm Al-$(CF_2)_n$-Al+2%Li-$(CF_2)_n$-Al#	7.60E+08 1.9%	1.23E+10 1.6%	5.39E+08 2.3%	0.65 2.5%	0.66 2.1%	0.69 3.0%	5.81 1.7%	18.3 1.7%	24.1 1.3%	3.25E-11 2.0%
skm430	39.4cm Al - 39.6cm $(CF_2)_n$	1.02E+09 1.8%	5.98E+09 2.1%	9.04E+07 5.5%	0.64 2.3%	0.65 2.8%	0.69 6.8%	1.40 2.9%	3.8 3.1%	5.2 2.4%	1.45E-11 3.2%
skm437	70cm Al - 22cm $(CF_2)_n$	1.10E+09 1.9%	1.17E+10 1.4%	2.10E+08 3.6%	0.64 2.5%	0.64 1.9%	0.69 4.8%	4.70 1.6%	4.4 4.2%	9.1 2.2%	1.29E-11 2.6%
skm435	75cm Al - 22cm $(CF_2)_n$	1.08E+09 1.9%	1.12E+10 1.5%	2.00E+08 4.8%	0.62 2.6%	0.63 2.0%	0.64 5.8%	4.36 1.7%	3.8 5.0%	8.2 2.5%	1.21E-11 2.9%
skm434	80cm Al - 17cm $(CF_2)_n$	1.07E+09 1.9%	1.38E+10 1.3%	4.04E+08 2.8%	0.64 2.5%	0.64 1.8%	0.67 3.8%	7.14 1.5%	6.33 3.0%	13.5 1.6%	1.63E-11 2.1%
skm432	80.3cm Al - 21.6cm $(CF_2)_n$	1.02E+09 2.2%	1.06E+10 1.8%	1.62E+08 5.0%	0.63 2.9%	0.63 2.3%	0.66 6.6%	4.22 2.0%	2.80 5.6%	7.0 2.5%	1.10E-11 3.1%
std473	68cm AlF_3(70%)/ Al(30%)- 2cm Ti	9.13E+08 1.8%	1.30E+10 1.3%	1.16E+08 3.0%	0.66 2.4%	0.67 1.7%	0.68 4.0%	4.02 1.6%	6.35 2.2%	10.4 1.5%	1.33E-11 1.9%

The fast neutron filter/moderator design proposed by INEL for the WSU epithermal neutron beam extraction facility for BNCT[7]. This design consists of 0.635 cm thick plates repeating in the order of Al1100-$(CF_2)_n$-[Al+2%Li(natural)]-$(CF_2)_n$-Al1100. The total thickness of the fast neutron filter/moderator is 69.85 cm (Al1100 - 27.94 cm, $(CF_2)_n$ - 27.94 cm, Al+2%Li(nat.) - 13.97 cm).

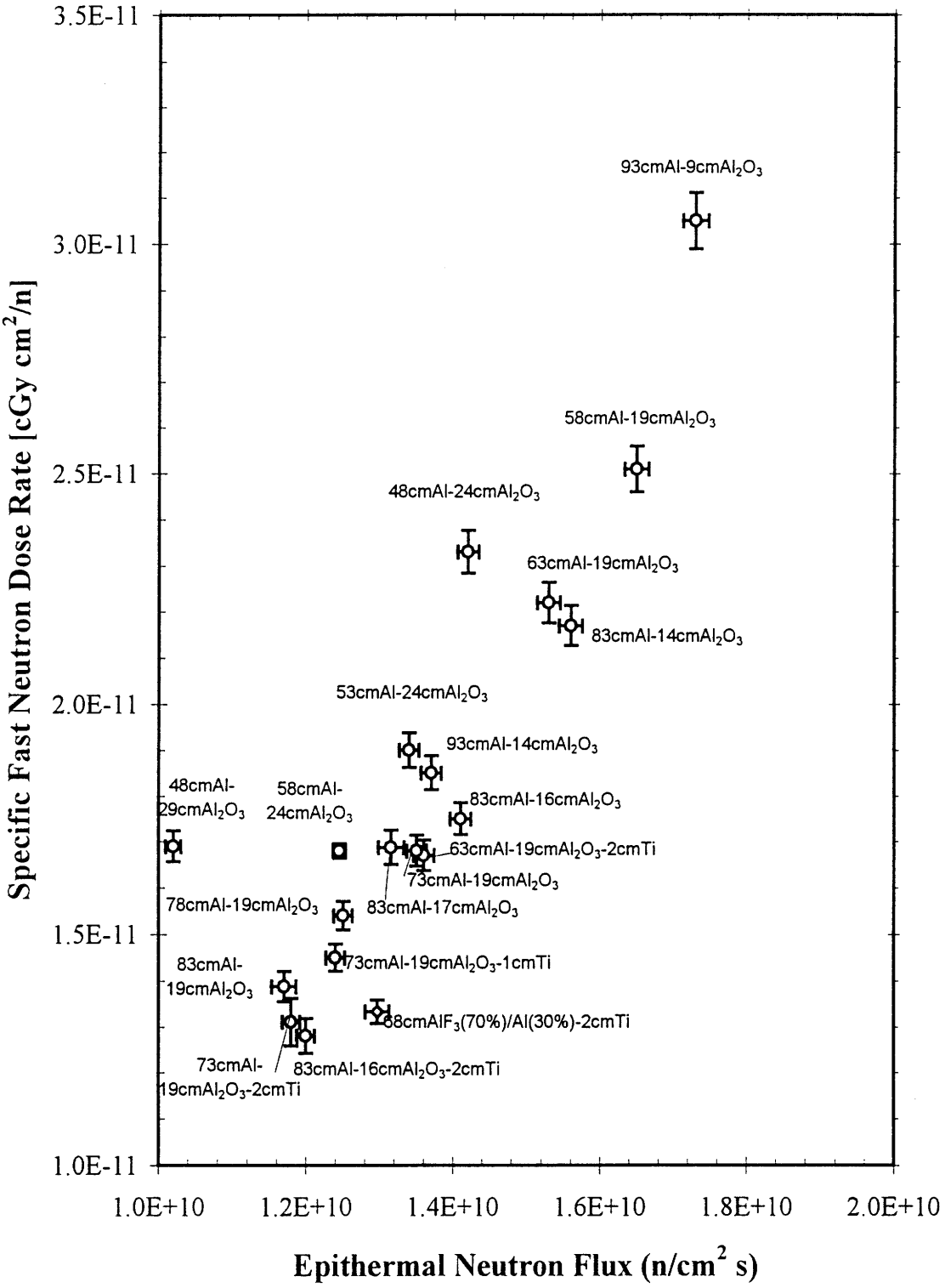

Figure 3.5 Epithermal neutron flux vs. specific fast neutron dose for various fast neutron filter/moderator designs composed of an Al block followed by an Al_2O_3 block. The label of each data point denotes the configuration of the filter/moderator design.

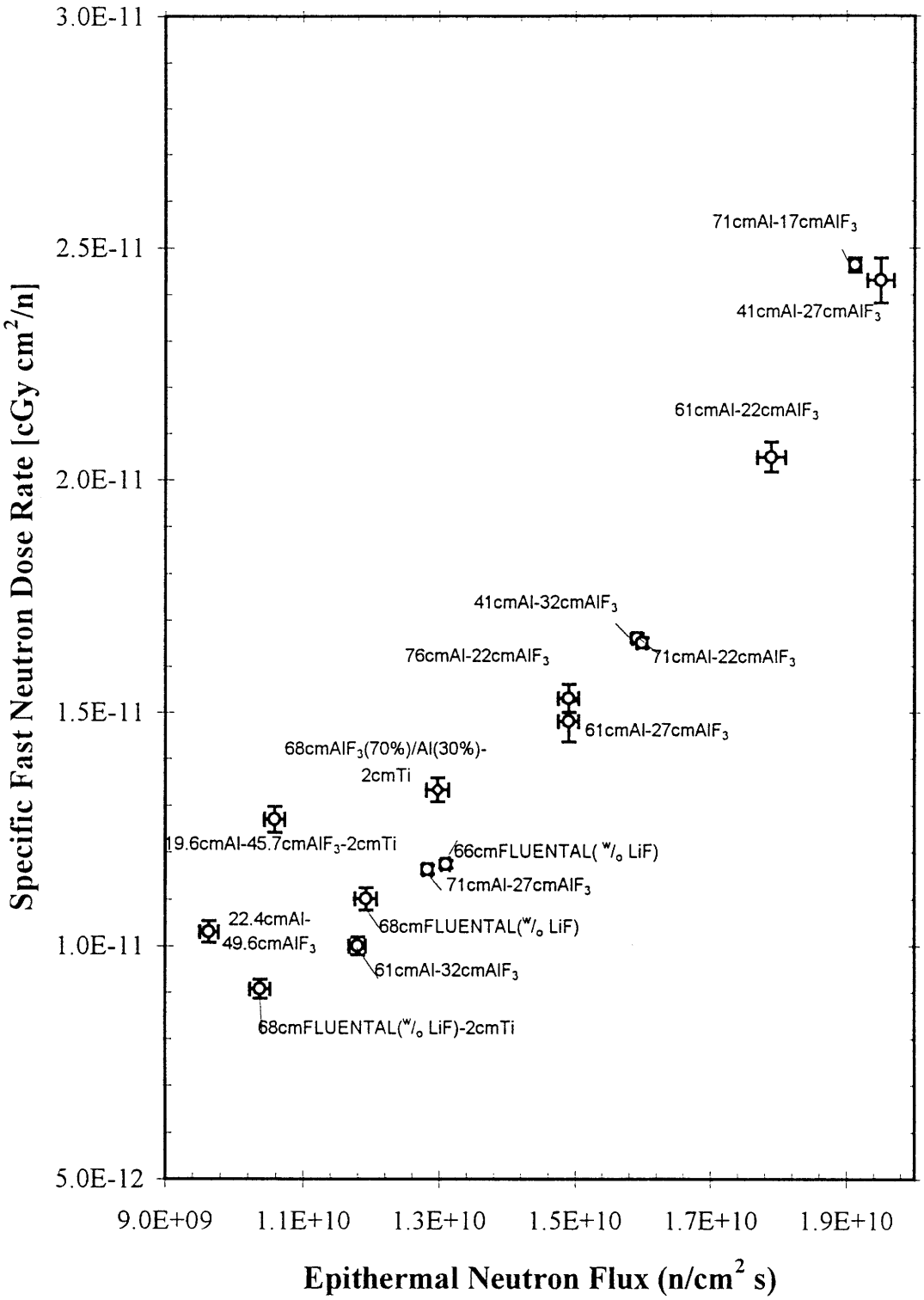

Figure 3.6 Epithermal neutron flux vs. specific fast neutron dose for various fast neutron filter/moderator designs composed of an Al block followed by an AlF_3 block. The label of each data point denotes the configuration of the filter/moderator design.

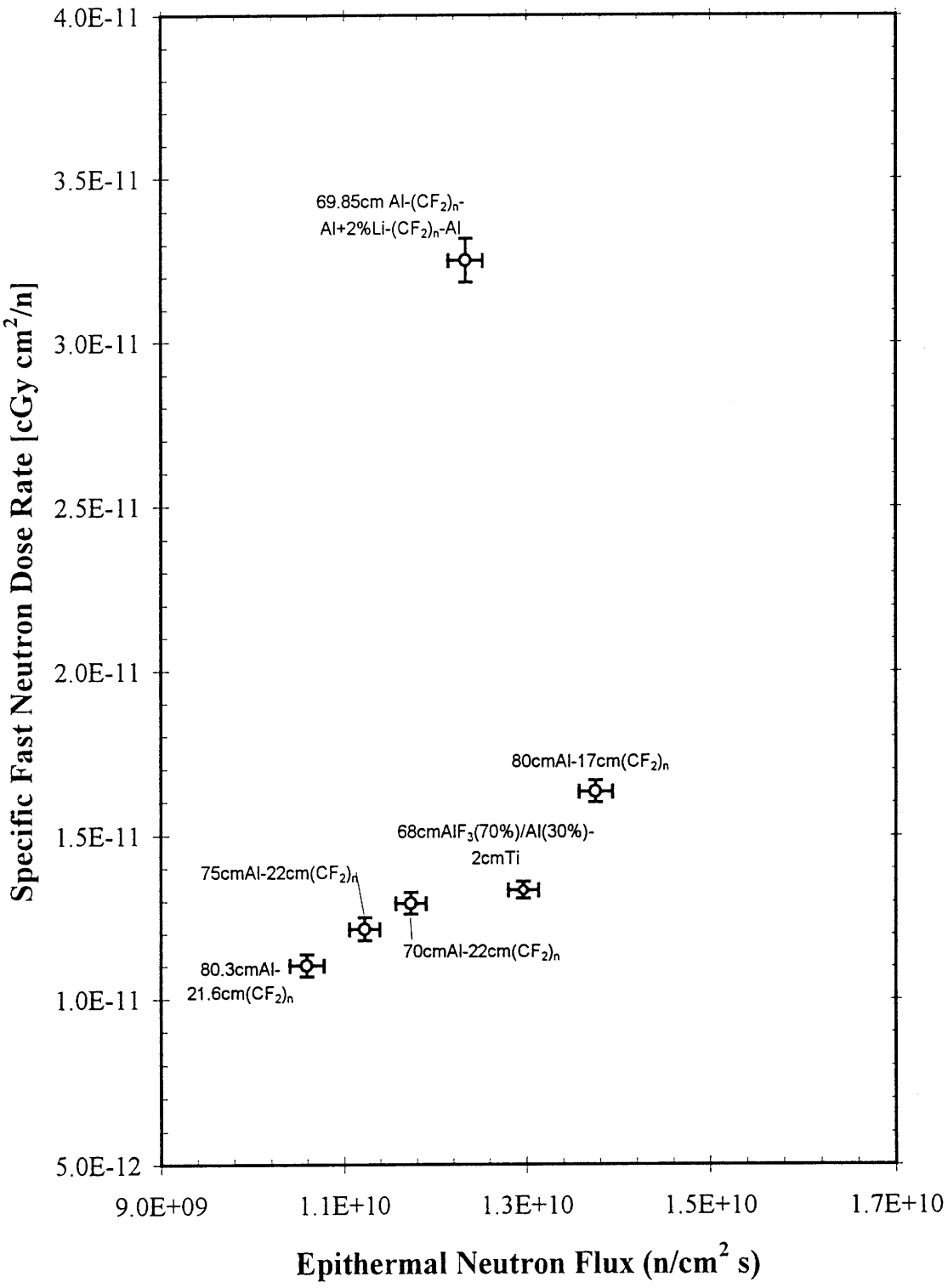

Figure 3.7 Epithermal neutron flux vs. specific fast neutron dose for various fast neutron filter/moderator designs composed of an Al block followed by an Teflon [$(CF_2)_n$] block. The label of each data point denotes the configuration of the filter/moderator.

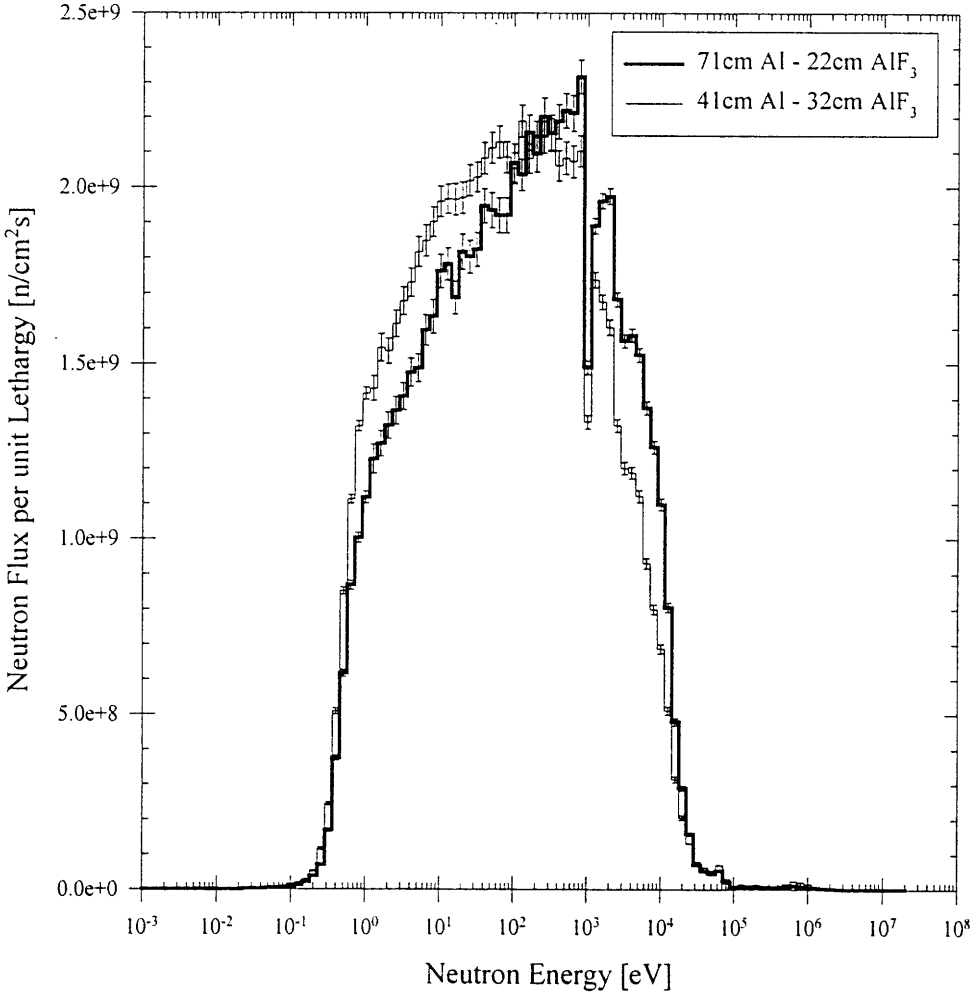

Figure 3.8 Comparison of the neutron flux spectra at the patient position generated by the fission converter beams with D_2O-cooled burned MITR-II fuel and the fast neutron filter/moderator designs using 71 cm Al - 22 cm AlF_3 (skm454) and 41 cm Al - 32 cm AlF_3 (skm457) shown in a linear scale. The reactor power was set at 5 MW.

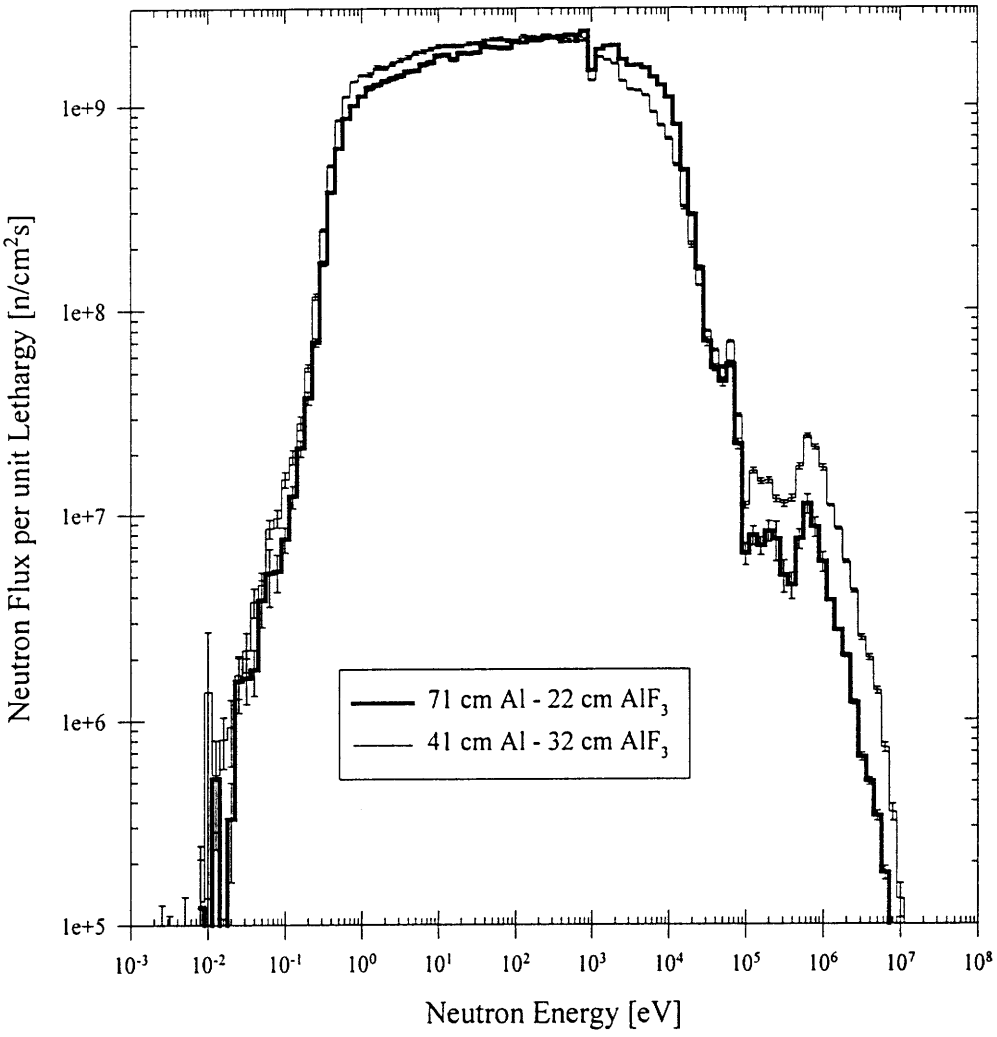

Figure 3.9 Comparison of the neutron flux spectra at the patient position generated by the fission converter beams with D_2O-cooled burned MITR-II fuel and the fast neutron filter/moderator designs using 71 cm Al - 22 cm AlF_3 (skm454) and 41 cm Al - 32 cm AlF_3 (skm457) shown in a log scale. The reactor power was set at 5 MW.

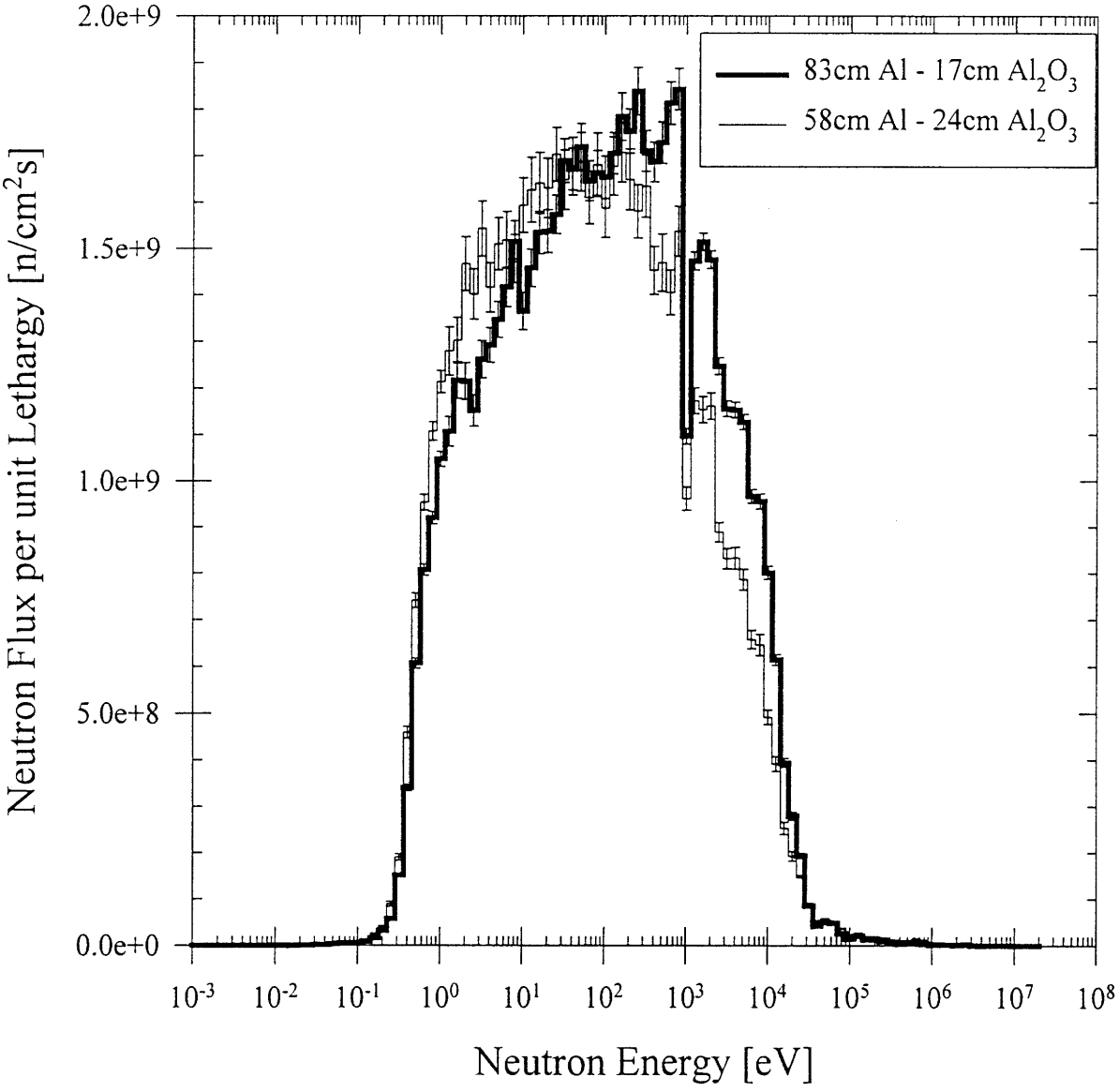

Figure 3.10 Comparison of the neutron flux spectra at the patient position generated by the fission converter beams with D_2O-cooled burned MITR-II fuel and the fast neutron filter/moderator designs using 83 cm Al - 17 cm Al_2O_3 (skm451) and 58 cm Al - 24 cm Al_2O_3 (skm463) shown in a linear scale. The reactor power was set at 5 MW.

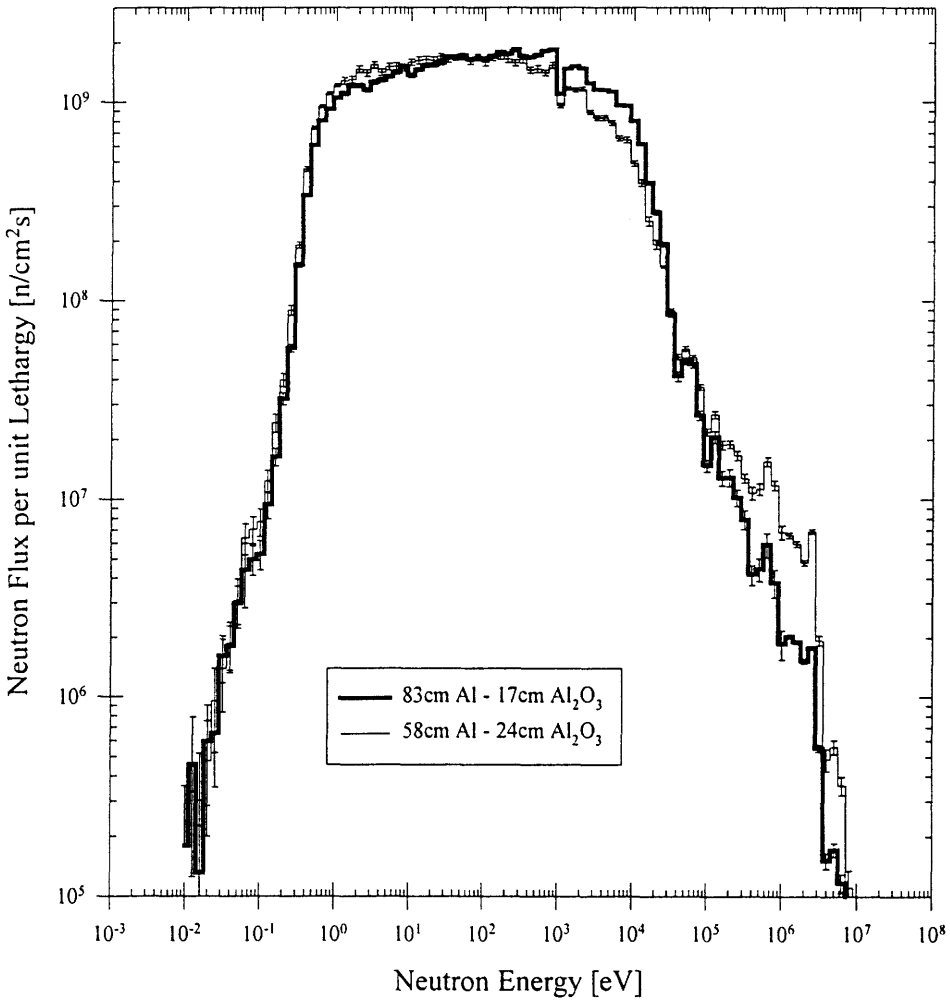

Figure 3.11 Comparison of the neutron flux spectra at the patient position generated by the fission converter beams with D_2O-cooled burned MITR-II fuel and the fast neutron filter/moderator designs using 83 cm Al - 17 cm Al_2O_3 (skm451) and 58 cm Al - 24 cm Al_2O_3 (skm463) shown in a log scale. The reactor power was set at 5 MW.

Since Teflon appears to be a promising candidate for the filter/moderator material, it is interesting to consider what is the effect of carbon in Teflon on beam performance. For this purpose, a few calculations were done for the designs using hypothetical Teflon from which carbon was removed. The results are presented with those for the designs with Teflon including carbon in Table 3.7. These calculations used a fast neutron filter/moderator composed of Al1100-$(CF_2)_n$-[Al+2%Li(natural)]-$(CF_2)_n$-Al1100 (INEL Design) proposed in Reference 7, where carbon in Teflon [$(CF_2)_n$] was kept or removed. The INEL design, which was proposed for the WSU epithermal neutron beam extraction facility for BNCT[7], repeats 0.635 cm thick plates in the order of Al1100-$(CF_2)_n$-[Al+2%Li(natural)]-$(CF_2)_n$-Al1100. The total thickness of the fast neutron filter/moderator is 69.85 cm (Al1100 - 27.94 cm, $(CF_2)_n$ - 27.94 cm, Al+2% Li(nat.) - 13.97 cm). In addition, a 6 cm or 10 cm thick Pb block was used as a photon shield, which was also used in Reference 7. The results show that the removal of carbon from Teflon increases the specific fast neutron dose by ~70% and the epithermal neutron flux by 70~80%. Therefore, it is found that carbon in Teflon decreases fast neutron contamination although it reduces beam intensity significantly as well.

Carbon is commonly used as a neutron moderator. It has very low absorption cross section and its total cross sections averaged over the epithermal and fast energy range with the spectrum of the fission converter beam are 4.71 b and 2.26 b, which are comparable to those of oxygen (epithermal - 3.74 b and fast - 2.52 b)[5]. Carbon does not behave as a band-pass filter. However, oxygen, which was shown to provide good filtration/moderation of fast neutrons, does not have any resonance peaks up to ~ 440 keV where it has the highest peak of ~ 17 b;[14] the magnitude of its resonance peak is not as large as those of fluorine. Then, it seems reasonable to expect that carbon would be used as a filter/moderator material as well as oxygen.

Motivated by these considerations, calculations were done using the combination of Al - C. The results are shown in Table 3.8. Design skm467 was made so that it contains the same numbers of Al and C atoms as those of Al and O atoms in Design skm451 (83 cm Al - 17 cm Al_2O_3). Table 3.8 shows that Design skm467 provides a beam performance which is similar to that of Design skm451 (28% lower epithermal neutron flux and 21% lower specific fast neutron dose). Moreover, it is seen that the filter design using 96 cm Al - 12 cm C (skm471) produces a beam which meets the design goals adequately.

Table 3.7 In-air beam performance for the filter/moderator designs composed of Al1100-$(CF_2)_n$-[Al+2%Li(natural)]-$(CF_2)_n$-Al1100 (INEL Design) where carbon in Teflon [$(CF_2)_n$] was kept or removed. These calculations used a fission converter composed of eleven burned MITR-II fuel elements (312 g ^{235}U per element) with D_2O cooling. The fast neutron filter/moderator is followed by a 0.04 cm Cd thermal neutron filter, a Pb photon shield with different thicknesses and a pyramidal collimator with a 15 cm thick lead lining, and is surrounded by a 10 cm thick lead reflector. The reactor power was set at 5 MW.

Run ID	Carbon in Teflon	Photon Shield	Φ_{th} n/cm^{2}s	Φ_{epi} n/cm^{2}s	Φ_f n/cm^{2}s	J_{th}/Φ_{th}	J_{epi}/Φ_{epi}	J_f/Φ_f	D_{fn} cGy/min	D_{fn}/Φ_{epi} cGycm^2/n	D_γ cGy/min	D_γ/Φ_{epi} cGycm^2/n
skm402	Yes	6cm Pb	8.27E+08 1.9%	1.31E+10 1.5%	6.03E+08 2.3%	0.66 2.5%	0.66 2.0%	0.69 3.0%	25.1 1.3%	3.19E-11 2.0%	2.7 2.2%	3.45E-12 2.6%
skm406	No	6cm Pb	4.01E+08 2.5%	2.22E+10 1.2%	2.29E+09 1.5%	0.65 3.3%	0.66 1.7%	0.68 2.0%	73.4 1.0%	5.52E-11 1.6%	3.2 2.4%	2.39E-12 2.7%
skm400	Yes	10cm Pb	6.97E+08 2.0%	1.06E+10 1.7%	4.34E+08 2.5%	0.65 2.6%	0.66 2.2%	0.69 3.3%	19.2 1.5%	3.03E-11 2.2%	1.3 1.9%	2.00E-12 2.5%
skm405	No	10cm Pb	3.82E+08 2.6%	1.90E+10 1.3%	1.72E+09 1.6%	0.63 3.5%	0.65 1.8%	0.68 2.1%	58.3 1.0%	5.11E-11 1.7%	1.5 1.9%	1.28E-12 2.3%

Table 3.8 In-air beam performance for the filter/moderator composed of an Al block followed by an graphite block with varying their thicknesses. These calculations used a fission converter composed of eleven burned MITR-II fuel elements (312 g ^{235}U per element) with D_2O cooling. The fast neutron filter/moderator is followed by a 0.04 cm Cd thermal neutron filter, an 8 cm Bi photon shield and a pyramidal collimator with a 15 cm thick lead lining, and is surrounded by a 10 cm thick lead reflector. The reactor power was set at 5 MW.

Run ID	Filter/moderator	Φ_{th} n/cm^{2}s	Φ_{epi} n/cm^{2}s	Φ_f n/cm^{2}s	J_{th}/Φ_{th}	J_{epi}/Φ_{epi}	J_f/Φ_f	D_{epi} cGy/min	D_{fast} cGy/min	D_{fn} cGy/min	D_{fn}/Φ_{epi} cGycm^2/n
skm467	96cm Al - 15cm C	1.02E+09 1.3%	9.45E+09 1.0%	2.07E+08 2.6%	0.61 1.7%	0.63 1.3%	0.63 3.3%	3.83 1.2%	3.71 2.8%	7.5 1.5%	1.33E-11 1.8%
skm471	96cm Al - 12cm C	1.06E+09 1.2%	1.20E+10 0.9%	3.83E+08 1.9%	0.62 1.6%	0.63 1.2%	0.65 2.5%	6.04 1.0%	6.40 2.1%	12.4 1.2%	1.73E-11 1.5%

For a quick comparisons between different combinations, several designs are selected for each combination and their results are presented in Table 3.9 and Figure 3.12. Table 3.9 shows the specific photon doses of the designs where the data are available. These results show that the filter/moderator designs using combinations/mixtures of Al and AlF_3 provide the best beam performance, i.e., a higher epithermal neutron flux and/or lower specific fast neutron dose. However, it will be shown in Section 3.3 that the difference in the specific fast neutron dose at such low levels does not affect in-phantom figures of merit significantly.

Comparing the results for the designs using 68 cm FLUENTAL (without LiF) with and without 2 cm Ti (Run ID - skm403 and skm426, respectively), one would see the effect of using a Ti filter on beam performance. Table 3.9 shows that the addition of the 2cm Ti reduces the specific fast neutron dose by 18% while decreasing the epithermal neutron flux by 13%. However, as will be discussed in Section 3.3, resonance peaks of Ti remove epithermal neutrons within the energy range of 3-10 keV, where the advantage depth would be maximized,[6] as well as undesired fast neutrons. Therefore, it is considered that the advantage of reducing fast neutron contamination with Ti would be offset by the reduction of the useful epithermal portion of the spectrum.

As for photon contamination, the 2 cm thick Ti layer does not increase the specific photon dose although Reference 5 identified Ti as a major photon generation source, which produces prompt gamma rays which accounts for ~ 26% of the photon contamination. This is likely because the 2 cm Ti filter is shielding photons as well as generating those. For photons with energies of 3-4 MeV, which are approximately the average energies of prompt gamma rays from Al (another major photon source), the mass attenuation coefficient of Pb and Fe are around 0.04 cm^2/g and 0.03 cm^2/g, respectively.[20] Since these values are considered to provide good approximations for those of Bi and Ti due to similarity of the atomic numbers between Pb and Bi and between Fe and Ti, the linear attenuation coefficients of Bi (Density = 9.8 g/cm^3) and Ti (Density = 4.5 g/cm^3) are

estimated as follows.

$$\mu(Bi) = 0.04\ [cm^2/g] * 9.8\ [g/cm^3] \sim 0.4\ [1/cm]$$

$$\mu(Ti) = 0.03\ [cm^2/g] * 4.5\ [g/cm^3] \sim 0.14\ [1/cm]$$

Therefore, roughly speaking, a 2 cm thick Ti layer is equivalent to a ~ 0.7 cm thick Bi layer in terms of photon attenuation. The parametric study of the Bi photon shield performed in Reference 5 shows that, in the beam design using a filter/moderator composed of 68 cm 70% AlF_3/30% Al - 2 cm Ti (the designs of the fission converter, reflector and collimator are different from those used here), a decrease in the thickness of Bi from 8 cm to 6 cm causes an increase in the photon dose rate at the patient position by ~100% (from 6.9 cGy/min to 14.2 cGy/min). Then, when 0.7 cm of Bi is removed, the photon dose rate is considered to increase by ~ 30 - 40 %. On the other hand, the photon dose analysis of Reference 5 which uses a filter/moderator composed of 68cm 70% AlF_3/30% Al - 2 cm Ti and an 8 cm Bi photon shield (again, the designs of the fission converter, reflector and collimator are different from those used here) indicates that the photon dose rate is increased by ~ 40% (from 5 cGy/min to 6.8 cGy/min) when the photon generation of the 2 cm Ti layer is turned on. As a result, it is considered that, when the 2 cm thick Ti layer is added, the increase in photon generation would be offset by the effect of increased photon attenuation. This consideration explains the small difference in the photon dose rate between Designs skm426 and skm403.

Table 3.9 Summary of in-air beam performance for the fast neutron filter/moderator designs using the combinations of Al-Al_2O_3, Al-AlF_3, Al-$(CF_2)_n$ and Al-C. These calculations used a fission converter composed of eleven burned MITR-II fuel elements (312 g ^{235}U per element) with D_2O cooling. The fast neutron filter/moderator is followed by a 0.04 cm Cd thermal neutron filter, an 8 cm Bi photon shield and a pyramidal collimator with a 15 cm thick lead lining, and is surrounded by a 10 cm thick lead reflector. The MITR reactor power was assumed to be 5 MW. D_{epi} and D_{fast} denote epithermal and fast components of the fast neutron dose rate (D_{fn}).

Run ID	Filter/moderator	Φ_{th} n/cm^{2}s	Φ_{epi} n/cm^{2}s	Φ_f n/cm^{2}s	J_{th}/Φ_{th}	J_{epi}/Φ_{epi}	J_f/Φ_f	D_{epi} cGy/min	D_{fast} cGy/min	D_{fn} cGy/min	D_{fn}/Φ_{epi} cGycm^2/n	$D\gamma$ cGy/min	$D\gamma/\Phi_{epi}$ cGycm^2/n
AlO2	48cm Al - 24cm Al_2O_3#	1.25E+09	1.42E+10	5.34E+08	0.64	0.66	0.67	6.51	13.36	19.9	2.33E-11	N.A.	N.A.
		1.7%	1.2%	2.2%	2.2%	1.6%	2.8%	1.4%	1.5%	1.1%	1.6%		
AlO21	83cm Al - 16cm Al_2O_3	8.95E+08	1.41E+10	4.99E+08	0.63	0.64	0.67	8.11	6.78	14.9	1.75E-11	N.A.	N.A.
		2.0%	1.4%	2.6%	2.7%	1.8%	3.5%	1.5%	2.7%	1.5%	2.0%		
skm451 (AlO22)	83cm Al - 17cm Al_2O_3	9.28E+08	1.32E+10	4.28E+08	0.62	0.65	0.65	7.30	6.02	13.3	1.69E-11	5.0	6.39E-12
		2.1%	1.3%	3.2%	2.7%	1.8%	4.0%	1.6%	3.4%	1.8%	2.2%	2.4%	2.8%
AlO27	83cm Al - 19cm Al_2O_3	8.99E+08	1.17E+10	2.90E+08	0.62	0.64	0.66	5.71	4.03	9.7	1.39E-11	5.1	7.27E-12
		2.1%	1.4%	3.6%	2.7%	1.9%	4.6%	1.6%	4.0%	1.9%	2.4%	1.8%	2.3%
skm457 (AlF2)	41cm Al - 32cm AlF_3	1.29E+09	1.59E+10	3.78E+08	0.64	0.66	0.69	7.36	8.50	15.9	1.66E-11	7.9	8.32E-12
		0.6%	0.4%	0.9%	0.7%	0.5%	1.2%	0.5%	0.6%	0.4%	0.6%	1.1%	1.2%
skm460	71cm Al - 17cm AlF_3	9.42E+08	1.91E+10	1.00E+09	0.63	0.64	0.67	14.56	13.71	28.3	2.46E-11	5.9	5.10E-12
		0.7%	0.4%	0.7%	1.0%	0.5%	0.9%	0.4%	0.8%	0.5%	0.6%	0.7%	0.8%
skm454	71cm Al - 22cm AlF_3	9.79E+08	1.60E+10	4.70E+08	0.62	0.64	0.67	9.55	6.29	15.8	1.65E-11	5.6	5.85E-12
		0.7%	0.4%	1.0%	0.9%	0.6%	1.3%	0.5%	1.1%	0.5%	0.7%	0.7%	0.8%
skm308 (AlF4m)	71cm Al - 27cm AlF_3	9.70E+08	1.28E+10	2.20E+08	0.62	0.64	0.66	6.06	2.89	9.0	1.16E-11	5.5	7.12E-12
		0.7%	0.5%	1.4%	0.9%	0.6%	1.8%	0.5%	1.6%	0.6%	0.8%	1.0%	1.1%
skm439	66 cm FLUENTAL w/o LiF	1.45E+09	1.31E+10	1.88E+08	0.65	0.66	0.69	4.04	5.19	9.2	1.17E-11	8.5	1.08E-11
		0.6%	0.5%	1.3%	0.8%	0.6%	1.7%	0.6%	0.8%	0.5%	0.7%	0.6%	0.8%
skm426	68 cm FLUENTAL w/o LiF	1.39E+09	1.19E+10	1.62E+08	0.65	0.67	0.68	3.52	4.35	7.9	1.10E-11	8.1	1.13E-11
		1.6%	1.3%	4.9%	2.2%	1.8%	6.0%	1.8%	2.8%	1.7%	2.2%	1.6%	2.1%
skm403	68 cm FLUENTAL w/o LiF - 2cm Ti	8.77E+08	1.04E+10	5.54E+07	0.64	0.66	0.68	2.61	3.03	5.6	9.07E-12	7.2	1.15E-11
		1.9%	1.4%	3.7%	2.5%	1.9%	5.0%	1.8%	3.0%	1.8%	2.3%	1.6%	2.1%

Table 3.9 (Continued)

Run ID	Filter/moderator	Φ_{th} n/cm^{2}s	Φ_{epi} n/cm^{2}s	Φ_f n/cm^{2}s	J_{th}/Φ_{th}	J_{epi}/Φ_{epi}	J_f/Φ_f	D_{epi} cGy/min	D_{fast} cGy/min	D_{fn} cGy/min	D_{fn}/Φ_{epi} cGycm^2/n	D_γ cGy/min	D_γ/Φ_{epi} cGycm^2/n
std473	68cm AlF_3(70%)/Al(30%) - 2cm Ti	9.13E+08 1.8%	1.30E+10 1.3%	1.16E+08 3.0%	0.66 2.4%	0.67 1.7%	0.68 4.0%	4.02 1.6%	6.35 2.2%	10.4 1.5%	1.33E-11 1.9%	8.0 1.5%	1.02E-11 2.0%
skm433	69.85 cm Al-$(CF_2)_n$-Al+2%Li-$(CF_2)_n$-Al##	7.60E+08 1.9%	1.23E+10 1.6%	5.39E+08 2.3%	0.65 2.5%	0.66 2.1%	0.69 3.0%	5.81 1.7%	18.3 1.7%	24.1 1.3%	3.25E-11 2.0%	2.2 1.9%	2.99E-12 2.4%
skm430	39.4cm Al - 39.6cm $(CF_2)_n$	1.02E+09 1.8%	5.98E+09 2.1%	9.04E+07 5.5%	0.64 2.3%	0.65 2.8%	0.69 6.8%	1.40 2.9%	3.8 3.1%	5.2 2.4%	1.45E-11 3.2%	10.5 1.1%	2.94E-11 2.4%
skm435	75cm Al - 22cm $(CF_2)_n$	1.08E+09 1.9%	1.12E+10 1.5%	2.00E+08 4.8%	0.62 2.6%	0.63 2.0%	0.64 5.8%	4.36 1.7%	3.8 5.0%	8.2 2.5%	1.21E-11 2.9%	7.0 1.9%	1.04E-11 2.4%
skm434	80cm Al - 17cm $(CF_2)_n$	1.07E+09 1.9%	1.38E+10 1.3%	4.04E+08 2.8%	0.64 2.5%	0.64 1.8%	0.67 3.8%	7.14 1.5%	6.33 3.0%	13.5 1.6%	1.63E-11 2.1%	6.4 2.1%	7.80E-12 2.4%
skm471	96cm Al - 12cm C	1.06E+09 1.2%	1.20E+10 0.9%	3.83E+08 1.9%	0.62 1.6%	0.63 1.2%	0.65 2.5%	6.04 1.0%	6.40 2.1%	12.4 1.2%	1.73E-11 1.5%	6.3 0.9%	8.67E-12 1.3%

BNL filter/moderator design

INEL filter/moderator design

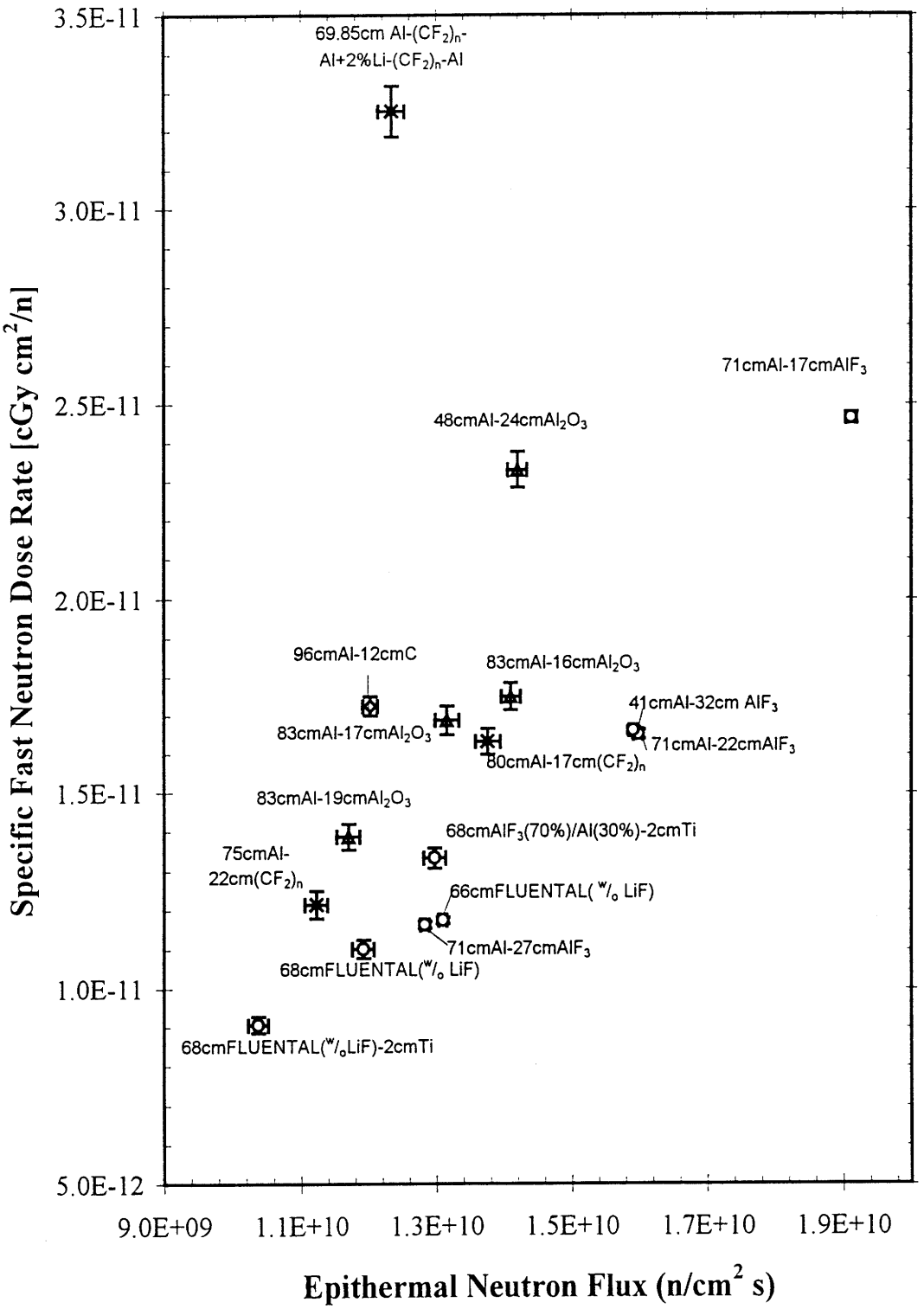

Figure 3.12 Epithermal neutron flux vs. specific fast neutron dose for various fast neutron filter/moderator designs using the combinations of Al-Al_2O_3, Al-AlF_3, Al-(CF_2) and Al-C. The label of each data point denotes the configuration of the the filter/moderator design.

So far, the fast neutron filter/moderator using the combinations of Al-Al_2O_3, Al-AlF_3, Al-$(CF_2)_n$ and Al-C were examined extensively. The next material to be investigated is lead fluoride, PbF_2. The use of PbF_2, suggested by Hungyuan B. Liu[8], is interesting because it works by filtering fast neutrons utilizing fluorine as well as by shielding gamma rays with lead. By replacing oxygen or carbon in Al_2O_3 or $(CF_2)_n$ (these are considered as less desirable band-pass filters than fluorine) with fluorine in PbF_2, the beam performance could potentially be improved. In addition, resonance peaks of Pb in the epithermal energy range are not as high as those of Bi, which could provide another advantage for the use of PbF_2 in place of Bi. For this analysis, the beam designs using the filter/moderator composed of 80 cm Al - 17 cm $(CF_2)_n$ and 83 cm Al - 17 cm Al_2O_3 were changed so that the 8 cm Bi photon shield and a portion of Al_2O_3 or CF_2 in these designs were replaced with a 11cm thick PbF_2 block. The results of the calculations are presented in Table 3.10 with the results for the original filter/moderator designs, i.e., the designs with 80 cm Al - 17 cm $(CF_2)_n$ and 83 cm Al - 17 cm Al_2O_3 followed by an 8 cm Bi photon shield. The results show that these replacements provide slight improvements in beam intensity without increasing fast neutron contamination. The use of PbF_2 also decreases photon contamination by 13%. Although the use of PbF_2 appears to be attractive, its physical, chemical and engineering properties should be examined carefully before making a decision to use it for a practical design.

Table 3.10 Comparison of in-air beam performance of the beam designs with and without a PbF_2 photon shield. These calculations used a fission converter composed of eleven burned MITR-II fuel elements (312 g ^{235}U per element) with D_2O cooling. The fast neutron filter/moderator is followed by a 0.04 cm Cd thermal neutron filter, a PbF_2 or Bi photon shield and a rectangular collimator with 15 cm thick lead lining, and is surrounded by a 10 cm thick lead reflector. The reactor power was set at 5 MW.

Run ID	Filter/moderator	Photon Shield	Φ_{th} n/cm^{2}s	Φ_{epi} n/cm^{2}s	Φ_f n/cm^{2}s	J_{th}/Φ_{th}	J_{epi}/Φ_{epi}	J_f/Φ_f	D_{fn} cGy/min	D_{fn}/Φ_{epi} cGycm^2/n	$D\gamma$ cGy/min	$D\gamma/\Phi_{epi}$ cGycm^2/n
skm434	80cm Al - 17cm $(CF_2)_n$	8cm Bi	1.07E+09	1.38E+10	4.04E+08	0.64	0.64	0.67	13.5	1.63E-11	6.44	7.80E-12
			1.9%	1.3%	2.8%	2.5%	1.8%	3.8%	1.6%	2.1%	2.1%	2.4%
skm446	80cm Al - 11cm $(CF_2)_n$	11 cm PbF_2	1.63E+09	1.45E+10	4.30E+08	0.64	0.65	0.67	14.1	1.63E-11	5.90	6.78E-12
			1.5%	1.3%	2.6%	2.1%	1.7%	3.4%	1.4%	1.9%	2.1%	2.4%
skm451	83cm Al - 17cm Al_2O_3	8cm Bi	9.28E+08	1.32E+10	4.28E+08	0.62	0.65	0.65	13.3	1.69E-11	5.04	6.39E-12
			2.1%	1.3%	3.2%	2.7%	1.8%	4.0%	1.8%	2.2%	2.4%	2.8%
skm447	83cm Al - 11cm Al_2O_3	11 cm PbF_2	1.55E+09	1.45E+10	4.48E+08	0.63	0.64	0.66	13.8	1.59E-11	4.85	5.56E-12
			1.8%	1.3%	3.0%	2.3%	1.7%	3.7%	1.5%	2.0%	2.2%	2.5%

3.3 In-Phantom Beam Performance

So far, fast neutron filter/moderators using different combinations of materials were examined in terms of in-air beam performance. This section will present dose-depth profiles and in-phantom figures of merit (i.e., the advantage depth, advantage ratio and advantage-depth dose rate) using several promising filter/moderator designs, including the explanation of the effect of variation of the neutron spectrum caused by different filter/moderator materials. The descriptions of the computational method and figures of merit used for the in-phantom analysis have been provided in Chapter 1.

In this analysis, boron uptake was assumed to be 40 ppm ^{10}B in tumor with a tumor-to-normal uptake ratio of 3.5:1; the values of boron concentration and uptake ratio used here have been observed for intravenous infusion of BPA-fructose,[16] which is the only drug currently approved by the US FDA as a boron-delivery drug for BNCT.[19] The RBE's which are used are 3.2 for neutrons, 1.0 for photons, 3.8 for boron in tumor, 1.35 for boron in normal tissue. These are the same as those used in the clinical trial of BNCT at MIT/BIDMC[17] with the exception that for photons, an RBE value of 0.5 is used because of the long irradiation times required for the current beam at MITR-II. The calculations used a fission converter composed of eleven D_2O-cooled MITR-II burned fuel elements. The fast neutron filter/moderator is followed by a 0.04 cm Cd thermal neutron filter, an 8 cm Bi photon shield and a pyramidal collimator with a 15 cm thick lead lining. This filter/moderator is surrounded by a 10 cm thick lead reflector. The reactor power was assumed to be 5 MW.

In examining the in-phantom figures of merit, a reader should recognize that the AD and AR are generally the most important figures of merit; maximization of ADDR is secondary to that of

AD and AR because the designs of the fission converter beam which have been developed in Reference 5 and the current study provide ADDR's which are more than adequate for any therapeutic irradiation.

Fast neutron filter/moderator designs selected for this analysis and resulting in-phantom figures of merit are presented in Table 3.11 along with their in-air figures of merit. In this table, the ratio of ADDR to the number of epithermal neutrons crossing the unit area at the patient position (J_{epi}) for each design is presented to compare the result with that of Reference 6, where the in-phantom figures of merit were calculated using the neutron beam which had a constant number of neutrons crossing the source plane per unit area. Also, for comparison, in-phantom beam performance of the beam design proposed in Reference 5 (std473) is shown. As an example of the dose-depth profile, the one for a unilateral irradiation with the fast neutron filter/moderator design composed of 71 cm Al - 27 cm AlF_3 (skm308) is shown with its dose components in Figure 3.13. As discussed below, variation of the in-phantom figures of merit concerning beam quality (AD and AR) for different filter/moderator designs shown in Table 3.11 is very small. Therefore, the shapes of the dose depth profiles produced by the other designs are expected to be very similar to that of Design skm308. The dose-depth profiles for a bilateral irradiation using this beam design is compared with those using the currently available MIT M67 beam[13] in Figure 3.14. In addition, the profiles of epithermal and thermal neutron fluxes as a function of depth in the head phantom produced by Design skm308 are presented in Figure 3.15. Although in-phantom figures of merit for the combination of Al - C is not evaluated, a consideration of its in-phantom beam performance based on the neutron spectrum will be presented below.

Table 3.11 shows various filter/moderator designs which provide comparable or better performance than the beam design proposed in Reference 5. All of the designs provide deep penetration of the beam (the AD of 9.3-9.8 cm extends significantly beyond the centerline of the

head phantom) and large therapeutic gain (the AR is around 5). Moreover, they produce advantage depth dose rates of 400-600 RBE cGy/min. The advantage parameters for the current MIT medical beam (M67 beam) based on the same assumptions of ^{10}B uptake and RBE values calculated by Reference 5 are: AD = 7.0 cm, ADDR = 8.8 RBE cGy/min and AR = 2.6. Compared to this beam, the designs of the fission converter beam in Table 3.11 double the advantage ratio and increase the advantage depth by 2 to 3 cm. Moreover, they provide an advantage depth dose rate ~ 50 to 70 times higher than that of the current beam.

Figure 3.13 shows that the effect of fast neutron and photon contamination of the beam is indeed negligible relative to the irreducible background of hydrogen and nitrogen capture in the phantom (i.e., dose components of induced photons and induced protons from the $^{14}N(n,p)$ reaction). The largest single background component is due to normal tissue concentrations of ^{10}B from the boron delivery agent. This dose component will decrease and beam performance would be further improved as better compounds are developed. For example, using an advanced tumor-targeting compound with a tumor-to-normal tissue concentration ratio of 10:1, the AD and AR increase to 10.6 cm and 7.0 respectively (advantage depth dose rate decreases to 273 RBE cGy/min) for the same filter/moderator design (71 cm Al - 27 cm AlF_3). Figure 3.14 shows that a bilateral irradiation using this beam design provides an AR of 4.8 which is significantly larger than that of the current MIT M67 beam (AR = 3.1). It is indicated by Figure 3.15 that the peak thermal neutron flux in the phantom is $2.9*10^{10}$ n/cm^{2}s, which occurs at around 2.5 cm depth. The ratio of peak to surface thermal flux is around 5. The M67 beam at MITR provides a peak thermal neutron flux of $2.2*10^8$ n/cm^{2}s at around 2 cm with a peak to surface flux ratio of ~ 3, which was measured in an ellipsoidal water phantom by Reference 18. Since the ^{10}B dose is directly proportional to the thermal neutron flux, it is recognized that the thermal flux profile of the fission converter beam provides significant reduction of radiation damage near the surface, increasing the

therapeutic dose at depth and improving beam penetration relative to the M67 beam.

The effect of the variation of neutron spectrum caused by different filter/moderator designs on the in-phantom figures of merit and the dose depth profile will be analyzed. First, the neutron spectra at the patient position generated by the filter/moderator designs using 83 cm Al - 17 cm Al_2O_3 (skm451), 71 cm Al - 27 cm AlF_3 (skm308) and 80 cm Al - 17 cm $(CF_2)_n$ (skm434), which provide almost the same beam intensities ($1.3*10^{10}$ to $1.4*10^{10}$ n/cm^{2}s), are compared in Figure 3.16 using a linear scale and in Figure 3.17 using a log scale. Interestingly, the shapes of these spectra are very similar in the epithermal energy range; they differ appreciably only in the fast energy region (skm451 and skm434 have higher fast neutron flux than skm308). Because of the similarity of the neutron spectra in the epithermal range and the very low level ($< 2.0*10^{-11}$ cGy cm^2/n) of fast neutron contamination, the AD's and AR's (indicators of beam quality) are almost the same and only the ADDR's vary approximately in proportion to beam intensity for these beam designs (note that J_{epi}/Φ_{epi} is almost constant for the filter/moderator designs shown in Table 3.11; then, the ADDR/J_{epi} is constant when the ADDR varies in proportion to Φ_{epi}). The neutron spectrum for the design using 96 cm Al - 12 cm C (skm471) at the patient position is also presented in Figure 3.15 and 3.16. One should note that this design also produces a very similar epithermal spectrum to those of the other designs. Because this design maintains fast neutron contamination at as low a level as others while producing comparable epithermal neutron flux, it is expected that this design would produce comparable in-phantom beam performance in terms of both beam intensity and quality relative to the others.

Next, the results for the designs using 71 cm Al - 27 cm AlF_3 (skm308), 68 cm 70% AlF_3/30% Al (96% theoretical density) with 2 cm Ti (std473) and 66 cm FLUENTAL $^{w}/_{o}$ LiF (skm439), which produce almost the same epithermal neutron flux at the patient position, are compared to examine the effect of increasing the amount of fluorine in the filter/moderator from

that of 71cm Al - 27 cm AlF_3 (skm308). The neutron spectra at the patient position for these filter/moderator designs are shown in Figures 3.18 (linear scale) and 3.19 (log scale). Figure 3.18 shows that the low energy portion of the epithermal region is increased and the high energy portion is decreased as the amount of fluorine in the filter/moderator is increased. In other words, the larger amount of fluorine softens the spectrum in the epithermal region. For Design std473, the resonance peaks of Ti above 3 keV also contribute to reduction of the high energy portion of the epithermal region. On the other hand, in Figure 3.19, it is noted that Designs std473 and skm439 increase the flux in the fast energy range above ~30 keV relative to Design skm308, which is due to less Al in Designs std473 and skm439. Although Designs std473 and skm439 provide lower specific fast neutron doses than skm308, they also decrease the useful portion of the spectrum from 100 eV to 10 keV.

As for in-phantom figures of merit, Design skm308 (71cm Al - 27 cm AlF_3) has slightly higher advantage depth than Design std473 (68 cm 70% AlF_3/30% Al - 2cm Ti) and Design skm439 (66 cm FLUENTAL $^{W}/_{O}$ LiF). It is also noted that, again, ADDR varies approximately in proportion to beam intensity (i.e., $ADDR/J_{epi}$ is approximately constant). Moreover, the advantage ratio does not vary for these designs. Likely explanations for these observations are given by the results of the ideal beam study in Reference 6, which examined the effect of the neutron energy, emission angle and beam size relative to the target size on in-phantom figures of merit. As for energy dependency, this study showed the following results: AD is maximized roughly at 2 - 10 keV. ADDR as a function of neutron energy shows a wavelike shape for neutrons with small emission angles (30 degrees or less), which is maximized roughly at 0.5 or 1.0 eV and minimized at 1 - 2 keV, before increasing at higher energies. This wavelike shape disappears and becomes almost flat as the emission angle increases. AR is maximized at the thermal energy region decreasing very slowly in the epithermal region and abruptly above ~ 10 keV. Since the portion of

the spectrum increased for Design skm308 ranges approximately from 100 eV to 30 keV, it is likely that its AD is higher than those for Designs std473 and skm439. Since the fast neutron flux is very low compared to the epithermal flux for these three designs, their AR's are likely to be the same. In addition, the variation of ADDR in the epithermal energy range shown in Reference 6 appears to be very small. Therefore, because of this behavior of ADDR in the epithermal range and very low fast neutron contamination of these beam designs, it is expected that the difference in the neutron spectrum shown in Figures 3.18 and 3.19 does not affect $ADDR/J_{epi}$. The dose-depth profiles of these three designs are presented in Figure 3.20.

Finally, the filter/moderator designs using 71 cm Al - 27 cm AlF_3 (skm308), 71 cm Al - 22 cm AlF_3 (skm454) and 71 cm Al - 17 cm AlF_3 (skm460) are examined. By comparing the beam performance of these designs, one can see the effect of decreasing the thickness of the AlF_3 layer. The neutron spectra for these filter/moderator designs are depicted in Figures 3.21 (linear scale) and 3.22 (log scale). In addition, dose-depth profiles produced by these designs are shown in Figure 3.23, where the dose component due to fast neutrons is presented to show the effect of the change in fast neutron contamination. In Figures 3.21 and 3.22, it is noted that the high energy portion of the epithermal region increases significantly as well as the fast neutron flux with decreasing thickness of the AlF_3 layer. As a result, Design skm460 (71 cm Al - 17 cm AlF_3) produces a specific fast neutron dose of $2.46*10^{-11}$ $cGycm^2/n$, which is above the design goal. However, although the specific fast neutron dose is increased above the nominal design goal, the advantage depth and advantage ratio are maintained at the same level while the advantage depth dose rate increases in proportion to the epithermal neutron flux. Hence, it is concluded that, within the range of low fast neutron contamination considered here, the beam quality is not degraded. Based on this result, the design goal for fast neutron contamination ($D_{fn}/\Phi_{epi} < 2*10^{-11}$ $cGycm^2/n$) is considered lower than necessary. Figure 3.23 illustrates that the effect of fast neutron

contamination is very small except for the location very close to the surface for these designs. In addition, the analyses of dose-depth profiles in the case of zero ^{10}B in normal tissue for these designs show that the contribution from the fast neutron component to the peak normal tissue dose is negligible. These observations support the above conclusion.

The neutron spectra generated by the designs using 41 cm Al - 32 cm AlF_3 (skm457) and 71 cm Al - 22 cm AlF_3 (skm454) were compared in Section 3.2. The results of in-phantom analysis for these designs show that the difference in the neutron spectrum between these designs does not affect beam quality (AD and AR) but varies ADDR slightly.

Table 3.11 In-phantom beam performance for different fast neutron filter/moderator designs. Boron uptake was assumed at 40 ppm ^{10}B in tumor with a tumor-to-normal tissue uptake ratio of 3.5:1. The RBE's are 3.2 for neutrons, 1.0 for photons, 3.8 for boron in tumor, 1.35 for boron in normal tissue. These calculations used a D_2O cooled fission converter composed of eleven burned MITR-II fuel elements (fuel loading is 312 g-^{235}U per element) at a MITR reactor power of 5 MW. The fast neutron filter/moderator is surrounded by a 10 cm thick lead reflector. It is followed by a 0.04 cm Cd thermal neutron filter, an 8 cm Bi photon shield and a pyramidal collimator with a 15 cm thick lead lining and a beam aperture size of 20 cm*20 cm.

Run ID	Fast Neutron Filter/Moderator	Filter/Moderator Material	Φ_{epi} n/cm^{2}s	D_{fn}/Φ_{epi} cGycm^2/n	$D\gamma/\Phi_{epi}$ cGycm^2/n	J_{epi}/Φ_{epi}	AD cm	ADDR RBEcGy/min	AR	ADDR/J_{epi} RBEcGycm^2/n
skm451 (AlO22)	83cm Al - 17cm Al_2O_3	Al 2866kg, O 350kg	1.32E+10 1.3%	1.69E-11 2.2%	6.39E-12 2.8%	0.65 1.8%	9.7	417	5.0	8.20E-10
skm460	71cm Al - 17cm AlF_3	Al 2289kg, F 367kg	1.91E+10 0.4%	2.46E-11 0.6%	5.10E-12 0.8%	0.64 0.5%	9.8	605	5.0	8.18E-10
skm454	71cm Al - 22cm AlF_3	Al 2340kg, F 474kg	1.60E+10 0.4%	1.65E-11 0.7%	5.85E-12 0.8%	0.64 0.6%	9.7	501	5.0	8.17E-10
skm308 (AlF4m)	71cm Al - 27cm AlF_3	Al 2391kg, F 582kg	1.28E+10 0.5%	1.16E-11 0.8%	7.12E-12 1.1%	0.64 0.6%	9.7	402	5.0	8.21E-10
skm457 (AlF2)	41cm Al - 32cm AlF_3	Al 1548kg, F 690kg	1.59E+10 0.4%	1.66E-11 0.6%	8.32E-12 1.2%	0.66 0.5%	9.6	525	4.9	8.38E-10
std473	68cm AlF_3(70%)/Al(30%) - 2cm Ti	Al 1050kg, F 985kg Ti 99kg	1.30E+10 1.3%	1.33E-11 1.9%	1.02E-11 2.0%	0.67 1.7%	9.5	435	4.9	8.39E-10
skm439	66 cm FLUENTAL w/o LiF	Al 1138kg, F 1038kg	1.31E+10 0.5%	1.17E-11 0.7%	1.08E-11 0.8%	0.66 0.6%	9.3	455	4.9	8.74E-10
skm434	80cm Al - 17cm $(CF_2)_n$	Al 2383kg, C 97kg F 306kg	1.38E+10 1.3%	1.63E-11 2.1%	7.80E-12 2.4%	0.64 1.8%	9.6	443	4.9	8.37E-10

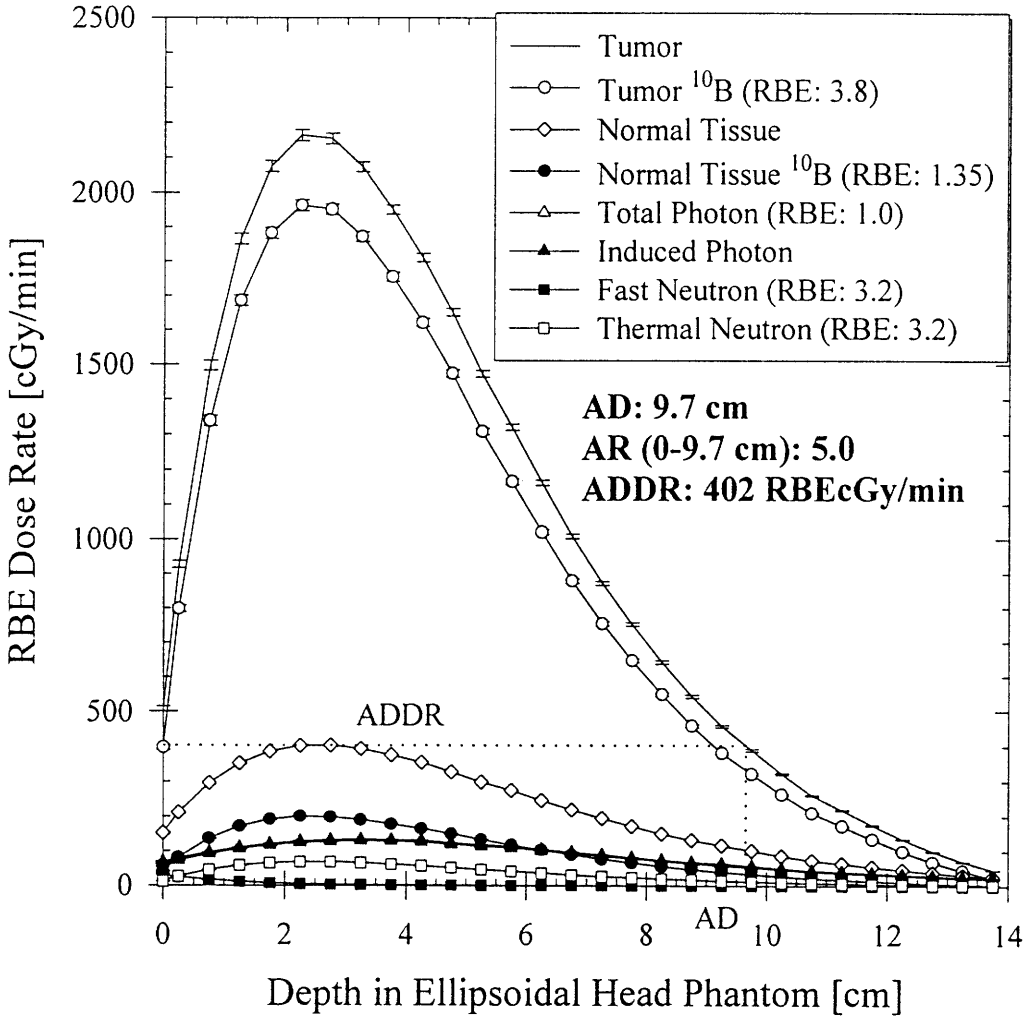

Figure 3.13 Dose-depth profiles for unilateral irradiation produced by the fission converter beam with D_2O-cooled burned MITR-II fuel and the fast neutron filter/moderator design composed of 71 cm Al - 27 cm AlF_3 (skm308). The filter/moderator is followed by a 0.04 cm Cd thermal neutron filter, an 8 cm Bi photon shield and a pyramidal collimator with 15 cm thick lead lining, and is surrounded by a 10 cm thick lead reflector. The beam aperture size is 20 cm* 20 cm. The MITR reactor power was set at 5 MW. Boron uptake was assumed at 40 ppm ^{10}B in tumor with a tumor-to-normal uptake ratio of 3.5:1.

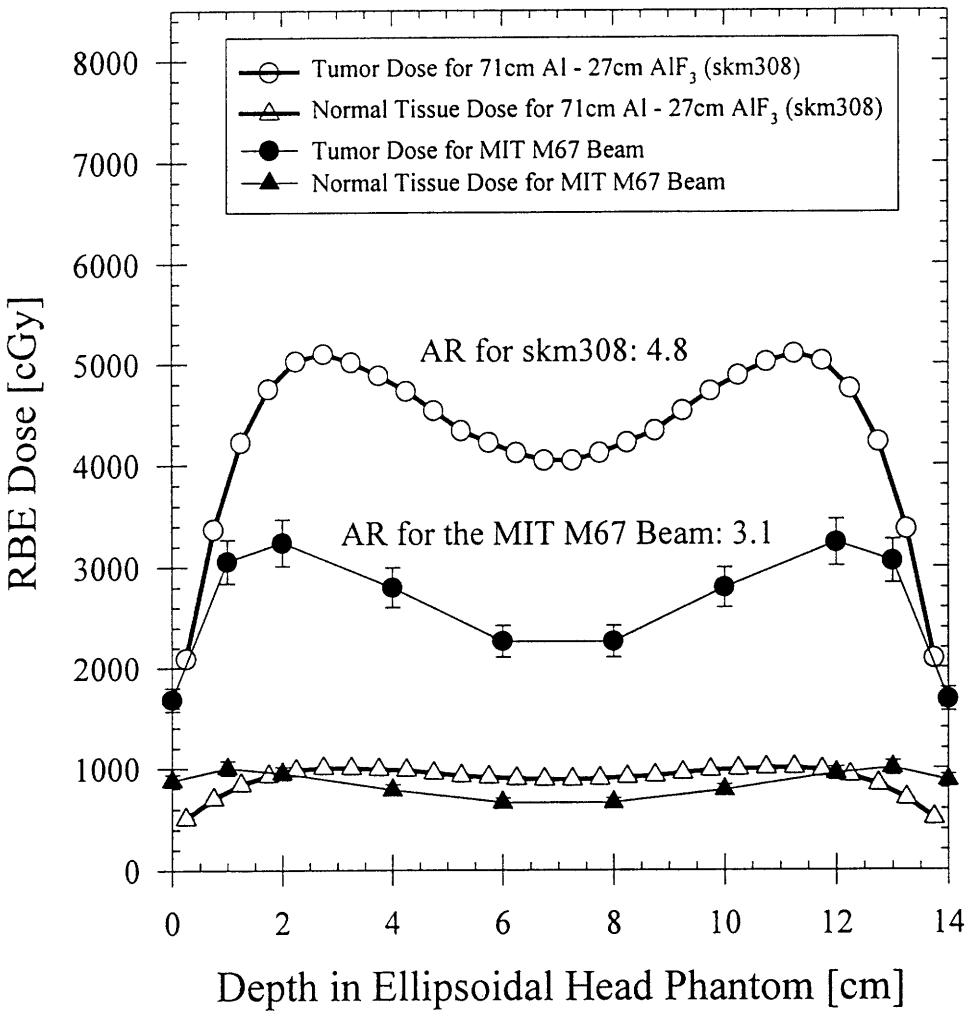

Figure 3.14 Comparison of dose-depth profiles for bilateral irradiations calculated for the fission converter beam with D_2O-cooled burned MITR-II fuel and measured for the MIT M67 beam at a reactor power of 5 MW. The doses are normalized so that the maximum normal tissue dose is equal to 1000 cGy. The fast neutron filter/moderator of the fission converter beam is composed of 71 cm Al - 27 cm AlF_3 (skm308). The filter/moderator is followed by a 0.04 cm Cd thermal neutron filter, an 8 cm Bi photon shield and a pyramidal collimator with a 15 cm thick lead lining, and is surrounded by a 10 cm thick lead reflector. The beam aperture size is 20 cm* 20 cm. Boron uptake was assumed at 40 ppm ^{10}B in tumor with a tumor-to-normal uptake ratio of 3.5:1. The RBE's are 3.2 for neutrons, 1.0 for photons, 3.8 for boron in tumor, 1.35 for boron in normal tissue.

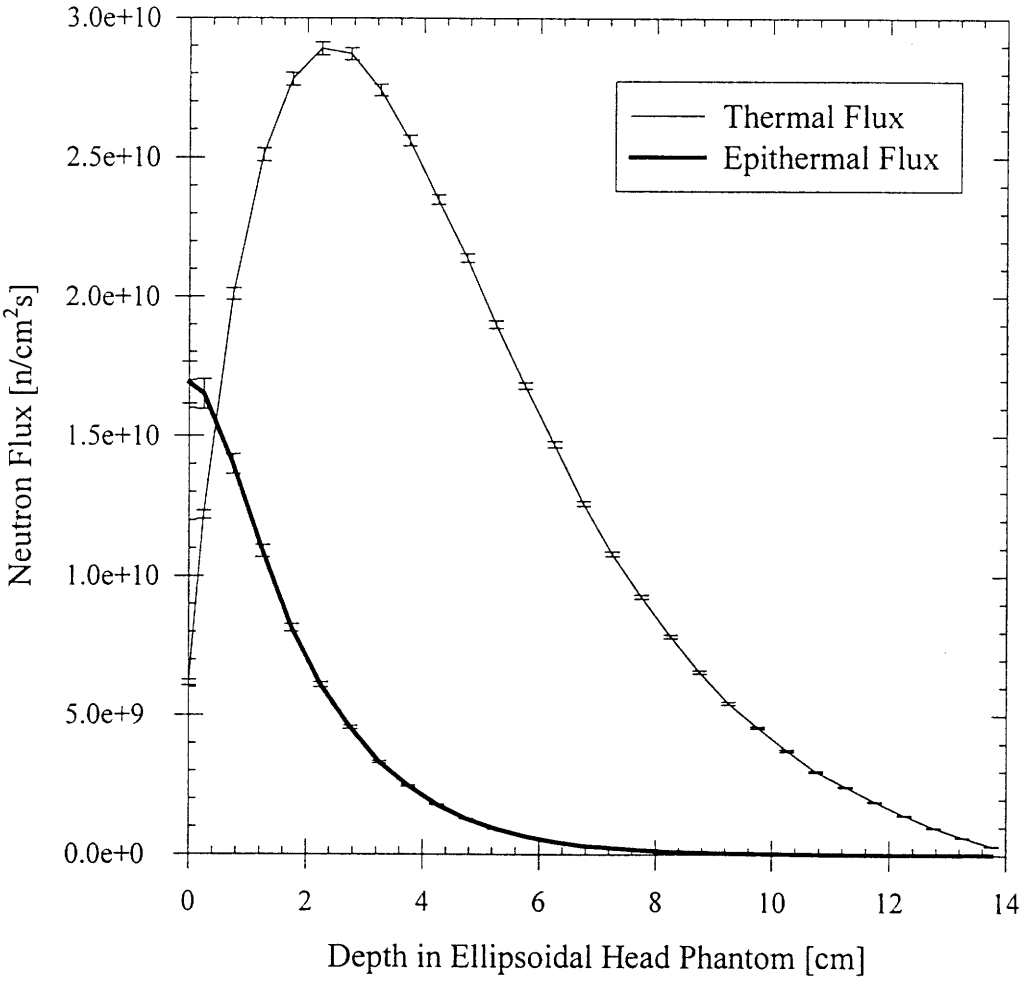

Figure 3.15 Profiles of epithermal and thermal neutron fluxes as a function of depth in the head phantom produced by the fission converter beam with D_2O-cooled burned MITR-II fuel and the fast neutron filter/moderator composed of 71 cm Al - 27 cm AlF_3 (skm308). The filter/moderator is followed by a 0.04 cm Cd thermal neutron filter, an 8 cm Bi photon shield and a pyramidal collimator with 15 cm thick lead lining, and is surrounded by a 10 cm thick lead reflector. The beam aperture size is 20 cm* 20 cm. The MITR reactor power was set at 5 MW.

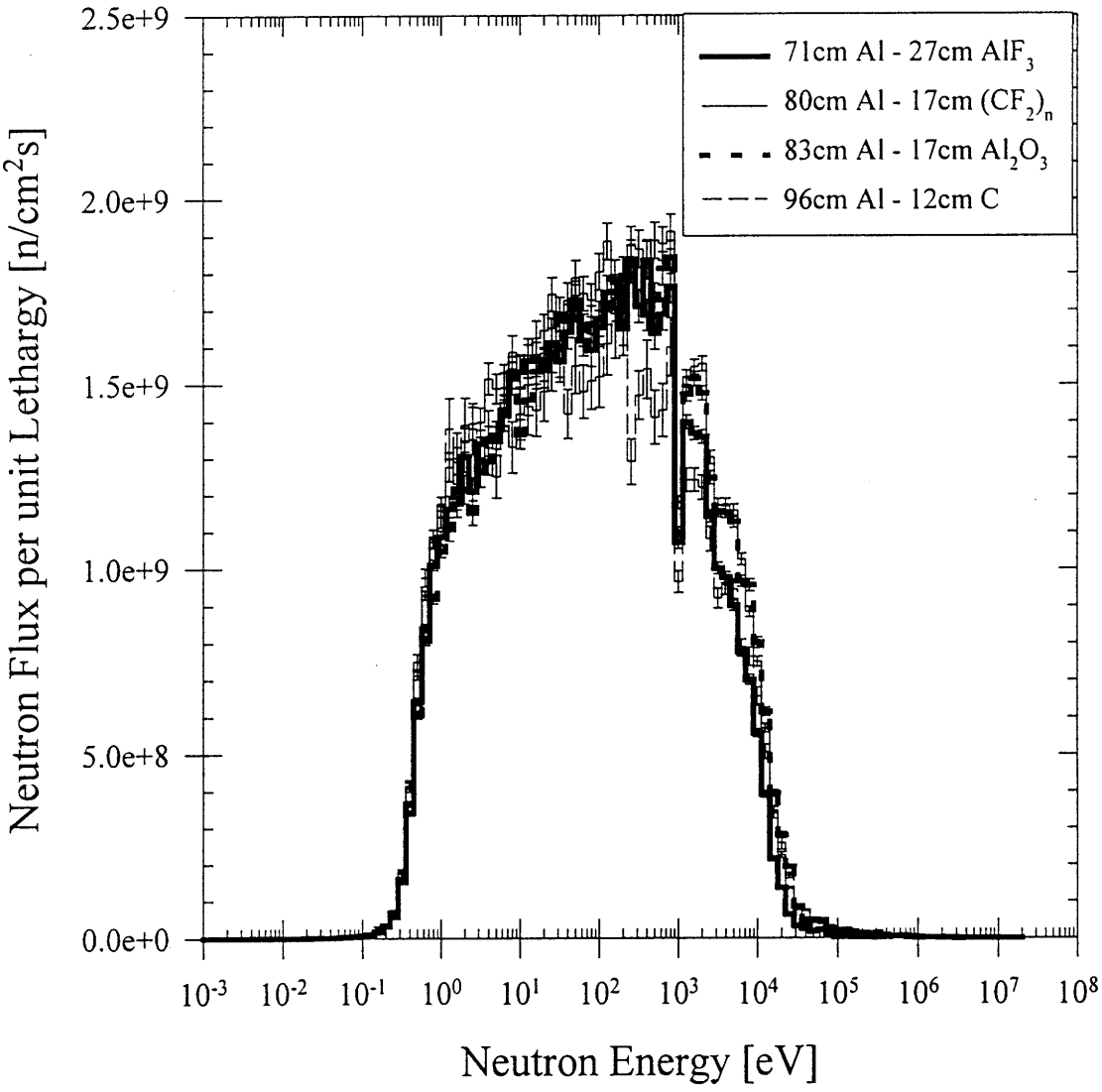

Figure 3.16 Comparison of the neutron flux spectra at the patient position generated by the fission converter beams with D_2O-cooled burned MITR-II fuel and the fast neutron filter/moderator designs using 83 cm Al - 17 cm Al_2O_3 (skm451), 71 cm Al - 27 cm AlF_3 (skm308), 80 cm Al - 17 cm $(CF_2)_n$ (skm434) and 96 cm Al - 12 cm C (skm471) shown in a linear scale. The reactor power was set at 5 MW.

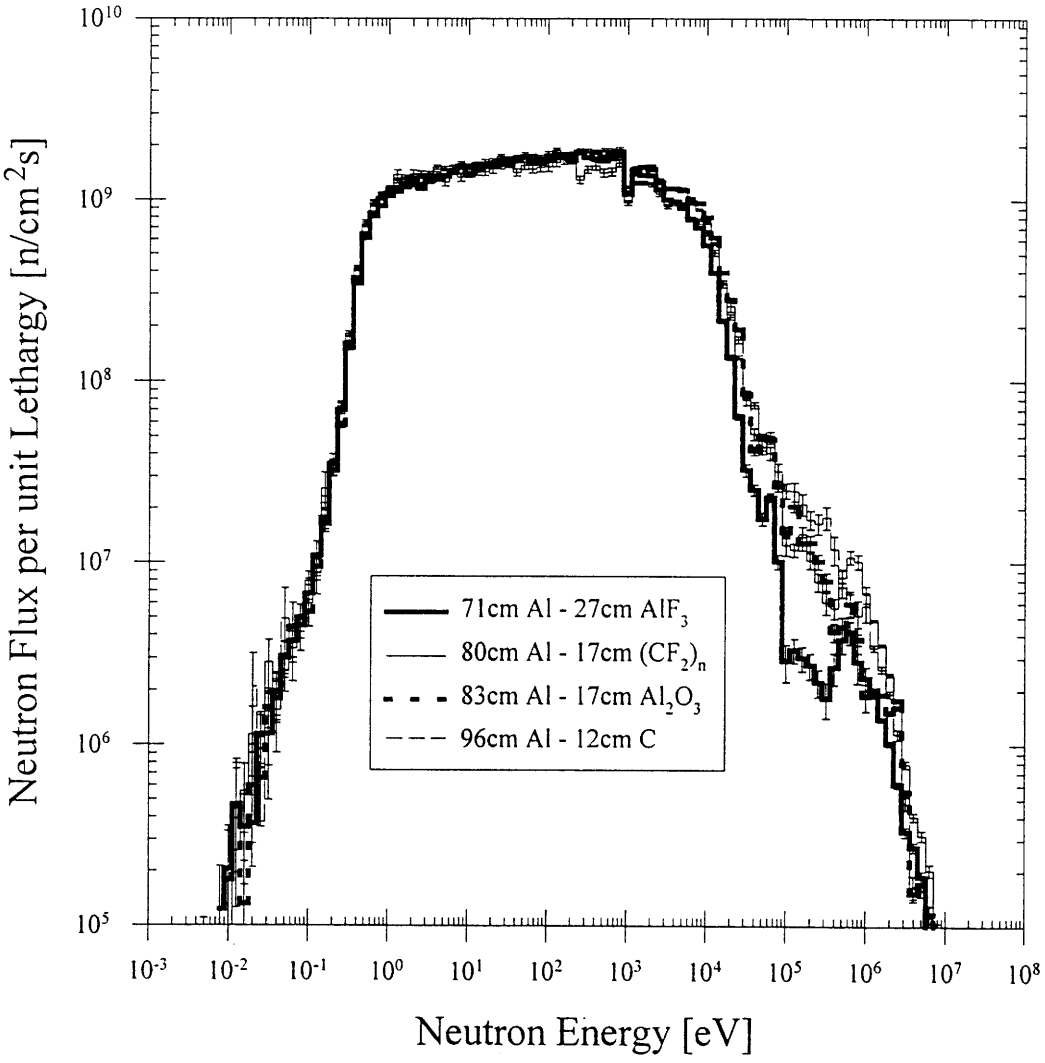

Figure 3.17 Comparison of the neutron flux spectra at the patient position generated by the fission converter beams with D_2O-cooled burned MITR-II fuel and the fast neutron filter/moderator designs using 83 cm Al - 17 cm Al_2O_3 (skm451), 71 cm Al - 27 cm AlF_3 (skm308), 80 cm Al - 17 cm $(CF_2)_n$ (skm434) and 96 cm Al - 12 cm C (skm471) in a log scale. The reactor power was set at 5 MW.

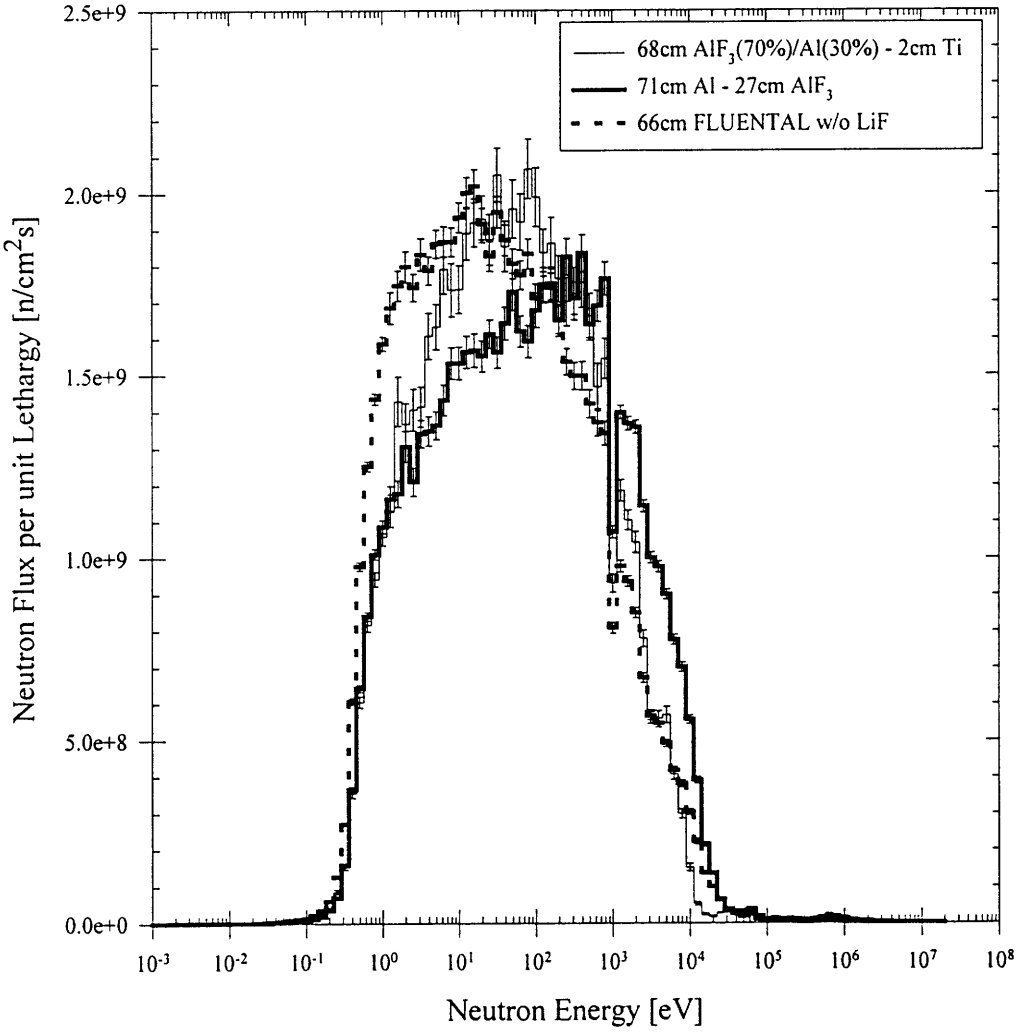

Figure 3.18 Comparison of the neutron flux spectra at the patient position generated by the fission converter beams with D_2O-cooled burned MITR-II fuel and the fast neutron filter/moderator designs using 71 cm Al - 27 cm AlF_3 (skm308), 68 cm AlF_3(70%)/Al(30%) - 2 cm Ti (std473), and 66 cm FLUENTAL $^{w}/_{o}$ LiF (skm439) in a linear scale. The reactor power was set at 5 MW.

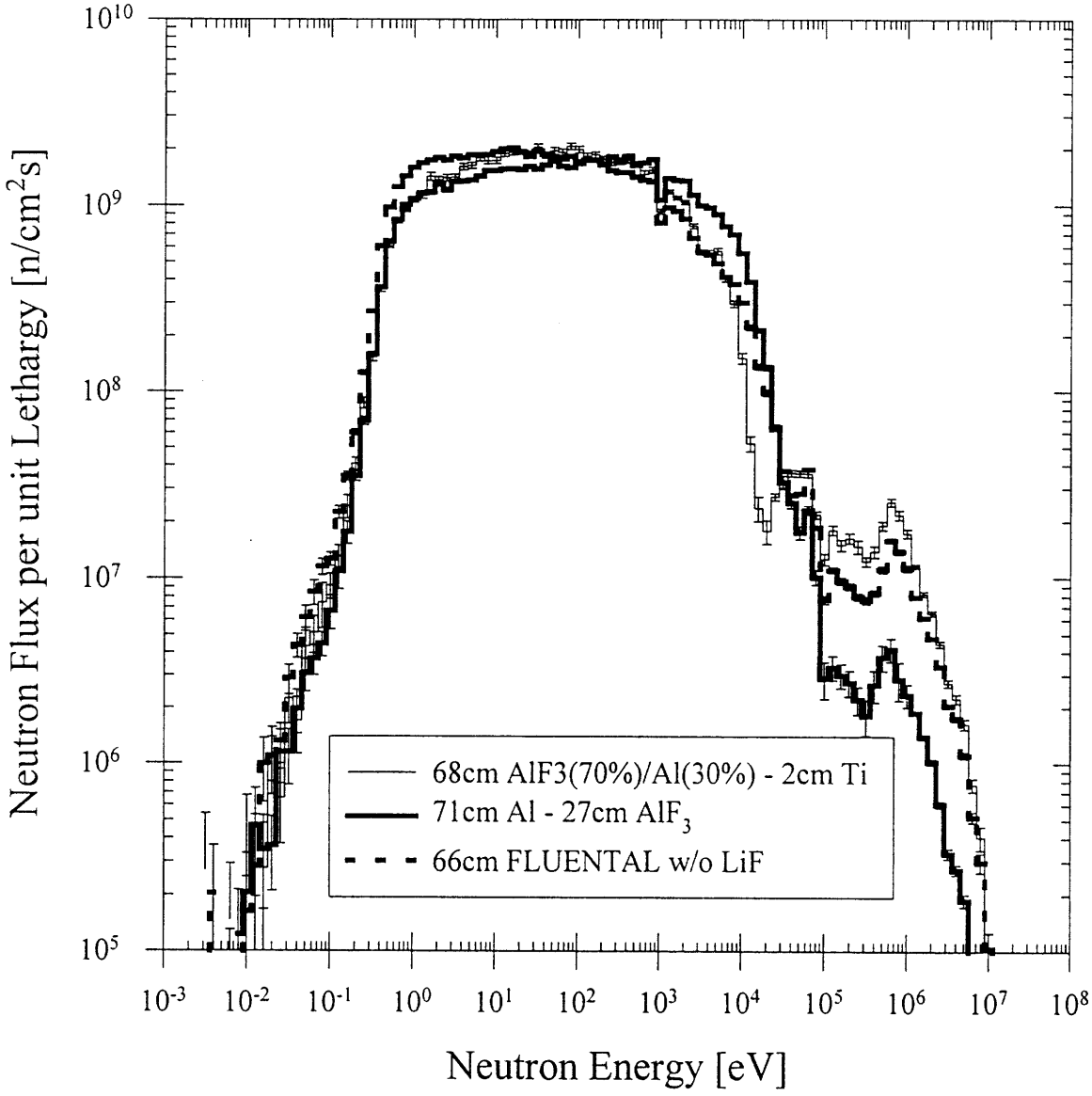

Figure 3.19 Comparison of the neutron flux spectra at the patient position generated by the fission converter beams with D_2O-cooled burned MITR-II fuel and the fast neutron filter/moderator designs using 71 cm Al - 27 cm AlF_3 (skm308), 68 cm AlF_3(70%)/Al(30%) - 2 cm Ti (std473), and 66 cm FLUENTAL $^{w}/_{o}$ LiF (skm439) in a log scale. The reactor power was set at 5 MW.

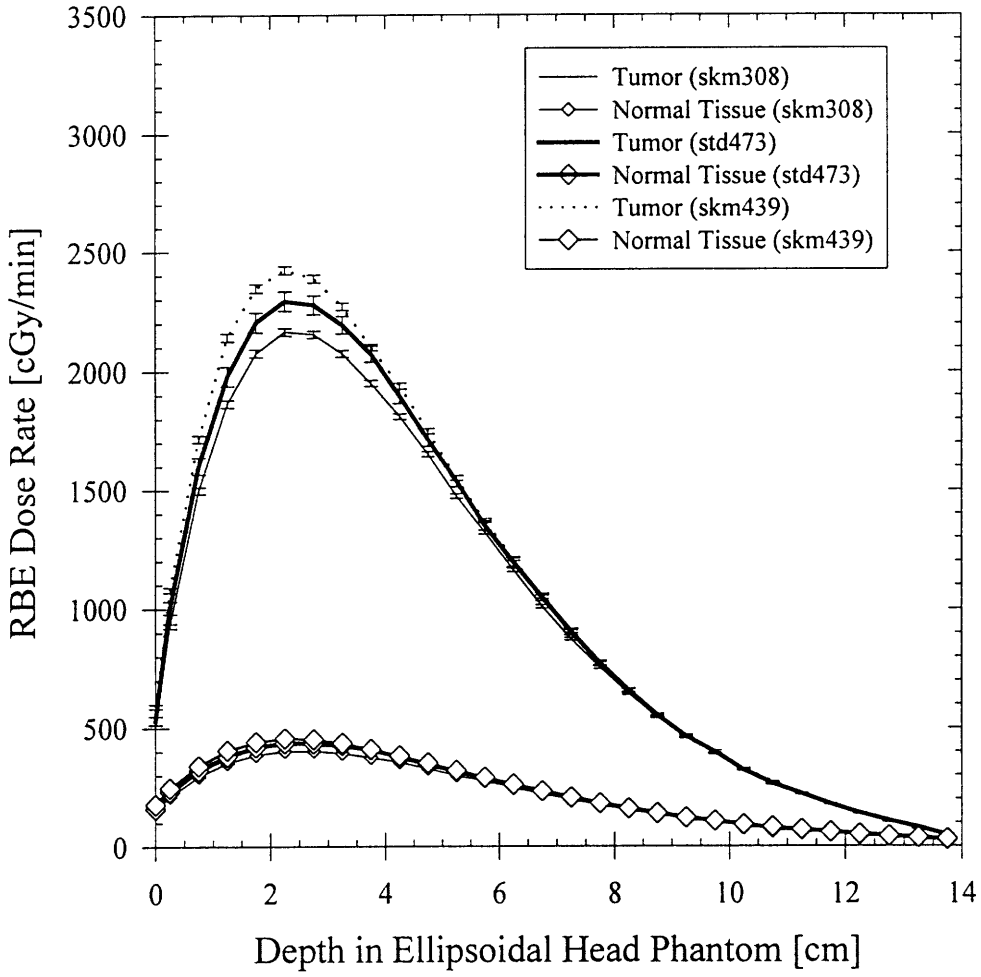

Figure 3.20 Comparison of dose-depth profiles for unilateral irradiation produced by the fission converter beams with D_2O-cooled burned MITR-II fuel and the fast neutron filter/moderator designs using 71 cm Al - 27 cm AlF_3 (skm308), 68 cm 70% AlF_3/30% Al - 2 cm Ti (std473) and 66 cm FLUENTAL $^{W}/_{O}$ LiF (skm460). Boron uptake was assumed at 40 ppm ^{10}B in tumor with a tumor-to-normal uptake ratio of 3.5:1. The RBE's are 3.2 for neutrons, 1.0 for photons, 3.8 for boron in tumor, 1.35 for boron in normal tissue. The reactor power was set at 5 MW.

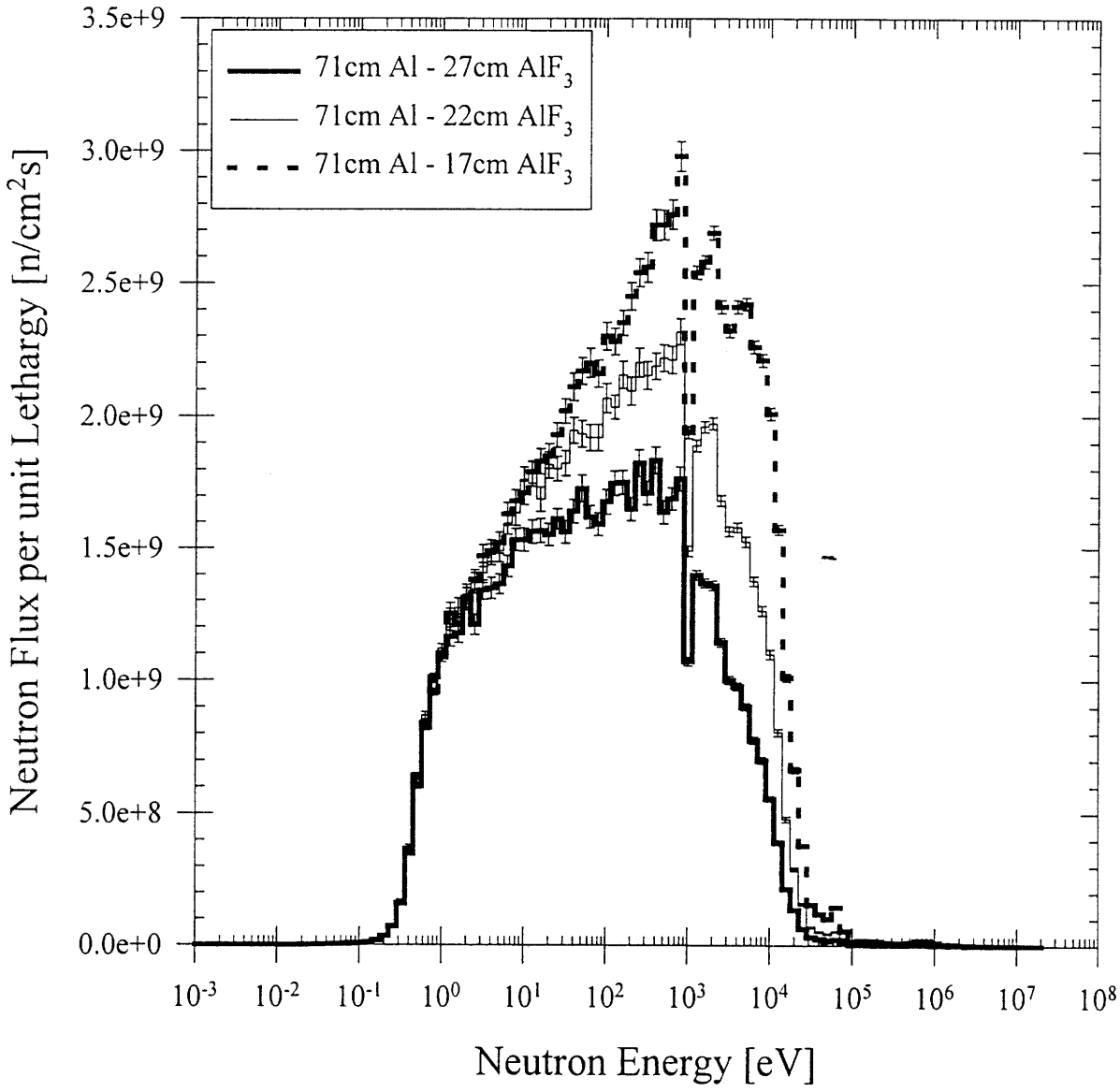

Figure 3.21 Comparison of the neutron flux spectra at the patient position generated by the fission converter beams with D_2O-cooled burned MITR-II fuel and the fast neutron filter/moderator designs using 71 cm Al - 27 cm AlF_3 (skm308), 71 cm Al - 22 cm AlF_3 (skm454), and 71 cm Al - 17 cm AlF_3 (skm460) in a linear scale. The reactor power was set at 5 MW.

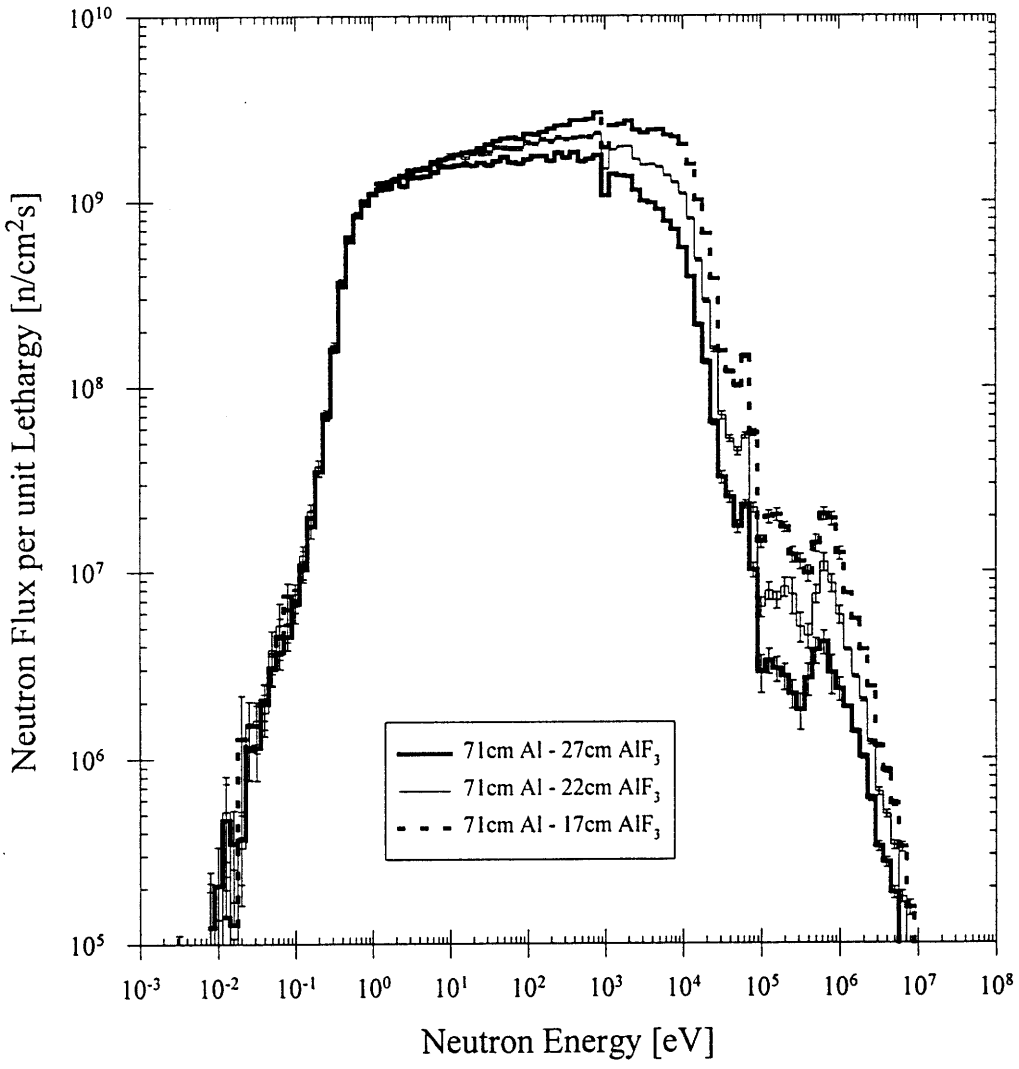

Figure 3.22 Comparison of the neutron flux spectra at the patient position generated by the fission converter beams with D_2O-cooled burned MITR-II fuel and the fast neutron filter/moderator designs using 71 cm Al - 27 cm AlF_3 (skm308), 71 cm Al - 22 cm AlF_3 (skm454), and 71 cm Al - 17 cm AlF_3 (skm460) in a log scale. The reactor power was set at 5 MW.

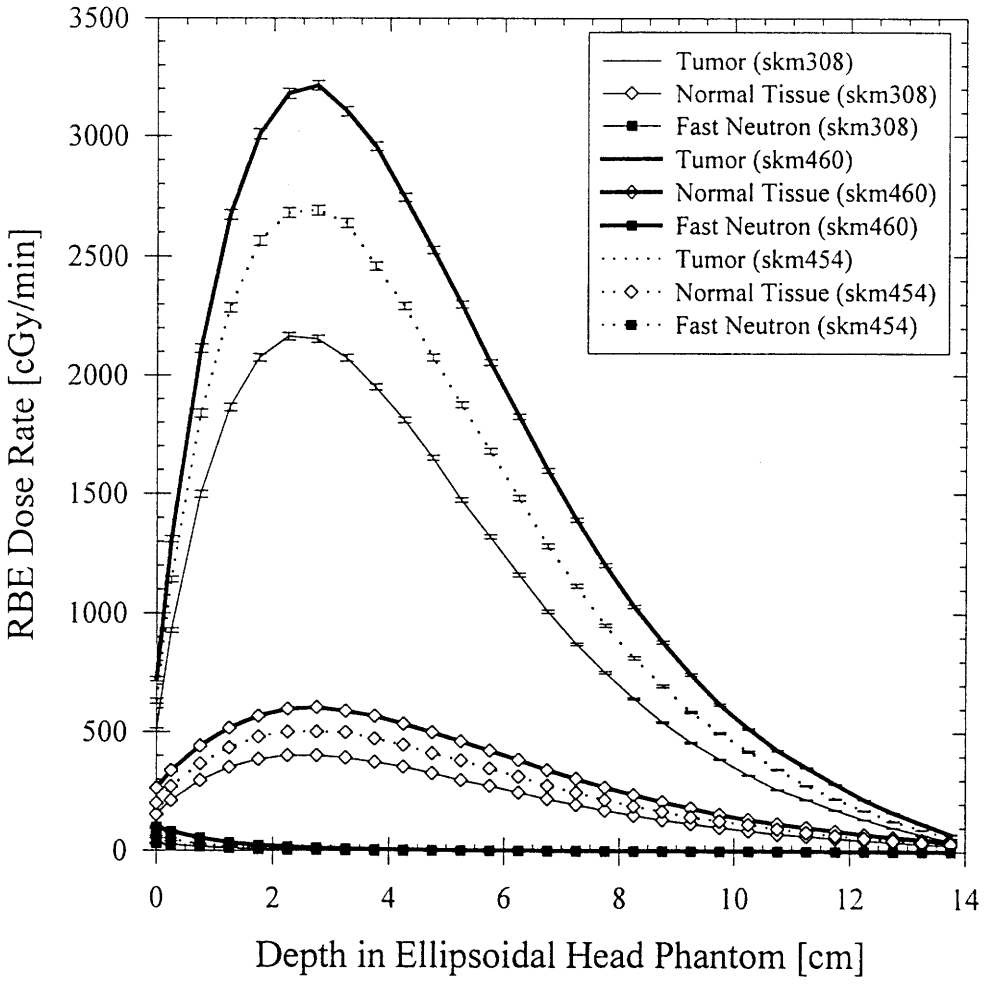

Figure 3.23 Comparison of dose-depth profiles for unilateral irradiations using the fission converter beams with D_2O-cooled burned MITR-II fuel and the fast neutron filter/moderator designs composed of 71 cm Al - 27 cm AlF_3 (skm308), 71 cm Al - 22 cm AlF_3 (skm454) and 71 cm Al - 17 cm AlF_3 (skm460). Boron uptake was assumed at 40 ppm ^{10}B in tumor with a tumor-to-normal uptake ratio of 3.5:1. The RBE's are 3.2 for neutrons, 1.0 for photons, 3.8 for boron in tumor, 1.35 for boron in normal tissue. The reactor power was set at 5 MW.

3.4 Analysis of the Thermal Neutron Filter

Among conventional thermal neutron absorbers, Cd, ^{6}Li, and ^{10}B, Cd was selected in Reference 5 because of its better transmission of epithermal neutrons due to the abrupt drop of its absorption cross section at 0.4 eV compared to other materials which have 1/v absorption cross sections. The thermal neutron filter used a 0.04 cm thick layer of Cd placed just downstream of the fast neutron filter/moderator, which absorbs 99% of incident 0.025 eV thermal neutrons while absorbing only 1% of 1 keV epithermal neutrons. A major drawback of using Cd is its emission of high energy gamma rays upon neutron capture. To mitigate this problem, the Cd thermal neutron filter was placed in front of a thick photon shield. Considering that photon contamination for the beam designs shown in Table 3.9 is essentially negligible compared to inherent hydrogen capture gamma in the tissue (i.e., D_{γ}/Φ_{epi}, $<< 2*10^{-10}$cGycm^2/n), the use of 0.04 cm Cd is justified for this beam. However, there are several ways to reduce photon contamination from the thermal neutron filter, e.g., the use of ^{6}Li or ^{10}B.

Some calculations were done to examine the effect of using ^{6}Li with filter/moderator designs which consist of FLUENTAL with or without 1% natural LiF (by weight). The LiF used here was uniformly distributed in FLUENTAL. If it was not used, a 0.04 cm Cd sheet was used as a thermal neutron filter. The results are summarized in Table 3.12. Comparison of the results of the designs using different materials for the thermal neutron filter shows that specific photon dose is reduced by a factor of 3-4 and epithermal neutron flux is decreased by ~20 % when $1^{w}/_{o}$ LiF(nat.) is used in place of a 0.04 cm Cd sheet. A significant reduction of the photon contamination is achieved due to suppression of radiative capture in Al caused by thermal neutron removal by the uniformly distributed ^{6}Li as well as removal of the Cd sheet. It should be recognized that, when using $1^{w}/_{o}$ LiF, very low photon contamination ($3*10^{-12}$ to $4*10^{-12}$ cGycm^2/n) would enable one to reduce

the thickness of the photon shield (8 cm Bi) significantly and regain beam intensity. However, the study of photon shield in Reference 5 showed that the reduction of the thickness of Bi photon shield by 50% (i.e., from 8 cm to 4 cm) would increase the epithermal neutron flux by 20% while increasing the specific photon dose by a factor of ~3. Therefore, the net benefit of replacing the 0.04 cm Cd sheet with $1^{w}/_{o}$ LiF uniformly distributed in FLUENTAL is expected to be insignificant.

Another way of reducing the effect of Cd photon production is to move a part or the whole of the Cd filter upstream to take advantage of the shielding effect of filter/moderator materials. To see this shielding effect of the filter/moderator for Cd capture gamma rays, a calculation was done using two separate 0.02 cm thick Cd sheets instead of one 0.04 cm Cd sheet, one of which was located in the middle of the fast neutron filter/moderator composed of 71 cm Al - 27 cm AlF_3 and the other was placed at the original location (i.e., downstream of the filter/moderator and in front of the photon shield). The results for the single and split-sheet designs are compared in Table 3.13. The results show that, although the relocation of the Cd filter reduces photon contamination by 16%, it also causes an undesired increase in the thermal neutron flux by 19%.

From the results presented so far, it is concluded that relocating a Cd sheet or replacing it with ^{6}Li does not appear to be advantageous. One should also note that the trade-off between the advantage of reduced photon contamination and the disadvantage of increased thermal neutron contamination and/or reduced epithermal beam intensity has to be taken into account in designing the thermal neutron filter.

Table 3.12 In-air beam performance for beam designs using different thermal neutron filters, ^{6}Li or Cd. These calculations used LiF which was uniformly distributed in FLUENTAL or a 0.04 cm Cd sheet which was located downstream of the fast neutron filter/moderator and in front of the photon shield. The materials used for the fast neutron filter/moderator are FLUENTAL and Titanium. The fission converter consists of eleven burned MITR-II fuel elements (312 g ^{235}U per element) with D_2O cooling. The neutron filters are followed by an 8 cm Bi photon shield and a pyramidal collimator with 15 cm thick lead lining, and is surrounded by a 10 cm thick lead reflector. The reactor power was assumed to be 5 MW.

Run ID	Fast Neutron Filter/Moderator & Thermal Neutron Filter	Φ_{th} n/cm²s	Φ_{epi} n/cm²s	Φ_f n/cm²s	J_{th}/Φ_{th}	J_{epi}/Φ_{epi}	J_f/Φ_f	D_{fn} cGy/min	D_{fn}/Φ_{epi} cGycm²/n	$D\gamma$ cGy/min	$D\gamma/\Phi_{epi}$ cGycm²/n
skm439	66cm FLUENTAL w/o LiF - 0.04cm Cd	1.45E+09 0.6%	1.31E+10 0.5%	1.88E+08 1.3%	0.65 0.8%	0.66 0.6%	0.69 1.7%	9.2 0.5%	1.17E-11 0.7%	8.5 0.6%	1.08E-11 0.8%
skm450	66cm FLUENTAL w/ 1%LiF	1.07E+09 2.0%	1.02E+10 1.5%	1.53E+08 4.8%	0.66 2.6%	0.66 1.9%	0.66 5.9%	7.5 1.8%	1.23E-11 2.3%	1.8 3.0%	2.98E-12 3.3%
skm403	68cm FLUENTAL w/o LiF - 2cm Ti - 0.04cm Cd	8.77E+08 1.9%	1.04E+10 1.4%	5.54E+07 3.7%	0.64 2.5%	0.66 1.9%	0.68 5.0%	5.6 1.8%	9.07E-12 2.3%	7.2 1.6%	1.15E-11 2.1%
skm404	68cm FLUENTAL w/ 1%LiF - 2cmTi	5.85E+08 2.4%	8.03E+09 1.6%	4.31E+07 4.0%	0.65 3.1%	0.66 2.1%	0.70 5.6%	4.5 1.9%	9.45E-12 2.5%	2.0 3.0%	4.09E-12 3.3%

Table 3.13 In-air beam performance for beam designs using different configurations of the Cd thermal neutron filter. Design skm436 used two 0.02 cm thick Cd sheets; one was located in the middle of the fast neutron filter/moderator composed of 71 cm Al - 27 cm AlF_3 and the other was placed at the original location (i.e., downstream of the filter/moderator and in front of the photon shield). Designs skm308 had one 0.04 cm thick Cd sheet behind the filter/moderator. The fission converter consists of eleven burned MITR-II fuel elements (312 g ^{235}U per element) with D_2O cooling. The neutron filters are followed by an 8 cm Bi photon shield and a pyramidal collimator with a 15 cm thick lead lining, and is surrounded by a 10 cm thick lead reflector. The reactor power was assumed to be 5 MW.

Run ID	Fast Neutron Filter/moderator & Thermal Neutron Filter	Φ_{th} n/cm²s	Φ_{epi} n/cm²s	Φ_f n/cm²s	J_{th}/Φ_{th}	J_{epi}/Φ_{epi}	J_f/Φ_f	D_{fn} cGy/min	D_{fn}/Φ_{epi} cGycm²/n	$D\gamma$ cGy/min	$D\gamma/\Phi_{epi}$ cGycm²/n
skm308	71cm Al - 27cm AlF_3 with one 0.04 cm Cd sheet	9.76E+08 2.5%	1.30E+10 1.4%	2.36E+08 4.2%	0.61 3.0%	0.63 1.9%	0.64 5.4%	9.3 1.8%	1.19E-11 2.3%	5.4 3.1%	6.95E-12 3.4%
skm436	71cm Al - 27cm AlF_3 with two 0.02 cm Cd sheets	1.16E+09 1.9%	1.34E+10 1.4%	2.20E+08 3.9%	0.63 2.5%	0.63 1.8%	0.67 5.1%	9.3 1.9%	1.16E-11 2.4%	4.7 2.5%	5.83E-12 2.8%

3.5 Conclusion

Sensitivity analyses of the fast neutron filter/moderator and thermal neutron filter were performed using MCNP. The fast neutron filter/moderator designs using the combinations of Al-Al_2O_3, Al-AlF_3, Al-$(CF_2)_n$ and Al-C were analyzed in terms of both in-air and in-phantom beam performance. The study of different arrangements (i.e., ordering of materials) of the filter/moderator materials showed how the different arrangements of Al and complementary elements (fluorine, oxygen or carbon) affect the neutron spectrum. This study also provided physical insight into the roles that the Al and complementary elements play in neutron moderation in the filter/moderator. The effect of varying materials and their dimensions on neutron spectrum and in-phantom figures of merit were examined in detail. This study showed that epithermal neutron beams with high quality and high intensity can be designed using many combinations of these four materials. These designs provide deep penetration of the beam (the AD's of 9.3-9.8 cm extend significantly beyond the centerline of the head phantom) and a large therapeutic gain (the AR is around 5). Moreover, they produce the ADDR's of 400-600 RBE cGy/min. Compared to the current MIT medical beam, they double the advantage ratio and increase the advantage depth by 2 to 3 cm. Furthermore, they provide advantage depth dose rates ~ 50 to 70 times higher than that of the current beam, potentially reducing irradiation times from several hours to just a few minutes. The results also indicated that the variation of the neutron spectrum caused by the use of different filter/moderator configurations, which meet the design criteria ($D/\Phi_{epi} < 2*10^{-11}$ cGy cm^2/n) does not affect beam quality because the fast neutron contamination is maintained at a very low level compared to the irreducible background due to hydrogen and nitrogen capture. The final design of the filter/moderator should be selected from the range of designs which were shown to provide excellent beam performance in this study taking engineering properties and costs of the

materials into consideration. Although the use of fluorine-containing materials would be accompanied with concern for decomposition and release of chemically active fluorine, one can take advantage of the shielding effect of a thick aluminum block by locating the fluorine-containing materials behind it, where the radiation level and temperature would be reduced relative to a location near the fission converter.

The analysis of the thermal neutron filter examined alternative ways to reduce or eliminate photon contamination caused by radiative capture in the Cd sheet. The studies of splitting/relocating the Cd sheet or replacing it with ^{6}Li showed that the advantage of reduction of photon contamination would be offset by undesired consequences, increasing the thermal neutron flux or decreasing the epithermal neutron flux. The low level of photon contamination which is well below the design goal ($2*10^{-11}$ $cGycm^2/n$) justifies the use of a Cd thermal neutron filter. Moreover, the current thickness of the Bi photon shield (8 cm) can be reduced to increase beam intensity. Therefore, in constructing the beam, it is recommended to make a Bi photon shield composed of several slabs in order to adjust its thickness.

Chapter 4 will present the result of the sensitivity study of the collimator design, which particularly examined the effect of beam directionality and beam size on in-phantom beam performance.

3.6 References

1. H. Rief, R.Van Heusden, and G.Perlini, "Generating Epithermal Neutron Beams for Neutron Capture Therapy in Small Reactors," *Advances in Neutron Capture Therapy,* Edited by A.H.Soloway *et al.,* Plenum Press, New York, 1993.

2. I. Auterinen, and P. Hiismaki, "Epithermal BNCT Neutron Beam Design for a TRIGA II Reactor," *Advances in Neutron Capture Therapy*, Edited by A.H.Soloway *et al.*, Plenum Press, New York, 1993.

3. S. D. Clement, J. R. Choi, R. G. Zamenhof, J. C. Yanch, and O. K. Harling, "Monte Carlo Methods of Neutron Beam Design for Neutron Capture Therapy at the MIT Research Reactor (MITR-II)," *Neutron Beam Design, Development, and Performance for Neutron Capture Therapy,* Edited by O.K.Harling *et al.*, Plenum Press, New York, 1990.

4. R. M. Brugger, T. J. Less, and G. G. Passmore, "An Intermediate-Energy Neutron Beam for NCT at MURR," Workshop on NCT, Jan. 1986, BNL-51994, Brookhaven National Laboratory (1986).

5. W. S. Kiger, III, *Neutronic Design of a Fission Converter-Based Epithermal Beam for Neutron Capture Therapy* , Nucl. E. Thesis, Massachusetts Institute of Technology, 1996

6. J. C. Yanch and O. K. Harling, "Dosimetric Effects of Beam Size and Collimation of Epithermal Neutrons for Boron Neutron Capture Therapy," *Rad. Res.* 135: 131-145, 1993.

7. J. M. Ryskamp, F. J. Wheeler, C. A. Wemple, K. D. Watts, D. W. Nigg, and P. J. Matonis, "Design of the WSU Epithermal Neutron Beam Extraction Facility for BNCT," *INEL BNCT Research Program, Annual Report 1995*, INEL-96/0139, Idaho National Engineering Laboratory, 1996.

8. H. B. Liu, "PbF_2 Compared to Al_2O_3 and AlF_3 to Produce an Epithermal Neutron Beam for Radiotherapy," *Med. Phys.* 23 (2), February 1996.

9. I. Auterinen and P. Hiismaki, "Design of an Epithermal Neutron Beam for the TRIGA Reactor in Otaniemi," *CLINCT BNCT Workshop Helsinki 1993,* Edited by Iiro Auterinen and Merja Kallio, TKK-F-A-718,1994.

10. Personal Communication from Iiro Auterinen and VTT-Chemical Technology in Finland.

11. H. B. Liu, R. M. Brugger, D. C. Rorer, P. R. Tichler, and J. P. Hu, "Design of a High-Flux Epithermal Neutron Beam Using ^{235}U Fission Plates at the Brookhaven Medical Research Reactor," *Med. Phys.* 21(10), October 1994.

12. H. B. Liu, R. M. Brugger, D. C. Rorer, "Enhancement of the Epithermal Neutron Beam at the Brookhaven Medical Research Reactor," *Advances in Neutron Capture Therapy,* Edited by A.H.Soloway *et al.,* Plenum Press, New York, 1993.

13. Personal Communication from K. Riley

14. Neutron Cross Sections, Third Edition, BNL-325, 1975.

15. J. E. Turner, *Atoms, Radiation and Radiation Protection*, McGraw-Hill, Inc., 1992.

16. C. S. Yam, *Microdosimetric Studies for Neutron Capture Therapy and Techniques for Capture Element Selection*, Ph. D. Thesis, Massachusetts Institute of Technology, 1995.

17. R. G. Zamenhof, "Procedures for Phase-I Study of Boron Neutron Capture Therapy for Glioblastoma Multiforme & Intracranial Melanoma at the New England Deaconess Hospital & the Massachusetts Institute of Technology", Protocol IND No. 46,176/No. 5, original submitted to FDA on Nov. 8, 1995.

18. R. D, Rogus, *Design and Dosimetry of Epithermal Neutron Beams for Clinical Trials of Boron Neutron Capture Therapy at the MITR-II Reactor,* Ph. D. Thesis, Massachusetts Institute of Technology, 1994.

19. Personal Communication from O. K. Harling.

20. A. B. Chilton, J. K. Shultis and R. E. Faw, *Principles of Radiation Shielding,* Prentice-Hall, Inc., Englewood Cliffs, New Jersey, 1984.

CHAPTER FOUR

Sensitivity Study of the Collimator Design - Effect of Beam Directionality and Beam Size

4.1 Introduction

A collimator is used in the medical neutron beam for several reasons, which include:

1. To minimize the dose to the tissue outside the target by delimiting the beam with a properly sized beam aperture
2. To reflect neutrons which enter the collimator region and guide them to the target position
3. To adjust the angular distribution (directionality) of the neutron beam

The importance of the third reason is suggested by Reference 1; that is, a beam with more forward-oriented directionality (higher J/Φ) is expected to improve effective beam penetration. A series of parametric studies to optimize the lining and shape of the collimator was performed (see Reference 2). The analysis of the collimator lining in Reference 2 was primarily aimed at identifying liner materials which maximizes beam intensity without degrading beam quality; that is, it tried to optimize the collimator design in terms of the second reason. Nickel, bismuth, lead and graphite were considered as candidates for the collimator liner materials and in-air beam performance was examined for varying thicknesses. The analysis of the collimator shape was concerned with improving the beam directionality (measured by the current-to-flux ratio, J/Φ) without reducing the beam intensity significantly (i.e., optimization in terms of the third reason). The in-air beam performance for four types of the collimator shapes, i.e., cone, pyramidal, funnel

and focusing designs were examined. As a result of these studies, Reference 2 proposed a pyramidal collimator with a 15 cm thick lead lining.

There are several neutronic parameters which are considered to affect in-phantom beam performance significantly:

(1) Beam intensity (i.e., epithermal neutron flux)

(2) Neutron energy distribution or neutron spectrum (including fast neutron contamination)

(3) Gamma contamination

(4) Neutron angular distribution (beam directionality)

(5) Beam size relative to the target size (or neutron spatial distribution)

The beam intensity is affected by the whole beam design including the neutron source. The neutron spectrum (including fast neutron contamination) and gamma contamination parameters are primarily determined by the type of the neutron source and neutron filters (the fast neutron filter/moderator and the thermal neutron filter). Chapter 1 and 3 discussed the effect of these parameters (especially the neutron spectrum) on the in-phantom figures of merit using the standard head phantom for different coolant types and different filter/moderator designs. As for the last two parameters, neutron angular distribution and beam size, Reference 3 performed an extensive sensitivity study using ideal beams, i.e., monoenergetic, photon-free neutron beams with varying maximum neutron emission angles (the maximum angle into which neutrons are allowed to be emitted from the source). This study revealed complicated dependencies of in-phantom figures of merit on beam size and beam directionality. Since these two parameters are mainly determined by the collimator, Reference 3 is expected to provide a lot of useful information for practical collimator design.

This chapter will discuss the effect of beam directionality and beam size on in-phantom beam performance using a realistic collimator design. The current-to-flux ratio was used as a measure of beam collimation as was in Reference 2. To examine beam-size dependency, the neutron flux profile across the surface at the beam edge (normal to the beam axis) was tallied. This study concentrated on the analysis for the standard water-filled head phantom, which was described in Section 1.4.3. The reader should recognize that the effects of beam size and beam directionality are dependent on the size and shape of the target so that care has to be taken in applying the results presented here to the study of other targets such as extremities.

Section 4.2 will review the definition of the current-to-flux ratio (J/Φ) used in MCNP calculations. In Section 4.3, the in-air analysis of collimator designs with varying beam directionality (J/Φ) and beam size will be discussed. Then, Section 4.4 will evaluate in-phantom beam performance of the collimator designs by calculating one and two dimensional dose distributions.

4.2 Definition of the Current-to-Flux Ratio (J/Φ) in MCNP

Consider a tally surface (area A) described in Figure 4.1, where the i-th particle is passing with the weight w_i and polar angle θ_i (between the tally surface normal and the trajectory of the particle). According to the definitions used in MCNP,[4] the surface current per unit area (Tally Type 1 modified by the tally segment card, J) and the surface flux (Tally Type 2, Φ) are tallied as follows:

$$J = \sum_i \{ w_i / A \}$$

$$\Phi = \sum_i \{ w_i / (|\mu_i| A) \} \quad , \quad (\mu_i = \cos \theta_i)$$

where the $|\mu_i|$ is set to 0.05 if $|\mu_i| < 0.1$. Then, the current-to-flux ratio (J/Φ) is given by

$$J/\Phi = [\sum_i \{ w_i / A \}] / [\sum_i \{ w_i / (|\mu_i| A) \}]$$

$$= [\sum_i \{ w_i / (w |\mu_i|) \}]^{-1} \qquad (w = \sum_i w_i)$$

As the beam becomes more isotropic, $|\mu_i|$ becomes smaller on average; then J/Φ becomes smaller. On the other hand, for a monodirectional (parallel) beam impinging on the surface vertically, $|\mu_i|$'s for all the particles are equal to one; then J/Φ is also equal to one. Therefore, this parameter represents how forward-oriented the beam is. When it is used, care has to be taken because its definition varies for different computational methods (the reader should recognize that the definition of J in MCNP is neither net current nor positive current nor negative current but the number of particles crossing a surface).

As an example of the use of this parameter, a neutron beam whose cosine of emission angle is uniformly distributed from $cos\ \theta_{max}$ to 1 (= $cos\ 0\ ^{o}$), which was used in Reference 3, is considered. It is assumed that the right-hand side of the surface is vacuum and N particles are impinging on the surface with the same weight w_0 ($w = N*w_0$). In this case, J in MCNP should be equal to the net current at the tally surface because there are no particles going backward; then, $|\mu_i|=\mu_i$. J/Φ is calculated by

$$J/\Phi = [\sum_{i=1}^{N} \{w_0/(w\mu_i)\}]^{-1} = [(1/N)\sum_{i=1}^{N} (1/\mu_i)]^{-1} = [E(1/\mu)]^{-1}$$

where $E(1/\mu)$ is the expectation value of $1/\mu_i$. Since μ is uniformly distributed from $cos\ \theta_{max}$ to 1 as shown in Figure 4.2, the probability density function for μ is given by

$$f(\mu) = 1/(1-cos\ \theta_{max}) \quad (cos\ \theta_{max} \leq \mu \leq 1)$$

or

$$= 0 \qquad (0 \leq \mu < cos\ \theta_{max})$$

Hence, $E(1/\mu)$ is given by

$$E(1/\mu) = \int_0^1 f(\mu)(1/\mu)\, d\mu$$

$$= \int_{cos\ \theta_{max}}^1 f(\mu)(1/\mu)\, d\mu = -ln(cos\ \theta_{max})/(1-cos\ \theta_{max}) \quad (cos\ \theta_{max} \geq 0.1)$$

or

$$= \int_{0.1}^{1} f(\mu)(1/\mu)\, d\mu + \int_{\cos\theta_{max}}^{0.1} f(\mu)(1/0.05)\, d\mu$$

$$= \{ln10+20(0.1-\cos\theta_{max})\}/(1-\cos\theta_{max}) \quad (0 \leq \cos\theta_{max} < 0.1)$$

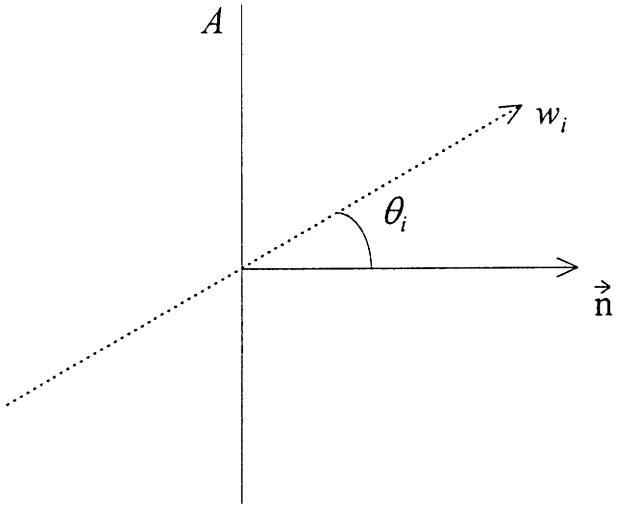

Figure 4.1 Schematic view of a tally surface (area A) through which the i-th particle is passing with the weight w_i and polar angle θ_i (between the tally surface normal and the trajectory of the particle).

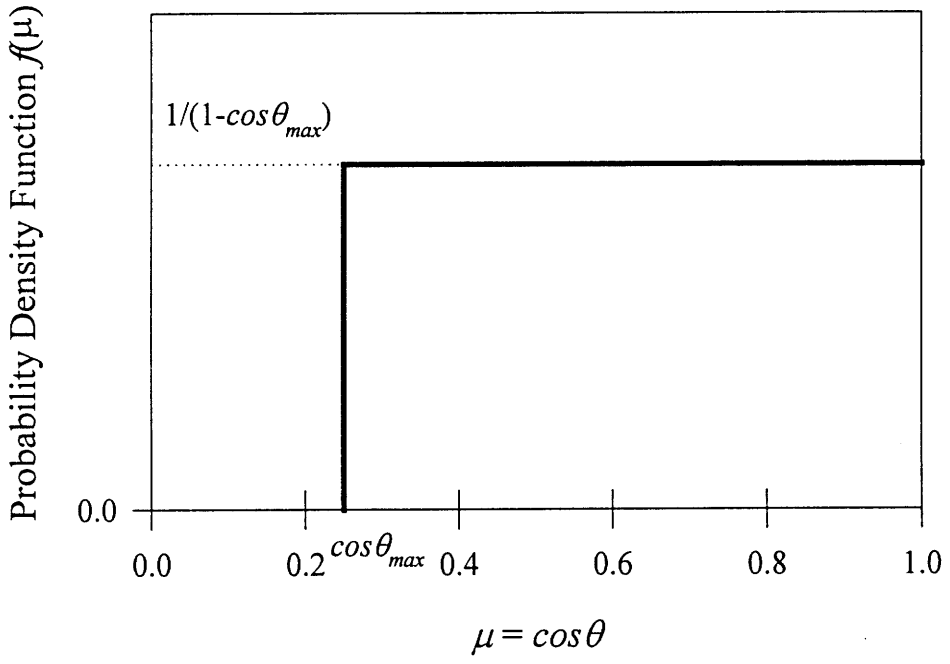

Figure 4.2 The probability density function for μ, which is uniformly distributed from 1 (= $cos\ 0\ ^{o}$) to $cos\ \theta_{max}$.

J/Φ equals the inverse of E($1/\mu$). The values of J/Φ for several θ_{max}'s calculated using the analytical solution above are presented in Table 4.1. It was confirmed that these values agree completely with the results from the MCNP simulation using the geometry and the angular distribution illustrated in Figures 4.1 and 4.2.

Although these results would provide insight of how neutrons with a large polar angle affect J/Φ defined in MCNP, one should recognize that the probability density function of μ for a realistic medical beam is significantly different from the one considered here.

Table 4.1 J/Φ with varying θ_{max} calculated by the analytical solution. It was confirmed that these results agree completely with those from the MCNP simulation using the geometry and the angular distribution illustrated in Figures 4.1 and 4.2.

θ_{max}	0°	30°	45°	60°	67°#	84.3° ($\cos\theta_{max}$=0.1)	85°	90°
J/Φ	1.0	0.931	0.845	0.721	0.651	0.391	0.357	0.232

The fission converter beam with a pyramidal collimator lined with 15 cm thick lead, which is assumed for the reference in this analysis, produces a current-to-flux ratio of ~0.65.

4.3 In-Air Analysis of the Collimator Design

This section will describe the first step of the study, i.e., evaluating beam intensity, directionality and size (neutron spatial distribution) for different collimator configurations. The study of the collimator shape in Reference 2 showed a trade-off between the current-to-flux ratio and beam intensity using funnel-shaped collimator designs. It showed that the 'straight' collimator (i.e., a 102.1 cm long tube with a cross-section of 20cm*20cm lined with 15 cm thick lead through the heavy concrete shielding), provides the highest current-to-flux ratio for epithermal neutrons (J_{epi}/Φ_{epi} = 0.78) among the tested designs with significant reduction of the epithermal neutron flux from that for the pyramidal collimator (i.e., from $1.3*10^{10}$ n/cm^{2}s to $1.4*10^{9}$ n/cm^{2}s) . Since these collimator designs did not provide substantial improvement in the current-to-flux ratio without large reductions of beam intensity and since the benefit of improved beam directionality was unclear, the pyramidal collimator was selected for the 'final' beam design. The trade-off between the current-to-flux ratio and beam intensity was also mentioned in Reference 5. Considering these results of Reference 2, the current study presented here carried out a parametric analysis to identify collimator designs which achieve high J/Φ without significant reduction of beam intensity. In addition, in-air beam performance of collimator designs with different beam aperture sizes was evaluated.

As for the collimator configuration to improve J/Φ, this study first reviewed the design study of the epithermal neutron beam using ^{235}U fission plates performed by BNL,[6] where MCNP was also utilized for beam analysis. The proposed beam design was shown to provide a high J/Φ (0.78) although the beam path at the irradiation port is short, only 20 cm. This beam path is surrounded by photon shields (Bi - 5 cm, Pb -10 cm) and a neutron absorber (lithiated polyethylene). The reported

J/Φ for the BNL design was confirmed in Reference 2, which constructed a portion of the BNL beam design (around the beam path) and examined beam directionality from it. Reference 2 showed that angular redistribution (increasing J/Φ) occurs as neutrons approach the patient position due to loss of large angle neutrons.

From these results, it was surmised that the lithiated polyethylene (Li-poly) at the irradiation port of the BNL beam design works as a beam delimiter and remove neutrons with large angles relative to the beam axis. Therefore, the current study examined collimator configurations using a Li-poly delimiter. The Li-poly used here contains 7% ^{6}Li by mass. Two collimator configurations were considered, whose cross-sectional views are shown in Figure 4.3 (funnel type) and Figure 4.4 (truncated pyramid type). The funnel-shaped collimator consists of a four-sided sloped portion lined with 15 cm thick lead and a 20 cm long straight portion with the square cross section surrounded by a Li-poly delimiter which covers the whole beam cross-section except for the beam aperture. The other collimator design is a truncated pyramid-shaped collimator with 15 cm thick lead lining, where the last *t* cm (t =0, 10, 20 and 30) long part of the lining in front of the patient position was replaced with Li-poly. It should be noted that, compared to that of the pyramidal design, the beam aperture of the funnel design subtends a smaller solid angle for neutrons at the surface of the Bi photon shield or the lead collimator lining to travel through toward the patient position without entering the Li-poly region. As for beam aperture, two different sizes, 20 cm*20 cm or 10 cm*10 cm, were considered. The pyramidal collimator with no Li-poly delimiter (i.e., t = 0 cm) with a beam aperture of 20 cm*20 cm corresponds to the one used in the 'final' beam design proposed in Reference 2 (std473), which was assumed for the reference design in this analysis.

The calculations used a fission converter composed of eleven burned MITR-II fuel elements (312 g ^{235}U per element) with D_2O cooling, which is followed by the fast neutron filter/moderator composed of 68 cm 70% AlF_3/30% Al - 2 cm Ti, a 0.04 cm Cd thermal neutron filter and an 8 cm

Bi photon shield. The filter/moderator is surrounded by a 10 cm thick lead reflector. The reactor power was assumed to be 5 MW. In-air figures of merit (except for the specific photon dose) produced with these collimator designs are summarized in Table 4.2. A plot of epithermal neutron flux vs. J_{epi}/Φ_{epi} for these designs is depicted in Figure 4.5. These results suggest that a higher J/Φ is obtained when neutrons with large angles to the beam axis which would be reflected by the collimator liner near the beam aperture otherwise are removed by the Li-poly delimiter. Also, a high J/Φ is accompanied by a great loss of beam intensity as indicated in the previous studies. Comparison of the results for Designs std473 and skm311 which have the same beam aperture size of 20 cm*20 cm indicates that the epithermal neutron flux is reduced by a factor of ~3 to increase J_{epi}/Φ_{epi} from 0.67 to 0.87. Comparison between skm464 and skm468 with the same beam aperture size of 10 cm*10 cm shows that an increase in J_{epi}/Φ_{epi} from 0.68 to 0.91 is obtained with a concomitant reduction in the epithermal neutron flux by a factor of ~6. A great reduction of large angle neutrons which results in the improved J/Φ and loss of beam intensity due to the use of a Li-poly delimiter is shown by Figure 4.6, which depicts the normalized neutron current angular distributions at the patient position for different collimator configurations with the beam size of 20 cm*20 cm (std473, skm304, skm311) . The angular distributions are described as a function of μ, which is the cosine of the angle between the particle trajectory and the beam axis, and are normalized to one at the maximum tally bin. Regarding this figure, it should be emphasized that these beams are already very forward-oriented. Neutrons passing within 32^{o} account for 50-80% of the total neutrons entering the beam aperture.

One should note that the use of a Li-poly delimiter also significantly affects the neutron spatial distribution around the beam aperture. Figure 4.7 shows vertical profiles of neutron flux centered on the beam axis at the patient position for Designs std473, skm304, skm311. It is noted that the intensities drop off rapidly at the side of the beam aperture, i.e., the 'effective' beam size

decreases when a Li-poly delimiter is used because it absorbs neutrons impinging on it. The photon dose profile is also changed by the use of a Li-poly delimiter for several reasons which include the different photon-shielding properties of Pb and Li-poly. Although the variation of the photon profile does not affect the in-phantom beam performance, it is a concern for radiation protection. Analysis of the photon dose profile at the patient position will be discussed in Chapter 5.

It is also noted from the results for all collimator designs that the fast neutron contamination increases as the J/Φ increases because the epithermal neutron flux decreases more rapidly than the fast neutron dose rate. However, the specific fast neutron dose is still below the design goal for all designs shown in Table 4.2. Therefore, the effect of fast neutron contamination is considered to be negligible relative to the irreducible background due to hydrogen and nitrogen capture.

Comparison of the results for Designs std473 and skm468 indicates that the reduction of beam aperture size from 20 cm*20 cm to 10 cm*10 cm for the pyramid collimator with only a lead lining (no Li-poly delimiter) does not affect the in-air beam performance including J/Φ. Since a large portion of neutron flux (~80%) at the patient position is due to neutrons scattered by the collimator lining[2], the change in the beam aperture size considered here would not affect the beam intensity, directionality or neutron spectrum. On the other hand, the results for Designs skm311 and skm464 shows that J/Φ increases with a significant reduction of beam intensity when the beam aperture size is decreased for the funnel-shaped collimator with a Li-poly delimiter. This is because the solid angle which the beam aperture subtends for neutrons to travel through without entering the Li-poly becomes smaller as the beam aperture size is decreased.

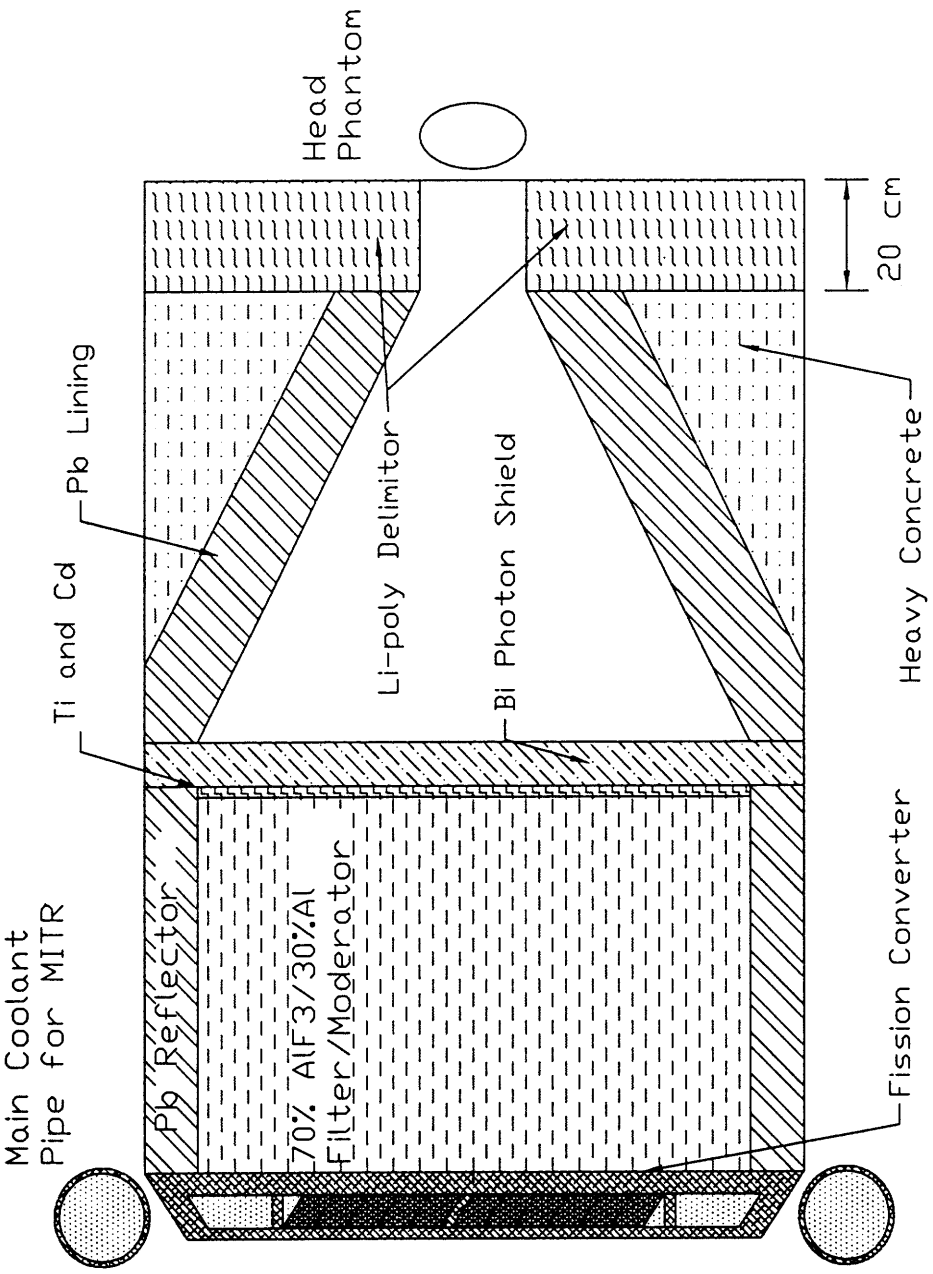

Figure 4.3 Cross-sectional view of the funnel-shaped collimator design. This type of collimator consists of a four-sided sloped portion lined with 15 cm thick lead and a 20 cm long straight portion with the square cross section surrounded by a Li-poly delimiter which covers the whole beam cross-section except for the beam aperture.

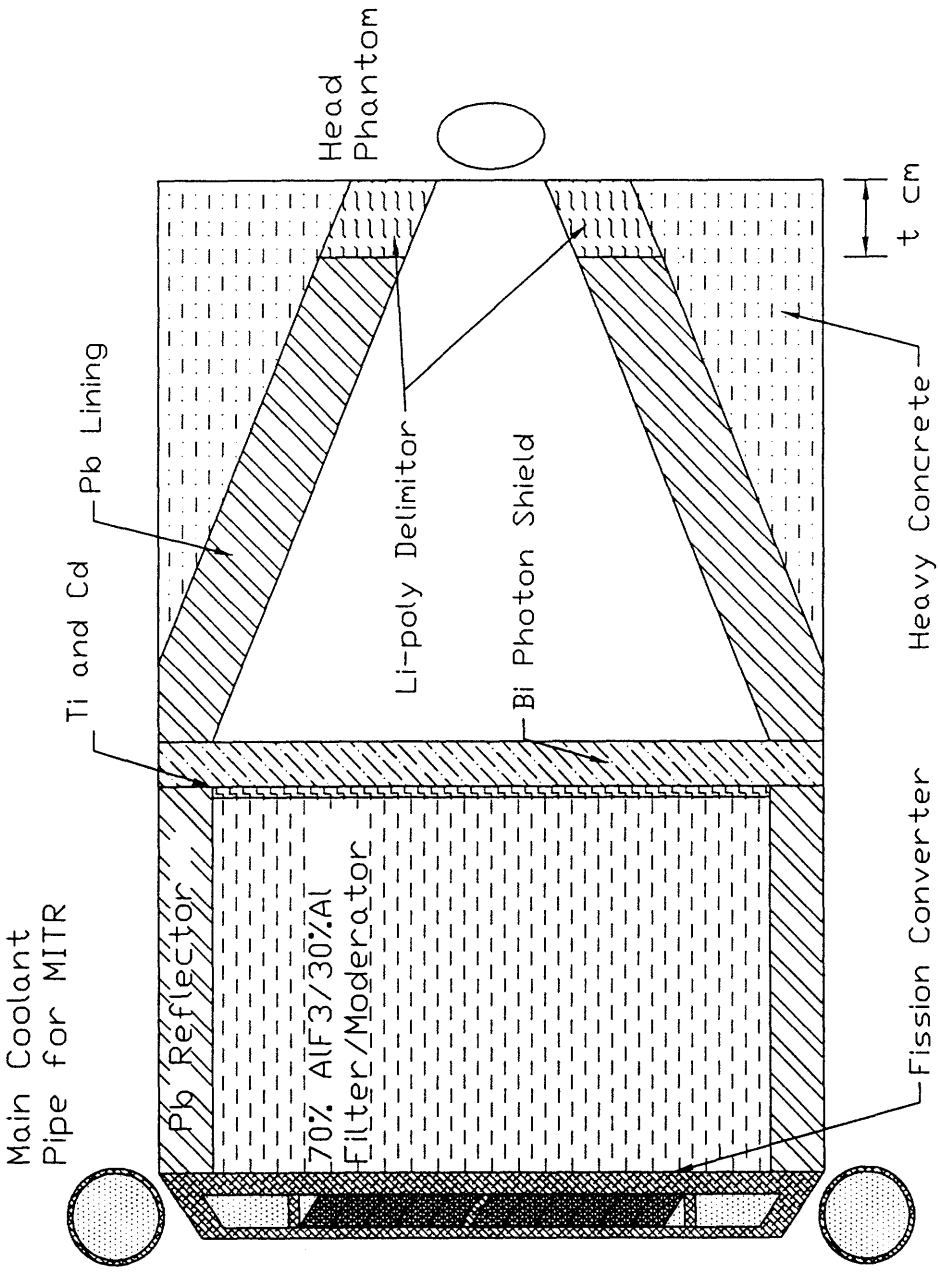

Figure 4.4 Cross-sectional view of the truncated pyramid-shaped collimator design. This design has a 15 cm thick lead lining, where the last *t* cm (t =0, 10, 20 and 30) long part of the lining in front of the patient position was replaced with Li-poly.

Table 4.2 In-air beam performance for different collimator designs. The funnel-shaped collimator consists of a four-sided sloped portion lined with a 15 cm thick lead lining and a 20 cm long straight portion with the square cross section surrounded by a Li-poly delimiter which covers the whole beam cross-section except for the beam aperture. The pyramidal collimator is lined with 15 cm thick lead, where the last *t* cm (t = 0, 10, 20 and 30) long part of the lining in front of the patient position was replaced with Li-poly. These calculations used a fission converter composed of eleven burned MITR-II fuel elements (312 g ^{235}U per element) with D_2O cooling, which is followed by a fast neutron filter/moderator composed of 68 cm 70% AlF_3/30% Al - 2 cm Ti, a 0.04 cm Cd thermal neutron filter and an 8 cm Bi photon shield. The filter/moderator is surrounded by a 10 cm thick lead reflector.

Run ID	Collimator Shape	Length of the Li-poly Portion cm	Beam Aperture Size	Φ_{th} n/cm^{2}s	Φ_{epi} n/cm^{2}s	Φ_f n/cm^{2}s	J_{th}/Φ_{th}	J_{epi}/Φ_{epi}	J_f/Φ_f	D_{fn} cGy/min	D_{fn}/Φ_{epi} cGycm^2/n
std473	Pyramid	0	20cm*20cm	9.13E+08	1.30E+10	1.16E+08	0.66	0.67	0.68	10.4	1.33E-11
				1.8%	1.3%	3.0%	2.4%	1.7%	4.0%	1.5%	1.9%
skm468	Pyramid	0	10cm*10cm	9.06E+08	1.28E+10	1.08E+08	0.64	0.68	0.69	9.9	1.29E-11
				2.8%	1.6%	4.3%	3.4%	2.0%	5.6%	1.9%	2.5%
skm311 (skm200)	Funnel	20	20cm*20cm	3.30E+08	4.45E+09	4.32E+07	0.82	0.87	0.88	4.0	1.49E-11
				1.1%	0.6%	1.0%	1.4%	0.9%	1.5%	0.5%	0.8%
skm464	Funnel	20	10cm*10cm	1.55E+08	2.19E+09	2.18E+07	0.86	0.91	0.91	2.14	1.62E-11
				2.5%	1.5%	2.4%	3.4%	2.1%	3.5%	1.0%	1.8%
skm304 (skm204)	Pyramid	10	20cm*20cm	7.03E+08	9.33E+09	8.20E+07	0.72	0.77	0.78	7.5	1.34E-11
				0.9%	0.5%	0.8%	1.2%	0.7%	1.1%	0.4%	0.7%
skm202	Pyramid	20	20cm*20cm	5.99E+08	7.92E+09	7.17E+07	0.74	0.80	0.81	6.5	1.37E-11
				2.6%	1.6%	2.2%	3.5%	2.2%	3.2%	1.2%	2.0%
skm205	Pyramid	30	20cm*20cm	5.48E+08	6.99E+09	6.51E+07	0.75	0.81	0.83	6.0	1.42E-11
				2.6%	1.6%	2.4%	3.5%	2.3%	3.5%	1.2%	2.0%

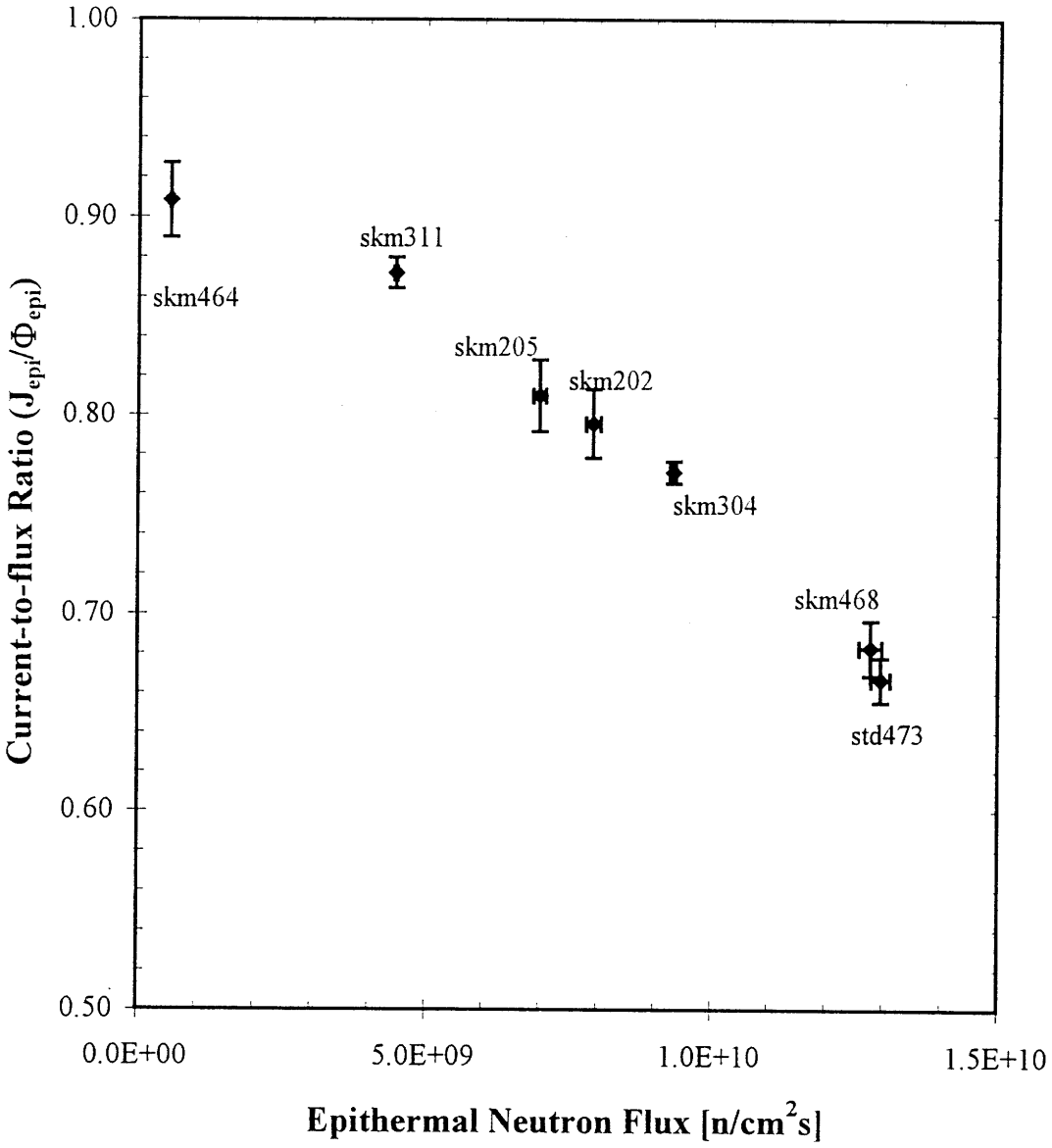

Figure 4.5 Epithermal neutron flux vs. current-to-flux ratio for different collimator designs shown in Table 4.2. The label of each data point denotes Run-ID of each collimator design.

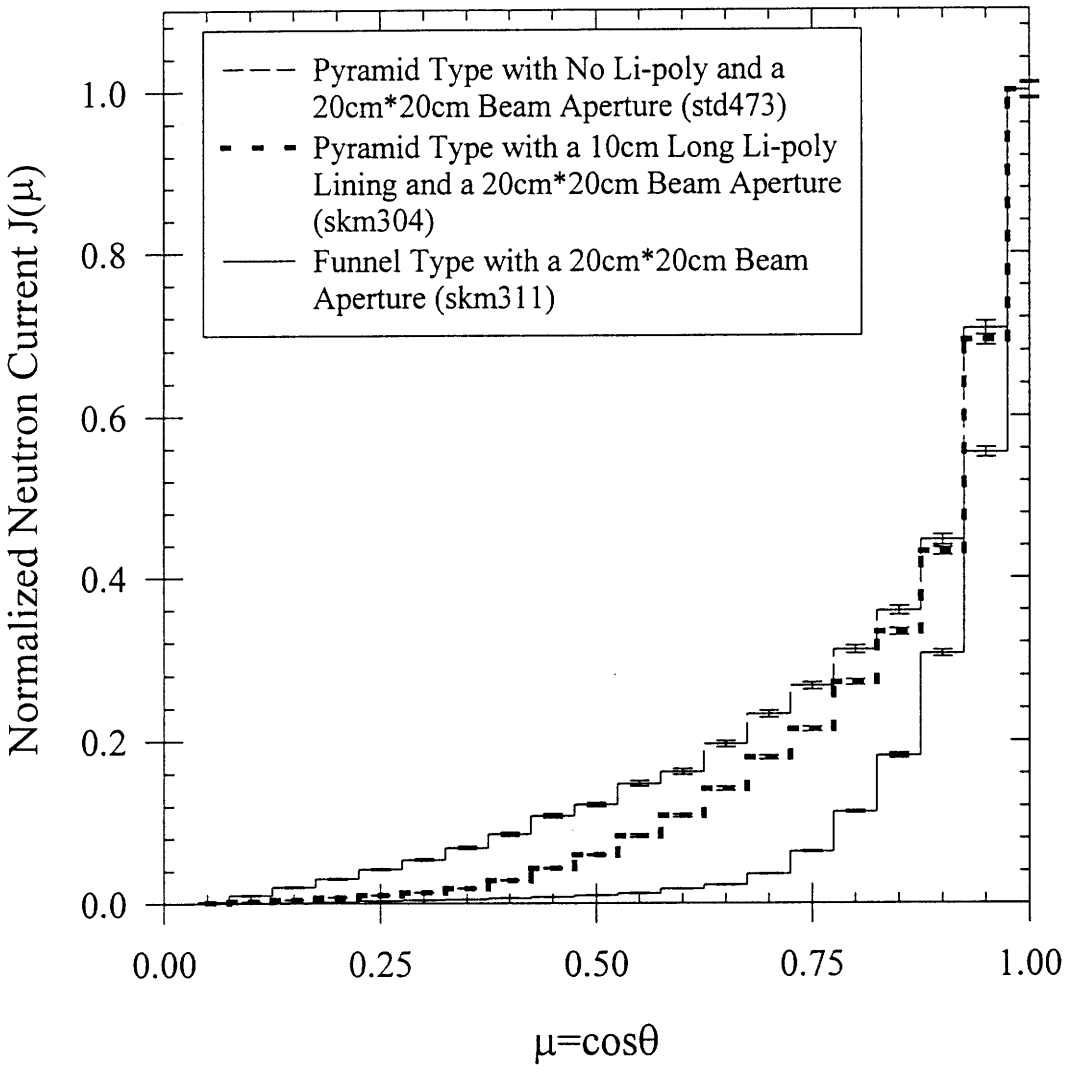

Figure 4.6 Normalized neutron current angular distribution at the patient position for different collimator designs described as a function of μ (the cosine of the angle between the particle trajectory and the beam axis). The angular distribution is normalized to one at the maximum tally bin. The funnel-shaped collimator (skm311) has a four-sided sloped portion lined with 15 cm thick lead and a 20 cm long straight portion with the square cross section surrounded by a Li-poly delimiter. The pyramidal collimators of std473 and skm304 are lined with 15 cm thick lead, where the last *t* cm (t = 0 and 10) long parts of the lining in front of the patient position are replaced with Li-poly. All of these designs have a 20 cm* 20 cm beam aperture.

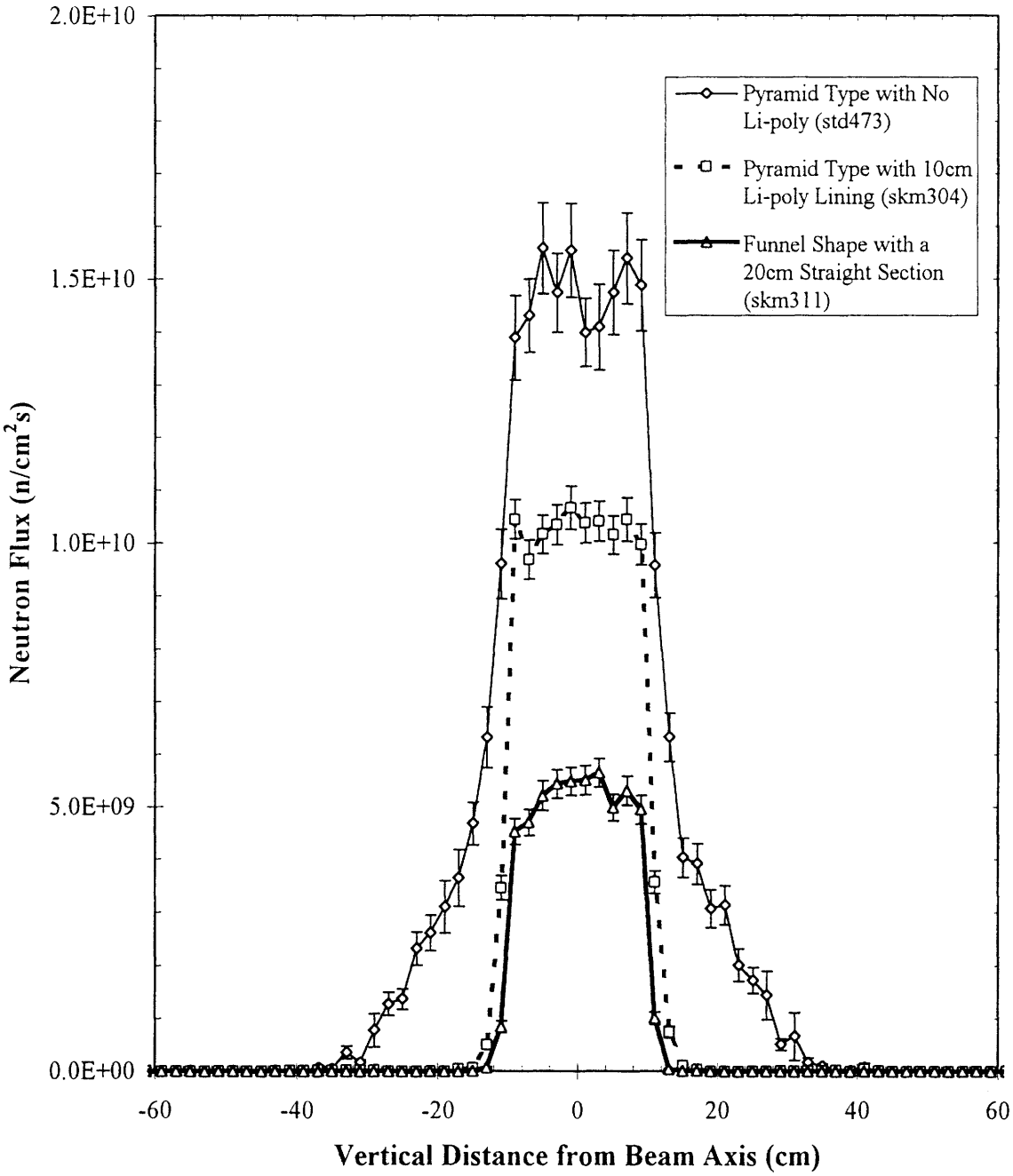

Figure 4.7 Vertical profiles of neutron flux of all energies centered on the beam axis at the patient position for Designs std473, skm304 and skm311. Design skm311 has a funnel-shaped collimator composed of a four-sided sloped portion with 15 cm thick lead lining and a 20 cm long straight portion with the square cross section surrounded by a Li-poly delimiter. Design std473 and skm304 have pyramidal collimators lined with 15 cm thick lead, where the last t cm (t = 0 and 10) long parts of the lining in front of the patient position are replaced with Li-poly. All of these designs have a 20 cm*20 cm beam aperture.

4.4 In-Phantom Analysis

The next step in the analysis of the different collimator designs is to examine beam performance in the standard head phantom. Originally, the effect of variation of beam directionality on the in-phantom figures of merit was the main interest of this study. However, as is shown later, it turned out that the beam size (neutron spatial distribution) plays an very important role in determining the in-phantom parameters. Therefore, in this section, emphases are placed on both beam size and beam directionality in presenting the results.

Four collimator designs, skm304, skm311, skm464 and skm468 were selected for in-phantom analysis and compared with Design std473. The in-phantom figures of merit (including ADDR/J_{epi}) produced by these collimator designs are presented as well as in-air figures of merit (including the specific photon dose) in Table 4.3. In this table, one should note that the specific photon dose increases as J/Φ increases because the epithermal neutron flux decreases more rapidly than the photon dose rate as was seen for the specific fast neutron dose. Although Designs skm311 and skm464 produce specific photon doses which are greater than the design goal, their values are still well below the peak dose due to the irreducible gamma component from hydrogen capture (~ $2*10^{-10}$ cGycm^2/n). Therefore, the effect of the incident gamma rays should be very small.

First, the results for Designs std473, skm304 and skm311, which have the beam aperture size (20 cm*20 cm) as large as the maximum dimension of the head phantom, are compared. (A beam with the size of the aperture as large as or larger than the maximum dimension of the phantom is called a 'large beam' in the following discussion.) To understand variation of beam performance for these designs, one should recognize that these designs have different 'effective' beam sizes as well as different directionalities (J/Φ) as discussed in Section 4.3 (the angular distributions and vertical profiles of neutron flux at the patient position for these three designs are presented in

Figures 4.6 and 4.7).

Table 4.3 shows that, for these three beam designs, AD decreases as J/Φ increases (i.e. as the beam is more collimated) while ADDR decreases approximately in proportion to the epithermal neutron current (J_{epi}) and AR is constant. The trend of decreasing AD with increasing J/Φ contradicts the perception that better collimation would provide better beam penetration[1]. The reason for this trend will be well explained below in terms of beam size dependency of the in-phantom figures of merit.

It is instructive to compare these results with those of Reference 3 to obtain insight into the effects of angular and beam-size dependencies on in-phantom beam performance. However, one should recognize that Reference 3 examined the effects of these parameters separately by varying one parameter with the other fixed while, in the actual beam design, these parameters are varied simultaneously. Therefore, a comparison between the current results and those of Reference 3 is not straight-forward .

As for the AD, Reference 3 indicated that AD is reduced as the maximum emission angle (θ_{max}) increases for a large beam while AD increases as the beam size increases for a "fairly well-collimated" beam with θ_{max} at 30^{o} or lower. The trend for AD shown in Table 4.3 suggests that the effect of beam-size outweighs that of the angular dependency for the collimator designs considered here, which would reduce AD as the 'effective' beam size is decreased. This conclusion is supported by Figure 4.8, which compares the 2D dose distributions produced by Design std473 and skm311 in an actual human head model. These dose distributions were created by W.S Kiger using the treatment planning software MacNCTPLAN developed by our research group at BIDMC[7,9] and the CT-image data of the head of one of the human subjects treated in the GBM protocol at MIT/BIDMC. Each curve denotes the iso-dose contour which represent the locations

where the same ratio of tumor dose to the maximum normal tissue dose is achieved (the ratio is expressed in percent). Therefore, therapeutic gains are obtained in the region bounded by the 100% curve. In this figure, it is seen that the iso-dose contours expand as the effective beam size increases, especially on the anterior and posterior sides of the head (a reader should remember that Design std473 has a larger effective beam size than Design skm311 as shown in Figure 4.7). This is likely because the epithermal neutrons coming from the sides of the beam aperture with large angles also provide therapeutic dose; therefore, the advantage depth, which is the depth at which the tumor dose is equal to the maximum normal tissue dose, becomes greater. The expansion of the iso-dose contours is consistent with the result of the study of improved neutron collimators at BNL,[8] where the expansion of the curves of the iso-thermal neutron fluence rate distribution was observed when the irradiation aperture of the collimator made of Li-poly was enlarged from 8 cm to 12 cm.

Concerning ADDR, Fig. 13 of Reference 3 indicates that, when beam size is as large as or larger than the target, ADDR's produced by beams with the constant number of neutrons crossing the source plane per unit area are almost constant with varying θ_{max} or beam size. Since the effective beam sizes of Designs std473, skm304 and skm311 (20 cm*20 cm or more) are larger than the target size, the constant ADDR/J_{epi} observed for these three designs can be explained by the effects of both angular distribution and beam-size.

For the beam-size dependency of AR, although Reference 3 mentions that AR decreases as beam size increases for "relatively parallel beams" with θ_{max} equal to or less than 45°, it is seen in Fig. 16 of Reference 3 that increases in AR with decreasing beam size (diameter) from 33.0 cm to 12.0 cm for $\theta_{max} \leq 30^{o}$ appear to be small. Also, as for its angular dependency, Reference 3 explains "the large dependency of AR on θ_{max} [is] reduced as the size of the beam approaches the

size of the phantom itself" (p142). Because the effective beam sizes of these designs are larger than the target size, their AR's may be constant although their angular distribution and effective beam sizes vary significantly.

Next, Designs std473 and skm468 are compared. The neutron angular and spatial distributions are shown in Figures 4.9 and 4.10, respectively. As shown in Figure 4.9, these designs produce almost the same neutron angular distribution shape, which is expected from their similar J/Φ's. However, they have significantly different spatial distributions, i.e., different effective beam sizes due to reduction of the beam aperture from 20 cm*20 cm to 10 cm*10 cm. The comparison of these designs is interesting because we can examine the effect of changing the beam size without having significant variation of beam directionality.

The results in Table 4.3 indicate that AD and ADDR/J_{epi} decrease with decreasing beam size while AR is almost unchanged. The decrease in AD can be explained by its beam-size dependency for a well-collimated beam described above (i.e., AD increases with increasing beam size). The trend of ADDR is explained by the results shown in Fig. 13 of Reference 3, which indicates that ADDR decreases as the beam size is reduced from that comparable to the phantom, especially when θ_{max} is large (i.e., $\theta_{max} \geq 45^{o}$). As for the beam-size dependency of AR, since the effective beam size of Design skm468 appears to be still larger than the beam size with a 12 cm diameter in Reference 3, AR may be unchanged for the same reason as explained above.

Finally, the results for Designs skm468 and skm464, which have a small beam aperture size relative to the phantom (10 cm*10 cm) are compared. The reader should remember that Design skm464 provides significantly higher J/Φ than Design skm468 due to the use of the Li-poly delimiter. Figures 4.11 and 4.12, which depict neutron angular and spatial distributions at the patient position for these designs, show a great reduction of large angle neutrons and significantly

reduced effective beam size due to the use of a Li-poly delimiter in Design skm464. Table 4.3 shows that AD decreases as the effective beam size decreases, which is expected based on the beam-size dependency of AD as mentioned above, while $ADDR/J_{epi}$ and AR are kept approximately constant. As for ADDR, Fig. 11 and Fig 12 of Reference 3 shows that ADDR increases as θ_{max} decreases while ADDR decreases as the beam size decreases. Since the use of a Li-poly delimiter causes reduction of the number of large angle neutrons (thereby, increasing J/Φ) and effective beam size simultaneously, the effect of beam-size on $ADDR/J_{epi}$ may be balanced with by the influence of angular dependency so that $ADDR/J_{epi}$ remains unchanged. As for the beam size dependency of AR, Reference 3 indicates that AR increases as the beam size decreases for a relatively parallel beam. On the other hand, the angular dependence of AR has a complex behavior, i.e., reduction in AR with increasing θ_{max} for a small beam and the opposite trend for a large beam. Therefore, it is difficult to explain how these dependencies affect the behavior of AR based on the information provided by Reference 3 when significant variations of both effective beam size (large beam to small beam) and angular distribution occur simultaneously as in this case.

For better understanding the differences in in-phantom beam performance between the collimator designs which vary beam directionality and/or effective beam size significantly, the profiles of thermal and epithermal neutron fluxes produced by Designs std473, skm311 and skm464 are compared in Figure 4.13 and Figure 4.14. In Figure 4.14, the thermal neutron flux profiles normalized to one at the peak are presented to compare their shapes. Figure 4.13 shows that the peak thermal neutron flux in the head phantom decreases as beam intensity decreases. Figure 4.14 indicates that, although the depth where the peaks occur are unchanged (~ 2.5 cm) for these beam designs, the thermal neutron profile drops off more rapidly beyond the peak depth as the effective beam size is reduced, which explains the decrease in the advantage depth with

decreasing the effective beam size. The dose-depth profiles for these designs are presented in Figure 4.15.

Table 4.3 Comparison of in-phantom figures of merit produced by different collimator designs. The funnel-shaped collimator (skm311 and skm464) consists of a four-sided sloped portion with 15 cm thick lead lining and a 20 cm long straight portion with the square cross section surrounded by a Li-poly delimiter which covers the whole beam cross-section except for the beam aperture. The pyramidal collimator is lined with 15 cm thick lead, where the last *t* cm (t = 0 for std473, skm468 and t = 10 for skm304) long part of the lining in front of the patient position was replaced with Li-poly. These calculations used a fission converter composed of eleven burned MITR-II fuel elements (312 g ^{235}U per element) with D_2O cooling, which is followed by a fast neutron filter/moderator composed of 68 cm 70% AlF_3/30% Al - 2 cm Ti, a 0.04 cm Cd thermal neutron filter and an 8 cm Bi photon shield. The filter/moderator is surrounded by a 10 cm thick lead reflector.

Run ID	Collimator Shape	Beam Aperture Size	Φ_{epi} n/cm^{2}s	J_{epi}/Φ_{epi}	D_{fn}/Φ_{epi} cGycm^2/n	$D\gamma/\Phi_{epi}$ cGycm^2/n	AD cm	ADDR RBE cGy/min	AR	ADDR/Jepi RBE cGycm^2/n
std473	Pyramid	20cm*20cm	1.30E+10 1.3%	0.67 1.7%	1.33E-11 1.9%	1.02E-11 2.0%	9.5	435	4.9	8.39E-10
skm468	Pyramid	10cm*10cm	1.28E+10 1.6%	0.68 2.0%	1.29E-11 2.5%	1.06E-11 2.4%	9.0	362	5.0	6.91E-10
skm304 (skm204)	Pyramid	20cm*20cm	9.33E+09 0.5%	0.77 0.7%	1.34E-11 0.7%	1.46E-11 1.0%	9.3	356	4.9	8.26E-10
skm311 (skm200)	Funnel	20cm*20cm	4.45E+09 0.6%	0.87 0.9%	1.49E-11 0.8%	2.28E-11 1.0%	9.1	206	4.9	8.82E-10
skm464	Funnel	10cm*10cm	2.19E+09 1.5%	0.91 2.1%	1.62E-11 1.8%	3.26E-11 2.2%	8.5	79	4.9	6.63E-10

This page is the back side of Table 4.3.

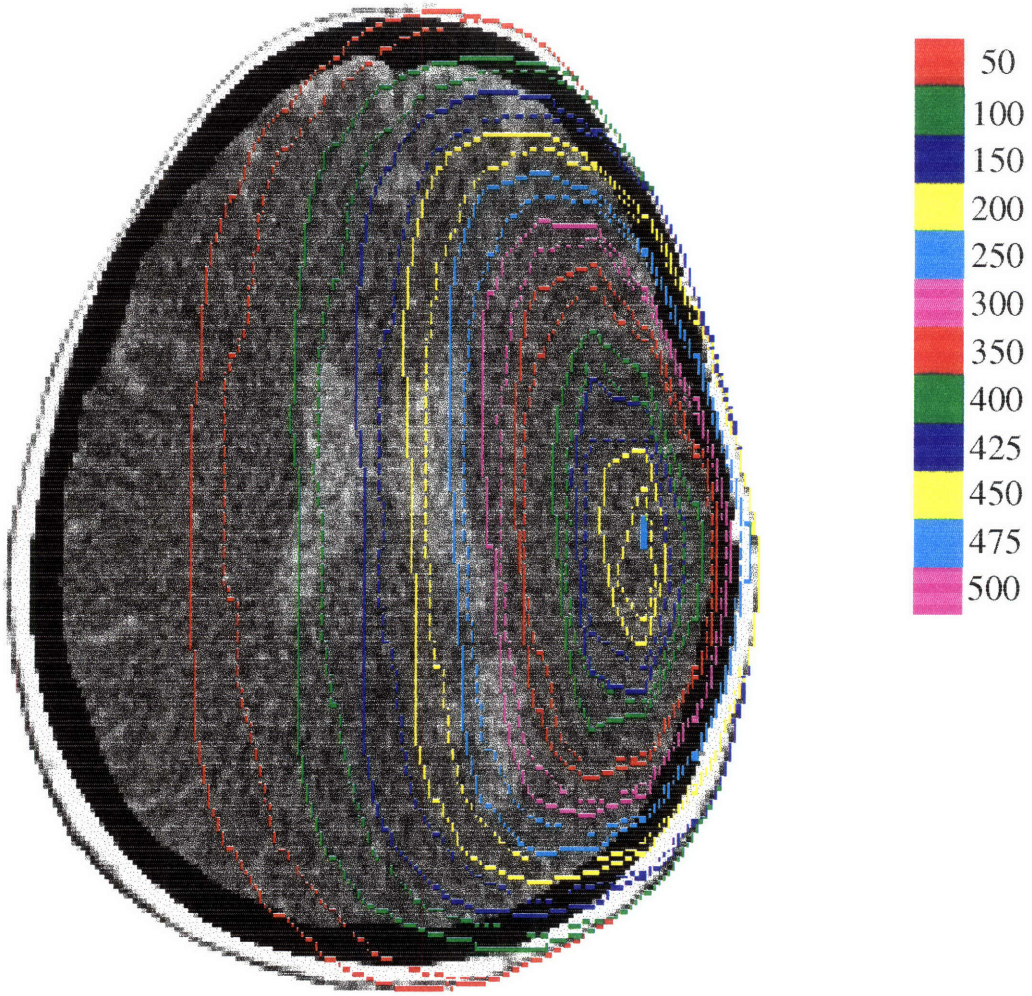

Figure 4.8 Two dimensional dose distributions produced by Designs std473 (solid curve) and skm311 (dashed curve) using the data of actual human head. Each curve denotes the iso-dose contour which represents the locations where the same ratio of tumor dose to the maximum normal tissue dose is achieved. The number besides the color bar denotes the ratio in percent for each color. Design std473 uses a pyramidal collimator with a 15 cm thick lead lining and no Li-poly. Design skm311 has a funnel-shaped collimator with a four-sided sloped portion lined with 15 cm thick lead and a 20 cm long straight portion with the square cross section surrounded by a Li-poly delimitor. Both collimator designs have a 20 cm*20 cm beam aperture.

This page is the back side of Figure 4.8.

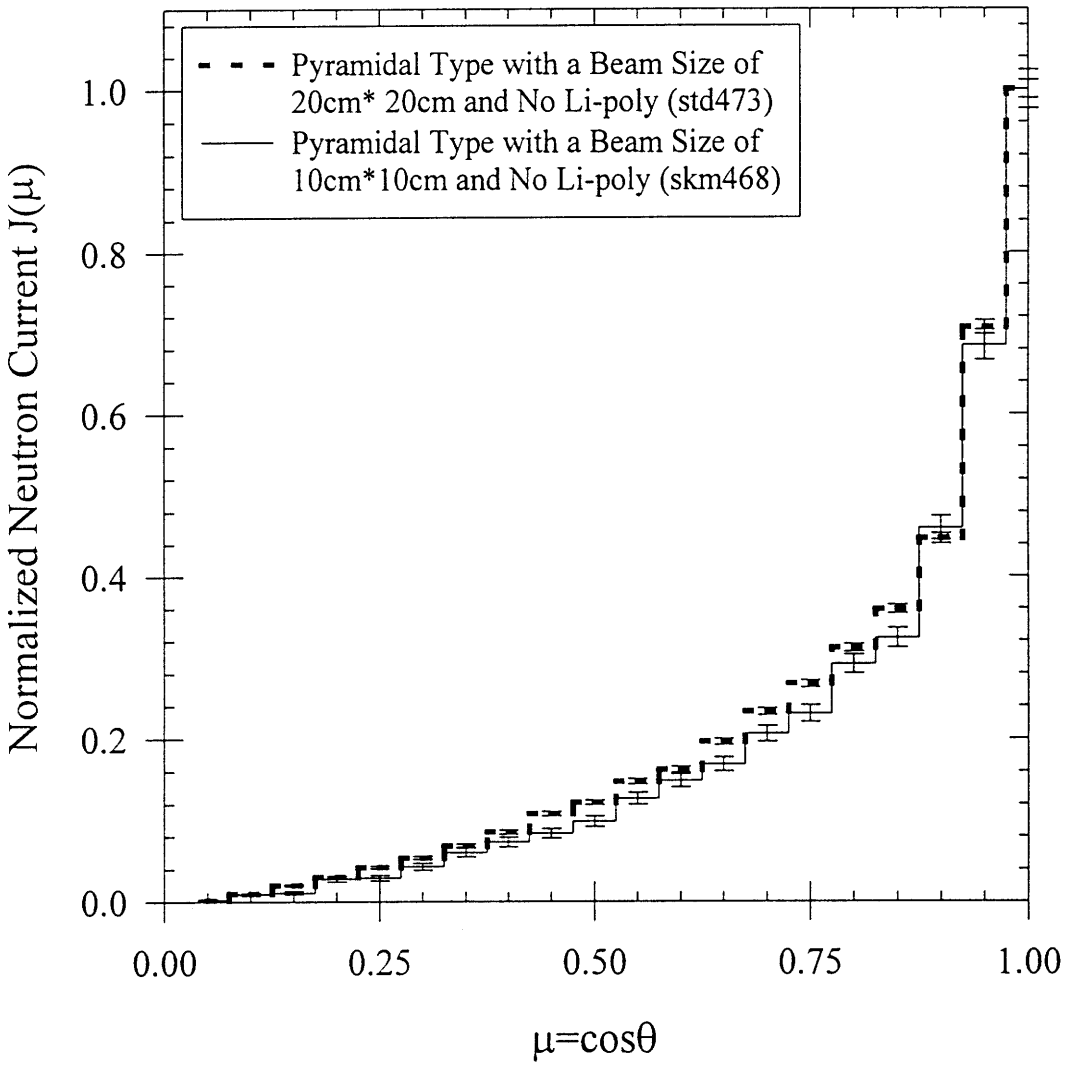

Figure 4.9 Normalized neutron current angular distribution at the patient position for the pyramidal collimator designs with different beam aperture sizes. The angular distribution is described as a function of μ (the cosine of the angle between the particle trajectory and the beam axis). The angular distribution is normalized to one at the maximum tally bin. Both designs use pyramidal collimators lined with 15 cm thick lead and no Li-poly delimiter and have different beam aperture sizes (20 cm*20 cm for std473 and 10 cm*10 cm for skm468).

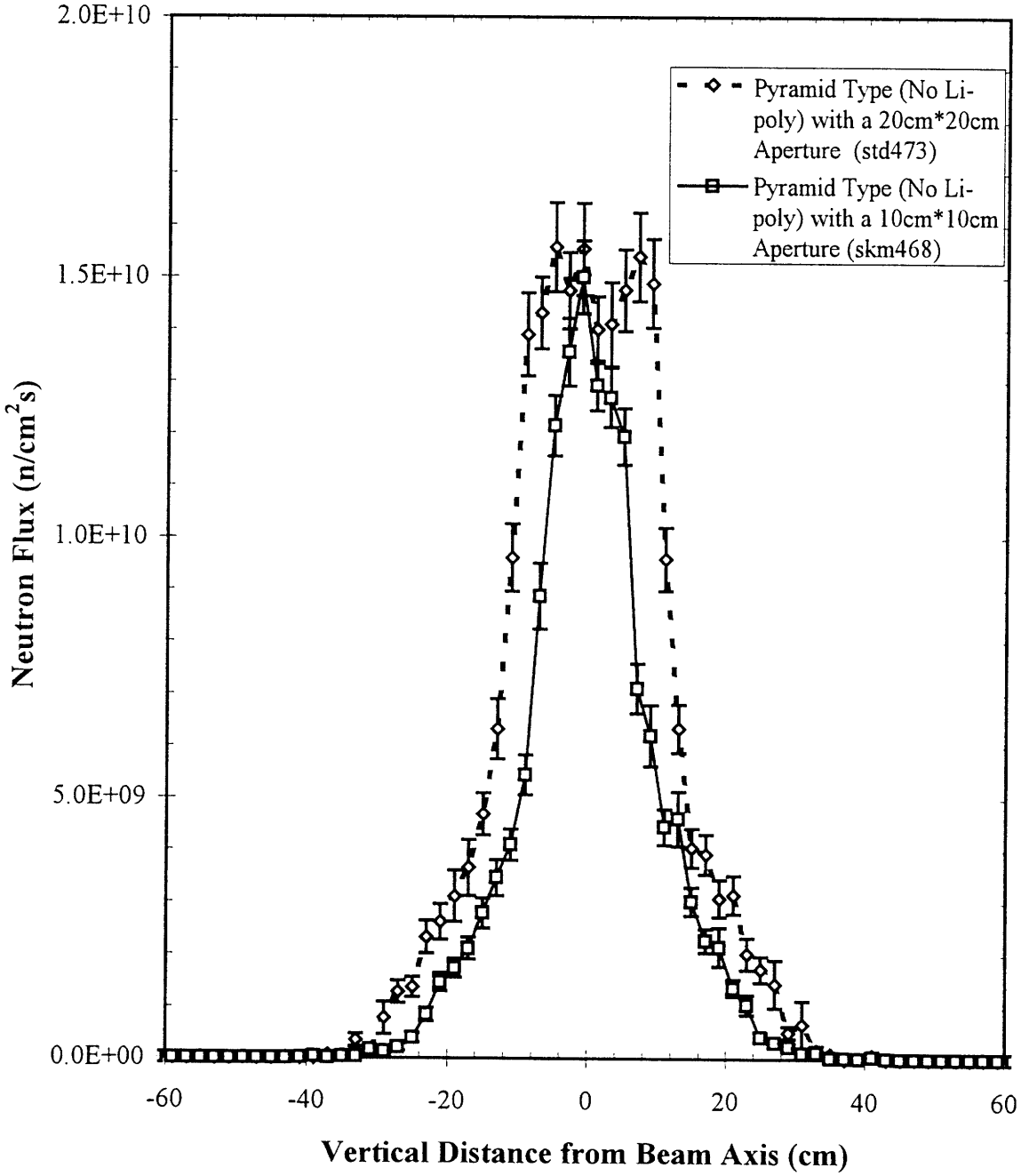

Figure 4.10 Vertical profiles of neutron flux of all energies centered on the beam axis at the patient position for Designs skm468 and std473. Both designs use pyramidal collimators lined with 15 cm thick lead and no Li-poly delimiter and have different beam aperture sizes (20 cm* 20 cm for std473 and 10 cm*10 cm for skm468).

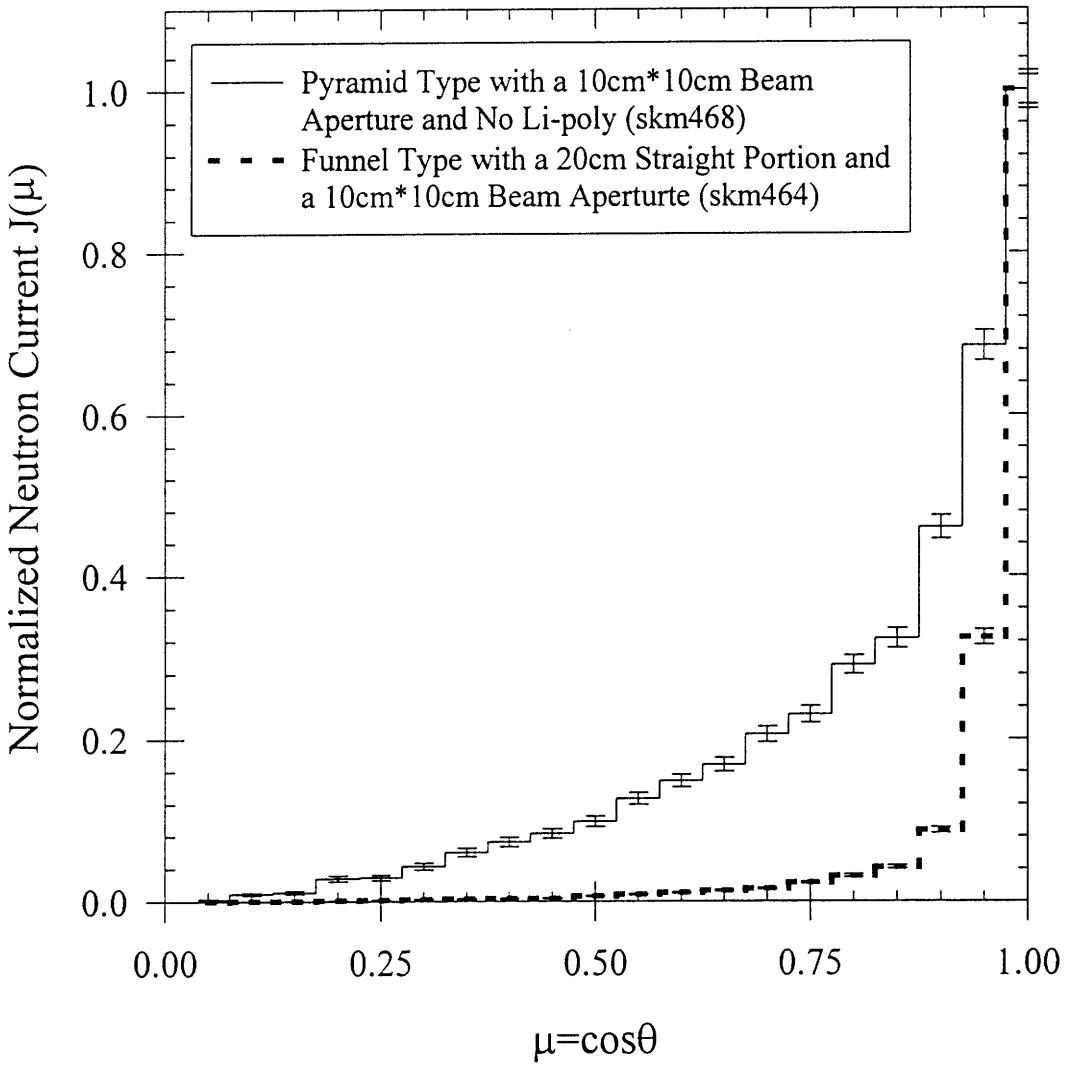

Figure 4.11 Normalized neutron current angular distribution at the patient position for the different collimator configurations. The angular distribution, which is described as a function of μ (the cosine of the angle between the particle trajectory and the beam axis), is normalized to one at the maximum tally bin. Design skm468 uses a pyramidal collimator lined with 15 cm thick lead and no Li-poly delimiter. Design skm464 has a funnel-shaped collimator composed of a four-sided sloped portion lined with 15 cm thick lead and a 20 cm long straight portion with the square cross section surrounded by a Li-poly delimiter. Both designs have the beam aperture with a size of 10 cm*10 cm.

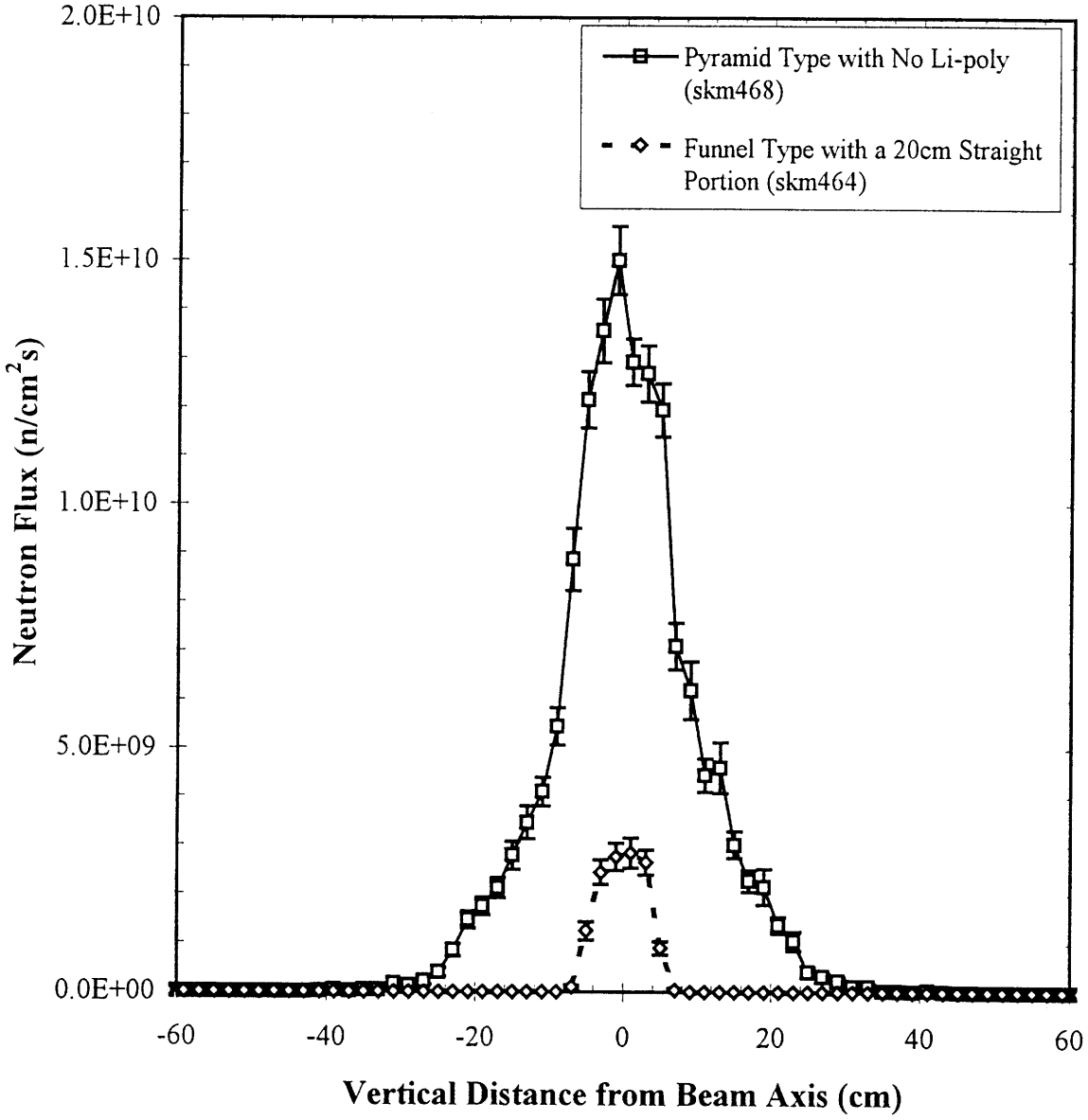

Figure 4.12 Vertical profiles of neutron flux of all energies centered on the beam axis at the patient position for Designs skm468 and skm464. Design 468 uses a pyramidal collimator lined with 15 cm thick lead and no Li-poly. Design 464 has a funnel-shaped collimator composed of a four-sided sloped portion lined with 15 cm thick lead and a 20 cm long straight portion with the square cross section surrounded by a Li-poly delimiter. Both designs have the beam aperture with a size of 10 cm*10 cm.

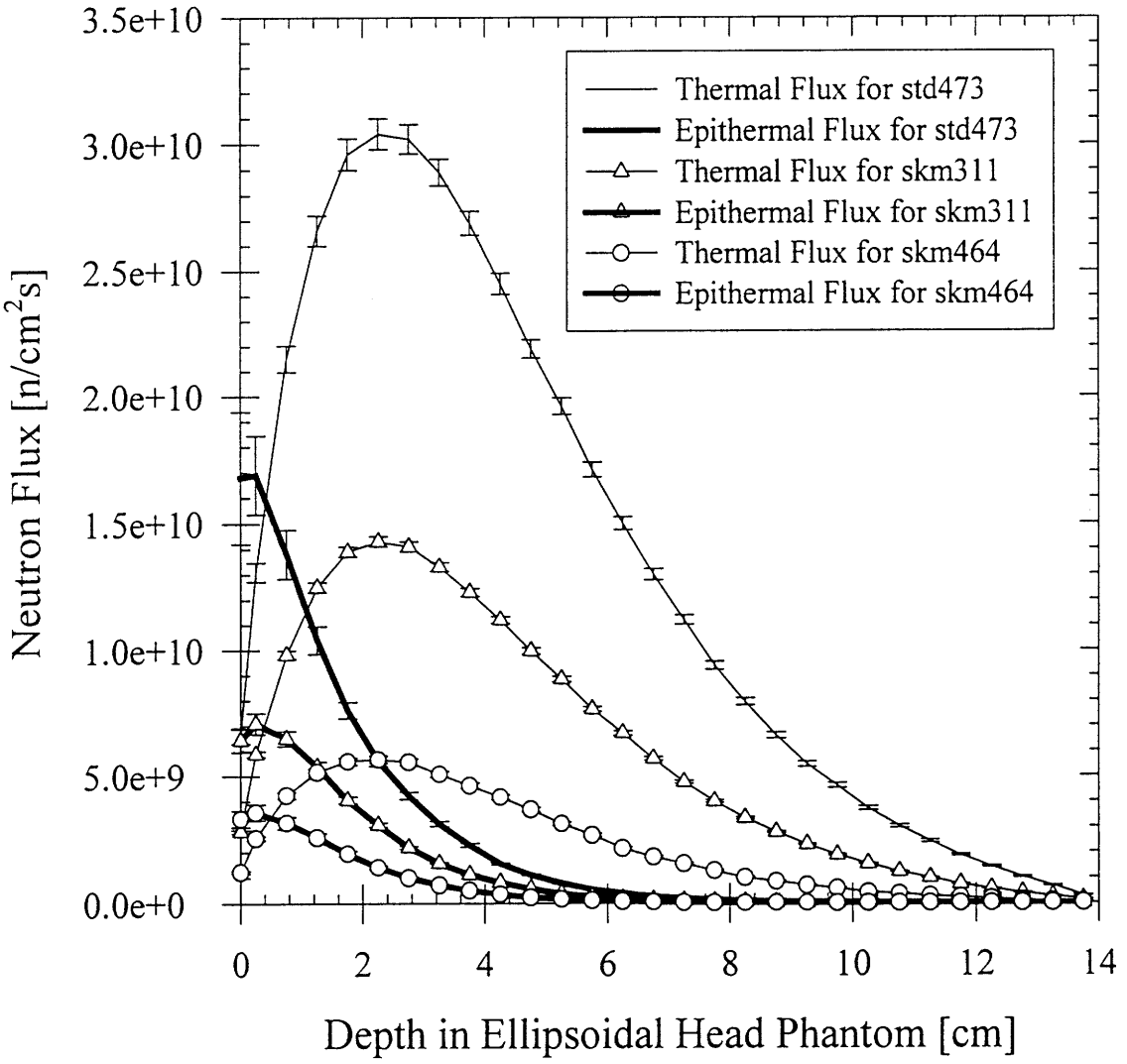

Figure 4.13 Profiles of the epithermal and thermal neutron fluxes as a function of depth in the head phantom produced by Designs std473, skm311 and skm464. Design std473 has a pyramidal collimator lined with 15 cm thick lead and no Li-poly delimiter and a 20 cm*20 cm beam aperture. Designs skm311 and skm464 use funnel-shaped collimators with a four-sided sloped portion with 15 cm thick lead lining and a 20 cm long straight portion with the square cross section surrounded by a Li-poly delimiter and different beam aperture sizes (20 cm*20 cm for skm311 and 10 cm*10 cm for skm464). The reactor power was set at 5 MW.

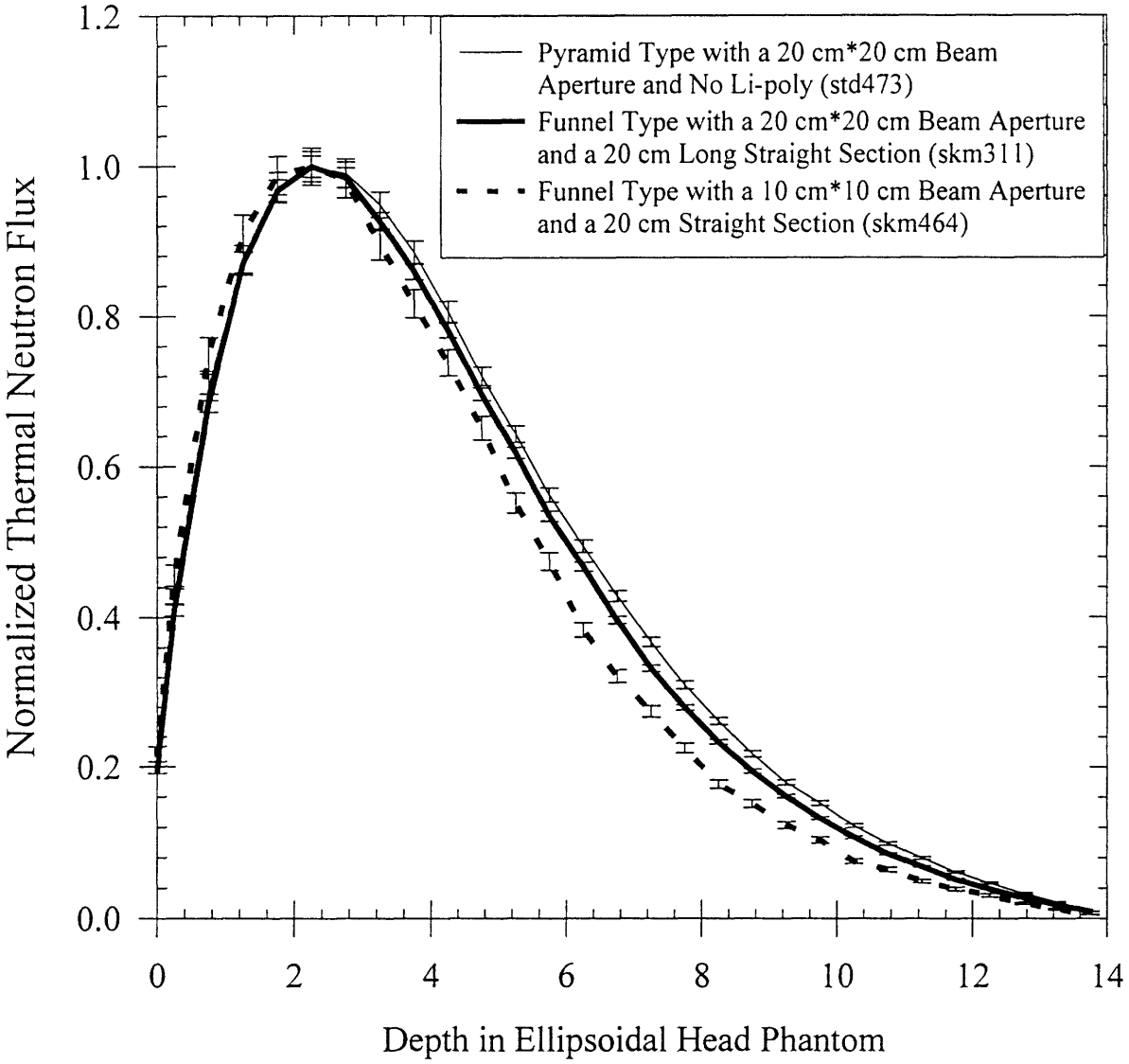

Figure 4.14 Thermal neutron profiles as a function of depth in the head phantom produced by Designs std473, skm311 and skm464. The profiles are normalized to one at the peaks. Design std473 has a pyramidal collimator lined with 15 cm thick lead and no Li-poly delimiter and a 20 cm*20 cm beam aperture. Designs skm311 and skm464 use funnel-shaped collimators with a four-sided sloped portion with 15 cm thick lead lining and a 20 cm long straight portion with the square cross section surrounded by a Li-poly delimiter and different beam aperture sizes (20 cm*20 cm for skm311 and 10 cm*10 cm for skm464).

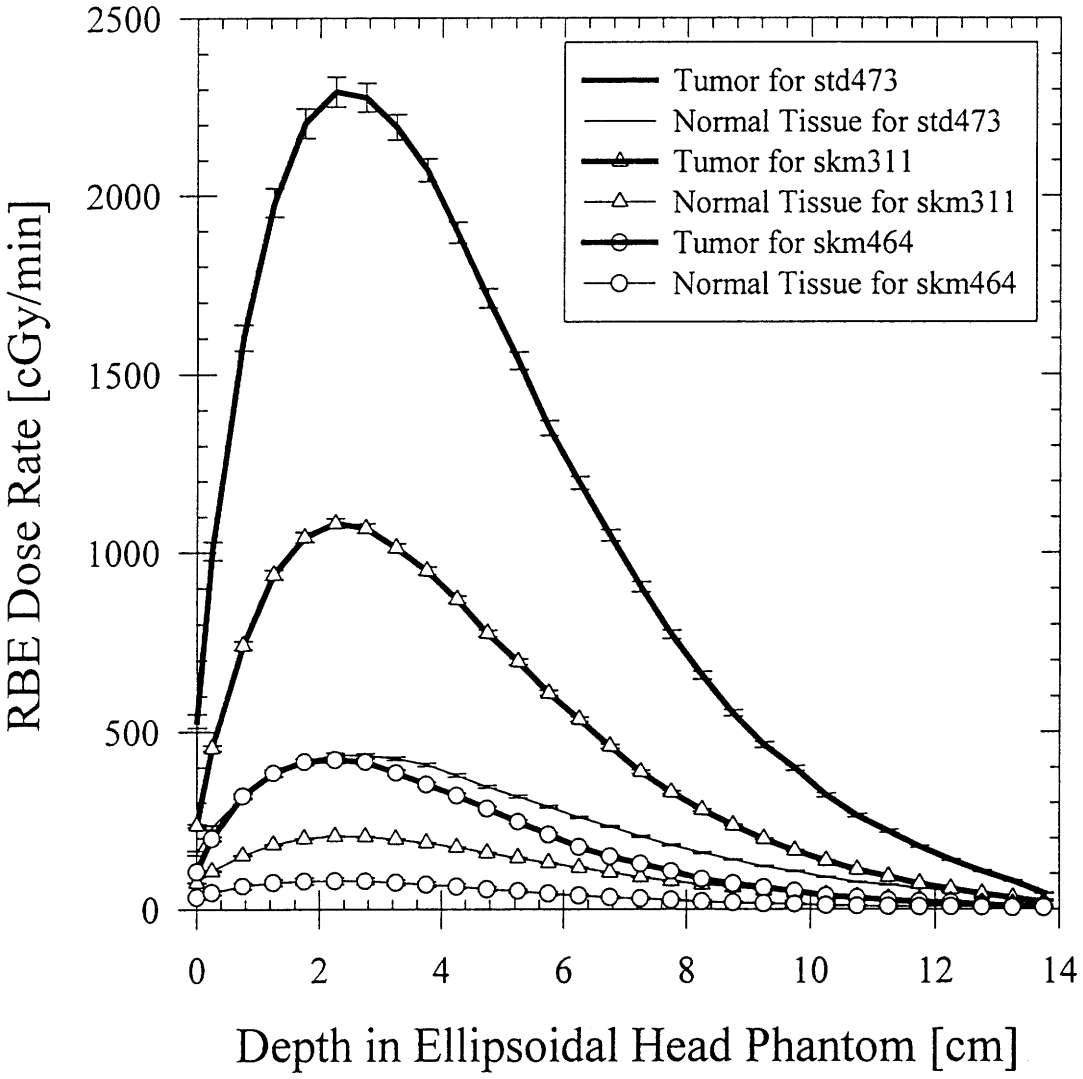

Figure 4.15 Comparison of dose-depth profiles for unilateral irradiation produced by Designs std473, skm311 and skm464. Design std473 has a pyramidal collimator lined with 15 cm thick lead and no Li-poly delimiter and a 20 cm*20 cm beam aperture. Designs skm311 and skm464 use funnel-shaped collimators with a four-sided sloped portion with a 15 cm thick lead lining followed by a 20 cm long straight portion with the square cross section surrounded by a Li-poly delimiter and with different beam aperture sizes (20 cm*20 cm for skm311 and 10 cm*10 cm for skm464). The reactor power was set at 5 MW. Boron uptake was assumed at 40 ppm ^{10}B in tumor with a tumor-to-normal uptake ratio of 3.5:1. The RBE's are 3.2 for neutrons, 1.0 for photons, 3.8 for boron in normal tissue. The reactor power was set at 5 MW.

4.5 Conclusion

The effect of variations of beam size and beam directionality on in-phantom figures of merit was examined by using different collimator designs (funnel and pyramid types) using a Li-poly delimiter and varying the beam aperture size. First, the effect of different collimator configurations and beam aperture sizes on neutron angular and spatial distributions at the patient position were examined. Then, in-phantom analyses were performed for the different collimator designs. The results of these analyses were compared with the angular-distribution and beam-size dependencies of the in-phantom parameters reported by the ideal beam studies of Reference 3. It was shown that many of the trends of in-phantom figures of merit may be explained by the results of Reference 3. One interesting conclusion derived from this study is that, although using a Li-poly delimiter provides a high current-to-flux ratio due to removal of neutrons impinging on the head phantom with large angles, it does not improve beam penetration; on the contrary, the advantage depth is decreased with concomitant great reduction of the advantage depth dose rate. It was indicated that significant reduction of beam aperture size (from 20 cm*20 cm to 10 cm*10 cm) decreases both ADDR and AD in the head phantom even though the angular distribution is unchanged.

There are two purposes for the use of a beam delimiter made of neutron absorber: to minimize the neutron dose outside the beam aperture to protect the patient from unnecessary radiation exposure and to adjust beam directionality. For the treatment of tumors such as glioblastoma multiforme in the brain, the dose is desired to be spatially uniform in the entire brain; therefore, a beam size comparable to the head should be used in the treatment. Based on the results of this analysis, for such a large beam, the adjustment of beam directionality (i.e. improvement of the current-to-flux ratio) by using a beam delimiter would result in significant reduction of beam intensity without improving (rather, slightly degrading) effective beam penetration. Therefore, the

use of a beam delimiter for the second purpose is considered to provide no benefit. In finalizing the collimator design, one has to optimize the trade-off between the advantage of reduction of the neutron dose outside the beam aperture and the disadvantage of significant reduction of beam intensity and slight degradation of beam penetration by using a beam delimiter made of a neutron absorber such as lithiated polyethylene. It would be worth paying attention to the discussion of Reference 8, which suggests that the expansion of beam aperture beyond 15.2 cm might cause a great concern of the whole-body irradiation risk. The use of a whole-body shield, i.e., a board or a sheet containing a neutron absorber which covers a while body except for a target would be an effective way of reducing undesired exposure to neutrons. The change of gamma dose profile around the beam aperture caused by the use of the beam delimiter should also be considered. As will be shown in Chapter 5, the use of a Li-poly delimiter which replaces a portion of lead collimator lining in front of the patient position increases the gamma dose outside the beam aperture even though it reduces neutron dose there.

Chapter 5 will present the results of various neutronic calculations necessary for engineering design and safety considerations of the fission converter beam.

4.6 References

1. R. L. Moss, O. Aizawa, D. Beynon, R. Brugger, G. Constantine, O. Harling, H. B. Liu, and P.Watkins, "The Requirements and Development of Neutron Beams for Neutron Capture Therapy of Brain Cancer," *Journal of Neuro-oncology,* to be published.

2. W. S. Kiger,III, *Neutronic Design of a Fission Converter-Based Epithermal Beam for Neutron Capture Therapy* , Nucl. E. Thesis, Massachusetts Institute of Technology, 1996.

3. J. C. Yanch and O. K. Harling, "Dosimetric Effects of Beam Size and Collimation of Epithermal Neutrons for Boron Neutron Capture Therapy," Rad.Res.135: 131-145, 1993.

4. J. F. Briesmeister, Ed., MCNP - A General Monte Carlo N-Particle Transport Code, *Version 4A,* LA-12625-M, Los Alamon National Laboratory, 1993.

5. J. M. Ryskamp, F. J. Wheeler, C. A. Wemple, K. D. Watts, D. W. Nigg, and P. J. Matonis, "Design of the WSU Epithermal Neutron Beam Extraction Facility for BNCT," *INEL BNCT Research Program, Annual Report 1995*, INEL-96/0139, Idaho National Engineering Laboratory, 1996.

6. H. B. Liu, R. M. Brugger, D. C. Rorer, P. R. Tichler, and J. P. Hu, "Design of a high-flux epithermal beam using ^{235}U fission plates at the Brookhaven Medical Research Reactor," *Medical Physics*, 21(10), October 1994.

7. R. G. Zamenhof, S. D. Clement, O. K. Harling, J. F. Brenner, D. E. Wazer, H. Madoc-Jones, and J.C.Yanch, "Monte Carlo Based Dosimetry and treatment Planning for Neutron Capture Therapy of Brain Tumors," *Neutron Beam Design, Development, and Performance for Neutron Capture Therapy* Edited by O.K.Harling et al., Plenum Press, New York,1990.

8. H. B.Liu, D. D. Greenberg, and J. Capala, "An Improved Neutron Collimator for Brain Tumor Irradiations in Clinical Boron Neutron Capture Therapy", *Medical Physics*, 23(12), December 1996.

9. W. S. Kiger III, R. G. Zamenhof, G. R. Solares, E. L. Redmond II, C.-S. Yam, "MacNCTPlan: An Improved Macintosh-Based BNCT Treatment Planning Program," Transactions of ANS, Vol. 75, Nov. 1996.

CHAPTER FIVE

Neutronic Calculations Related to the Engineering Considerations on the Fission Converter Beam

5.1 Introduction

In the previous chapters, sensitivity studies of the main components of the fission converter beam, i.e., the fission converter, the neutron filters and the collimator, have been described. For the engineering design, there are several aspects of the system which require information from neutronic analysis, e.g., thermal hydraulics and radiation protection. This chapter will present the analyses of some of these aspects.

5.2 Results of the Analysis

The aspects or factors analyzed in the current study are as follows:

- Effect of changing the cross-sectional area of the fast neutron filter/moderator
- Effect of core gamma rays
- Reactivity insertion in MITR due to the fission converter
- Tritium production rate in a D_2O-cooled fission converter
- Heat deposition in the fission converter

- Transverse and Vertical Power Profiles in individual fuel-plates
- Effect of impurities in the fast neutron filter/moderator and collimator liner materials
- Shielding of photons outside the beam aperture

The following sections will describe the result of the analysis of each item listed above.

5.2.1 Effect of Changing the Cross-Sectional Area of the Fast Neutron Filter/Moderator

Reference 1 pointed out the need to optimize the width and height of the fast neutron filter/moderator because increases in the specific fast neutron dose were observed when the collimator design is changed so that the volume of the filter/moderator composed of 68 cm 70% AlF_3/30% Al - 2 cm Ti is reduced by narrowing the beam cross section while the thicknesses of these materials are fixed. Hence, to investigate the effect of changing the cross-sectional area of the filter/moderator, an MCNP calculation was performed. The model used here consists of a D_2O-cooled fission converter with eleven burned MITR-II fuel elements (312 g ^{235}U per element) followed by a fast neutron filter/moderator using 68 cm 70% AlF_3/30% Al - 2cm Ti, a 0.04 cm Cd thermal neutron filter, an 8 cm Bi photon shield and a pyramidal collimator with a 15 cm thick lead lining. The filter/moderator is surrounded by a 10 cm thick lead reflector. The cross-sectional area of the filter/moderator was increased from 105 cm*105 cm to 125 cm*125 cm (the total cross-sectional area of the beam including the reflector thickness was increased from 125 cm*125 cm to 145 cm*145 cm). The resulting in-air beam performance is compared with the original design (using the filter/moderator with the cross-sectional area of 105 cm*105 cm) in Table 5.1. This comparison shows that the increase in the volume of the filter/moderator material by 42% due to increasing its cross-sectional area augments the epithermal neutron flux by 15% while reducing the

specific fast neutron dose by 11%, which is likely due to reduced transverse leakage. Although the width of 125 cm for the original beam design is close to the maximum horizontal dimension available in the thermal column, there would be room for the beam cross-section to be extended in the vertical direction[1]. Therefore, it is worthwhile to perform an optimization study of the beam cross-sectional area.

Table 5.1 Comparison of in-air beam performance of the beam designs using fast neutron filter/moderators with different cross-sectional areas. These calculations used a fission converter composed of eleven burned MITR-II fuel elements (312 g ^{235}U per element) with D_2O cooling, which is followed by a fast neutron filter/moderator composed of 68 cm 70% AlF_3/30% Al - 2 cm Ti, a 0.04 cm Cd thermal neutron filter, an 8 cm Bi photon shield and a pyramidal collimator with a 15 cm thick lead lining. The filter/moderator is surrounded by a 10 cm thick lead reflector. The reactor power was set at 5 MW. The statistical error (one standard deviation) of each result is listed below the value.

Run ID	Cross-sectional Area of the Filter/Moderator	Φ_{epi} n/cm^{2}s	D_{fn}/Φ_{epi} cGycm^2/n	J_{epi}/Φ_{epi}
std473	105cm*105cm	1.30E+10 1.3%	1.33E-11 1.9%	0.67 1.7%
skm103	125cm*125cm	1.50E+10 1.2%	1.19E-11 1.9%	0.64 1.6%

5.2.2 Effect of the Core Gamma Rays

The computational method developed in Reference 1 decouples the MITR-II reactor model from the fission converter beam model. Since the former model is used in a neutron-only run (i.e., only neutron histories are stored in the surface source at the edge of the graphite reflector) for

computational efficiency, the calculations have not taken into account gamma rays generated in the reactor model. Therefore, the photon dose at the patient position due to gammas from the MITR-II reactor region (core gamma rays) was evaluated in the current study.

First, a rough estimate was obtained by a manual calculation. As the photon dose at the radial surface of the MITR-II core tank (26 cm from the core centerline) is estimated to be about 10^8 rad/hr according to the previous measurement,[2] the photon dose rate due to core gamma rays at the patient position (303 cm from the core centerline) is roughly estimated by the following equation:

$$D_{patient} = D_{core\ tank} * (26/303)^2 * \exp(- \sum_i \mu_i * x_i)$$

where, μ_i and x_i are the linear attenuation coefficient for 2 MeV photons (this energy was selected because prompt fission gammas below this energy account for ~70% of the total energy release due to prompt fission gammas)[3] and the thickness of material i which exists between the core and the patient position, and $D_{core\ tank}$ is assumed to be 10^8 rad/hr. One should note that this calculation neglects the photon buildup factor because a rough estimate of it is included in the Monte Carlo simulation which follows. The materials considered here and the data assumed for these materials are summarized in Table 5.2. Graphite was not included in this analysis because the 14-inch window provides a pathway for photons.

Table 5.2 Linear attenuation coefficients for 2 MeV photons and thicknesses of the materials which intervene between the core and the patient position. The mass attenuation coefficient data were obtained from Reference 3.

Material	μ (1/cm)	x (cm)
D_2O	0.049 (data for H_2O was used)	37 (Reactor Reflector 34 + FC# coolant 3)
Al	0.12	77 (FC 7 + Filter/Moderator 70)
U	0.90	0.92 (in FC)
Bi	0.44 (data for Pb was used)	8

'FC' stands for 'Fission Converter'

Following the hand calculation, an MCNP calculation was done to obtain the photon dose rate at the patient position due to prompt gamma rays generated in the reactor core region. First, a criticality run in the coupled neutron-photon mode was performed to store photon histories in the surface source at the edge of the graphite reflector. This photon surface source was subsequently transported through the fission converter beam in a photon only run. Energy independent weight windows were used in these calculations. The fission converter beam model used here consists of a fission converter composed of eleven burned MITR-II fuel elements (312 g ^{235}U per element) with D_2O cooling, which is followed by a fast neutron filter/moderator composed of 68 cm 70% AlF_3/30% Al - 2 cm Ti, a 0.04 cm Cd thermal neutron filter, an 8 cm Bi photon shield and a pyramidal collimator with 15 cm thick lead lining and a beam aperture of 20 cm*20 cm. The filter/moderator is surrounded by a 10 cm thick lead reflector. The reactor power was set at 5 MW.

The results of the hand and MCNP calculations are presented in Table 5.3. For comparison, the result of the MCNP calculation without accounting for core gamma rays (i.e., only taking photons from the fission converter beam model into account) is also presented in this table. It is seen that the effect of core prompt gamma rays is very small compared to that of gamma rays

generated in the fission converter beam model. One should note that the photon dose rate calculated by MCNP is only due to prompt gamma rays. The effect of delayed core gamma rays is considered negligible compared to that of the prompt core gamma rays based on the calculation of the effect of delayed core gamma rays for the 4IH1 experiment configuration performed by W. S. Kiger.[5] Therefore, it is concluded that the effect of photons from the reactor core region is very small compared to that of photons from the components of the fission converter beam due to the large distance between the reactor core and the patient position and the shielding of various materials between these locations. By comparing the results of the MCNP and hand calculations, one can obtain a rough estimate of the buildup factor for the fission converter beam, which is around 13.

Table 5.3 Photon dose rate at the patient position due to photons generated in the MITR-II reactor region (core gamma rays). The MCNP calculations used a fission converter composed of eleven burned MITR-II fuel elements (312 g ^{235}U per element) with D_2O cooling, which is followed by a fast neutron filter/moderator composed of 68 cm 70% AlF_3/30% Al - 2 cm Ti, a 0.04 cm Cd thermal neutron filter, an 8 cm Bi photon shield and a pyramidal collimator with a 15 cm thick lead lining. The filter/moderator is surrounded by a 10 cm thick lead reflector. The statistical error (one standard deviation) of each MCNP calculation is listed below the value. The reactor power was assumed to be 5 MW. The fission converter power obtained in the calculation is 78 kW.

Computational Method	Photon Dose Rate cGy/min
MCNP calculation with core prompt gamma ray only	0.38 9%
Hand Calculation of core gamma rays (prompt + delayed)	0.029
MCNP calculation without core prompt gamma ray	8.0 2%

5.2.3 Reactivity Insertion Due to the Fission Converter

Since the fission converter contains a significant amount of ^{235}U, it is expected to increase the multiplication of neutrons in the system (reactor + converter) although the interaction between the reactor core and the fission converter was shown to be very small.[1] The insertion of positive reactivity has to be restricted to below the reactivity insertion limit (0.2% $\Delta k/k$) for movable experiments in MITR-II.[6] Some efforts had been made using MCNP or CITATION to estimate the reactivity insertion due to the fission converter.[1] However, they were not able to provide a definitive answer to this question because of large statistical uncertainty or inaccuracy of the computational model. To resolve this question, the coupled core-fission converter model was modified to include a Cd shutter and criticality runs were performed with varying shutter positions (open or closed) to examine the change in the multiplication factor (k_{eff}) of the system due to the operation of the fission converter.

The computational model used here contains the MITR-II core with 24 fuel elements and 3 solid aluminum dummy elements and the fission converter with eleven D_2O-cooled burned MITR-II fuel elements (312 g ^{235}U per element) or eleven H_2O-cooled fresh elements (510 g ^{235}U per element). According to Reference 1, these fission converter designs produce the lowest and the highest k_{eff}'s, respectively, among the possible combinations of fuel loading and coolant. The Cd shutter, composed of a 0.0508cm thick Cd layer sandwiched with 0.3175 cm thick aluminum on both sides,[1] is located in front of the fission converter. The bottom of this shutter is raised 81.9 cm above or lowered 81.9cm below the beam centerline when it is open or closed. All of the other beam components (a fast neutron filter/moderator composed of 68 cm 70% AlF_3/30% Al -2 cm Ti, a 0.04 cm Cd thermal neutron filter, a 10 cm lead reflector, an 8 cm Bi photon shield and a pyramidal collimator with a 15 cm lead lining) are included in the model. To improve the statistics,

criticality calculations had ~1000-2000 fission cycles , which required ~5000 minutes on a 200 MHz Intel Pentium Pro computer.

The resulting k_{eff}'s and fission converter powers are summarized in Table 5.4. The fission converter power for each case is compared with that from the fixed-source run using the same fission converter model (shown in the parentheses immediately below the result), which was performed in Reference 1 or the current study; the results show reasonable agreement (power differences of at most 3%). From these results, reactivity insertion due to the operation of the fission converter is calculated as follows (the error after the value denotes one standard deviation).

For the D_2O-cooled fission converter with burned fuel

0.00035 ± 0.00060 $\Delta k/k$

For the H_2O-cooled fission converter with fresh fuel

0.00125 ± 0.00071 $\Delta k/k$

Although the statistical errors are still significant because the reactivity change is so small, these results suggest that, in the case of the H_2O-cooled fission converter with fresh fuel, the reactivity insertion might exceed the limit. Therefore, the procedure to open the Cd shutter should be carefully planned during preoperational testing so as not to cause positive reactivity exceeding the limit. Although the power difference between a criticality calculation and fixed-source calculation is very small, the results for the cases with the Cd shutter closed should be examined carefully because one third of the fuel containing cells of the fuel elements in the fission converter had no fission source points in those cases due to very poor penetration of thermal neutrons into the Cd shutter. This poor sampling of the fission source in some regions could bias the results. Obtaining more accurate results for these cases would require a different approach such as use of perturbation theory as suggested in Reference 1, which is now available in MCNP4B.

Table 5.4 The multiplication factors and fission converter powers calculated using the coupled core-fission converter model. The fission converter power for each case is compared with that from the fixed-source run using the same fission converter model. The Cd shutter was incorporated in the model. The error denotes one standard deviation of each value. The reactor power was assumed to be 5 MW.

Run ID	Fuel Type	Coolant Type	Shutter Position	Nominal source size	# of cycles	k_{eff} w/ 1σ	FC Power (kW) w/ 1σ
react1	Burned	D_2O	Closed	4000	1110	1.00455±0.00048	0.521±0.006 (0.523±0.004)#
react3	Burned	D_2O	Open	4000	2060	1.00490±0.00036	79.6±0.05 (81.5±0.24)#
reac11	Fresh	H_2O	Closed	4000	1010	1.00417±0.00051	1.818±0.011 (1.759±0.012)##
react5	Fresh	H_2O	Open	4000	1015	1.00543±0.00050	124.8±0.10 (125.5±0.25)#

Fixed source calculation in Reference 1

Fixed source calculation in the current study

5.2.4 Tritium Production Rate in the D_2O-Cooled Fission Converter

If D_2O is used as a coolant in the fission converter, tritium (^3H) production is an issue from a radiological standpoint. For this reason, an MCNP calculation as well as a hand calculation were performed to estimate the ^3H production rate in the fission converter. These calculations used a fission converter with D_2O-cooled eleven burned MITR-II fuel elements (312 g U-235 per element). Two beam models were used; one contains the Cd shutter (closed) and the other does not (i.e. opened shutter). All the components of the beam (a filter/moderator composed of 68 cm 70% AlF_3/30% Al - 2 cm Ti, a 0.04 cm Cd thermal neutron filter, a 10 cm Pb reflector, an 8 cm Bi photon shield and a pyramidal collimator with a 15 cm lead lining) were included in the models. The reactor power was set at 5 MW. The results are presented in Table 5.5.

Table 5.5 MCNP calculations of tritium production rate in a fission converter when the Cd shutter is open or closed. These calculations used a fission converter with D_2O-cooled eleven burned MITR-II fuel elements (312 g U-235 per element). The statistical error (one standard deviation) is listed immediately below each value. The reactor power was assumed to be 5 MW.

Run ID	Cd Shutter	^3H Production Rate atom/s
tri01	Open (No shutter)	2.19×10^{12} 0.3%
tri03	Closed (-81.9cm)	5.83×10^{10} 1.4%

Assuming that, within one year (365 days), the fission converter will be operated for 608 hr (20 patients per day and 5 minutes per patient) and shut down for the rest of the time (8162 hr) with the reactor operating at 5 MW, the amount of ^3H produced in a year is given by

$(2.19\times10^{12}[\text{atom/s}]\times608[\text{hr}] + 5.83\times10^{10}[\text{atom/s}]\times8162[\text{hr}])\times 60[\text{min/hr}]\times60[\text{s/min}]$

$= 6.51\times10^{18}$ [atom/yr]

Since the decay constant of ^{3}H is given by

$\ln2/(12.3[\text{yr}]\times365\times24\times60\times60) = 1.787\times10^{-9}[1/\text{s}]$,

the activity of ^{3}H accumulated within one year is,

6.51×10^{18} [atom/yr] $\times 1.787\times10^{-9}$[1/s] $= 1.16\times10^{10}$ [Bq/yr] = 0.314 [Ci/yr]

where the decay of ^{3}H is neglected.

Assuming that the total volume of the D_2O coolant in the fission converter is ~1900 *l* (~500 US gal.), the tritium production rate per unit mass of the coolant is given by,

$0.314[\text{Ci/yr}]/(1900[l]\times1.10445[\text{kg/}l]) = 1.5\times10^{-4}[\text{Ci/kg·yr}]$

It should be mentioned that the calculations described above do not account for ^{3}H production above the top boundary of the model of the fission converter (98.8 cm above the beam axis). However, its effect is expected to be small because the thermal neutron flux above the top boundary is expected to be significantly lower than in the locations surrounding the fuel elements, where the major portion of tritium is produced.

For hand calculations, the following data/assumptions were used:

- Thermal cross section for (n,γ) reaction of deuterium, σ : 0.5×10^{-3} [b][7]
- The atomic density of deuterium in heavy water, N: 0.066272 [atom/barn-cm]
- Average thermal neutron flux in the fission converter, ϕ_{th}:

  5.1×10^{11} [n/cm^2·s] when the Cd shutter is open (tallied at the interface between coolant and rear inner tank in an MCNP calculation)

  5.1×10^{9} [n/cm^2·s] when the Cd shutter is closed
- Decay constant of ^{3}H, λ: 1.787×10^{-9}[1/s]

Then, neglecting decay, the amount of ^3H generated in D_2O coolant in the fission converter within one year is given by:

$$N(^3H) = N\sigma\phi_{th}\times(\text{time})\times(\text{volume})$$

$$= 0.066272[\text{atom/barn-cm}]\times 0.5\times10^{-3}\ [\text{b}]\times(5.1\times10^{11}\ [\text{n/cm2}\cdot\text{s}]\times 608\ [\text{hr}] + 5.1\times10^{9}\ [\text{n/cm2}\cdot\text{s}]\times 8152[\text{hr}])\times 60\times 60\times 100\times 10^{3}[\text{cm}^3]$$

$$= 4.19\times10^{18}[\text{atom/yr}]$$

The accumulation of activity of ^3H in one year is

$$4.19\times10^{18}\ [\text{atom/yr}]\times 1.787\times10^{-9}[\text{1/s}] = 7.47\times10^{9}[\text{Bq/yr}] = 0.202\ [\text{Ci/yr}]$$

This result is 36% lower than that from the MCNP calculation. However, these results agree reasonably well considering significant simplifications employed for the hand calculation.

5.2.5 Heat Deposition in the Fission Converter

The energy release caused by fission reactions in the fission converter was already calculated in Reference 1. However, for thermal-hydraulic analysis of the fission converter, the energy deposition in various parts of the fission converter is required. Therefore, MCNP calculations were performed to calculate detailed energy deposition distributions using the track length cell energy deposition tally (F6). The coupled core-fission converter model with an H_2O-cooled fission converter composed of eleven fresh fuel elements (510 g ^{235}U per element), which was used in the reactivity insertion study, was also employed in this study. The energy deposition caused by neutrons and photons from the MITR-II core was taken into account in the calculation. The reactor power was assumed to be 5 MW. The results are shown in Table 5.6 for the fuel region, and in Table 5.7 for coolant and structural material (aluminum - mostly in the fission converter tanks) of

the fission converter. These results are summarized as follows:

Energy deposition in a H_2O-cooled fresh-fuel fission converter

(The number in the parenthesis denotes one standard deviation)

Fuel: 108.9 kW (0.2%)

Fuel + Coolant: 111.1 kW (0.2%)

Fuel + Coolant + Structural Material (Al): 112.8 kW (0.1%)

Total Effective Energy Release by Fission: 126.5 kW (0.2%)

Regarding this calculation, it should be mentioned that delayed fission energy release, which is around 6% of the total effective energy release, is not taken into account in this calculation. Also, the energy due to delayed gamma rays from the structural materials (primarily Al) and the energy deposited above the top boundary of the computational model of the fission converter (98.8 cm above the beam centerline) are not taken into account. The effect of the last two energies are expected to be very small for the following reasons:

- According to the study of the delayed gamma rays from ^{28}Al in Reference 1, the dose rate at the patient position due to these gamma rays are negligible relative to that due to prompt gamma rays of Al, which is the major photon producer in the fast neutron filter/moderator. Therefore, it is expected that the effect on energy deposition of delayed gammas from Al is also negligible compared to that of its prompt gammas.
- Because the top boundary of the model is far from the beam centerline (98.8 cm), the radiation level above the top boundary is expected to be significantly lower than that in the fuel region, where most of energy deposition in the coolant occurs (~ 70%).

Table 5.6 Energy deposition in the fuel elements of the fission converter. The calculation used a coupled core-fission converter model where the fission converter consists of eleven fresh MITR-II fuel elements (510 g U-235 per element) cooled with H_2O. The statistical error (one standard deviation) is listed immediately below each value. The reactor power was assumed to be 5 MW.

Fuel Element	Fuel			Effective Energy Release by Fission kW
	Fuel Meat kW	Cladding kW	Total kW	
1	7.15 0.6%	0.05 0.2%	7.20 0.6%	8.39 0.6%
2	7.89 0.6%	0.07 0.2%	7.96 0.6%	9.24 0.6%
3	9.67 0.5%	0.08 0.2%	9.75 0.5%	11.32 0.5%
4	11.15 0.5%	0.09 0.2%	11.24 0.5%	13.05 0.5%
5	12.06 0.5%	0.10 0.2%	12.16 0.5%	14.12 0.5%
6	12.43 0.5%	0.10 0.2%	12.53 0.5%	14.56 0.5%
7	12.25 0.5%	0.10 0.2%	12.35 0.5%	14.34 0.5%
8	11.10 0.5%	0.09 0.2%	11.19 0.5%	12.99 0.5%
9	9.52 0.5%	0.08 0.2%	9.60 0.5%	11.14 0.5%
10	7.70 0.6%	0.07 0.2%	7.76 0.6%	9.01 0.6%
11	7.11 0.6%	0.05 0.2%	7.16 0.6%	8.34 0.6%
Total	108.02 0.2%	0.89 0.1%	108.90 0.2%	126.50 0.2%

Table 5.7 Energy deposition in the coolant (H_2O) and the structural material (aluminum) of the H_2O-cooled fission converter with eleven fresh fuel elements. The components which contain most of the aluminum considered here are the converter tank walls.

	Coolant					Structural Material (Aluminum)
	Between the Fuel Plates	Above the Fuel Elements	Below the Fuel elements	Side of the Fuel Elements	Coolant Total	
Energy Dep. kW	1.496 0.1%	0.277 0.4%	0.239 0.5%	0.167 0.8%	2.178 0.1%	1.762 0.2%

5.2.6 Transverse and Vertical Power Profiles in Individual Fuel Plates

In addition to energy deposition, a detailed profile of power generation (i.e., effective energy release by fission reactions) in individual fuel plates of the fission converter is required for thermal hydraulic analysis (e.g., to calculate a hot channel factor). Therefore, the following calculations were performed:

5.2.6.1 Calculation of transverse power profiles in a fission converter with eleven fresh fuel elements and either H_2O or D_2O cooling

The power profiles calculated on a fuel-plate basis for both H_2O and D_2O coolants are shown in Figure 5.1. Since one element contains 15 fuel plates, the total number of plates is 165. The power generation for each plate is described in the appendix. One can see the detailed structure in these profiles. The peaks occur at the sides of the fuel elements where the coolant thickness between the fuel plates is larger, especially around the Al cross-tie. The power increases very rapidly at the lateral ends of the fuel region where the fuel plates face the side reflector. The results are summarized as follows:

H_2O-cooled fresh fuel fission converter

Fission converter power: 125.7 kW

Max. power per plate: 1.12 kW

Fuel plate with max. power: Plate 1 of Element 7

Nuclear hot channel factor#: 1.12*165/125.7 = 1.47

D_2O-cooled fresh fuel fission converter

Fission converter power: 104.9 kW

Max. power per plate: 0.975 kW

Fuel plate with max. power: Plate 1 of Element 7

Nuclear hot channel factor: 1.53

#Nuclear hot channel factor =

(max. power per plate) * (the number of fuel plates)/ (total fission converter power)

5.2.6.2 Calculation of the vertical power profile for the fuel plate with max. power generation

Section 5.2.6.1 showed that Plate 1 of Element 7, which is located next to the central Al cross-tie, is the hottest fuel plate for both H_2O and D_2O cooling. Hence, the axial power distribution for this plate with H_2O cooling was calculated. The vertical profile of average linear power density is shown in Figure 5.2. The numerical result is presented in the appendix. From this calculation, the peak to average ratio is 23.79 [W/cm]* 56.8325[cm]/1122[W]=1.21.

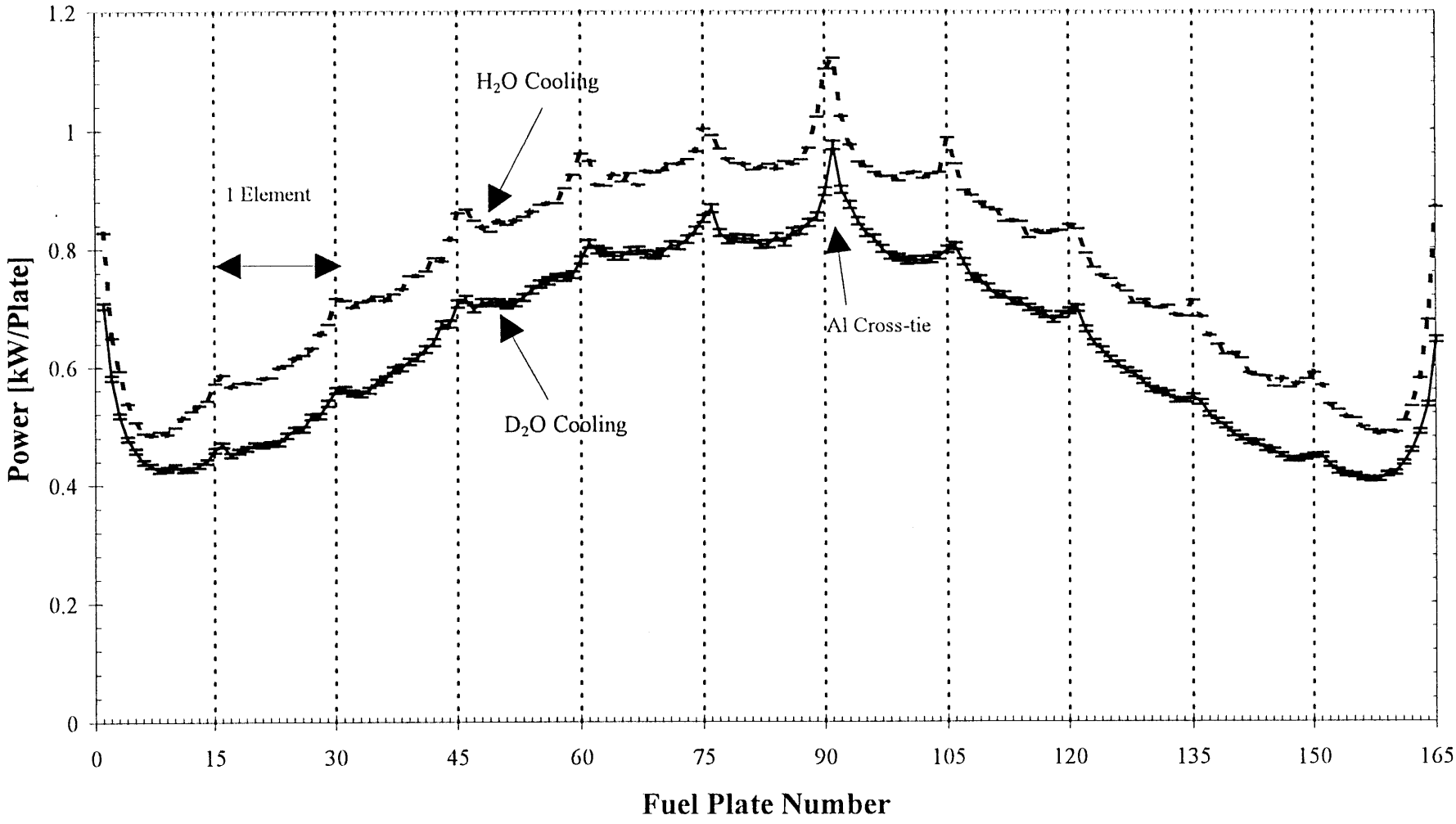

Figure 5.1 Transverse power profile in a fission converter with eleven fresh MITR-II fuel elements and H_2O or D_2O cooling.

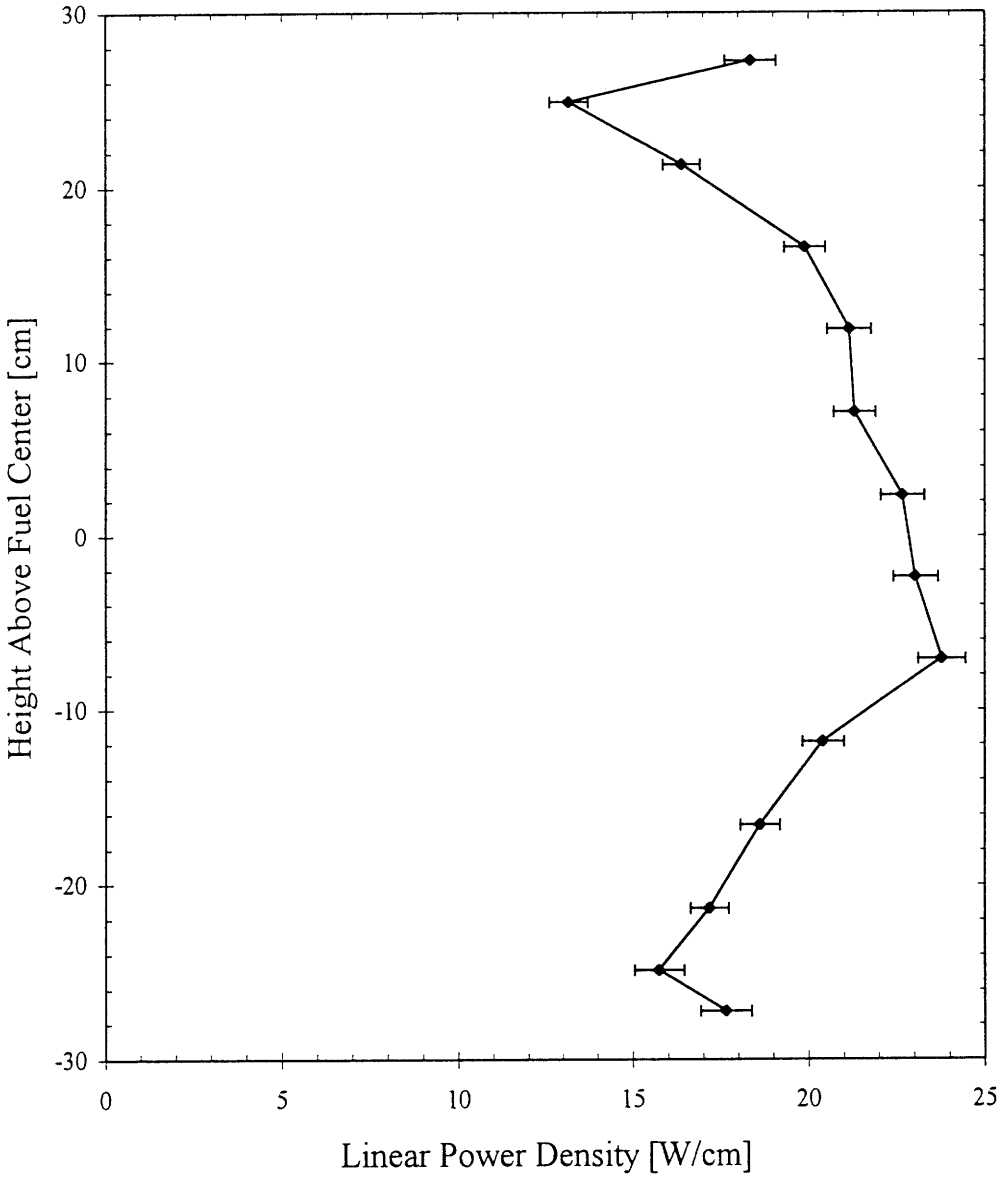

Figure 5.2 Vertical power profile for Plate 1 of Element 7, which is the hottest fuel plate, in an H_2O-cooled fission converter using fresh MITR-II fuel. The ordinate shows the height of the centers of the segments.

5.2.7 Effect of Impurities in the Fast Neutron Filter/Moderator and Collimator Materials

In Reference 1 and the current study, impurities in most of the materials used in the beam design were not taken into account. However, it is possible that the impurities might affect beam performance in various ways such as to increase photon production due to radiative capture. Although the detailed compositions of the materials which would be used in the actual beam construction are not currently available, it is meaningful to estimate the effect of impurities based on the chemical requirement of each material because it would provide some information about how significant the effect of the impurities is. Therefore, sensitivity analyses of the impurities were performed using MCNP based on the chemical requirements from ASTM standards.[8] One should remember the limitation of MCNP calculations in terms of photon production; that is, MCNP does not take account of the delayed (activation) gamma rays. Therefore, the computational results of photon contamination presented here account for only capture (prompt) gamma rays.

First of all, the materials to be analyzed were identified. The filter/moderator, where Al is the main component, would be important for the impurity study because of its large volume relative to the other components and its function of determining the neutron spectrum. The photon shield (Bi) and collimator lining (Pb) would have to be examined carefully, especially in terms of photon contamination, because they are not shielded from the patient position. However, Bi was removed from the scope of this analysis because the experience with Bi in the MIT M67 beam has shown no problem due to impurities and provides confidence with using it as long as material of the same quality is available. Impurities in the Cd thermal neutron filter are expected to have a small impact because Cd is already a major source of photon contamination, its thickness is very small (only 0.04 cm), and its impurities shown in the chemical requirement do not appear to affect

the neutron spectrum significantly.[8] As a result of these considerations, Al and Pb were selected for the analysis. The chemical requirements for Al and Pb from ASTM standards are presented in Table 5.8. Al1100 and Al6061 and common lead (L50049) were chosen for the candidates. The calculations used a fission converter composed of eleven burned MITR-II fuel elements (312 g ^{235}U per element) with D_2O cooling, which is followed by a fast neutron filter/moderator (71 cm Al - 27 cm AlF_3 for the analysis of Al and 68 cm 70% AlF_3/30% Al - 2 cm Ti for the analysis of Pb), a thermal neutron filter (0.04 cm Cd), a photon shield (8 cm Bi) and a pyramidal collimator with a 15 cm thick lead lining. The filter/moderator is surrounded by a 10 cm thick lead reflector. The reactor power was set at 5 MW. The nuclear data mentioned in the following discussions are from References 7, 11, 12, 13 and 14.

Table 5.8 Chemical requirements for Al1100, Al6061 and common lead in weight percent from ASTM standards.[8] The limit described by a single value denotes weight percent maximum unless stated otherwise.

Material	Chemical Compositions w/o
Al1100	Si+Fe 0.95, Cu 0.05-0.2, Mn 0.05, Zn 0.10, Other Elements 0.05(each) 0.15(total), Al 99.00min
Al6061	Si 0.40-0.8, Fe 0.7, Cu 0.15-0.40, Mn 0.15, Mg 0.8-1.2, Cr 0.04-0.35, Zn 0.25, Ti 0.15 Other Elements 0.05(each) 0.15(total), Al remainder
Common Lead (L50049)	Ag 0.005, Cu 0.0015, As+Sb+Sn 0.002, Zn 0.001, Fe 0.002, Bi 0.050, Pb 99.94 min.

As for aluminum, the compositions (in weight percent) of Al1100 and Al6061 used in the MCNP model based on their chemical requirements are shown in Table 5.9. The weight fraction of each impurity was set to its limit to consider bounding cases; as a result, the fraction of aluminum in Al1100 becomes less than the requirement. In the case of Si and Fe in Al1100, the fraction of either one (Si in Type I and Fe in Type II) was set to the limit. As for 'other elements', cobalt,

chromium and nickel were added with 0.05% for each. It should be mentioned that zinc (0.10% max. for Al1100 and 0.25% max. for Al6061) is not included in these compositions because of lack of data in the neutron cross section library of MCNP4A.

Table 5.9 The compositions of Al1100 and Al6061 used in the MCNP model (in weight percent).

Material	Composition $w/_o$
Al1100 (Type I)	Si 0.95, Cu 0.2, Mn 0.05, Cr 0.05, Co 0.05, Ni 0.05, Al 98.65
Al1100 (Type II)	Fe 0.95, Cu 0.2, Mn 0.05, Cr 0.05, Co 0.05, Ni 0.05, Al 98.65
Al6061	Si 0.8, Fe 0.7, Cu 0.4, Mn 0.15, Mg 1.2, Cr 0.35, Ti 0.15, Co 0.05, Ni 0.05, Al 98.65

Table 5.10 In-air beam performance for filter/moderator designs composed of 71 cm Al - 27 cm AlF_3 where pure aluminum, Al1100 or Al6061 is used as the Al block. These calculations used a fission converter composed of eleven burned MITR-II fuel elements (312 g U-235 per element) cooled with D_2O. The filter/moderator is followed by a thermal neutron filter (0.04 cm Cd), a photon shield (8 cm Bi) and a pyramidal collimator with a 15 cm thick lead lining. The statistical error (one standard deviation) is listed immediately below each value. The reactor power was set at 5 MW.

Run ID	Material for Al block	Φ_{th} n/cm²s	Φ_{epi} n/cm²s	Φ_f n/cm²s	J_{th}/Φ_{th}	J_{epi}/Φ_{epi}	J_f/Φ_f	Dγ cGy/min	D_γ/Φ_{epi} cGycm²/n	D_{fn} cGy/min	D_{fn}/Φ_{epi} cGycm²/n
skm308	Al (no impurity)	9.70E+08 1%	1.28E+10 0%	2.20E+08 1%	0.62 0.9%	0.64 0.6%	0.66 1.8%	5.5 1%	7.12E-12 1.1%	9.0 0.6%	1.16E-11 0.8%
skm419	Al1100 TypeI	9.13E+08 2%	1.27E+10 1%	2.09E+08 3%	0.63 2.1%	0.63 1.5%	0.68 4.1%	5.4 2%	7.09E-12 2.4%	8.7 1.4%	1.14E-11 1.8%
skm420	Al1100 TypeII	9.44E+08 2%	1.24E+10 1%	2.17E+08 3%	0.62 2.2%	0.64 1.5%	0.66 4.1%	5.2 2%	6.93E-12 2.5%	8.8 1.5%	1.18E-11 1.9%
skm421	Al6061	8.93E+08 1.9%	1.17E+10 1.2%	2.09E+08 3.2%	0.62 2.4%	0.64 1.5%	0.66 4.2%	5.0 1.8%	7.04E-12 2.1%	8.4 1.6%	1.19E-11 1.9%

The aluminum in the 71 cm Al block of the filter/moderator was replaced with either Al1100 or Al6061 shown in Table 5.9 (AlF_3 was assumed to be pure). The results of the calculations are summarized in Table 5.10. It is noted that beam intensity is slightly reduced (by 9%) when Al6061 is used. However, beam quality (fast neutron and photon contamination) is not changed significantly by the impurities in aluminum.

As for photon contamination due to prompt gammas from Zn in aluminum, its influence should be small relative to that of Al because the weight fraction of Zn is very small (< 0.25%) and its radiative capture cross section for thermal neutrons (~ 1 b) is not very large compared to that of Al (~ 0.2 b). The effect of Zn on the neutron spectrum is also expected to be small because of its small weight fraction although it has several resonance peaks in the epithermal range as high as ~ 500 barns.

Concerning delayed gammas which are not taken into account in MCNP calculations, Reference 1 examined the effect of activation products from Al (^{28}Al), F (^{20}F), Ti (^{51}Ti) , Ni (^{65}Ni) and Bi (^{210}Bi and $^{210}Bi^{m}$) using the beam design which consists of a fast neutron filter/moderator with 63 cm AlF_3 - 3*2 cm Al - 2*2 cm Ti surrounded by a 5 cm thick nickel reflector and an 8 cm thick Bi photon shield. It indicated that the photon dose due to these activation products are negligible compared to the prompt photon dose. Therefore, the effects of delayed gammas from Ni and Ti included in Al1100 and Al6061 as impurities should also be negligible. As for delayed gamma rays from activated Zn (primarily ^{65}Zn and ^{69}Zn, σ_{act} = ~ 0.8 b for ^{65}Zn and ~ 0.1 b for ^{69}Zn, $T_{1/2}$ = 244 d for ^{65}Zn and 14 h for ^{69}Zn, $E\gamma$ = 1.12 MeV for ^{65}Zn and 0.439 MeV for ^{69}Zn), their effects are considered to be negligible because their activation cross sections and photon energies are not so different from those of ^{27}Al (σ_{act} = ~ 0.2 b, $E\gamma$ = 1.78 MeV). Since the filter/moderator is followed by a thick Bi photon shield, the effect of both prompt and delayed gamma rays from the impurities in the filter/moderator is expected to be

insignificant. However, the effect of other activation products such as ^{56}Mn with $\sigma_{act} = \sim 13$ b, $T_{1/2} = 2.6$ h, $E\gamma = 0.847$ MeV (99%), 1.81 MeV (27%), 2.11 MeV (14%) has to be analyzed to confirm that it is small.

Next, the impurity analysis for lead will be discussed. The composition of common lead used in the MCNP model is shown in Table 5.11. Again, the weight fraction of each impurity was set to the limit. In the case of As and Sn, the fraction of either one (Sn in Type I and As in Type II) was set to the limit. Antimony (0.002%max.) and zinc (0.001% max.) were not included due to lack of data in the neutron cross section library.

Table 5.11 The compositions of common lead used in the MCNP model (in weight percent).

Material	Composition $w/_o$
Common lead (Type I)	Ag 0.005, Cu 0.0015, Sn 0.002, Fe 0.002, Bi 0.050, Pb 99.9395
Common lead (Type II)	Ag 0.005, Cu 0.0015, As 0.002, Fe 0.002, Bi 0.050, Pb 99.9395

Table 5.12 In-air beam performance for collimator designs using pure lead or common lead for the lining. These calculations used a fission converter composed of eleven burned MITR-II fuel elements (312 g U-235 per element) cooled with D_2O followed by a filter/moderator (68 cm 70% AlF_3/30% Al - 2 cm Ti), a thermal neutron filter (0.04 cm Cd), a photon shield (8 cm Bi) and a pyramidal collimator with a 15 cm thick lead lining. The statistical error (one standard deviation) is listed immediately below each value. The reactor power was assumed to be 5 MW.

Run ID	Material for Al block	Φ_{th} n/cm²s	Φ_{epi} n/cm²s	Φ_f n/cm²s	J_{th}/Φ_{th}	J_{epi}/Φ_{epi}	J_f/Φ_f	$D\gamma$ cGy/min	$D\gamma/\Phi_{epi}$ cGycm²/n	D_{fn} cGy/min	D_{fn}/Φ_{epi} cGycm²/n
std473	Lead (no impurity)	9.1E+08 2%	1.3E+10 1%	1.2E+08 3%	0.66 2%	0.67 2%	0.68 4%	8.0 2%	1.0E-11 2%	10.4 1%	1.3E-11 2%
skm417	Common Lead Type I	9.35E+08 1%	1.30E+10 1%	1.14E+08 2%	0.64 1.8%	0.66 1.2%	0.68 3.2%	8.7 2%	1.12E-11 1.9%	10.1 1.1%	1.29E-11 1.4%
skm418	Common Lead Type II	9.41E+08 1.0%	1.29E+10 0.7%	1.14E+08 1.7%	0.64 1.3%	0.66 0.9%	0.69 2.2%	9.0 1.3%	1.16E-11 1.4%	10.2 0.8%	1.32E-11 1.1%

The results of the calculations are shown in Table 5.12. The results indicate that the specific photon dose is slightly increased (by 12-16%) when the impurities are added to lead while the epithermal neutron flux and the specific fast neutron dose are unchanged. The increases in the specific photon dose are likely due to radiative capture by Ag, which generates prompt gammas of ~ 2.4 MeV (on average) with a radiative capture cross section for thermal neutrons of ~ 64 barns. As for the effect of Zn and Sb on photon contamination, they have radiative capture cross sections for thermal neutrons which are rather small compared to that of Ag (Zn ~1 b, ^{121}Sb ~6 b, ^{123}Sb ~4 b). Therefore, their contribution would not be significant as long as the effects of their activation products are negligible. However, if accumulated, activated Sb (mainly the following two isotopes, ^{122}Sb with $T_{1/2}$ of 2.7 d, and ^{124}Sb with $T_{1/2}$ of 60.2 d) might cause significant photon contamination. Regarding the neutron spectrum, the effects of Zn and Sb are considered to

be insignificant because they are contained in the collimator lining and their weight fractions are very small (< 0.002%) although Sb has very high resonance peaks (as high as ~3000 b) in the epithermal range.

It should be emphasized that detailed analyses of photon contamination due to impurities, especially the effect of their activation products such as ^{56}Mn in aluminum, ^{122}Sb, ^{124}Sb and ^{76}As (σ_{act} = ~ 4b, $T_{1/2}$ = 26.3 h) in lead, are required before finalizing the beam design. The accumulation of activated elements depends on the impurities, neutron flux and operation schedule (i.e. irradiation time). These analyses should be based on the composition data provided by neutron activation analysis using samples of the materials which would actually be used in the beam.

5.2.8 Shielding of Photons Outside the Beam Aperture

Reference 1 showed that horizontal and vertical photon dose profiles at the patient position rise steeply outside of the 15 cm thick lead collimator lining because of the high photon production in the high density concrete shielding. For the purpose of radiation protection, photons from the concrete region have to be shielded adequately. Therefore, photon generation in the concrete region was analyzed and a new photon shield was considered in the current study. The beam design used here consists of a fission converter composed of eleven burned MITR-II fuel elements (312 g ^{235}U per element) with D_2O cooling, which is followed by a fast neutron filter/moderator composed of 68 cm 70% AlF_3/30% Al - 2 cm Ti, a 0.04 cm Cd thermal neutron filter, an 8 cm Bi photon shield and a pyramidal collimator with a 15cm thick lead lining (in a few calculations, collimator designs with Li-poly delimiters were also considered). The filter/moderator is surrounded by a 10 cm thick lead reflector.

First, photon generation in the heavy concrete will be discussed. The vertical photon dose

profiles centered on the beam axis at the patient position produced by the beam design using heavy concrete is analyzed in Figure 5.3. The profiles in the cases where heavy concrete cells were voided or photon generation of only particular elements (Ti, Fe, ^{10}B) in heavy concrete was turned on using the PIKMT card are also presented. The comparison of the profiles for the calculations with and without heavy concrete confirms that the peaks of the photon dose profiles outside the collimator lining are caused by photon generation in the heavy concrete region. The profiles for the calculations where photon generation from Ti (thermal absorption cross section is ~6 b, average photon energy is 3.6 MeV), Fe (thermal absorption cross section is ~3 b, average photon energy is 3.4 MeV) and ^{10}B (thermal absorption cross section is ~3840 b, average photon energy is 0.48 MeV) [7] is turned on show that photons from these elements account for almost all the photon dose outside of the collimator lining. It is interesting to consider the reason why the profiles have a peak about 30 cm off the beam axis, where the interface between the lead collimator lining and heavy concrete intersects with the surface at the beam edge which is normal to the beam axis . The likely explanation is as follows. Neutrons penetrate through the lead collimator lining although gamma rays are attenuated significantly there. Since the heavy concrete is doped with ^{10}B, thermal neutrons would not travel deeply into it; in other words, neutrons would be absorbed near the interface between the collimator lining and heavy concrete. Around $\pm$ 30 cm from the beam axis, the interface is very close to the beam edge and capture gammas will pass through a very thin layer of heavy concrete to escape to the patient position. However, as the distance from the beam axis increases, the thickness of heavy concrete between the interface and the surface at the beam edge increases, which results in greater photon attenuation. As a result, the photon dose profile is peaked around the intersection of the surface at the beam edge with the interface between the collimator lining and heavy concrete.

Next, the effect of using regular concrete will be examined. The regular concrete used in this calculation is LOS ALAMOS (MCNP) MIX described in Reference 9, whose composition is compared with that of heavy concrete in Table 5.13. Figure 5.4 shows vertical photon dose profiles for beam designs using regular concrete. For comparison, the profile for the beam using heavy concrete is also shown in this figure. One of the designs using regular concrete has a 6 cm lead photon shield behind the regular concrete as shown in Figure 5.5.

Table 5.13 Compositions of heavy concrete and regular concrete in weight percent. The data of heavy concrete is that used in the study of Reference 1. Regular concrete used here is LOS ALAMOS (MCNP) Mix from Reference 9.

Concrete	Composition $w/_o$
Regular	H 0.453, O 51.26, Si 36.036, Al 3.555, Na 1.527, Ca 5.791, Fe 1.378
Heavy	H 0.381, O 32.6, Si 2.12, Ca 4.54, Mg 1.84, Fe 38.0, Ti, 19.9, ^{10}B 0.116, ^{11}B 0.512

The results presented in Figure 5.4 show that regular concrete produces significantly higher photon dose outside the beam aperture relative to heavy concrete. The lower photon dose rate for heavy concrete is explained by two factors: heavy concrete contains ^{10}B (0.116% by weight), which would absorb thermal neutrons and suppress the emission of other higher energy capture gammas, and: heavy concrete contains significant amounts of relatively high Z materials such as Fe and Ti, which would provide photon shielding. The result for the beam with a 6 cm thick lead shield suggests that even very high photon dose (higher than that at the patient position in the direct beam) produced by regular concrete can be reduced to a very low level by using a lead shield with the thickness of ~ 10 cm.

Finally, the photon dose profile for the beam design using a Li-poly delimiter will be

considered. The vertical photon dose profiles at the patient position for Designs std473 (pyramidal collimator with no Li-poly), skm304 (pyramidal collimator with 10 cm long Li-poly lining) and skm311 (funnel-shaped collimator with a 20 cm thick Li-poly delimiter), which have the same size of the beam aperture (20 cm*20 cm), are compared in Figure 5.6 (see Figures 4.3 and 4.4 for their geometries). It is noted that Design skm304 broadens the high photon dose rate region around the beam aperture compared to std473. This is because the last 10 cm of collimator lining was replaced with Li-poly in skm304 so that the effective beam aperture size for photons was enlarged. The photon dose profile of Design skm311 drops more slowly beyond $\pm$ 10 cm (physical beam aperture size) than that of Design std473 because photons with large angles can pass through the Li-poly delimiter and reach off-axis locations; that is, photons are diverging after exiting the lead collimator region. Interestingly, the peaks around $\pm$ 30 cm are not observed for Designs skm304 and skm311. The possible explanations are as follows. For Design skm304, most of neutrons are absorbed by the 10 cm long Li-poly lining; then, capture gamma rays have to pass through at least 10 cm of heavy concrete to escape, which attenuates them significantly. On the other hand, in Design skm311, a 20 cm thick Li-poly delimiter, which covers the whole beam cross section except for the beam aperture, is considered to have a photon shielding effect. For 3 MeV photons, H_2O has a mass attenuation coefficient of ~0.040 cm^2/g.[3] Since polyethylene and water have similar properties in terms of density (polyethylene 0.95 g/cm^3, H_2O 1 g/cm^3) and effective atomic number, (polyethylene, 5.5, H_2O 7.4)[10], the mass attenuation coefficient of polyethylene is expected to be close to that of H_2O. Then, using the data of H_2O for polyethylene, the linear attenuation coefficient for polyethylene is ~0.038 [1/cm]. Therefore, neglecting the buildup, a 20 cm thick layer of polyethylene attenuate 3 MeV photons to ~50%. For lower energy photons, attenuation due to polyethylene is more significant.

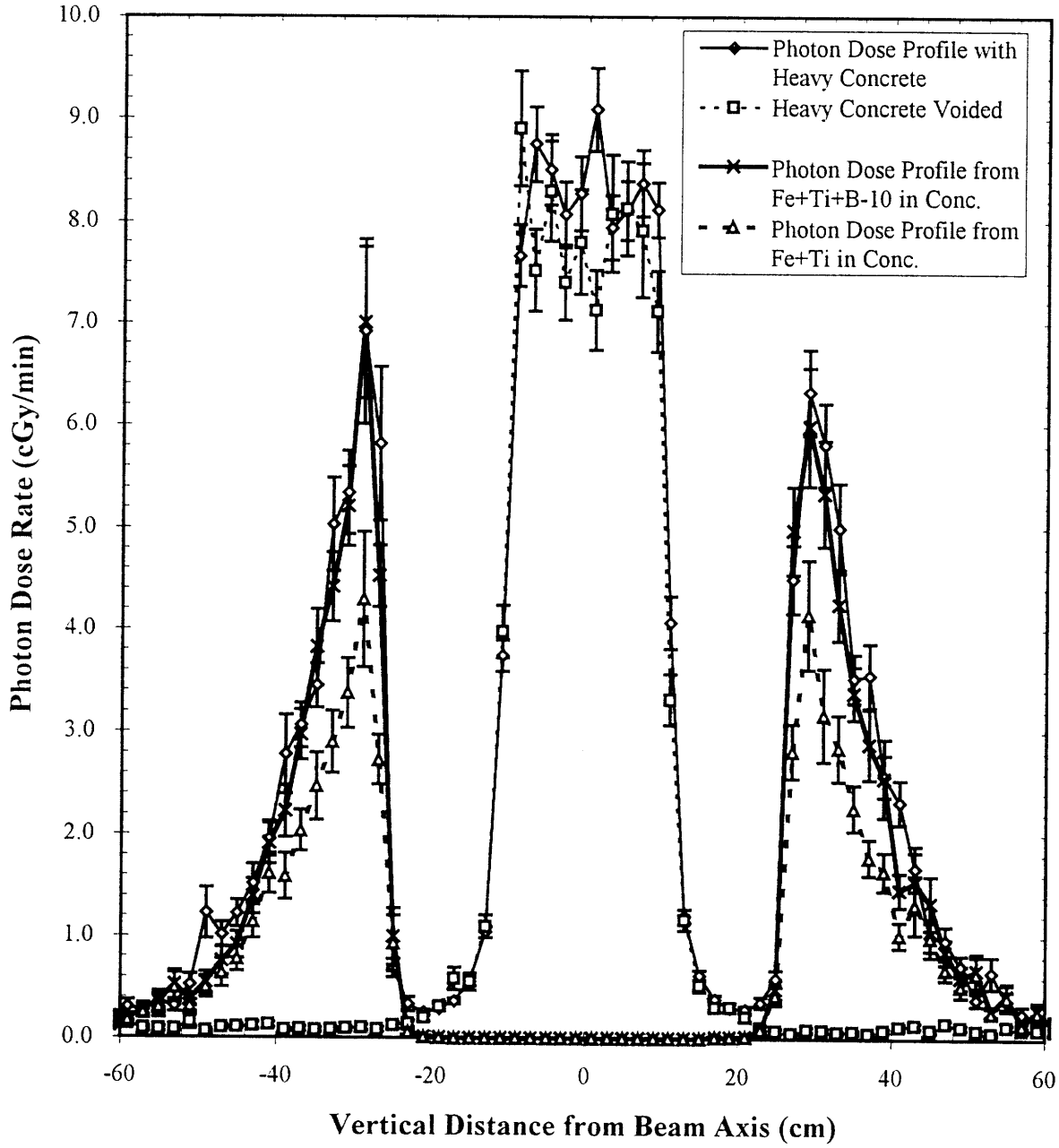

Figure 5.3 Vertical photon dose rate profiles centered on the beam axis at the patient position for the beam designs using heavy concrete. The profile labeled 'Heavy Concrete Voided' is for the beam design with heavy concrete cells voided. The profiles due to photons from particular elements (Fe, Ti, and ^{10}B) are also presented.

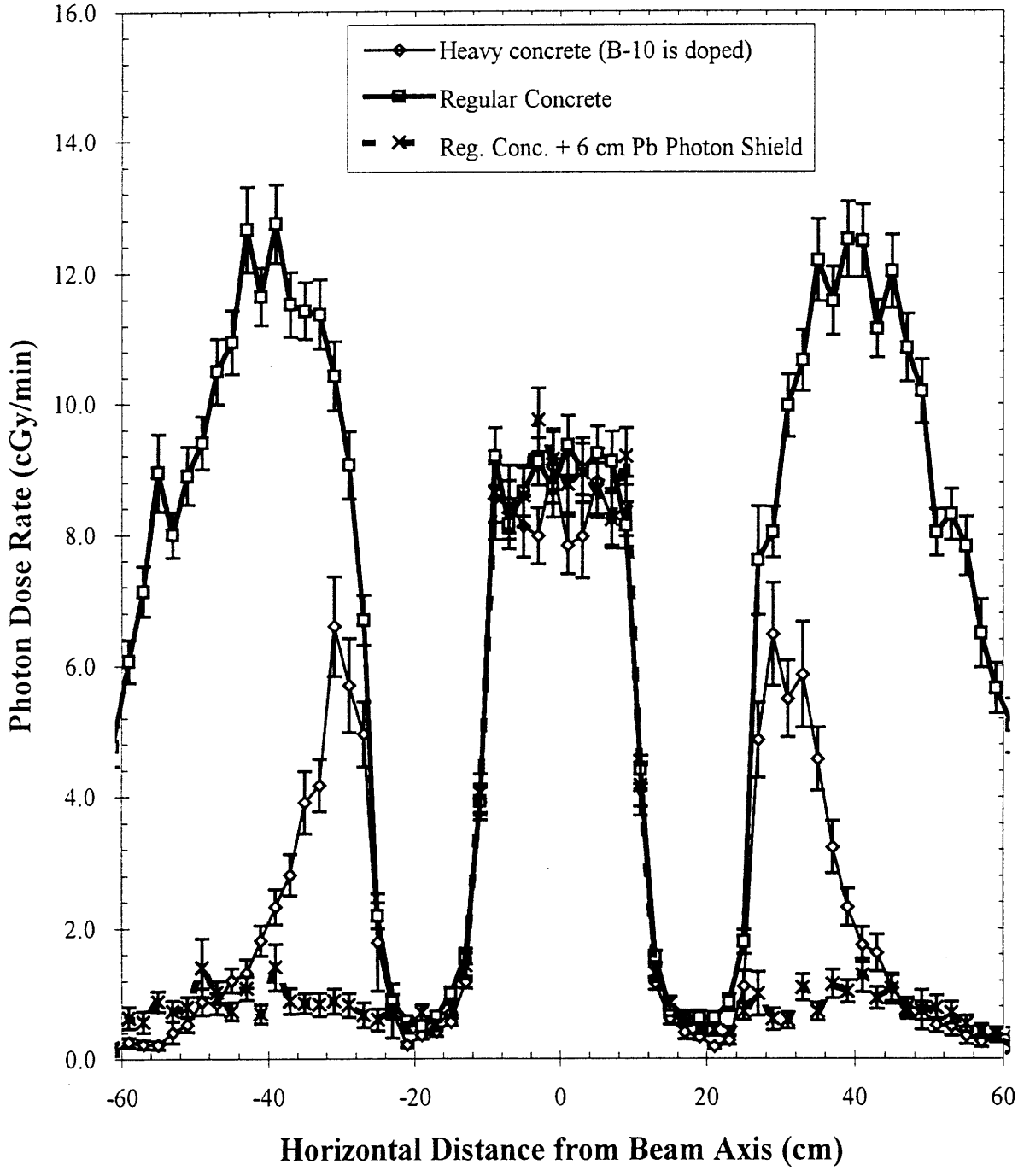

Figure 5.4 Comparison of vertical photon dose rate profiles for the beam designs using heavy and regular concrete.

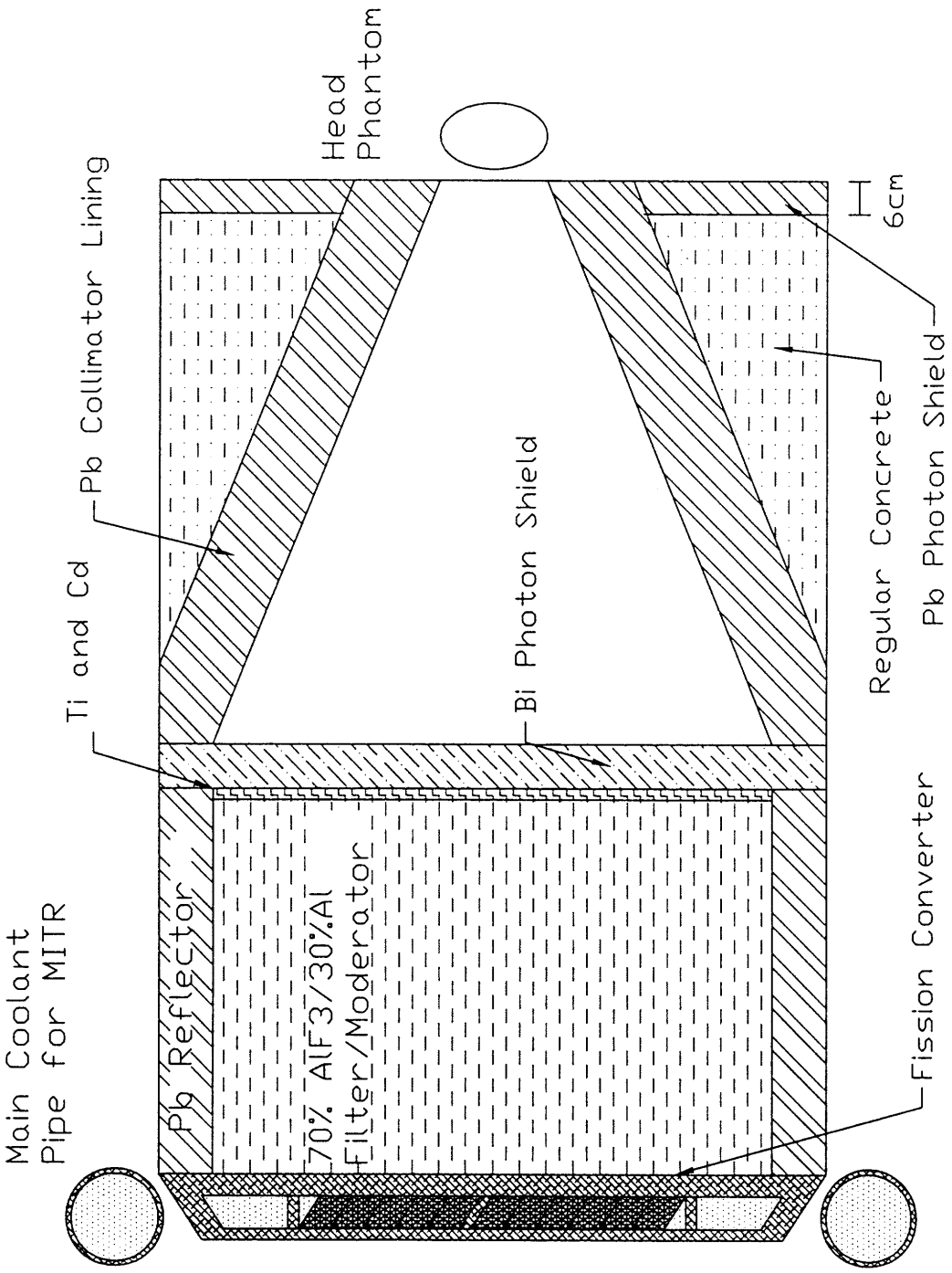

Figure 5.5 The cross-sectional view of the beam design using regular concrete followed by a 6 cm thick lead photon shield.

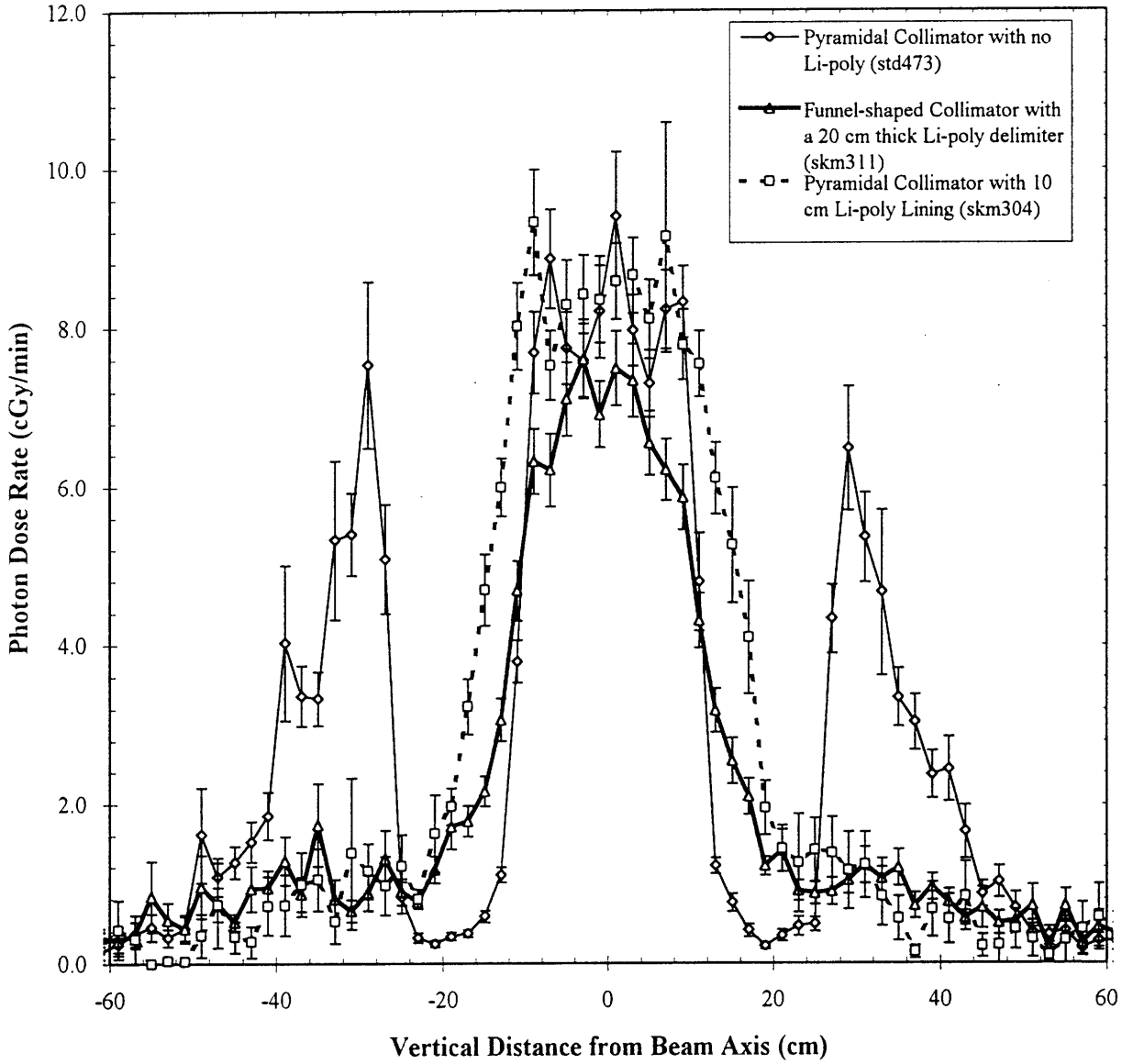

Figure 5.6 Vertical profiles of photon dose rate centered on the beam axis at the patient position for Designs std473, skm304 and skm311.

5.3 Conclusion

Various neutronic calculations related to engineering considerations of the fission converter beam in terms of several aspects such as thermal hydraulics and radiation protection were performed. The conclusions derived from these calculations are summarized as follows:

- Increasing the cross-sectional area of the fast neutron filter/moderator raises beam intensity.
- The effect of the gamma rays from the MITR-II reactor core is negligible.
- The reactivity insertion due to a H_2O-cooled fission converter might exceed the reactivity insertion limit (0.2% $\Delta k/k$).
- The effects of impurities listed in the chemical requirements of ASTM standards on beam intensity, neutron spectrum and photon contamination due to prompt gamma rays are expected to be very small. However, further impurity analyses based on the composition data provided by neutron activation analysis, especially regarding the effect of accumulation of activated elements, are required.
- Gamma rays produced in the concrete (heavy or regular) can be shielded adequately by a lead layer with the thickness of ~ 10 cm.

In addition, detailed information about tritium production rate, heat deposition and detailed power profiles in the fission converter was obtained. The results of these analyses will be integrated into the overall design of the fission converter beam facility. The photon shielding outside the beam aperture (i.e., shielding of the gamma rays produced in the concrete region) will be considered in the discussion of the proposal for the designs of the collimator and concrete region in Chapter 6.

5.4 References

1. W. S. Kiger, III, *Neutronic Design of a Fission Converter-Based Epithermal Beam for Neutron Capture Therapy*, Nucl. E. Thesis, Massachusetts Institute of Technology, 1996.
2. S. T. Boerigter, *An Investigation of Neutron-Irradiation Induced Segregation in Austenitic Stainless Steels,* Sc. D. Thesis, Massachusetts Institute of Technology, 1992.
3. A. B. Chilton, J. K. Shultis and R. E. Faw, *Principles of Radiation Shielding,* Prentice-Hall, Inc., Englewood Cliffs, New Jersey, 1984.
4. J. E. Turner, *Atoms, Radiation, and Radiation Protection,* McGraw-Hill Inc., New York, 1992.
5. Personal Communication from W. S. Kiger.
6. Technical Specifications for the Massachusetts Institute of Technology Research Reactor, Facility License No.R-37, 1975.
7. D. J. Hughes, et al., *Neutron Cross Sections,* 2nd Edition and Supplements, BNL-325 1958, 1960, 1964, 1965.
8. 1996 Annual Book of ASTM Standards.
9. C. D. Harmon, II, *et al.*, *Criticality Calculations with MCNP: A Primer,* LA-12827-M, Los Alamos National Laboratory, 1994.
10. A. E. Profio, *Radiation Shielding and Dosimetry*, John Wiley & Sons., 1979
11. *Engineering Compendium on Radiation Shielding*, edited by R. G. Jaeger *et al.*, Springer-Verlag New York Inc., 1968.
12. S. F. Mughabghab, *et al.*, *Neutron Cross Sections*, 3rd Edition, BNL-325, 1975.

13. M. D. Glascock, *Neutron Activation Analysis Tables*, Research Reactor Facility, University of Missouri, July 1985

14. G. Erdtmann, W. Soyka, *The Gamma Rays of the Radionuclides,* Verlag Chemie, Weinheim, 1979.

CHAPTER SIX

Summary and Recommendations for Future Analysis

6.1 Summary

Sensitivity analyses were performed for the neutronic designs of the main components of the fission converter beam: the fission converter, the neutron filters and the collimator. In the analyses of the fast neutron filter/moderator and the collimator, great emphasis was placed on in-phantom figures of merit using the water-filled ellipsoidal head phantom described in Section 1.4.3 to evaluate beam performance of different designs. In addition, various neutronic calculations required for the engineering design were performed. This chapter will summarize the implications of these analyses and recommendations for future analysis.

In the sensitivity analysis of the fission converter design, the effect of using different fuel configurations (multi-plate reactor type MITR-II fuel vs. single plate type fuel) was examined with the expectation that reduced volume fraction of coolant in the single plate fuel fission converter might offset the disadvantage of the H_2O coolant which overmoderates the useful portion of the neutron spectrum without a commensurate reduction of fast contamination. However, this analysis showed that, although the single plate type fuel can have considerably higher fuel loading than the MITR-II fuel, the fresh MITR-II fuel provides comparable beam performance to the single plate fuel for either H_2O or D_2O cooling. Moreover, in spite of its much lower volume fraction of coolant, an H_2O-cooled single plate fuel fission converter with the minimum coolant thickness

(0.16 cm) does not improve beam performance significantly relative to a D_2O-cooled burned MITR-II fuel fission converter. Therefore, it is concluded that both burned and fresh MITR-II fuel are as efficient generators of epithermal neutron beams, especially with D_2O coolant, as the single plate fuel. The study of the fuel spacing effect showed that increasing the spacing between the fuel elements increases power without improving the epithermal neutron flux or the specific fast neutron dose. Reference 1 showed that increases in the D_2O layer thickness on the upstream side reduce the epithermal neutron flux in proportion to the fission converter power and that increases in the thickness of the downstream D_2O layer cause a significant loss of epithermal neutron flux while decreasing the specific fast neutron dose slowly. From these results, it is concluded that, because the MITR-II fuel already has a large coolant volume fraction, increases in the thickness of the coolant layers surrounding the fuel elements does not reduce fast neutron contamination enough to offset the loss of beam intensity.

The sensitivity analysis of the filter/moderator design indicated that the epithermal neutron beams with high intensity and high quality can be designed using many combinations of filter/moderator materials, i.e., Al-Al_2O_3, Al-AlF_3, Al-$(CF_2)_n$ and Al-C. These designs provide deep penetration of the beam (the AD's of 9.3-9.8 cm extend significantly beyond the centerline of the head phantom) and large therapeutic gain (the AR's are around 5) for a boron-delivery drug such as BPA-fructose. Moreover, they produce ADDR's of 400-600 RBE cGy/min, which enable a complete irradiation in a few minutes. Compared to the current MIT medical beam, they double the advantage ratio and increase the advantage depth by 2 to 3 cm. Moreover, they provide an advantage depth dose rate ~ 50 to 70 times higher than that of the current beam. It was also shown that the variation of the neutron spectrum caused by the use of different filter/moderator configurations which meet the design goals ($D/\Phi_{epi} \leq 2*10^{-11}$ $cGycm^2/n$) does not affect beam quality because the fast neutron and photon contamination is maintained at a very low level

compared to the irreducible background dose due to nitrogen and hydrogen capture. The final design of the filter/moderator can be selected from the range of designs which were shown to provide adequate beam performance in the current study, while taking engineering properties and costs of the materials into consideration. As for the materials which are accompanied with concern for decomposition and release of chemically active species (e.g., fluorine in AlF_3 or Teflon), the analysis showed that one can take advantage of the shielding effect of a thick aluminum filter block by locating such materials behind it, where the radiation levels and temperature would be reduced relative to a location near the fission converter.

The sensitivity analysis of the collimator design and the analysis of photon generation in the concrete shielding provided insight into how the collimator and the concrete regions should be designed. The collimator study examined the effect of using a beam delimiter made of a neutron absorbing material (i.e., lithiated polyethylene) and of changing the size of the beam aperture on in-phantom beam performance. It showed that, although the use of a Li-poly delimiter increases the current-to-flux ratio because of removal of neutrons impinging on the target at large angles relative to the beam axis, it does not improve beam penetration; on the contrary, the advantage depth is decreased due to the decrease in effective beam size. Moreover, the advantage depth dose rate is greatly reduced when a Li-poly delimiter is used. Therefore, in designing the collimator, one has to optimize the trade-off between the advantage of reduction of the neutron dose outside the beam aperture and the disadvantage of significant reduction of beam intensity and slight degradation of beam penetration when using a beam delimiter for irradiations of a head target. The analysis of photon generation in the concrete shielding showed the need to locate a photon shield on the downstream (i.e. patient) side of the concrete. It also suggested that a lead photon shield with a thickness of ~10 cm would provide adequate shielding for either heavy or regular concrete. From the results of these analyses, the design of the collimator and concrete regions shown in Figure 6.1

is recommended.

Lead shielding should completely cover the outside of the beam aperture to attenuate gamma rays coming from the Bi photon shield and those generated in the concrete. In addition, a layer of neutron absorber should be placed on the downstream side of the concrete. Although the neutron flux profile at the patient position for Design skm304 shows that neutron flux is reduced very significantly outside the beam aperture by replacing the last 10 cm lead collimator lining with Li-poly, it would be preferable to have a neutron shield which covers the overall area outside the delimiter in case neutrons penetrating through the lead collimator lining and the concrete cause appreciable dose (this might be the case when regular concrete without neutron absorber is used). For the material of the neutron shield, ^{10}B -containing material could be used if it is located on the concrete side and is followed by the photon shield. The thicknesses of the photon and neutron shields depend on the compositions (i.e., shielding properties) of concrete.

Furthermore, it is recommended to install a removable variable-size beam delimiter which consists of a lead layer followed by a neutron-absorbing material layer at the patient end. For the neutron absorber, a lithium-containing material such as lithiated polyethylene is recommended because of low photon generation due to neutron absorption in it. Several types of beam delimiters with different thicknesses of lead and Li-containing material layers and different beam aperture sizes can be used to adjust beam intensity, effective beam size, and beam directionality, which would be optimized for different targets (e.g., head, extremities, etc.)

As for the type of concrete, heavy concrete with neutron absorber (e.g. ^{10}B, ^{6}Li) is recommended in terms of both photon and neutron shielding. However, regular concrete would also be acceptable when photon and neutron shields with adequate thicknesses are used.

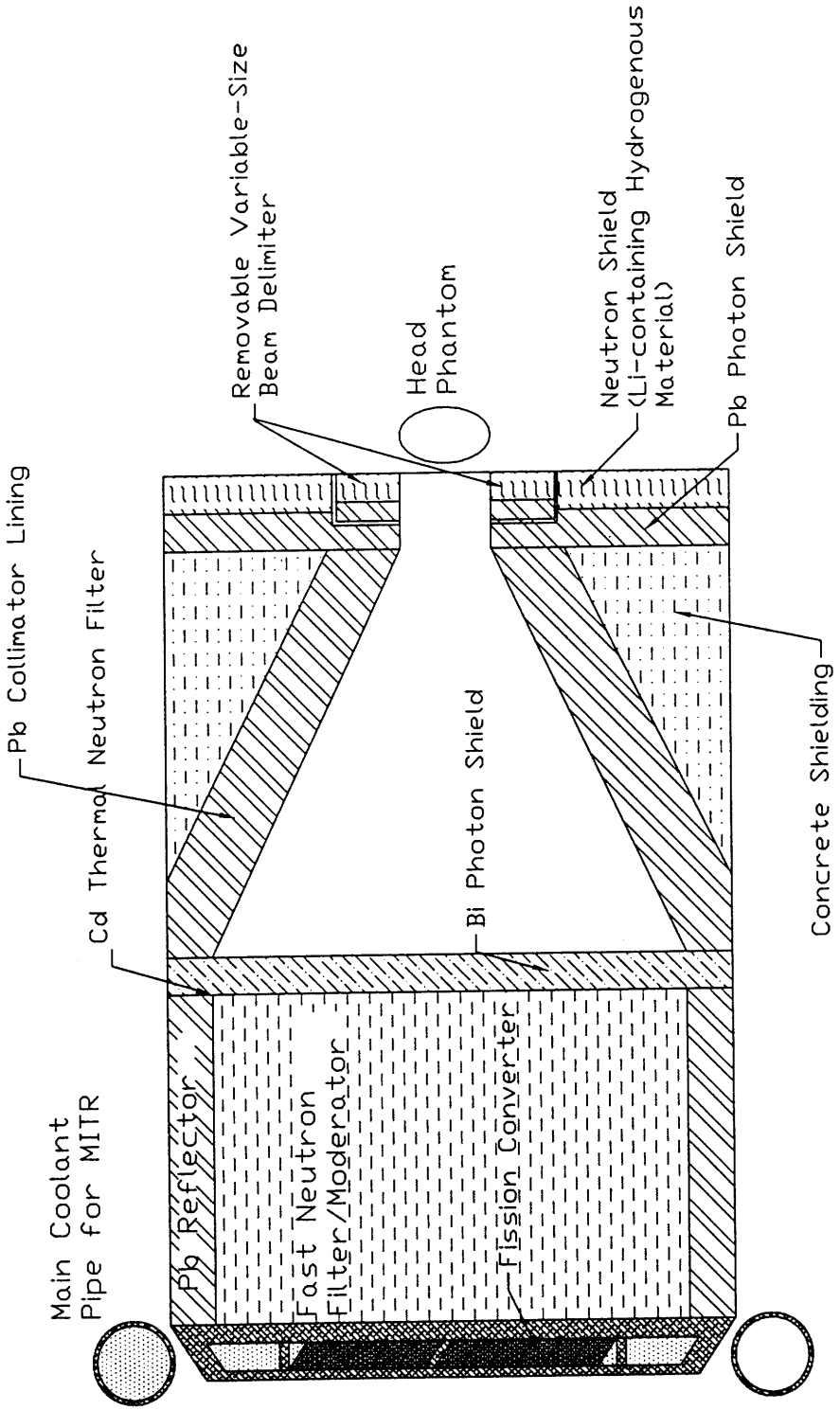

Figure 6.1 Cross-sectional view of a beam design with a removable variable-size beam delimiter at the end of the collimator and neutron and photon shields on the downstream side of the concrete.

6.2 Recommendations for Future Analysis

Although an extensive series of studies has been performed in Reference 1 and the current study for the neutronic design of the fission converter beam, there still remain several factors to be analyzed in order to finalize the beam design. The following items were identified based on the results of the current study. The reader should refer to Chapter 6 of Reference 1 for additional recommendations concerning future studies.

The selection of the best filter/moderator materials and fine-tuning of their dimensions have to be done taking engineering properties and costs of the materials into consideration. Especially, for a fluorine-containing material such as Teflon, one should consider a configuration which sandwiches it with sheets of Al for assuring structural strength and capturing fluorine released due to decomposition as suggested by Reference 2.

The configuration of the beam delimiter has to be optimized. The optimization of beam size (including neutron and photon dose profiles at the patient position) and beam directionality based on detailed in-phantom analysis for different targets should be realized in designing removable, variable-size beam delimiters. For irradiations of brain tumors, a beam delimiter should be designed to optimize the trade-off between the advantage of reducing the neutron dose outside the beam aperture and the disadvantage of significant loss of beam intensity and slight degradation of beam penetration.

The photon and neutron shields outside the beam aperture have to be optimized based on the composition data of concrete which will actually be used in the beam construction. Since the concrete has to support the heavy collimator unless a special frame is used to support it, mechanical strength would be an important factor for concrete selection.

The effect of bremsstrahlung on beam performance has to be analyzed. The MCNP

calculations done in Reference 1 and the current study have not taken account of bremsstrahlung for computational efficiency. Although it is expected not to be difficult to shield the bremsstrahlung, its effect should be analyzed to prepare appropriate shielding if required.

In addition to the items mentioned above, the following studies should be performed:

- Impurity study based on composition data obtained from neutron activation analyses of materials which will actually be used in the beam
- Optimization of the cross-sectional area of the fast neutron filter/moderator
- Consideration of a whole body shield to reduce undesired exposure outside the target region

6.3 References

1. W.S.Kiger,III, *Neutronic Design of a Fission Converter-Based Epithermal Beam for Neutron Capture Therapy*, Nucl. E. Thesis, Massachusetts Institute of Technology, 1996.

2. J. M. Ryskamp, F. J. Wheeler, C. A. Wemple, K. D. Watts, D. W. Nigg, and P .J. Matonis, "Design of the WSU Epithermal Neutron Beam Extraction Facility for BNCT," *INEL BNCT Research Program Annual Report 1995,* INEL-96/0139, Idaho National Engineering Laboratory, 1996.

APPENDIX

Numerical Results of the MCNP Calculations for Transverse and Vertical Power Profiles

This appendix describes the numerical results of the MCNP calculations for transverse and vertical power profiles in the fission converter. The power produced by individual fuel plates in the MITR-II fuel elements with H_2O or D_2O cooling are given in Table A.1 (H_2O cooling) and Table A.2 (D_2O cooling). The axial power distribution of Plate 1 of Element 7, which was identified as the hottest fuel plate, in the H_2O-cooled fission converter is provided in Table A.3.

Table A.1 Power generation for each fuel plate in a H_2O-cooled fresh fuel fission converter. The reactor power was assumed to be 5MW.

Fission Converter Power (kW) = 125.7 (Std. Dev. = 0.081%)

Element 1			Element 2			Element 3			Element 4		
Plate #	Power (kW)	Std Dev (%)	Plate #	Power (kW)	Std Dev (%)	Plate #	Power (kW)	Std Dev (%)	Plate #	Power (kW)	Std Dev (%)
1	0.828	1.09	1	0.586	1.19	1	0.713	1.10	1	0.867	1.02
2	0.651	1.14	2	0.567	1.18	2	0.701	1.08	2	0.848	1.02
3	0.594	1.20	3	0.573	1.18	3	0.710	1.10	3	0.838	1.01
4	0.538	1.23	4	0.573	1.17	4	0.713	1.08	4	0.829	1.00
5	0.507	1.23	5	0.573	1.17	5	0.720	1.09	5	0.846	1.01
6	0.488	1.24	6	0.581	1.17	6	0.713	1.07	6	0.841	1.02
7	0.485	1.27	7	0.581	1.16	7	0.723	1.06	7	0.848	1.01
8	0.491	1.28	8	0.599	1.16	8	0.732	1.06	8	0.855	1.00
9	0.486	1.24	9	0.603	1.16	9	0.754	1.06	9	0.863	1.00
10	0.498	1.25	10	0.615	1.13	10	0.754	1.03	10	0.875	0.99
11	0.513	1.25	11	0.620	1.13	11	0.763	1.05	11	0.877	0.99
12	0.525	1.24	12	0.632	1.12	12	0.785	1.05	12	0.878	0.99
13	0.535	1.21	13	0.656	1.12	13	0.779	1.04	13	0.903	0.98
14	0.542	1.19	14	0.673	1.11	14	0.816	1.05	14	0.925	0.95
15	0.572	1.19	15	0.716	1.13	15	0.861	1.03	15	0.961	0.96
Total	8.252	0.314	Total	9.150	0.297	Total	11.237	0.275	Total	13.055	0.257
Average	0.550	0.314	Average	0.610	0.297	Average	0.749	0.275	Average	0.870	0.257
Peaking Factor*	1.505		Peaking Factor	1.174		Peaking Factor	1.149		Peaking Factor	1.104	

* The ratio of peak to average power per plate for each fuel element

Table A.1 (Continued)

Element 5			Element 6			Element 7			Element 8		
Plate #	Power (kW)	Std Dev (%)	Plate #	Power (kW)	Std Dev (%)	Plate #	Power (kW)	Std Dev (%)	Plate #	Power (kW)	Std Dev (%)
1	0.949	0.97	1	0.991	0.95	1	1.120	0.90	1	0.944	0.97
2	0.909	0.96	2	0.969	0.94	2	1.023	0.92	2	0.899	0.95
3	0.907	0.96	3	0.953	0.94	3	0.975	0.93	3	0.890	0.97
4	0.925	0.96	4	0.945	0.93	4	0.947	0.93	4	0.879	0.98
5	0.914	0.95	5	0.943	0.94	5	0.939	0.95	5	0.869	0.98
6	0.929	0.96	6	0.934	0.95	6	0.929	0.95	6	0.865	0.99
7	0.908	0.95	7	0.937	0.94	7	0.922	0.94	7	0.846	0.98
8	0.932	0.96	8	0.944	0.95	8	0.923	0.95	8	0.847	0.99
9	0.929	0.96	9	0.936	0.95	9	0.915	0.94	9	0.846	1.00
10	0.933	0.94	10	0.948	0.94	10	0.928	0.96	10	0.818	0.99
11	0.944	0.93	11	0.943	0.93	11	0.929	0.95	11	0.829	1.00
12	0.943	0.94	12	0.950	0.93	12	0.920	0.96	12	0.825	1.01
13	0.951	0.94	13	0.970	0.92	13	0.927	0.95	13	0.829	1.00
14	0.965	0.95	14	1.022	0.92	14	0.929	0.94	14	0.831	1.00
15	1.002	0.96	15	1.103	0.92	15	0.987	0.96	15	0.840	0.99
Total	14.038	0.247	Total	14.488	0.242	Total	14.313	0.243	Total	12.855	0.255
Average	0.936	0.247	Average	0.966	0.242	Average	0.954	0.243	Average	0.857	0.255
Peaking Factor	1.071		Peaking Factor	1.142		Peaking Factor	1.174		Peaking Factor	1.101	

Table A.1 (Continued)

Element 9			Element 10			Element 11		
Plate #	Power (kW)	Std Dev (%)	Plate #	Power (kW)	Std Dev (%)	Plate #	Power (kW)	Std Dev (%)
1	0.833	1.02	1	0.684	1.09	1	0.568	1.20
2	0.792	1.02	2	0.652	1.11	2	0.535	1.19
3	0.768	1.02	3	0.637	1.11	3	0.525	1.22
4	0.754	1.02	4	0.620	1.09	4	0.514	1.24
5	0.749	1.03	5	0.623	1.11	5	0.511	1.21
6	0.736	1.04	6	0.614	1.13	6	0.497	1.22
7	0.727	1.06	7	0.589	1.12	7	0.491	1.23
8	0.706	1.05	8	0.585	1.14	8	0.486	1.25
9	0.713	1.05	9	0.583	1.16	9	0.490	1.25
10	0.700	1.05	10	0.566	1.14	10	0.488	1.25
11	0.698	1.06	11	0.578	1.18	11	0.507	1.24
12	0.703	1.06	12	0.564	1.18	12	0.532	1.22
13	0.688	1.06	13	0.571	1.16	13	0.580	1.20
14	0.685	1.08	14	0.578	1.17	14	0.679	1.15
15	0.712	1.09	15	0.589	1.18	15	0.869	1.09
Total	10.965	0.271	Total	9.033	0.294	Total	8.272	0.314
Average	0.731	0.271	Average	0.602	0.294	Average	0.551	0.314
Peaking Factor	1.140		Peaking Factor	1.136		Peaking Factor	1.576	

Table A.2 Power generation for each fuel plate in a D_2O-cooled fresh fuel fission converter. The reactor power was assumed to be 5MW.

Fission Converter Power (kW) = 104.88 (Std. Dev.= 0.1 %)

Element 1			Element 2			Element 3			Element 4		
Plate #	Power (kW)	Std Dev (%)	Plate #	Power (kW)	Std Dev (%)	Plate #	Power (kW)	Std Dev (%)	Plate #	Power (kW)	Std Dev (%)
1	0.704	0.736	1	0.468	0.878	1	0.561	0.891	1	0.715	0.851
2	0.582	0.763	2	0.451	0.871	2	0.555	0.900	2	0.699	0.845
3	0.518	0.785	3	0.457	0.891	3	0.554	0.895	3	0.709	0.879
4	0.479	0.818	4	0.462	0.903	4	0.560	0.884	4	0.709	0.822
5	0.458	0.850	5	0.468	0.899	5	0.574	0.892	5	0.709	0.841
6	0.439	0.858	6	0.468	0.893	6	0.579	0.892	6	0.705	0.805
7	0.433	0.879	7	0.470	0.903	7	0.595	0.903	7	0.709	0.823
8	0.425	0.865	8	0.471	0.882	8	0.599	0.876	8	0.718	0.832
9	0.427	0.875	9	0.484	0.908	9	0.609	0.894	9	0.731	0.824
10	0.432	0.893	10	0.494	0.928	10	0.616	0.911	10	0.740	0.815
11	0.426	0.895	11	0.494	0.910	11	0.630	0.903	11	0.746	0.805
12	0.427	0.876	12	0.516	0.909	12	0.642	0.902	12	0.752	0.805
13	0.434	0.885	13	0.517	0.910	13	0.672	0.893	13	0.752	0.796
14	0.440	0.867	14	0.538	0.981	14	0.673	0.857	14	0.756	0.768
15	0.459	0.882	15	0.560	0.901	15	0.707	0.876	15	0.781	0.776
Total	7.084	0.218	Total	7.317	0.235	Total	9.127	0.231	Total	10.929	0.211
Average	0.472	0.218	Average	0.488	0.235	Average	0.608	0.231	Average	0.729	0.211
Peaking Factor*	1.491		Peaking Factor	1.148		Peaking Factor	1.162		Peaking Factor	1.072	

* The ratio of peak to average power per plate for each fuel elemet

Table A.2 (Continued)

Element 5			Element 6			Element 7			Element 8		
Plate #	Power (kW)	Std Dev (%)	Plate #	Power (kW)	Std Dev (%)	Plate #	Power (kW)	Std Dev (%)	Plate #	Power (kW)	Std Dev (%)
1	0.808	0.794	1	0.868	0.759	1	0.975	0.695	1	0.804	0.721
2	0.798	0.785	2	0.827	0.733	2	0.900	0.704	2	0.778	0.722
3	0.794	0.817	3	0.815	0.731	3	0.874	0.716	3	0.752	0.729
4	0.787	0.777	4	0.818	0.741	4	0.846	0.722	4	0.748	0.732
5	0.788	0.795	5	0.817	0.751	5	0.826	0.723	5	0.734	0.741
6	0.797	0.786	6	0.816	0.744	6	0.817	0.732	6	0.722	0.741
7	0.797	0.776	7	0.807	0.741	7	0.799	0.715	7	0.721	0.739
8	0.791	0.779	8	0.808	0.732	8	0.788	0.716	8	0.710	0.734
9	0.789	0.770	9	0.820	0.742	9	0.784	0.732	9	0.709	0.731
10	0.794	0.768	10	0.811	0.732	10	0.779	0.723	10	0.699	0.741
11	0.807	0.760	11	0.828	0.742	11	0.781	0.730	11	0.693	0.740
12	0.805	0.760	12	0.830	0.723	12	0.781	0.721	12	0.688	0.742
13	0.816	0.770	13	0.844	0.722	13	0.782	0.721	13	0.679	0.740
14	0.832	0.749	14	0.854	0.742	14	0.787	0.722	14	0.687	0.741
15	0.851	0.758	15	0.897	0.729	15	0.799	0.722	15	0.693	0.740
Total	12.054	0.200	Total	12.460	0.191	Total	12.318	0.186	Total	10.817	0.190
Average	0.804	0.200	Average	0.831	0.191	Average	0.821	0.186	Average	0.721	0.190
Peaking Factor	1.058		Peaking Factor	1.080		Peaking Factor	1.187		Peaking Factor	1.115	

Table A.2 (Continued)

Element 9			Element 10			Element 11		
Plate #	Power (kW)	Std Dev (%)	Plate #	Power (kW)	Std Dev (%)	Plate #	Power (kW)	Std Dev (%)
1	0.698	0.730	1	0.539	0.785	1	0.449	0.829
2	0.663	0.739	2	0.518	0.794	2	0.433	0.839
3	0.641	0.747	3	0.506	0.803	3	0.422	0.862
4	0.628	0.758	4	0.499	0.801	4	0.417	0.850
5	0.612	0.749	5	0.485	0.811	5	0.415	0.869
6	0.604	0.758	6	0.478	0.821	6	0.410	0.856
7	0.592	0.758	7	0.472	0.812	7	0.408	0.861
8	0.586	0.769	8	0.470	0.821	8	0.409	0.861
9	0.574	0.767	9	0.460	0.829	9	0.417	0.868
10	0.560	0.767	10	0.457	0.840	10	0.420	0.838
11	0.557	0.769	11	0.449	0.848	11	0.436	0.849
12	0.553	0.793	12	0.443	0.851	12	0.458	0.823
13	0.542	0.776	13	0.442	0.842	13	0.489	0.804
14	0.542	0.784	14	0.445	0.841	14	0.535	0.774
15	0.548	0.793	15	0.448	0.855	15	0.645	0.755
Total	8.900	0.197	Total	7.110	0.212	Total	6.762	0.216
Average	0.593	0.197	Average	0.474	0.212	Average	0.451	0.216
Peaking Factor	1.177		Peaking Factor	1.136		Peaking Factor	1.431	

Table A.3 Axial power distribution of Plate 1 of Element 7 (fresh fuel) with H_2O Cooling

- The active fuel length in the model is 56.8325 cm.
- Power for the plate = 1122 W (Std. Dev. = 0.85%)

Height[#] cm	Avg. LPD[##] W/cm	Std. Dev. %
27.23	18.35	3.95%
24.86	13.16	4.24%
21.31	16.38	3.20%
16.58	19.89	2.91%
11.84	21.15	2.93%
7.10	21.31	2.78%
2.37	22.68	2.71%
-2.37	23.04	2.72%
-7.10	23.79	2.84%
-11.84	20.40	2.90%
-16.58	18.62	3.04%
-21.31	17.18	3.20%
-24.86	15.75	4.48%
-27.23	17.65	4.11%

The height of the center of each segment
Linear power density